NUCLEAR MAGNETIC RESONANCE AND MECHANISTIC STUDIES OF COBALT(III) COMPLEXES

BY

STEVE CHIK FUN AU-YEUNG

A Thesis

Submitted to the School of Graduate Studies

in Partial Fulfilment of the Requirements

for the degree of

Doctor of Philosophy

McMaster University

"If a man does not keep pace with his companions, perhaps it is because he hears a different drummer. Let him step to the music he hears, however measured or far away".

THOREAU

NUCLEAR MAGNETIC RESONANCE AND MECHANISTIC STUDIES OF COBALT(III) COMPLEXES

To My Brother William, My Family And

My Best Friend Inderjit

DOCTOR OF PHILOSOPHY (1983) McMaster University
(Chemistry) (Hamilton, Ontario)

TITLE: Nuclear Magnetic Resonance and Mechanistic Studies of Cobalt(III) Complexes

AUTHOR: Steve Chik Fun Au-Yeung, B.Sc. (Simon Fraser University)

SUPERVISOR: Professor D.R. Eaton

NUMBER OF PAGES: xxi, 271

ABSTRACT

This thesis describes a number of closely related studies on aspects of the chemistry of Co(III) complexes. Of particular interest are μ-peroxy Co(III) complexes formed by the addition of molecular oxygen to Co(II) containing solutions. These compounds have attracted much attention, partly because they can serve as models for biological oxygen carriers and partly because of their intrinsic chemical interest. A review of some of the pertinent chemistry is contained in Chapter One. A number of interesting questions which remain unanswered, particularly with respect to the unexpectedly rapid rates of ligand exchange reactions and the mechanisms of electron transfer reactions will be addressed in the present thesis.

There are also problems with respect to the characterisation of the complexes in solution particularly in cases where there are a number of isomeric possibilities. ^{59}Co NMR has not previously been applied to this area and the thesis reports the intitial results of such a study. Some necessary NMR theory is reviewed in Chapter Two. Experimental details for both the chemical and the NMR studies are contained in Chapter Three.

The application of ^{59}Co NMR to these di-oxygen complexes resulted in several interesting observations and NMR problems. These topics will be dealt with in Chapters Four, Five and Six. In Chapter Seven, the application of a model for assigning ^{59}Co resonances to Co di-oxygen complexes is presented. Finally, in Chapter Eight, some mechanistic studies

on ligand exchange and electron transfer reactions are described. Two appendices give computer programmes and some results on the characterisation of Fe compounds produced by oxidation with the Co di-oxygen complexes.

In order to achieve better resolution, high field experiments were performed using superconducting magnet instruments. In the course of these experiments an anomolous field dependence of the linewidths was observed. The interpretation of this effect is the subject of Chapters Four and Five. In the first of these chapters, linewidth measurements on 22 complexes at 3 different fields are reported. Qualitatively, the results are consistent with relaxation due to chemical shielding anisotropy but calculations show that the observed broadening is two to three orders of magnitude greater than expected from this source. Several other possible explanations are considered. It is concluded that the most likely origin of the effect lies in the contribution of antisymmetric components of the chemical shielding tensor, modulated by an abnormally long correlation time which is associated with the lifetimes of hydrogen bonding interactions. Although the existence of antisymmetric components in the shielding tensor has been recognised as theoretically possible for some time, there has been no previous experimental evidence for their importance. This model leads to two predictions - that there will be a large solvent dependence of the field effect and that the very unusual result of T_1 less than T_2 will be found if this relaxation mechanism is dominant. Measurements showing T_1

less than T_2 have not previously been reported. Chapter Five reports the results of experiments designed to check these predictions. The data support the proposed relaxation mechanism. Nine compounds have been examined in a number of different solvents and the results correlated with the Gutmann donor numbers of the solvents. The contributions of quadrupolar relaxation and scalar relaxation of the second kind to the linewidths are assessed. The measurement of very short T_1's (where T_1 becomes comparable with the instrumental pulse widths) presents some hazards but the predicted values relative to T_2 have been observed. These results suggest a new approach to the study of short lived hydrogen bonded second sphere intermediates of kinetic significance in transition metal complex reactions.

Chapter Six returns to the problem of assigning ^{59}Co resonances in complex mixtures. A model is developed for estimating both the chemical shift and the linewidth of an octahedrally coordinated Co(III) complex with any ligand arrangement. This model is tested by application to some 50 known complexes. ^{59}Co data on a number of these complexes have not been reported previously. The relative chemical shifts, particularly for complexes with similar ligands, can be calculated with some reliability. The agreement between calculated and observed linewidths is only qualitative but the results are nevertheless useful in making isomeric assignments. In Chapter Seven, this model is applied to Co di-oxygen complexes. Examples involving complex isomeric mixtures are discussed and its use in identifying inter-

mediates produced during the oxygenation of Co(II) solutions containing a variety of ligands is demonstrated.

Finally, in Chapter Eight, some mechanistic studies on Co di-oxygen complexes are described. The mechanism of ligand exchange reactions involving bis(salicylaldehyde)ethylenediimine Co(III) dioxygen complexes has been investigated by stopped-flow spectrophotometry. The initial step is dissociative ligand exchange. This result is contrasted with literature reports on similar reactions involving complexes containing amine ligands for which the initial step is electron transfer to the Co. The reasons for the high lability of this class of complexes are discussed. The reduction of several amine containing Co di-oxygen complexes by Fe(II) has been followed by stopped-flow spectrophotometry and by ^{59}Co NMR. In this case, the mechanistic results agree with literature reports on similar complexes but the interesting observation has been made that the different isomers react at different rates. The structures of the isomers have been assigned using ^{59}Co NMR.

Some of the results contained in this thesis are reported in the following publications:

i) Steve C.F. Au-Yeung and Donald R. Eaton, "Characterization of Cobalt-dioxygen complexes by means of High Field ^{59}Co NMR" Inorg. Chim. Acta, 76, L141-144 (1983).

ii) Steve C.F. Au-Yeung and Donald R. Eaton, "Chemical Shift Anisotropy and Second Sphere Hydrogen Bonding in Co(III) Complexes". J. Magn. Reson., 52(3), 351-365 (1983).

iii) Steve C.F. Au-Yeung and Donald R. Eaton, "The Solvent and Field Dependence of ^{59}Co NMR Linewidths", J. Magn. Reson., 52(3), 366-373 (1983).

iv) Steve C.F. Au-Yeung, Richard J. Buist and Donald R. Eaton, "Spin-Lattice Relaxation of Low Symmetry Co(III) Complexes", J. Magn. Reson., in press.

v) Steve C.F. Au-Yeung and Donald R. Eaton, "A Model for Estimating ^{59}Co Chemical Shifts and Linewidths and its application to Cobalt dioxygen complexes", Can. J. Chem., 61, 2431-41 (1983).

vi) Steve C.F. Au-Yeung and Donald R. Eaton, "The Kinetics and Mechanism of the Reaction of μ-Peroxy-bis(Salicylaldehyde)ethylenediimine Co(III) with Cyanide and Thiocyanate Ions". Inorg. Chem., in press.

ACKNOWLEDGEMENTS

The author wishes to express his deep appreciation for the unlimited support, guidance and good humour of his project supervisor Dr. D.R. Eaton. I would also like to thank the other members of the thesis supervisory committee, Drs. C.J.L. Lock and A. Corsini for their constant encouragement. Financial support from the Chemistry Department and McMaster University is gratefully acknowledged.

A special note of thanks to Dr. G. Dénès (C.N.R.S., France) for assistance in the Mössbauer work, and Mr. R.J. Buist for his technical assistance in parts of the NMR work without which this thesis could not have been completed. Linda Palmer is also thanked for her patience in typing this thesis.

To other good friends and colleagues who have contributed in many ways to the completion of this thesis, I sincerely thank you.

TABLE OF CONTENTS

TABLE OF CONTENTS (cont..)

TABLE OF CONTENTS (cont..) PAGE

TABLE OF CONTENTS (cont..) PAGE

TABLE OF CONTENTS (cont..)

TABLE OF CONTENTS (cont..)

LIST OF TABLES

List of Tables (cont..)

LIST OF TABLES (cont..)

LSIT OF TABLES (cont..)

LIST OF FIGURES

LIST OF FIGURES (cont..)

LIST OF FIGURES (cont..)

CHAPTER ONE

LITERATURE SURVEY OF COBALT DIOXYGEN COMPLEXES

SECTION 1.1 Introduction

Metal complexes which are capable of forming adducts with dioxygen without irreversible oxidation of the metal (M) or ligand (L) are known as oxygen carriers. The reverse reaction in equation 1.1 must be observable if a complex is to belong to this class.

$$nM(L) + O_2 \overset{K}{\rightleftharpoons} [M(L)]_nO_2 \quad n = 1,2 \qquad [1.1]$$

Such oxygen carriers are of great importance in the transport and storage of molecular oxygen in living systems (1.1) for the following general reasons:

i) molecular oxygen functions as the terminal electron acceptor in the electron transport chain. It is a necessity in the production of adenosinetriphosphate (ATP) for aerobic metabolism.

ii) molecular oxygen participates in reactions mediated by oxygenases and oxidases. The former involve catalysis of insertion reactions of oxygen whereas the latter involve the oxidation of organic substrates (1.4-1.5).

Table 1.1 summarizes the general properties of naturally occuring oxygen carriers involved in oxygen metabolism. Other metals (not listed in Table 1.1) are also believed to be active in aspects of oxygen metabolism. For example, the oxygen transport agent in photosynthesis is postulated to be manganese (Mn) (1.6-1.7) and the free radical reactions of vitamin B_{12} are believed to utilize both oxygen and Cobalt (1.8-1.9).

Table 1.1

Properties of Naturally Occuring Oxygen Carriers (1.2, 1.3)

	Hemoproteins		Hemerythrin	Hemocyanin
	Hemoglobin	Myoglobin		
Metal(M)	Fe^{n+}	Fe^{n+}	Fe^{n+}	Cu^{n+}
De-oxygenated form				
n	2	2	2	1
magnetic-electronic properties	h.s., S=2	h.s., S=2	h.s., S=2	d^{10}, S=0
Oxygenated form				
magnetic-electronic properties	diamagnetic	diamagnetic	μ_{eff}, temperature dependent, ground state diamagnetic	diamagnetic
M/O_2	1	1	2	2
Major function	transport	storage	storage	transport

Considerable progress has been made in elucidating the details of oxygen transport involving hemoglobin (1.10). Through studies of synthetic model systems in which simple compounds containing metal complexed to dioxygen, insight has been gained into the essential nature of the metal dioxygen bonding.

It is generally agreed in the literature that the fixation of molecular oxygen onto metal complexes takes place by a reversible one electron oxidative-addition reaction. The model of Pauling and others (1.11-1.13) involving a metal dioxygen σ-bond formation is favoured over that of Vaska's lateral π-bonding (1.14-1.15). The metal reversibly transfers an electron to the dioxygen, leading to a formally oxidized metal bonded to the formally reduced oxygen. A bonding scheme (1.16-1.18) with transfer of a metal d-electron to the oxygen π^*_{2p} orbital results in a σ-bond as well as possible oxygen to metal pπ-dπ back bonding. This viewpoint is supported by the bulk of the evidence in the literature. A significant balance between σ and dπ-pπ* back bonding is required for a good oxygen carrier (1.19-1.20). Therefore, the basic equilibrium for dioxygen complexation in oxygenation reactions can be visualized as

$$nML^{n+} + O_2 \overset{K}{\rightleftharpoons} (ML)_n^{n+}\ O{=}O \leftrightarrow (ML)_n^{(n+1)}\ \overset{+}{O}{-}\overset{-}{O} \qquad [1.2]$$

This bonding description has led to extensive investigation of the first row transition metals capable of one electron oxidation interactions with oxygen. Thus, Mn^{2+}, Fe^{2+}, Co^{2+}, Cu^{+} and Cr^{2+} all complex with oxygen due to their readily accessible higher oxidation states in reactions closely-similar to those of biologically relevant oxygen carriers. In general,

literature reports on the study of oxygen carriers can be divided into three main types;

i) Modes of binding and the properties of the oxygen carriers
ii) Dynamics of metal dioxygen binding in solution, and
iii) Reactions of dioxygen complexes.

(i) and (ii) are complementary to each other. For example, quantitative values obtained from measurements of the thermodynamics and kinetics of complexation directly reflect the strength of the σ-π bonding. Single crystal X-ray measurements of bond length and bond angles provide the necessary complementary information. In addition, E.S.R. measurements provide semi-quantitative values for spin density transferred from metal to oxygen for 1:1 complexes. A wealth of information is available on structural and dynamic aspects of oxygen carriers but only a limited effort has been made in the area of the substitution and redox reactions of simple dioxygen complexes.

The literature dealing with reversible oxygen carriers is vast but has been well reviewed. References to individual papers will therefore be omitted except for those immediately relevant to the present research. In this thesis, it is the subject of cobalt di-oxygen complexes that is of particular interest. The literature on these compounds is therefore reviewed as far back as 1960. For other oxygen carriers, little was known until the mid-seventies. General references are listed below:

i) Cobalt oxygen carriers (1.2, 1.3, 1.19, 1.21 - 1.48)
ii) Manganese oxygen carriers (1.49-1.51)

iii) Iron oxygen carriers (1.52-1.56)

iv) Copper oxygen carriers (1.57)

In addition, two other articles or books have appeared dealing with general aspects of bioinorganic chemistry (1.58-1.59), and one review article discusses the recent development of the Actinides as probes for biological reactions (1.60). In section 1.2, a general review of recent developments in Cobalt chemistry is given to complete the literature survey.

SECTION 1.2 General Review of Cobalt(III) Chemistry

In general, the work reported since the earlier days of Werner is divided into four broad areas, namely,

i) synthesis

ii) stereochemistry (including crystallography)

iii) kinetics, reactivity and mechanisms, and

iv) catalysis.

Recent review articles or books dealing with the systematic synthesis of Cobalt (III) complexes (1.61-1.62), optical and stereochemistry (1.63), substitution reactions (1.64) as well as catalytic topics (1.65-1.66) have been published. In addition, references for other areas of increasing interest, in recent years are compiled elsewhere (1.67-1.68).

General concepts for inorganic reaction mechanism are well covered in the books by Basolo and Pearson (1.69) and Wilkins (1.70). Older litera-

ture in this area includes the reviews by House (1.71) and Swaddle (1.72). Models for general electron transfer reaction have been reviewed by Bodek and Davis (1.73) and Davis (1.74). A summary of Werner's research in Cobalt(III) complexes is also available (1.75).

SECTION 1.3 Nomenclature

The term molecular oxygen refers only to the free uncombined oxygen molecule which is paramagnetic and has a triplet $^3\Sigma_g$ ground state. Dioxygen is used as a generic name for the O_2 species in any of its forms, with the restriction that there exist a covalent bond between the oxygen atoms. An M.O. description shows that the unpaired electrons in the $^3\Sigma_g$ ground state are found in the two degenerate antibonding $2p\pi_g^*$ orbitals leaving O_2 with a formal bond order of two and a vacancy for further addition of a single electron in both of the antibonding orbitals (Fig. 1.1).

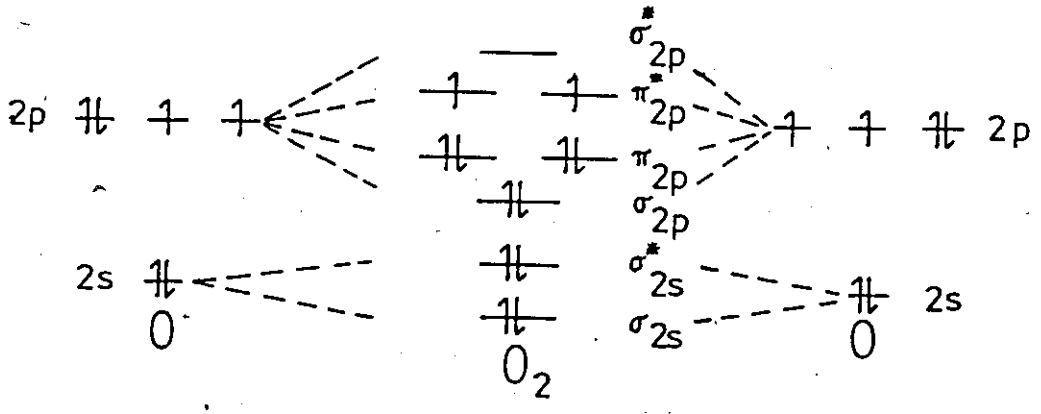

Figure 1.1 M.O. Diagram for Molecular Oxygen

The addition of a single electron results in the formation of a superoxide ($O_2^{\cdot -}$) anion with a total bond order of 1.5 whereas the addition of two electrons would result in the formation of the peroxide (O_2^{--}) anion with a bond order of one (Fig. 1.1).

SECTION 1.4 Cobalt Models

There are three main structural classes of Cobalt oxygen carriers.

a) Mononuclear $CoLO_2$

b) Binuclear $LCoO_2CoL$

c) Binuclear double bridge $LCoO_2(X)CoL$, X=OH, NH_2 or others

Thus, the mononuclear complexes can be regarded as superoxy Co(III) compounds and the binuclear complexes as Co(III)–peroxo–Co(III) compounds. This can be represented as follows:

1:1 complex - one metal atom to one molecule of O_2,

$$M^{2+}O_2\ (A) \leftrightarrow M^{3+}O\text{----}O^-\ (B)$$

2:1 complex - two metal atoms to one molecule of O_2,

$$M^{2+}O{=}O\ M^{2+}\leftrightarrow M^{3+}\ O^-{=}{=}O\ M^{2+}\leftrightarrow M^{2+}\ O{=}{=}O^-\ M^{3+}\leftrightarrow M^{3+}\ O^-\text{——}\ O^-\ M^{3+}$$
$$(A) \qquad (B) \qquad (C) \qquad (D)$$

In the case of the one to one complex, form (B) predominates whereas in the case of the two to one complex form (D) predominates.

SECTION 1.4.1 General Survey of Cobalt Dioxygen Complexes

Since the first discovery of Cobalt dioxygen complex in 1852, two major areas of research have emerged.

i) mechanistic study of reversible dioxygen activation (1.26, 1.76-1.82) because equilibrium between 1:1 and 2:1 complexes has been shown to be extremely solvent dependent (1.83, 1.84).

ii) synthetic design of Cobalt dioxygen complexes modelling biological systems both in aqueous and non-aqueous solution (1.85-1.87) because

it is believed that dioxygen travels through a hydrophobic environment to reach the metal coordination site in the natural system (1.88-1.89).

In general, two types of oxygenation kinetics are observed both in the solid state (1.90-1.95) and in solution (1.26, 1.76-1.82). A 1:1 complex obeys first order kinetics with equation 1.3 as the rate determining step whereas a 2:1 complex obeys second order kinetics with equation 1.4 being rate determining.

$$CoL^{2+} + O_2 \xrightarrow{k_1} LCo^{3+} \cdots O^-\!\!-\!\!-O^{\cdot} \qquad [1.3]$$

$$LCo^{3+} \cdots \bar{O}\!-\!\!-O^{\cdot} + CoL^{2+} \underset{k_{-2}}{\overset{k_2}{\rightleftharpoons}} LCo^{3+}\cdots\bar{O}\!-\!\!-\bar{O}\cdots{}^{3+}CoL \qquad [1.4]$$

In addition to 2:1 complex formation, μ-O_2-μ-ligand dibridged type complexes have also been identified and their kinetics of oxygenation has been demonstrated (1.8, 1.96-1.97) to obey equation 1.3 and 1.4 followed by a slow, first order intramolecular formation of the μ-ligand bridge. This type of μ-ligand bridge is believed to be common when two cis-metal sites are available for coordination under suitable conditions (1.96). For example, $[Coen_5O_2]^{4+}$ has been investigated extensively by various techniques (1.98). The proposed structures are shown in Figure 1.2. On the basis of ^{13}C NMR results, structure I of Figure 1.2 was concluded to be the most likely structure, but kinetic results are not available. It should be reiterated that mononuclear 1:1 complex, the intermediate in the formation of 2:1 dimer, has been inferred kinetically and that its actual existence has not been detected for systems where equations 1.3 and 1.4 are applicable in aqueous solution except for the complex $[Co(CN)_5O_2H]$ (1.99-1.101).

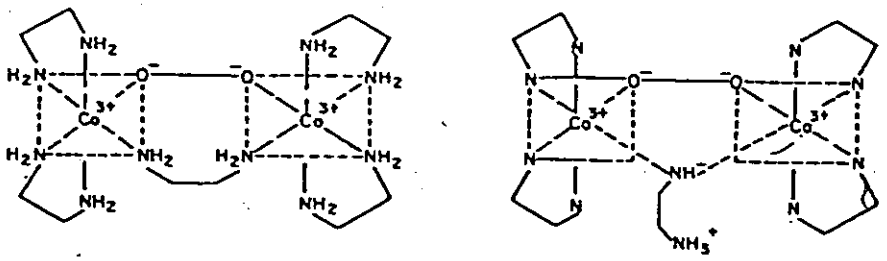

I II

Figure 1.2 Solution structures of $[Coen_5O_2]^{4+}$

In non-aqueous solution, much of the work has been concentrated in the elucidation of the electronic, structural and environmental factors of the 1:1 complex modelling the "cooperative" dioxygen binding in hemoglobin (1.102, 1.103). The subject is beyond this thesis, the reader is referred to many review articles in this area (1.104 - 1.110) with particular emphasis on the recent review by Smith and Pilbrow (1.109).

In summary, a literature survey indicates that most research interest remains centered about electronic, structural and environmental factors. There are increasing trends in the literature in exploiting Cobalt(III) as a probe for the active sites of enzymes (1.111 - 1.112). The energy of the lowest electronic absorption band has been found to be consistent with the average environment rule of Jorgensen (1.112). This behaviour allows qualitative identification of the environment (functional groups) in the active site of enzyme (1.112) leading to potential use of ^{59}Co NMR spectroscopy.

SECTION 1.4.2 Reactions of Co-Dioxygen Complexes

The redox, ligand substitution and decomposition reactions of 2:1 μ-peroxo type Cobalt oxygen complexes were investigated as early as the late sixties. However, it was not until the last two years (1981-82) that the mechanistic details were clarified. Before considering the reaction mechanisms in detail it is appropriate to examine briefly the structures of oxygen complexes in aqueous solution. —

(A) Structure of μ-Peroxo Cobalt Oxygen Complexes in Aqueous Solution $[(Co(NH_3)_5)_2O_2]^{4+}$

Upon addition of $[(Co(NH_3)_5)_2O_2](SO_4)_2 \cdot 2H_2O$ to ice cold 3M H_2SO_4, a red salt believed to be $[(Co(NH_3)_5)_2O_2H](HSO_3)_3SO_4$ is obtained (1.25). On the basis of UV/VIS spectroscopy, the structure of the red hydroperoxo salt was proposed to be either that of I or II (1.25) in Figure 1.3.

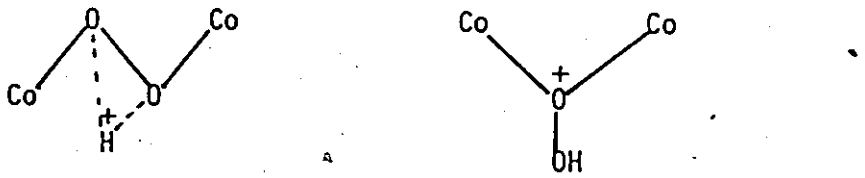

(I) (II)

Figure 1.3 Solution structure of the Hydroperoxo Complex $[(Co(NH_3)_5)_2O_2H]^{5+}$

It is known that form (I) of the μ-amido-μ-hydroperoxo-bis[ethylenediamine cobalt(III) complex is inert towards redox reaction with I^- whereas form (II) reacts slowly in 1M H_2SO_4 at 0°C. The reaction completes in approximately 30 mins. Under these conditions, the hydroperoxo complex of

$[(Co(NH_3)_5)_2O_2]^{4+}$ shows no detectable reactivity. This finding is therefore consistent with the proposed form(I). Cyclic voltammetry experiments conclusively demonstrated that protonation of the μ-peroxo ligands (1.113) occurs at pH less than 3.

Structure I is best described by the two forms (III).

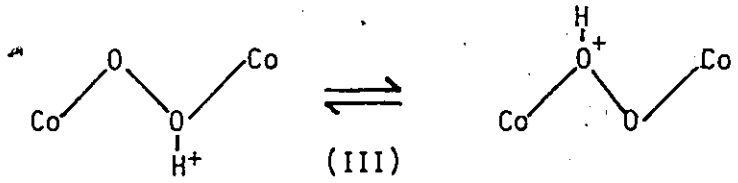

The exact location of the proton remains unknown. Repeated efforts in obtaining a single crystal of the hydroperoxo complex for both X-ray and neutron diffraction analysis by various groups remain unsuccessful.

$\underline{[(Co(CN)_5)_2O_2]^{6-}}$

The anion $[(Co(CN)_5)_2O_2]^{6-}$ is stable at high pH (>13) and undergoes reversible protonation between pH = 10 and 13 to give the pale yellow hydroperoxo complex $[(Co(CN)_5)_2O_2H]^{5-}$ at low temperature. The pK of this proton has been determined to be 12. The hydroperoxo complex disproportionates to the mononuclear hydroperoxo complex $[Co(CN)_5O_2H]^{3-}$ and the hydrolysed product $[Co(CN)_5H_2O]^{2-}$ when the pH ≤ 10. Further lowering of pH (∿5) causes production of H_2O_2 from the mononuclear hydroperoxo complex. This is summarized below.

$$[(Co(CN)_5)_2O_2]^{6-} + H^+ \underset{0.4°C}{\overset{\text{Argon}}{\rightleftharpoons}} [(Co(CN)_5)_2O_2H]^{5-} \qquad [1.5]$$

$$[(Co(CN)_5)_2O_2H]^{5-} + H_2O \longrightarrow [Co(CN)_5O_2H]^{3-} + [Co(CN)_5H_2O]^{2-} \qquad [1.6]$$

$$[Co(CN)_5O_2H]^{3-} + H_3O^+ \longrightarrow [Co(CN)_5H_2O]^{2-} + H_2O_2 \qquad [1.7]$$

HydroTysis of the mononuclear hydroperoxo complex is slow, so that it has proved possible to isolate the salt $K_3[Co(CN)_5(O_2H)]$ (1.114). This is the only known example of a mononuclear hydroperoxo Cobalt complex with monodentate ligands in its first coordination shell.

$[(Coen_2)_2(O_2)(NH_2)]^{3+}$

Dibridged complex formation is extremely common for Cobalt-amine type oxygen complexes. Continued study by various groups has led to a comprehensive understanding of the structural transformation properties in aqueous solution. Mori and Weil (1.115) have investigated in detail the dibridged complex $[Coen_2(\mu\text{-}O_2, NH_2)Coen_2]^{3+}$ using optical and kinetic measurements and concluded that the equilibrium relationship between the various species is consistent with Scheme 1.1. The crystal structures of both the α and γ ions have been determined. The structure of the α ion with the O-O distance of 1.48 Å is consistent with a typical peroxide (1.116). The nitrogen atom of the amido bridge has a tetrahedral angle.

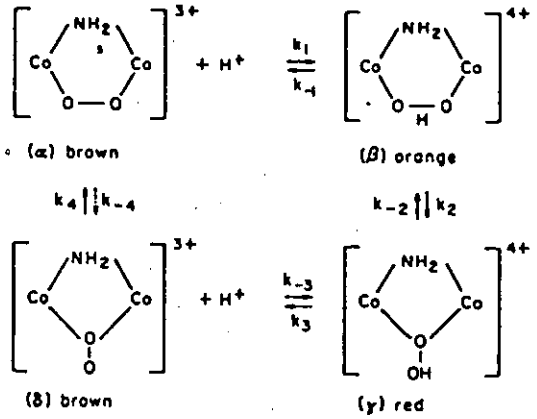

The chemical transformations of the μ-amido-μ-peroxobis[bis(ethylenediamine)cobalt(III)] 3+ ion (= α) in aqueous solution.

Scheme 1.1

The structure of the γ ion (1.117) demonstrates the unusual trivalent oxygen bridge. A more accurate structure determination is desirable due to disordering of the OH group. The isolation of the γ ion provides further support for the existence of a β form - the precursor to γ formation. In summary, equilibria between α, β, and γ forms are established in acidic aqueous solution. The less well characterized δ form is believed to be involved in the α, δ, γ equilibria in basic solution. In neutral solution the α form is stable for several hours.

(B) Redox Reactions

The redox chemistry of μ-dioxygen monobridged and dibridged complexes has been extensively studied. In general, reduction of the superoxo complex is believed to occur by an outer sphere mechanism whereas that of the peroxo complexes involves an inner sphere pathway. Scheme 1.2 suggested by Sykes (1.118) is reproduced below

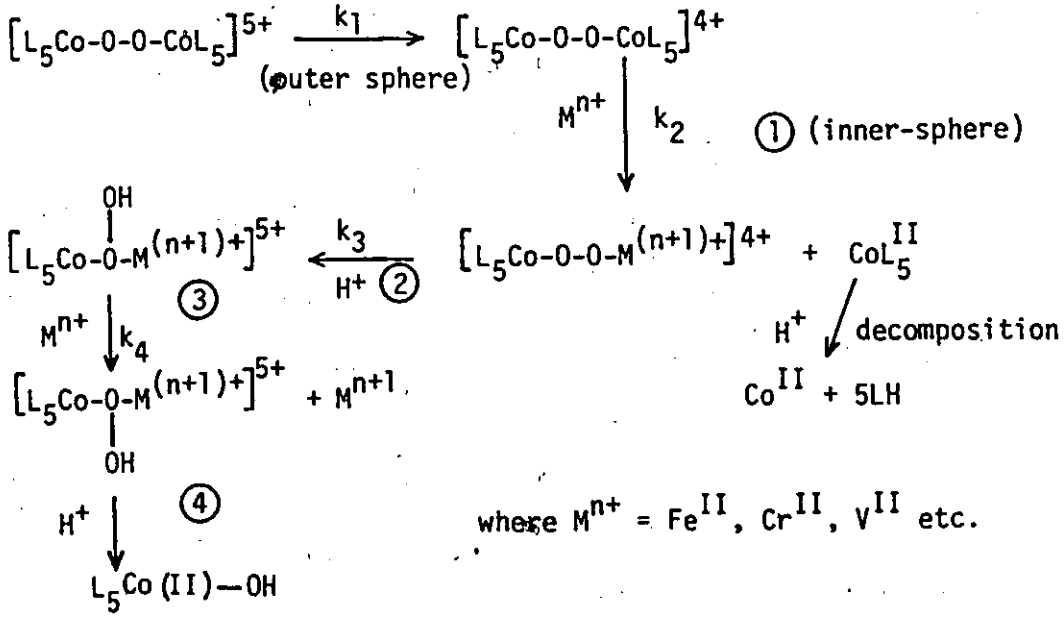

Scheme 1.2

Evidence for the inner-sphere product $L_5Co\text{-}O\text{-}O\text{-}M^{(n+1)+}$ has been provided by both Sykes (1.118) and Martell (1.119). By repeated stopped-flow scanning method, the intermediate optical spectrum was found to contain a Cobalt(III) chromophore at ∿500nm. This is believed to imply the retention of a formally Co(III) moiety in the intermediate. There is, however, no conclusive evidence for a protonated species beyond the second reduction step. Table 1.2 summarizes the bimolecular rate constants for some redox reactions. A special feature is that the inner-sphere rate constants for dibridged μ-peroxo complexes are generally larger than that for mono-bridged complexes. This is attributed to a spatially more exposed peroxo group due to the "lock in" effect of the second bridge as compared with the zig-zag arrangement of the monobridged μ-peroxo complex. In the latter, the peroxo ligand is spatially less accessible.

(C) Substitution and Intramolecular Redox Reaction-Mechanism of De-oxygenation.

For a long time, the substitution chemistry of μ-peroxo Cobalt dioxygen complexes remained a mystery because they exhibit apparently much higher reactivity (lability) than the classically inert Cobalt(III) compounds. This behaviour is inconsistent with the $Co^{III}O_2 \rightleftharpoons Co^{III}$ formalism. For example, the observation of the acid hydrolysis of $[(Co(NH_3)_5)_2O_2]^{4+}$ requires a stopped-flow apparatus to follow the reaction and some deoxygenation reactions have a half-life of less than 10 secs (1.120). Furthermore, substitution proceeds without retention of configuration. This has been demonstrated in one case by crystal structure analysis (1.121). Results of the earlier studies (1965 - 1975) are summarized in Scheme 1.3(1.122).

Table 1.2

Redox Rate Constants for Some Cobalt Dioxygen Complexes

Complex	Reductant	k_1 ($M^{-1}sec^{-1}$)	Mechanism	Ref.
μ-peroxo $[Co(tep))_2O_2]^{4+}$	Fe^{2+}	~3	I.S.	1.19
$[(Coen_2)_2(O_2)(OH)]^{3+}$	Fe^{2+}	400	I.S.	1.19
$[(Coen_2)_2(O_2)(NH_2)]^{3+}$	Cr^{2+}	2100	I.S.	1.18
	V^{2+}	7.7	I.S.	1.18
$[(Co(trien))_2(O_2)(OH)]^{3+}$	Fe^{2+}	25	I.S.	1.19
$[(Co(dien))_2(O_2)(OH)]^{3+}$	Fe^{2+}	140	I.S.	1.19
μ-superoxo $[(Co(NH_3)_5)_2O_2]^{5+}$	Fe^{2+}	0.03		
$[(Co(tep))_2O_2]^{5+}$	Fe^{2+}	380	O.S.	1.19
$[(Coen_2)_2)O_2)(NH_2)]^{4+}$	Cr^{2+}	$\geq 1.4 \times 10^5$	O.S.	1.18
	V^{2+}	$\geq 2.5 \times 10^5$	O.S.	1.18
$[(Co(NH_3)_4)_2(O_2)(NH_2)]^{4+}$	Fe^{2+}	25.2		1.2
$[(Co(bipy)_2)_2(O_2)(NH_2)]^{4+}$	Fe^{2+}	7000	O.S.	1.2
$[(Co(phen)_2)_2(O_2)(NH_2)]^{4+}$	Fe^{2+}	10,000	O.S.	1.2
$[(Co(trien))_2O_2]^{5+}$	Fe^{2+}	430	O.S.	1.2
$[(Coen_2H_2O)_2(O_2)]^{5+}$	Fe^{2+}	>8000		1.2
μ-hydroperoxo complex β-$[(Coen_2)_2(O_2H)(NH_2)]^{4+}$	Cr^{2+}	~16		1.119
	V^{2+}	~ 1		
γ$[(Coen_2)_2(O_2H)(NH_2)]^{4+}$	Cr^{2+}	≤0.1		1.118
	V^{2+}	≤1		

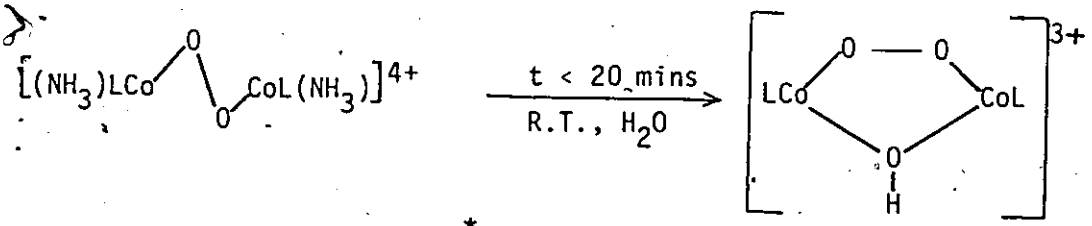

L = 2en, 2(R-pn), trien*, tren

* t < 40 mins.

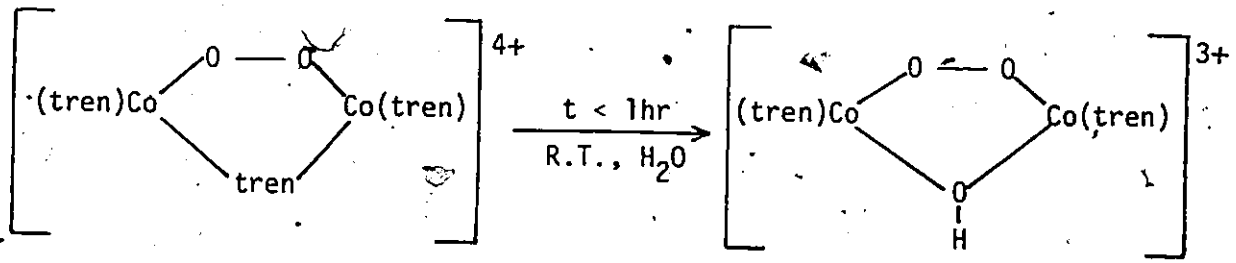

$$[(NH_3)(en)_2Co{-}O{-}O{-}Co(en)_2(NH_3)]^{4+} \xrightarrow[30°C/pH=7]{L=SCN^-,NO_2^-} [(L)(en)_2Co{-}O{-}O{-}Co(en)_2(L)]^{2+}$$

$$\text{trans-}[(NO_2)(en)_2Co{-}O{-}O{-}Co(en)_2(NO_2)]^{2+} \xrightarrow[R.T.]{CN^-} [(Co(en)(CN)_3)_2O_2]^{2-}$$

Scheme 1.3

This puzzle has been resolved very recently by various groups (1.113, 1.123, 1.124). The most important piece of work comes from the group of Fallab (1.123). They showed that the rates of acid decomposition, formation of the (μ-O_2,OH)-dibridged oxygen complex, and oxygen exchange for the complex $[(Co(tren)(MeNH_2))_2O_2]^{4+}$ are identical within experimental error. Their results are summarized below:

$$[(Co(tren)(CH_3NH_2))_2{}^{16}O_2]^{4+} \xrightarrow[\text{R.T.}]{{}^{16}O_2,k_{ex}} [(Co(tren)(CH_3NH_2))_2{}^{16}O_2]^{4+} + {}^{18}O_2 \qquad [1.8]$$

$$[(Co(tren)(CH_3NH_2))_2{}^{18}O_2]^{4+} \xrightarrow[\text{R.T. pH}\sim 1.5]{k_d} 2[Co(tren)(CH_3NH_2)]^{2+} + {}^{18}O_2 \qquad [1.9]$$

$$[(Co(tren)(CH_3NH_2))_2{}^{18}O_2]^{4+} \underset{\text{pH} \geq 1}{\overset{k_f}{\rightleftharpoons}} \left[(tren)Co\begin{smallmatrix}O-O\\ \diagdown\ \ \diagup\\ O\\ |\\ H\end{smallmatrix}Co(tren)\right]^{3+} + 2CH_3NH_2 \qquad [1.10]$$

$$k_{ex} \simeq k_d \simeq k_f \simeq 1 \times 10^{-3}\ \text{sec}^{-1}\ (t_{1/2} \simeq 700\ \text{sec})$$

The significance of these results is that all three reactions are controlled by the same rate determining step. From equation 1.8 and 1.10 this rate determining step involves complete breakdown of the $Co\begin{smallmatrix}O\\ \diagdown\\ \\ \diagup\\ O\end{smallmatrix}Co$ framework to reform a Co(II) aquo intermediate. In other words, an intramolecular redox process between the peroxo bridge and the two Cobalt centers is the rate determining step. In the presence of excess CH_3NH_2, the reverse reaction (equation 1.10) proceeds at a much slower rate ($k_{reverse} \leq 3.5 \times 10^{-5}\text{sec}^{-1}$, $t_{1/2} \geq 2 \times 10^4$sec). The rate of ${}^{18}O_2$ exchange with ${}^{16}O_2$ for the μ-O_2, μ-OH dibridged complex is slow ($k_{ex} \simeq 1.4 \times 10^{-5}\text{sec}^{-1}$, $t_{1/2} \simeq 5 \times 10^{-4}$ sec). Both the reverse rate constant and the exchange rate constant for the dibridged

species indicate that the rate determining step is consistent with a classically inert Co(III) center and is most likely determined by the cleavage of the hydroxo bridge.

Sykes (1.113) has independently demonstrated that the acid decomposition of the protonated hydroperoxo complex $[(Co(NH_3)_5)_2O_2H]^{5+}$ exhibits a pH dependence. It is suggested by Sykes that this result demonstrates an intramolecular electron transfer process. Protonation of the peroxo complex removes electron density from the peroxo bridge, thus decreasing its ability to participate in a redox process.

Saito and co-workers (1.124) examined the kinetics of decomposition of μ-O_2, OH dibridge formation and substitution reactions of NO_2^- for the complex $[(Co(en)_2(NH_3))_2O_2]^{4+}$ and arrived at the same conclusion, i.e., the rate determining step is decomposition and not direct substitution of the monobridged peroxo complex. The intermediate species is most likely a diaquo Cobalt(II) entity. The findings of the various groups are summarized by equations 1.11 - 1.15.

$$[L'LCo\text{-}O\text{-}O\text{-}CoLL']^{4+} + H^+ \overset{K}{\rightleftharpoons} [L'LCo\text{-}\underset{H^+}{O}\text{-}O\text{-}CoLL]^{4+} \qquad [1.11]$$

$$[L'LCo\text{-}O\text{-}O\text{-}CoLL']^{4+} \xrightarrow[\text{Redox}]{\text{Intramolecular}} L'Co^{3+}\cdots O_2^{\bullet} + Co^{II}LL'(H_2O) \qquad [1.12]$$

(rate determining)

$$L'LCo^{3+}\cdots O_2^{\bullet} \xrightarrow{\text{fast}} Co^{II}LL'(H_2O) + O_2 \qquad [1.13]$$

$$Co^{II}LL'(H_2O) \xrightarrow{\text{fast}} Co^{II}L(H_2O)_2 + L' \qquad [1.14]$$

$$Co^{II}L(H_2O)_2 \xrightarrow{\text{fast}} \text{products} \qquad [1.15]$$

In conclusion, substitution takes place via a labile Cobalt(II) intermediate following stepwise intramolecular oxidation of the peroxo bridge. There were no examples of direct substitution at the Cobalt(III) center for this class of complex prior to the results presented in this thesis.

SECTION 1.5 Purpose of This Work

An objective of this thesis is to develop the potential use of ^{59}Co NMR spectroscopy in studying Cobalt di-oxygen complexes as Cobalt is 100% abundant and is also a highly sensitive NMR nucleus. This technique is particularly useful in

i) structural identification of complexes and

ii) mechanistic studies of relatively slow reactions, NMR is far more sensitive to the details of electronic and molecular structure than absorption spectroscopy. A long term goal is to be able to utilize this technique as a direct probe in biological studies.

CHAPTER TWO

THEORY OF NUCLEAR MAGNETIC RELAXATION AND INTERMOLECULAR INTERACTIONS

SECTION 2.1 Introduction

Stemming from the poineering work of Bloembergen, Purcell and Pound (2.1), the NMR method has been developed into a major tool for studying both molecular structure and environment in liquids. More recently, applications to polymer and imaging studies have been developed (2.2-2.9). The structural studies are characterized by NMR parameters such as the chemical shifts (δ) and coupling constants (J_{AB}). The dynamics of molecular motions are characterized by time constants such as the spin-lattice relaxation time (T_1), the spin-spin relaxation time (T_2) and the correlation time (τ).

Two general approaches have been taken to obtain nuclear magnetic resonances in bulk materials. The continuous wave (CW) methods employs a continuous application of rf power while the spectrum is observed. The second approach makes use of short pulses of rf power at a single frequency and observation is made after the rf power is turned off. This is the "pulse" method or "free precession" technique first suggested by Bloch (2.10) and has led to the recent increases in sophistication in NMR. The same spectral information obtained by CW is obtained by this pulse method through mathematical Fourier analysis of the free inducation decay (FID) of the bulk magnetization. This is known as Fourier Transform (FT)-NMR spectroscopy because the sampling of NMR frequency is based on the

transformation properties of the time domain function to the corresponding frequency domain function (spectrum) by the Fourier method.

The advent of FT-NMR spectroscopy permits rapid determination of nuclear spin relaxation times and it is this subject that is of some concern to this thesis. The theory governing chemical shifts and relaxation will be examined in more detail below. Since the general theory of NMR is well developed and understood, and is readily available in many text books, it is omitted.

SECTION 2.2 Theory of Chemical Shifts of Co(III) Complexes

General Comments on Shielding

The fundamental idea of shielding is extremely simple. In an ideal situation where a "bare" (i.e., stripped of electrons) nucleus can be observed, the NMR frequency is in principle the same as that predicted by the theoretical expression for the Zeeman energy:

$$\hat{H} = g_N \beta_N H I_z \qquad [2.1]$$

where g_N is the nuclear g factor, β_N is the nuclear magneton and I_z is the component of the nuclear spin I in the z direction, usually chosen in the direction of the applied field H. In the presence of electrons, the electron cloud precesses freely about the uniformly applied magnetic field H and this electronic current generates a secondary magnetic field H' at the nucleus giving rise to an observed frequency shift. In other words, the NMR nucleus sees an effective field H_{eff}. This electronic effect is generally called the screening effect and σ is the screening or shielding constant. For a single

closed shell, free atom, the shielding constant can be estimated from the Lamb equation (2.11).

It is immediately apparent that the electron cloud no longer freely precesses about H for atoms embedded in a molecule. This leads to the following modification to the shielding constant σ:

i) the secondary field H' is not necessarily anti-parallel to $H(H_z)$ and the shielding constant becomes a tensor quantity,

ii) since shielding is an electronic effect, the wave function describing the molecular orbitals in which the electrons reside is modified. Therefore, movement of electrons is dependent upon the orbital angular momentum operator $\hat{L}$ and the molecular symmetry.

This problem was first resolved by Ramsey (2.12 - 2.14) and the resulting equation, in its explicit form is given below;

$$\sigma = \sigma^d + \sigma^p \qquad [2.2]$$

where $$\sigma^d_{\alpha\beta} = \frac{\mu_o e^2}{8\pi m} < 0|\sum_k r_k^{-3}(r_k^2\delta_{\alpha\beta} - r_{k\alpha}r_{k\beta})|0 > \text{ and}$$

$$\sigma^p_{\alpha\beta} = -\frac{\mu_o e^2}{8\pi m^2}\sum_n \left[<0|\sum_k r_k^{-3}\hat{L}_{k\alpha}|n><n|\sum\hat{L}_{k\beta}|0>+<0|\sum_k \hat{L}_{k\beta}|n><n|\sum_k r_k^{-3}\hat{L}_{k\alpha}|0>\right](E_n-E_0)^{-1} \qquad [2.3]$$

and the subscripts α and β label the x,y,z cartesian components of the shielding tensor, μ_o is the permeability constant, e is the elementary charge, m is the mass of the electron, r_k is the position of the k^{th} electron relative to the nucleus of interest, $\hat{L}_k$ is the position of the k^{th} electron angular momentum operator, $\delta_{\alpha\beta}$ is the Kronecker delta function ($\delta_{\alpha\beta} = 1$ if $\alpha=\beta$, $\delta_{\alpha\beta}=0$ if $\alpha\neq\beta$), $|0>$ and $|n>$ refer to the electronic ground and excited states of the molecule, and E_0 and E_n are the ground and excited state energies respectively where n goes from 0 to the continum σ^d is

known as the diamagnetic contribution to the shielding involving freely rotating electron clouds about the nucleus of interest and σ^p is called the paramagnetic contribution to the shielding describing the disruption to σ^d due to electrons in other nuclei in the molecule.

A complete evaluation of equation 2.2 is not possible since both the excited state wavefunctions and energies are in general unknown. However, σ^p can be simplified by employing the average excitation energy approximation. σ^p reduces to

$$\sigma^p_{\alpha\beta} = -\frac{\mu_o e^2}{4\pi m^2} \Delta E^{-1} [\langle 0 | \sum_k r_k^{-3} \hat{L}_{k\alpha} \sum \hat{L}_{k\beta} | 0 \rangle] \qquad [2.3]$$

where ΔE is the average excitation energy. This simplification involves the ground state wavefunctions only, which is readily obtained by the M.O. method. It is necessary to point out explicitly that some detailed calculations in the literature (2.15-2.18) suggest that contributions from energy states in the continum may be comparable to those from discrete energy states. Calculations also show that the σ^d contribution to shielding is relatively large, but the variation from compound to compound is small in comparison to the total shielding observed. This is consistent with the fact that σ^d is primarily determined by the core electrons which are relatively insensitive to chemical bonding. For the heavy atoms, this has been shown to be the case (2.18).

Cobalt Chemical Shifts

In general, Cobalt shielding is relatively well understood. There is, however, continued interest in evaluating Cobalt shielding constants since the low lying excited electronic states which mix with the ground

states cause a large paramagnetic contribution. A good understanding of these excited states has resulted from electronic absorption spectroscopy and ligand field theory, allowing low symmetry Cobalt(III) complexes to serve as an excellent test of the Ramsey equation. Within the framework of ligand field theory, equation 2.2 simplifies to

$$\sigma = \sigma^d - 1/3\alpha^p_{\alpha\alpha} \qquad [2.4]$$

$$\text{where} \quad \alpha^p_{\alpha\alpha} = 4\beta^2 \sum_n \left\langle \frac{1}{r^3} \right\rangle_c \frac{|\langle 0|\sum_k \hat{L}_{\alpha k}|n\rangle|^2}{E_n - E_o} = 4\beta^2 \sum_n \left\langle \frac{1}{r^3} \right\rangle_c \frac{k'^2}{\Delta E_n}$$

and α = x, y, z designates the direction of the principal axes system of the shielding tensor of the complex, β is the Bohr magneton, $\langle r^{-3} \rangle_c$ – the radical factor is the average value of r^{-3} for the valence electron in the complex (closely related to the charge distribution in complexes), k' is generally known as the orbital reduction factor evaluating the quenching effect of orbital angular momentum as a result of complex formation, and ΔE is the excitation energy from the ground to n excited states. In order to use equation 2.4, it is necessary to know σ^d, k' and ΔE. In general, ΔE can be determined experimentally from electronic absorption spectroscopy. As long as $|n\rangle$ is known, $\sum_n \Delta E$ can be evaluated. Equation 2.4 has the following implication when σ^d is assumed to be constant:

i) a linear relationship between σ_{iso} and ΔE^{-1} is expected for complexes with an approximately constant value of $\langle r^{-3} \rangle_c \, k'^2$. This situation arises when the metal ion is coordinated to a ligand donor atom belonging to the same periodic series in the periodic table or when the metal-ligand interaction takes on multiple bond character.

ii) convergence of correlation lines defined by different values of $\langle r^{-3} \rangle_c k'^2$ at $\Delta E^{-1} = 0$ is expected. The convergence point gives the value $\gamma_o (1 - \sigma^d)$.

iii) an average value for $\langle r^{-3} \rangle_c k'^2$ for each complex can be determined indirectly by measuring the dependences of the gyromagnetic ratio with respect to wave length within a temperature range via the fundamental relationship (2.19 - 2.21)'.

$$\gamma = \gamma_o(1-\sigma^d) + 32\gamma_o\beta^2 \langle r^{-3} \rangle_c k'^2 \lambda$$

$$\frac{d\gamma}{d\lambda} = 32\gamma_o\beta^2 \langle r^{-3} \rangle k'^2$$

where γ_o is the magnetogyric ratio of an unshielded Cobalt nucleus and λ is the wavelength.

This is only valid when temperature changes cause slight modification of the ligand field splitting. As a consequence, changes in $\langle r^{-3} \rangle k'^2$ are primarily determined by changes in occupancy of the vibrational modes of the complex. Equation 2.4 has been successfully applied and three correlation lines have been found (2.18, 2.22, 2.23) for Cobalt complexes corresponding to correlation with ligand donor atoms of the II(C,N.O), III(S,P,Cl) and IV(As,Se,Br) periodic series. Using 6.7a.u. for the $\langle r^{-3} \rangle_F k'^2$ (free ion value, k' = 1) obtained from a calculation using Hartree-Fock wave functions for a 3d electron of the Co^{3+} ion, the orbital reduction factors and their ratios to the free ion value for several Cobalt(III) complexes are collected in Table 2.1. With the exception of $Co(CN)_6^{3-}$, the donor atoms of the II periodic series have the same k' values. This deviation to a lower value is consistent with the larger covalency arising from $d\pi$-$p\pi^*$ overlap between metal and cyanide. For ligand donor atoms of the III and IV transition series, the k' values are relatively well behaved. Since $\langle r^{-3} \rangle_c k'^2 / \langle r^{-3} \rangle_F$ is a measure of co-

Table 2.1[a,b,c,d,e]

Orbital Reduction Factor and Nephelauxetic Ratios
For Octahedral Cobalt(III) Complexes

Type	Complex	$\langle r^{-3} \rangle_c k'^2$(a.u.)	$\langle r^{-3} \rangle_c k'^2 / \langle r^{-3} \rangle_F$	β_{35}
CoO_6	$Co(C_2O_4)_3^{3-}$	4.32	0.64	0.5
	$Co(CO_3)_3^{3-}$	4.26	0.64	0.49
	$Co(acac)_3$	4.36	0.65	
CoN_6	$Co(NH_3)_6^{3+}$	4.34	0.65	0.55
	$Coen_3^{3+}$	4.26	0.64	0.53
	$Copn_3^{3+}$			0.52
	$Co(NH_2OH)_6^{3+}$	4.32	0.64	
	$Co(NO_2)_6^{3-}$	4.28	0.64	
CoC_6	$Co(CN)_6^{3-}$	3.84	0.57	0.41
CoS_6	$Co(S_2CN(C_2H_5)_2)_3$	2.90	0.44	0.34
	$Co(S_2COC_2H_5)_3$	3.03	0.45	0.30
	$Co(S_2P(OC_2H_5)_2)_3$			0.36
	$Co(S_2CNH_2)_3$			0.33
CoP_6	$Co(P(OCH_2)_3CCH_3))_6^{3+}$	~3.61	~0.54	0.31
	$Co(P(OCH_3)_3)_6^{3+}$			0.27
CoCl	$Co(NH_3)_5Cl^{2+}$	3.49(Cl)	0.52	0.30
	tr-$Coen_2Cl_2^+$	3.49(Cl)	0.52	
	$Co(CN)_5Cl^{3-}$	3.53(Cl)	0.53	
$CoSe_6$	$Co(Se_2CN(CH_3)_2)_3$	3.15	0.47	
$CoAs_6$	$Co(triarsine)_3^{3+}$	3.07	0.46	
CoBr	$Co(NH_3)_5Br^{2+}$	3.30(Br)	0.49	
	tr-$Coen_2Br_2^+$	3.34(Br)	0.50	
	$Co(CN)_5Br^{3-}$	3.30(Br)	0.49	
CoI	$Co(NH_3)_5I^{2+}$	3.07(I)	0.46	
	$Co(CN)_5I^{3-}$	1.92(I)	0.29	

[a] Reference 2.21
[b] Reference 2.20
[c] Reference 2.24
[d] Reference 2.22
[e] Reference 2.25

valency as suggested by numerous groups (2.20-2.22) a correlation with the nephelauxetic ratio β_{35} is expected. Such a correlation was established by Juranic (2.21) leading to the series, in increasing order of covalency.

$$CoO_6 \simeq CoN_6 \leq CoC_6 \leq CoS_6 \simeq CoP_6 \simeq CoCl_6 \leq CoBr_6 \simeq CoAs_6 \simeq CoSe_6$$

In addition, this finding is in agreement with the calculation of Betteridge and Golding (2.18), in which the percentage of "spin" transferred to the ligands of the II, III, and IV transition series increases from 2.86% to 5.35% to 6.31%,respectively.

The intercept obtained from δ vs ΔE^{-1} plot gives the shielding of the hypothetical free ion value of Co^{3+} as -1.1% with respect to the standard reference $Co(CN)_6^{3-}$ (δ=0). Adding the calculated σ^d (2140 ppm) value by Dickinson (2.26), the "bare" Co nucleus can be assumed to resonate at a frequency corresponding to a shielding value of -1.3140%.

Juranic et. al. (2.27) have shown that deviation from the Ramsey expression in low symmetry complexes with ligand donor atoms of the same periodic series arises from inexact determination of the excitation energies ΔE_x, ΔE_y and ΔE_z. Using a deconvolution technique, the exact band position of the constituent components of the first absorption band are determined,therefore allowing a correct evaluation of the shielding constants $\sigma_{xx}^{(p)}$, $\sigma_{yy}^{(p)}$, and $\sigma_{zz}^{(p)}$. By plotting δ_{iso} versus the weighted average wavelength of the first absorption band, the Ramsey equation is found to be obeyed. The results of the exact shielding expressions for O_h, C_{4v}, D_{4h} and C_{2v} symmetry were given by Yamasaki (2.20) and Juranic (2.27) independently, and are collected in Table 2.4. The assignment of the electronic configurations

---

1% = 10,000 ppm

and d-orbitals associated with the shielding expressions are given in Tables 2.2 and 2.3.

In summary, recent understanding in Cobalt shielding has led to two main conclusions:

i) Experiments confirm that electron delocalization manifests itself by periodic decreases of the parameters k' and β as predicted by the ligand field theory.

ii) The effect of shielding produced by a series of ligands about a magnetic nucleus is independent of the central ion-a direct consequence of a well defined correlation between the magneto-chemical series of ligands or spectrochemical series and the field strength series of ligands (2.21), i.e., $\Delta/B_{Racah}^{\alpha}(\beta_{35}\lambda)^{-1}$

Recently, a theory for field dependent chemical shifts has been developed by Doddrell (2.23). The idea is based on the shielding contribution from a fourth-order perturbation treatment of paramagnetic currents originally suggested by Ramsey (2.12-2.14). The evidence provided is weak (2.29) thus warrenting further investigation in this area.

Finally, to complete the literature survey on this topic, a coupling constant has been reported recently (2.30) for the complex $[Co(P(OCH_3)_6)_6](BF_4)_3$ (δ = +304ppm J_{Co-p}^{3+} = 414 Hz). The lower value of $^1J_{Co-p}^{3+}$ as compared to that of $^1J_{Co-p}^{-1}$ (1225 Hz) has been attributed to a combination of structural and electronic effects.

Table 2.2[a]

Irreducible Representation of the Ground and First Excited Electronic Configuration of d^6 Complex Ion in O_h, D_{4h}, C_{4v}, or C_{2v} Symmetry Group

Electronic Configuration	Symmetry Group			
	O_h	D_{4h}	C_{4v}	C_{2v}
$(d_{xy})^2(d_{xz})^2(d_{yz})^2$	$^1A_{1g}$	$^1A_{1g}$	$^1A_1$	$^1A_1$
$(d_{xy})^2(d_{xz})^2(d_{yz})(d_{x^2-y^2})$		^1E_g	^1E	$^1A_2$
$(d_{xy})^2(d_{xz})(d_{yz})^2(d_{x^2-y^2})$		^1E_g	^1E	$^1B_2$
$(d_{xy})(d_{xz})^2(d_{yz})^2(d_{x^2-y^2})$		$^1A_{2g}$	$^1A_2$	$^1B_1$
$(d_{xy})^2(d_{xz})^2(d_{yz})(d_{z^2})$	$^1T_{1g}+{}^1T_{2g}$	$^1B_{2g}$	$^1B_2$	$^1A_2$
$(d_{xy})^2(d_{xz})(d_{yz})^2(d_{z^2})$		^1E_g	^1E	$^1B_2$
$(d_{xy})(d_{xz})^2(d_{yz})^2(d_{z^2})$		^1E_g	^1E	$^1B_1$

[a] Reference 2.27

Table 2.3[a]

Assignment of Real d Orbitals According to its Irreducible Representation in O_h, D_{4h}, C_{4v}, or C_{2v} Symmetry Group

Orbitals	O_h	D_{4h}	C_{4v}	C_{2v}
d_{xy}	t_{2g}	b_{2g}	b_2	b_1
d_{xz}	t_{2g}	e_g	e	b_2
d_{yz}	t_{2g}	e_g	e	a_2
$d_{x^2-y^2}$	e_g'	b_{1g}	b_1	a_1'
d_{z^2}	e_g''	a_{1g}	a_1	a_1''

[a] Reference 2.27

Table 2.4[a,b]

Shielding Tensor for Octahedral Cobalt(III) Complexes

Electronic configuration	^{59}Co Shielding	Electronic configuration	^{59}Co Shielding
O_h Symmetry		**C_{4v} Symmetry**	
$^1A_{1g}$ $(\tilde{t}_{2g})^2(\tilde{t}_{2g})^2(\tilde{t}_{2g})^2$	$\sigma^p_{zz}=8\beta^2\langle\frac{1}{r^3}\rangle\frac{\lvert\langle\tilde{t}_{2g}\rvert\ell_z\rvert\tilde{e}_g\rangle\rvert^2}{\Delta E_{^1A_{1g}\rightarrow{}^1T_{1g}}}$	$^1A_1$ $(\tilde{e}_2)^2(\tilde{e})^2(\tilde{e})^2$	$\sigma^p_{zz}=8\beta^2\langle\frac{1}{r^3}\rangle\frac{\lvert\langle\tilde{e}_2\rvert\ell_z\rvert\tilde{b}_1\rangle\rvert^2}{\Delta E_{^1A_1\rightarrow{}^1A_2}}$
$(\tilde{t}_{2g})^2(\tilde{t}_{2g})^2(\tilde{t}_{2g})(-\frac{1}{3}\tilde{e}_g'-\frac{\sqrt{3}}{2}\tilde{e}'')$	$\sigma^p_{xx}=8\beta^2\langle\frac{1}{r^3}\rangle\frac{\lvert\langle\tilde{t}_{2g}\rvert\ell_x\rvert-\frac{1}{2}\tilde{e}_g'-\frac{\sqrt{3}}{2}\tilde{e}_g''\rangle\rvert^2}{\Delta E_{^1A_{1g}\rightarrow{}^1T_{1g}}}$	$^1A_2$ $(\tilde{e}_2)(\tilde{e})^2(\tilde{e})^2(\tilde{b}_1)$	$\sigma^p_{xx}=8\beta^2\langle\frac{1}{r^3}\rangle\frac{\lvert\langle\tilde{e}\rvert\ell_x\rvert-\frac{1}{2}\tilde{b}_1-\frac{\sqrt{3}}{2}\tilde{a}_1\rangle\rvert^2}{\Delta E_{^1A_1\rightarrow{}^1E}}$
$^1T_{1g}$ $(\tilde{t}_{2g})^2(\tilde{t}_{2g})(\tilde{t}_{2g})^2(-\frac{1}{2}\tilde{e}_g'+\frac{\sqrt{3}}{2}\tilde{e}'')$			
$(\tilde{t}_{2g})(\tilde{t}_{2g})^2(\tilde{t}_{2g})^2(\tilde{e}_g')$	$\sigma^p_{yy}=8\beta^2\langle\frac{1}{r^3}\rangle\frac{\lvert\langle\tilde{t}_{2g}\rvert\ell_y\rvert-\frac{1}{2}\tilde{e}_g'+\frac{\sqrt{3}}{2}\tilde{e}''\rangle\rvert^2}{\Delta E_{^1A_{1g}\rightarrow{}^1T_{1g}}}$	^1E $(\tilde{e}_2)^2(\tilde{e})^2(\tilde{e})(-\frac{1}{2}\tilde{b}_1-\frac{\sqrt{3}}{2}\tilde{a}_1)$	
		$(\tilde{e}_2)^2(\tilde{e})(\tilde{e})^2(-\frac{1}{2}\tilde{b}_1+\frac{\sqrt{3}}{2}\tilde{a}_1)$	$\sigma^p_{yy}=8\beta^2\langle\frac{1}{r^3}\rangle\frac{\lvert\langle\tilde{e}\rvert\ell_y\rvert-\frac{1}{2}\tilde{b}_1+\frac{\sqrt{3}}{2}\tilde{a}_1\rangle\rvert^2}{\Delta E_{^1A_1\rightarrow{}^1E}}$
D_{4h} Symmetry		**C_{2v} Symmetry**	
$^1A_{1g}$ $(\tilde{b}_{2g})^2(\tilde{e}_g)^2(\tilde{e}_g)^2$	$\sigma^p_{zz}=8\beta^2\langle\frac{1}{r^3}\rangle\frac{\lvert\langle\tilde{b}_{2g}\rvert\ell_z\rvert\tilde{b}_{1g}\rangle\rvert^2}{\Delta E_{^1A_{1g}\rightarrow{}^1A_{2g}}}$	$^1A_1$ $(\tilde{b}_1)^2(\tilde{b}_2)^2(\tilde{a}_2)^2$	$\sigma^p_{zz}=8\beta^2\langle\frac{1}{r^3}\rangle\frac{\lvert\langle\tilde{b}_1\rvert\ell_z\rvert\tilde{a}_1'\rangle\rvert^2}{\Delta E_{^1A_1\rightarrow{}^1B_1}}$
$^1A_{2g}$ $(\tilde{b}_{2g})(\tilde{e}_g)^2(\tilde{e}_g)^2(\tilde{b}_{1g})$	$\sigma^p_{xx}=8\beta^2\langle\frac{1}{r^3}\rangle\frac{\lvert\langle\tilde{e}_g\rvert\ell_x\rvert-\frac{1}{2}\tilde{b}_{1g}\frac{\sqrt{3}}{2}\tilde{a}_{1g}\rangle\rvert^2}{\Delta E_{^1A_{1g}\rightarrow{}^1E_g}}$	$^1B_1$ $(\tilde{b}_1)(\tilde{b}_2)^2(\tilde{a}_2)(\tilde{a}_1')$	
		$^1A_2$ $(\tilde{b}_1)^2(\tilde{b}_2)^2(\tilde{a}_2)(-\frac{1}{2}\tilde{a}_1'-\frac{\sqrt{3}}{2}\tilde{a}_1'')$	$\sigma^p_{xx}=8\beta^2\langle\frac{1}{r^3}\rangle\frac{\lvert\langle\tilde{a}_2\rvert\ell_x\rvert-\frac{1}{2}\tilde{a}_1'-\frac{\sqrt{3}}{2}\tilde{a}_1''\rangle\rvert^2}{\Delta E_{^1A_1\rightarrow{}^1A_2}}$
^1E $(\tilde{b}_{2g})^2(\tilde{e}_g)^2(\tilde{e}_g)(-\frac{1}{2}\tilde{b}_{1g}-\frac{\sqrt{3}}{2}\tilde{a}_{1g})$			
$(\tilde{b}_{2g})^2(\tilde{e}_g)(\tilde{e}_g)^2(-\frac{1}{2}\tilde{b}_{1g}+\frac{\sqrt{3}}{2}\tilde{a}_{1g})$	$\sigma^p_{yy}=8\beta^2\langle\frac{1}{r^3}\rangle\frac{\lvert\langle\tilde{e}_g\rvert\ell_y\rvert-\frac{1}{2}\tilde{b}_{1g}+\frac{\sqrt{3}}{2}\tilde{a}_{1g}\rangle\rvert^2}{\Delta E_{^1A_1\rightarrow{}^1E_g}}$	$^1B_2$ $(\tilde{b}_1)^2(\tilde{b}_2)(\tilde{a}_2)^2(-\frac{1}{2}\tilde{a}_1'+\frac{\sqrt{3}}{2}\tilde{a}_1'')$	$\sigma^p_{yy}=8\beta^2\langle\frac{1}{r^3}\rangle\frac{\lvert\langle\tilde{b}_2\rvert\ell_y\rvert-\frac{1}{2}\tilde{a}_1'+\frac{\sqrt{3}}{2}\tilde{a}_1''\rangle\rvert^2}{\Delta E_{^1A_1\rightarrow{}^1B_2}}$

[a] Reference 2.20
[b] Reference 2.27

SECTION 2.3 Origin of Magnetic Relaxation and the Relaxation Times T_1 and T_2

Relaxation comes about because every molecule interacts with its surroundings. These interactions limit the lifetime of a spin state. In general, nuclear spins in large concentration (bulk material) are in thermal equilibrium with their surroundings (lattice) and are distributed among the energy levels according to the Boltzmann equation. Following disruption of this equilibrium by absorption of rf radiation (induced transition), the nuclear spin system returns to thermal equilibrium by mechanisms whereby the spins come to equilibrium at the lattice temperature by a first order relaxation process characterized by a time constant T_1. This process is called "spin-lattice relaxation" and the time constant T_1 is the spin-lattice relaxation time. It is a spontaneous (non-radiative) transition process and is a measure of the time taken for magnetic Zeeman energy of the spin system to be transferred to other degrees of freedom (lattice). A necessary condition that must be met for the establishment of thermal equilibrium (defined by this process) is that other spins are not involved.

As a consequence of large concentrations of nuclear spins separated by small distances in the bulk material, resonance line broadening occurs because each spin "sees" additional small local fields due to its neighbours. Since each local field possesses a different value, this gives rise to a distribution in the observed resonance frequencies in effect varying the relative energies of the nuclear spin levels. Variation of spin energy levels results from variation in spin coupling. Magnetic energy transfer is extremely rapid through this process because of immediate conservation

of energy. As a result, thermal equilibrium is quickly established within the spin system itself with a characteristic time constant T_2 often much shorter than T_1. This process is known as "spin-spin relaxation" and T_2 is the spin-spin relaxation time. This simple physical description of relaxation owes its origin to time dependent magnetic behaviour of the magnetic nucleus. For example, this can be interaction with lattice vibrations in a solid or random motion in a liquid. The important point is that a microscopic (local) fluctuating magnetic field originates in molecular motion and that molecular motion covers a wide range of frequencies. It is this unique property which makes possible relaxation.

In pulse NMR spectroscopy, relaxation phenomena can be visualized in terms of a classical precession model. This approach was first outlined by Bloch et. al. (2.10). The empirical foundation of the Bloch equation is as follows:

i) the time dependence of M, where M is a macroscopic magnetic moment resulting from an ensemble of "free" spins in a magnetic field H, is described by the equation of motion

$$\frac{dM}{dt} = \gamma M \times H$$

ii) in a static field, $H_o = H_z$, the equilibrium value of the magnetization M_o in this static field become M_z and M_o obeys the Curie susceptibility.

$$M_z = M_o = \chi_o H_z = \frac{N\gamma^2\hbar^2 I(I+1)}{3kT} H_z$$

Under this condition, the time dependence of M_z returning to equilibrium can be described accurately by the equation

$$\frac{dM_z}{dt} = - \frac{(M_z - M_o)}{T_1}$$

T_1 is the spin-lattice (longitudinal) relaxation time.

iii) when components perpendicular to H_z are generated due to disruption of equilibrium, the interacting spins (either with each other or with the surroundings creating local magnetic fields) cause the transverse magnetization to decay to zero at a rate described by the equations.

$$\frac{dM_x}{dt} = - \frac{M_x}{T_2}, \qquad \frac{dM_y}{dt} = - \frac{M_y}{T_2}$$

T_2 is the spin-spin (transverse) relaxation time.

From these arguments, the equations of motion about the three axes are formulated and are generally known as the Bloch equations;

$$\frac{dM_x}{dt} = \omega_o M_y - \frac{M_x}{T_2}, \quad \frac{dM_y}{dt} = -\omega_o M_x - \frac{M_y}{T_2} \qquad [2.5]$$

$$\frac{dM_z}{dt} = - \frac{(M_z - M_o)}{T_1}$$

A second important result is that the Bloch equations predict definitively that the absorption signal is of the Lorentzian shape:

$$g(\omega) = \frac{T_2}{\pi} \cdot \frac{1}{1 + T_2^2(\omega - \omega_o)^2} \qquad [2.6]$$

T_2 determines the width of the unsaturated resonance signal at half height, therefore, providing a simple means of measuring T_2.

In order to understand relaxation time data in terms of molecular motions quantitatively, it is necessary to derive mathematical functions

describing the random time behaviour of motions. In other words, we are seeking solutions to the frequency distribution of thermal motions. This is achieved by the use of a correlation function $G(\tau)$ and its Fourier transform partner $J(\omega)$, the spectral density (power) function. Since we are interested in the self-correlation of motions, the correlation function is called the auto-correlation function.

$$J(\omega) = \int_{-\infty}^{+\infty} G(\tau) e^{i\omega\tau} d$$

$$G(\tau) = \overline{f(t) f^{*}(t + \tau)}$$

where $f(t)$ is the function modelling the random molecular motion.

Although it has been said earlier that molecular motion covers a wide frequency range, the important frequencies are those that are effective in causing relaxation. These are motions with frequencies which cause spin reorientation (transition) and modulation of the spin energy levels. It has been shown that these frequencies are at zero frequency, at the nucleus resonance ω_o, and at twice this resonance frequency, $2\omega_o$ for like spins (2.31). The low frequency component, i.e., $\omega = o$ has been demonstrated to be ineffective towards the T_1 relaxation process, whereas the high frequency components affect both T_1 and T_2. Physical interpretation of the physics behind these results is given by Andrew (2.32). For interaction between unlike spins I and S, $2\omega_o$ is replaced by $\omega_I + \omega_S$ and the low frequency component by $\omega_I - \omega_S$.

To calculate the auto-correlation function, it is necessary to find suitable models for molecular motions; for example, models such as M-diffusion, J-diffusion, and anisotropic rotor,etc. In solution, the isotropic Brownian motion

has been widely used to formulate the random position functions. This random walk model is due to Debye (2.33). The problem is formulated as diffusion over the surface of a sphere with a radius defined by the distance of closest approach for the interaction between two spins. The general solution of this problem is the normalized spherical harmonics $Y_{\ell m}(\theta,\phi)$ of order ℓ (2.33), where $\ell = 0,1,2$ because for magnetic resonance, second order tensors are of primary concern. r,θ,ϕ are defined by the usual spherical polar coordinates. In the Bloch formalism, τ, obtained from the Fourier transform of the autocorrelation function is defined as the time constant (lifetime) of an exponential decay function characterizing a distinct type of fluctuation. The power function $J(\omega)$ is a measure of the probability of finding molecular motion at the frequency ω characterized by τ.

In summary, the general approach for the calculation of relaxation rate is straight-forward once all the parameters required are known.

An exceptionally clear example for relaxation calculation is given by Carrington and McLachlan (2.34). It is clear that spin relaxation calculation is a typical example of semi-classical treatment of a system. In the next section, the various interactions governing the efficiencies of relaxation will be examined and the results will be given.

SECTION 2.4 Line Broadening Mechanisms - Relaxation and Non-Relaxation

In this section, the line broadening mechanisms which arise from both relaxation and non-relaxation origin will be examined, namely;

i) Dipole-Dipole relaxation

ii) Spin-rotation relaxation

iii) Scalar relaxation

iv) Quadrupolar relaxation

v) Chemical shielding anisotropy relaxation

vi) Magnetic field alignment effect (non-relaxation)

SECTION 2.4.1 Dipole-Dipole Relaxation

Dipole-dipole interaction results from the magnetic coupling between two or more magnetic dipole moments. The strength of the interaction depends on the relative orientation and separation of the spins. Relaxation arises when the dipolar coupling tensor D(t) is modulated by tumbling motions and the components of the D_{jk} become a random function of time. The interaction Hamiltonian for two unlike spins I and S is of the form

$$\hat{H}_{DD} = I \cdot D(t) \cdot S$$

Dipole-dipole relaxation is the most extensively studied of all the relaxation mechanisms, and is the most important for nuclei of spin I = 1/2. Detailed derivations of the relaxation rates are readily available (2.31 - 2.35). The results are given below (2.35).

$$\frac{1}{T_1^I} = \frac{2}{5} \frac{\gamma_I^2 \gamma_S^2 \hbar^2 S(S+1)}{r_{IS}^6} \left[\frac{1}{3} \cdot \frac{\tau_2}{1+(\omega_I-\omega_S)^2\tau_2^2} + \frac{\tau_2}{1+\omega_I^2\tau_2^2} + \frac{2\tau_2}{1+(\omega_I+\omega_S)^2\tau_2^2} \right] \quad [2.7]$$

$$\frac{1}{T_2^I} = \frac{1}{5} \frac{\gamma_I^2 \gamma_S^2 \hbar^2 S(S+1)}{r_{IS}^6} \left[\frac{4}{3}\tau_2 + \frac{1}{3} \cdot \frac{\tau_2}{1+(\omega_I-\omega_S)^2\tau_2^2} + \frac{2\tau_2}{1+\omega_S^2\tau_2^2} + \frac{\tau_2}{1+\omega_I^2\tau_2^2} + \frac{2\tau_2}{1+(\omega_I+\omega_S)^2\tau_2^2} \right] \quad [2.8]$$

When I = S, equations 2.7 and 2.8 simplify to equation 2.9 and 2.10.

$$\frac{1}{T_1} = \frac{2}{5} \cdot \frac{\gamma_I^4 \hbar^2 I(I+1)}{r_{ij}^6} \left[\frac{\tau_2}{1+\omega^2\tau_2^2} + \frac{4\tau_2}{1+4\omega^2\tau_2^2} \right] \qquad [2.9]$$

$$\frac{1}{T_2} = \frac{1}{5} \cdot \frac{\gamma_I^4 \hbar^2 I(I+1)}{r_{ij}^6} \left[3\tau_2 + \frac{5\tau_2}{1+\omega^2\tau_2^2} + \frac{2\tau_2}{1+4\omega^2\tau_2^2} \right] \qquad [2.10]$$

Note: r_{ij}^{-6} is replaced by $\sum_j r_{ij}^{-6}$ if a molecule contains several equivalent spins and $\frac{1}{n}\sum_{i=1} r_{ij}^{-6}$ for n non-equivalent spins.

In nonviscous (mobile) liquids where the relationship $(\omega_o\tau_2)^2 \ll 1$, a condition referred to as <u>extreme narrowing</u> (frequency independent) is met, equations 2.9 and 2.10 reduces to 2.11.

$$\frac{1}{T_1} = \frac{1}{T_2} = \frac{2\gamma^4\hbar^2 I(I+1)}{r_{ij}^6} \tau_2 \qquad [2.11]$$

SECTION 2.4.2 <u>Spin-Rotation Relaxation</u>

The spin-rotation interaction is an example of magnetic interaction via indirect nucleus-electron coupling. When a molecule rotates, the electrons about the nucleus undergo rotation with the molecule about the nucleus at an average distance r from the nucleus. The circulating electronic current generated, as a result of rotation motion, creates a magnetic moment μ_J proportional to the average value of the rotational angular momentum J of the molecule. The rate of fluctuation of J is determined by the mean angular velocity of the molecule and is inversely

proportional to θ, the moment of inertia. Due to the fluctuation of J, a local fluctuating magnetic field is seen at the nucleus, therefore giving rise to a relaxation mechanism. The Hamiltonian is given by

$$\hat{H}_{SR} = -\hbar I \cdot C(t) \cdot J$$

where C(t) is the spin-rotation coupling tensor and I is the nuclear spin. The derivation of relaxation rates is given by Spiess (2.35) and the results are tabulated in Table 2.5.

Table 2.5

Relaxation Rates Through Spin-Rotation Interaction

	$1/T_1^{SR} = 1/T_2^{SR}$
Asymmetric rotor, c may be asymmetric	$\frac{2}{3}\frac{kT}{\hbar^2}\sum_{i,j=x,y,z}\theta_j c_{ij}^2 \tau_{J_j}$
$\vec{\theta}$ and c have common principal axes system, c symmetric	$\frac{2}{3}\frac{kT}{\hbar^2}(\theta_x c_{xx}^2 \tau_{J_x} + \theta_y c_{yy}^2 \tau_{J_y} + \theta_z c_{zz}^2 \tau_{J_z})$
As above but moreover symmetric top	$\frac{2}{3}\frac{kT}{\hbar^2}(2\theta_\perp c_\perp^2 \tau_{J_\perp} + \theta_\parallel c_\parallel^2 \tau_{J_\parallel})$
Spherical top	$\frac{2}{3}\frac{kT}{\hbar^2}(2\theta_\perp c_\perp^2 + \theta_\parallel c_\parallel^2)\tau_J$
Linear molecule	$\frac{4}{3}\frac{kT}{\hbar^2}\theta c^2 \tau_J$

Four points are to be noted:

i) τ_J is the angular momentum correlation time and is a measure of the length of time a molecule is in the J'th rotational state.

ii) In the isotropic diffusion model, the isotropic rotational reorientation time τ_2 is related to the angular momentum correlation time τ_J (2.36).

$$\tau_2\tau_J = \frac{1}{C} \cdot \frac{\theta}{kT} \qquad \text{where C is a numerical constant (2.37)}$$

The relaxation time for a spin-rotation mechanism increases with decreasing temperature which is opposite to all other relaxation mechanisms.

iii) The calculation of the relaxation rate usually invokes: (a) the extreme narrowing condition since only rapid rotations are important for this mechanism, and (b) instead of using the fourier transform of the autocorrelation function in calculating spectral densities, simple time integrals are used (2.35).

iv) Antisymmetric components C_{ij} of the spin-rotation tensor are possible if the moment of inertia tensor $\theta(t)$ has a principal axes system where $\theta_{xx} \neq \theta_{yy} \neq \theta_{zz}$.

SECTION 2.4.3 Scalar Relaxation

In order to induce relaxation it is necessary that the observing spin experiences a fluctuating local magnetic field. When two spins I and S are coupled together, the coupling Hamiltonian has the form

$$\hat{H}_{SC} = I \cdot J_{iso} \cdot S$$

where J_{iso} is the scalar (spin-spin) coupling constant. Under well defined conditions, i.e. the relaxation times of both the I and S spins are long as compared to J_{iso}^{-1} (J_{iso} may be time dependent because of exchange), the exchange lifetime, τ_{ex}, is much longer than J_{iso}^{-1}. If the above conditions are not met, it would have the following effect as observed through I:

i) if only $\tau_{ex} << J_{iso}^{-1}$ that is, the exchange is rapid, the spin-spin structure of the covalently bonded resonances collapses as for a normal chemical exchange situation. The local magnetic field is defined by $J_{iso}(t)\ S/\gamma_I$ and $J_{iso} = 0$ when I and S are uncoupled and J_{iso} is finite when I and S are coupled. As a result of the fluctuation of J_{iso}, $\hbar J_{iso}(t)\ I \cdot S$ becomes a relaxation mechanism. In general, any process that induces a fluctuation in J_{iso} is referred to as scalar (spin-spin) relaxation of the first kind.

ii) if the relaxation time of S is short compared to the coupling constant, i.e., $T_1^S << J_{iso}^{-1}$, by an independent mechanism the local field becomes $J_{iso}S(t)/\gamma_I$ providing a relaxation mechanism. The above condition imposes the restriction that the observed coupling constant J_{iso} be replaced by $\langle J_{iso} \rangle$ because the relaxation time of spin S is a random function of time. Secondly, the spin system S can be treated as being part of the "lattice" because of its short relaxation time and the lattice is assumed to be in thermal equilibrium. This is referred to as scalar relaxation of the second kind. An example of this occurs when S is a quadrupole nucleus ($I>1/2$) and its relaxation is dominated by quadrupole interactions.

The results for the relaxation rates derived from the Bloch equation for both scalar relaxation of the first and second kind have been shown to take the same form (2.31, 2.35);

$$\frac{1}{T_1^I} = \frac{2}{3} S(S+1) J_{iso}^2 \frac{\tau_2^s}{1+(\omega_I-\omega_s)^2\tau_2^{s2}} \qquad [2.12]$$

$$\frac{1}{T_2^I} = \frac{1}{3} S(S+1) J_{iso}^2 (\tau_1^s + \frac{\tau_2^s}{1+(\omega_I-\omega_s)^2\tau_2^{s2}}) \qquad [2.13]$$

where I is the observing nucleus, $\tau_2^s = \tau_1^s = \tau_{ex}$ for scalar relaxation of the first kind and $\tau_2^s = \tau_2^s$, $\tau_1^s = T_1^s$ for scalar relaxation of the second kind. A final comment is that this relaxation mechanism is frequency dependent due to the term $(\omega_I-\omega_S)$.

SECTION 2.4.4 Quadrupolar Relaxation

A nucleus with spin I > 1/2 possesses a nuclear quadrupole moment. When a quadrupolar nucleus is placed in an environment where electric charges are distributed asymmetrically about the nucleus, an electric field gradient is produced at the nucleus. For example, this could arise from covalent bonding in which bonding p or d electrons produce a large non-centrally symmetric field. This "local" electric field gradient interacts with the nuclear quadrupole moment with an interaction Hamiltonian of the form

$$\hat{H}_Q = I \cdot A \cdot I$$

where A is the symmetric second rank quadrupole coupling tensor defined as the product of the traceless quadrupole moment tensor Q_{jk} and the traceless field gradient tensor at the origin $\left(\frac{\partial^2 V}{\partial X_j \partial X_k}\right)_{r=o}$. The details are given by Abragam (2.31). In the presence of a magnetic field, the Zeeman levels split into 2I + 1 (non-degenerate) levels with 2I transitions obeying the selection rule $\Delta m = \pm 1$.

In solution, molecules undergo a rapid reorientation (tumbling) motion, the time average of the field gradient is zero, the original non-degeneracy is removed and the degeneracy of the Zeeman levels are restored. The coupling tensor A(t) becomes a random function of time, and the nucleus encounters a fluctuating field gradient, therefore, providing a relaxation mechanism. In the Brownian motion model, the complete equation describing the relaxation rates is given below (2.35);

$$\frac{1}{T_1} = \frac{3}{200}\left(\frac{e^2qQ}{\hbar}\right)^2\left(1+\frac{\eta_Q^2}{3}\right)\frac{2I+3}{I^2(2I-1)}\left[\frac{\tau_2}{1+\omega^2\tau_2^2} + \frac{4\tau_2}{1+4\omega^2\tau_2^2}\right] \qquad [2.14]$$

$$\frac{1}{T_2} = \frac{3}{400}\left(\frac{e^2qQ}{\hbar}\right)^2\left(1+\frac{\eta_Q^2}{3}\right)\frac{2I+3}{I^2(2I-1)}\left[3\tau_2 + \frac{5\tau_2}{1+\omega^2\tau_2^2} + \frac{2\tau_2}{1+4\omega^2\tau_2^2}\right] \qquad [2.15]$$

where $\left(\frac{e^2qQ}{\hbar}\right)$ is the quadrupole coupling constant, η_Q is the asymmetry parameter defined as

$$\eta_Q = \frac{V_{xx} - V_{yy}}{V_{zz}}$$, V_{ii} are the components of the field gradient tensor in the principal axes system and τ_2 is the rotational reorientation time. In the limit of extreme narrowing $(\omega\tau_2)^2 << 1$, equations 2.14 and 2.15 reduces to the simple form:

$$\frac{1}{T_1} = \frac{1}{T_2} = \frac{3}{40}\left(\frac{e^2qQ}{\hbar}\right)^2\left(1+\frac{\eta_Q^2}{3}\right)\frac{2I+3}{I^2(2I-1)}\tau_2 \qquad [2.16]$$

The distinct feature of this relaxation mechanism is that $\frac{1}{T_{1,2}} \alpha \left(\frac{e^2qQ}{\hbar}\right)x\left(1+\frac{\eta_Q^2}{3}\right)$ under this condition.

SECTION 2.4.5 · Relaxation via Chemical Shielding Anisotropy

The origin of shielding was discussed in Section 2.2. The shielding constants can differ appreciably about the principal axes with values $\sigma_{xx} \neq \sigma_{yy} \neq \sigma_{zz}$. In solution, rapid tumbling causes a time average of σ_{ii}, i.e., $\bar{\sigma}_{iso} = \frac{1}{3}(\sigma_{xx}+\sigma_{yy}+\sigma_{zz})$ where σ_{iso} is the isotropic shielding. The nucleus sees a fluctuation in the local magnetic field on a very short time scale and the shielding tensor randomizes with time providing a relaxation mechanism.

Unlike the other second rank tensors pertinent to magnetic resonance spectroscopy, the general character of the shielding tensor is asymmetric (2.38). In general, any second rank tensor can be decomposed into the sum of an isotropic part $\bar{\sigma}_{iso}$, a traceless symmetric anisotropic (symmetric) part $\sigma_{ij}^{(s)}$, and an antisymmetric part $\sigma_{ij}^{(a)}$, i.e.,

$$\sigma_{ij} = \bar{\sigma}_{iso} + \sigma_{ij}^{(a)} + \sigma_{ij}^{(s)}$$

where

$$\bar{\sigma}_{iso} = \frac{1}{3}(\Sigma_i \sigma_{ii})\delta_{ij}$$

$$\sigma_{ji}^{(s)} = \sigma_{ij}^{(s)} = 1/2(\sigma_{ij} + \sigma_{ji}) - \bar{\sigma}_{iso}\delta_{ij}$$

$$\sigma_{ij}^{(a)} = -\sigma_{ji}^{(a)} = 1/2(\sigma_{ij} - \sigma_{ji})$$

For a symmetric second rank tensor:

$$\sigma_{ij}^{(2)} = \bar{\sigma}\delta_{ij} + \sigma_{ij}^{(s)}$$

there is always a principal axes system (XYZ) for which the matrix $\sigma^{(2)}$ is diagonalized with the diagonal elements being the principal elements obeying the convention:

$$|\sigma_{zz}^{(2)}| > |\sigma_{xx}^{(2)}| > |\sigma_{yy}^{(2)}|$$

Also $\sigma_{xx} + \sigma_{yy} + \sigma_{zz} = 0$ for a traceless tensor, and the principal components can be reduced further by defining the asymmetry parameter η,

$$\eta = \frac{\sigma_{xx} - \sigma_{yy}}{\sigma_{zz}} \qquad 0 \leq \eta \leq 1$$

i.e., the second rank symmetric tensor can be characterized by two principal values instead of three.

The asymmetric part $\sigma^{(a)} \equiv \sigma^{(1)}$ cannot be diagnoalized in the $\sigma^{(2)}$ axes system. The axes system where $\sigma^{(1)}$ can be brought into diagonal form is rotated with respect to the XYZ system of $\sigma^{(2)}$. The transformation function is given by Wigner Rotation Matrices (2.35). The importance of the antisymmetric part of the second rank tensor is that it can represent a pseudo vector quantity such that the presence of real asymmetry in the tensor can be associated with non-vanishing pseudo-vector interaction. The principal axes of an asymmetric second rank tensor are not necessarily orthogonal (2.38).

It is also well known (2.39) that antisymmetric tensors of second rank can be reduced to pseudo tensors of various ranks. For example, a pseudo tensor of rank zero is a pseudo scalar (pseudo meaning the scalar undergoes changes with coordinate transformation) such as scalar density or capacity. Within this context, the definition of density or capacity remains consistent with its physical meaning. In other words, a scalar capacity (volume) can be filled or emptied of a scalar density. An example of this situation is charge densities in a region of space where orbitals

overlap in a bonding interaction.

Asymmetry in the NMR shielding tensor has been treated by Schneider (2.38) and Haebelern (2.40). Schneider has explicitly shown that the effect of asymmetry manifests itself as a "second order" (quadratic in shielding) effect and its magnitude is controlled by shielding itself. By group theoretical analysis, Buckingham (2.41) has calculated the possibility of non-vanishing components for asymmetry of the shielding tensor and their results are tabulated in Table 4.10. The general conclusion from these results is that the antisymmetric term may be important in nuclei with large chemical shift ranges, e.g., ^{59}Co and ^{207}Pb. Therefore, in the analysis of relaxation rates, the antisymmetric term is not necessarily zero. The complete expression for the relaxation rates is given by Spiess (2.35);

$$\frac{1}{T_1} = \gamma_I^2 B_o^2 \left[\frac{2}{3}(\Delta_a\sigma)^2 \frac{\tau_1}{1+\omega^2\tau_1^2} + \frac{2}{15}\Delta\sigma^2\left(1+\frac{\eta_{cs}^2}{3}\right)\frac{\tau_2}{1+\omega^2\tau_2^2}\right] \qquad [2.17]$$

$$\frac{1}{T_2} = \gamma_I^2 B_o^2 \left[\sigma_{iso}^2 \tau_o + \frac{1}{3}(\Delta_a\sigma)^2 \frac{\tau_1}{1+\omega^2\tau_1^2} + \frac{1}{15}\Delta\sigma^2\left(1+\frac{\eta_{cs}^2}{3}\right)\left[\frac{4}{3}\tau_2 + \frac{\tau_2}{1+\omega^2\tau_2^2}\right]\right] \qquad [2.18]$$

$$\Delta\sigma = \sigma_{zz} - 1/2(\sigma_{xx} + \sigma_{yy})$$

$$\eta_{cs} = \frac{\sigma_{xx} - \sigma_{yy}}{\sigma_{zz}}$$

$$\Delta_a\sigma = [(P_{xy}^{cs})^2 + (P_{xz}^{cs}) + (P_{yz}^{cs})^2]^{1/2}$$

Under the extreme narrowing condition and when $\Delta_a\sigma = 0$, equation 2.12 reduces to the standard form with $T_1/T_2 = 7/6$.

SECTION 2.4.6 Alignment Effects ($\Delta\chi$) Induced by Magnetic Fields

In the strictest sense, this is a line splitting mechanism, however, when the line splitting is small and resolution is low, it appears as a line broadening. The theoretical criteria are as follows:

i) the molecule must have anisotropic diamagnetic susceptibility tensor (χ) components,

ii) Boltzmann statistics can be applied to estimate the alignment with the magnetic field, and

iii) disturbance of the ordering is due to Brownian motion.

If the anisotropy in the susceptibility components is large, the magnetic field, under high field condition, tends to align these molecules along the direction of the field, H_0. On the other hand, molecules undergo rapid Brownian motion destroying the magnetically ordered domain leading to a small alignment at thermal equilibrium. For quadrupole nuclei, the average value of the field gradient becomes non-zero leading to a small perturbation of the Zeeman levels, thus inducing a quadrupole line splitting. The theory is due to Lohman and Maclean (2.42-2.45). The appropriate Hamiltonian (2.42) is given below:

$$\hat{H}_Q = \sqrt{\frac{3}{2}}\left[\frac{eQ}{h} \cdot \frac{1}{6I(2I-1)}\right]\left[3(I_z)^2 - I^2\right] \times$$

$$\left[\sqrt{\frac{3}{2}}\left\langle\frac{3}{2}\cos^2\theta - \frac{1}{2}\right\rangle V_{zz} + \sqrt{\frac{3}{8}}\left\langle\sin^2\theta \cdot \cos^2\phi\right\rangle (V_{xx} - V_{yy})\right.$$

$$+ \sqrt{\frac{3}{8}} \left\langle \sin^2\theta \sin 2\phi \right\rangle (V_{xy} + V_{yx}) + \sqrt{\frac{3}{2}} \left\langle \cos\theta \sin\theta \cos\phi \right\rangle (V_{xz} + V_{zx})$$

$$+ \sqrt{\frac{3}{2}} \left\langle \cos\theta \sin\theta \sin\phi \right\rangle (V_{yz} + V_{zy}) \Bigg] \qquad [2.19]$$

where $\langle \ldots \rangle$ are the averages of the motional parameters, θ is the angle between the principle axis and the applied field H_o, ϕ is defined as in spherical coordinates, V_{ij} (ij=x,y,z) are the components of the field gradient tensor and I is the spin of the nucleus. For molecules with axial symmetry i.e., a three-fold or higher symmetry axis, equation 2.19 reduces to

$$\hat{H}_Q = \left[\frac{eQ}{h} \cdot \frac{1}{4I(2I-1)}\right]\left[\left\langle \frac{3}{2}\cos^2\theta - \frac{1}{2} \right\rangle V_{zz}\left[3(I_z')^2 - I^2\right]\right] \qquad [2.20]$$

because ϕ averages to zero. For C_{2v} symmetry $\sin\theta$ averages to zero, therefore equation 2.19 reduces to

$$\hat{H}_Q = \left[\frac{eQ}{h} \cdot \frac{1}{4I(2I-1)}\right]\left[\left\langle \frac{3}{2}\cos^2\theta - \frac{1}{2} \right\rangle V_{zz} + \frac{1}{2}\left\langle \sin^2\theta\cos 2\phi \right\rangle (V_{xx} - V_{yy})\right]$$

$$\times\left[3(I_z')^2 - I^2\right]$$

$\eta_Q = \frac{V_{xx} - V_{yy}}{V_{zz}}$, then substitution yields

$$\hat{H}_Q = \left[\frac{eQ}{h} \cdot \frac{1}{4I(2I-1)}\right] V_{zz}\left[\left\langle \frac{3}{2}\cos^2\theta - \frac{1}{2} \right\rangle + \frac{\eta_Q}{2}\left\langle \sin^2\theta\cos 2\phi \right\rangle\right] \cdot \left[3(I_z')^2 - I^2\right] \qquad [2.21]$$

The motional parameters are

$$\left\langle \frac{3}{2}\cos^2\theta - \frac{1}{2} \right\rangle = \frac{1}{15}\, x_{zz} - \frac{1}{2}(x_{xx}+x_{yy})\, \frac{H_o^2}{kT}$$

$$\left\langle \sin^2\theta\cos 2\phi \right\rangle = \frac{1}{15}\, (x_{xx} - x_{yy})\, \frac{H_o^2}{kT} \qquad [2.22]$$

where k = Boltzmann constant and T = temperature. The calculation of line splitting is straightforward.

SECTION 2.5 Inter-Molecular Interactions

SECTION 2.5.1 General Survey

Various authors have proposed different models to account for relaxation rates of quadrupole ions in solution. The assumptions vary from purely electrostatic to weakly covalent overlap interactions between solvent and ion. Valiev (2.46-2.50) suggested that the relaxation rate results from both vibrational motion of the solvent molecule in the solvated complex and translational motion of the solvent molecules governed by a random radial distribution. Alternatively, Hertz (2.51-2.52) proposed an electrostatic theory assuming that the dipoles of the solvent molecules in the immediate environment of the quadrupole ion are considered to contribute a small perturbation modulated by molecular motion of the solvent in this vicinity. This approach, however, involves numerous parameters which require independent estimation as well as various approximations;

i) motion correlation between solvent molecules and the solute at the closest distance of approach is neglected.

ii) orientational motion of solvent molecules is entirely random.

iii) infinite dilution conditions apply, i.e., solute-solute interactions are absent.

This is known as the fully randomized model (FRD). The most important feature of this model is that a discrete solvation shell does not exist.

Within the same framework, Hertz has modified the FRD model to one with a discrete solvation shell. There are two limits to this modification. The first is the non-oriented solvation (NOS) model in which the motions of the solvent molecule within the first solvation shell is entirely randomized. The second is the fully oriented solvation (FOS) model for which the solvent dipoles of the first solvation shell are radially oriented about the solute molecule. Allowance has been made to accomodate ion-ion interaction, i.e., finite concentration. In general, most experimental results fall between the NOS and FOS limits. In principle, if the assumption that the charge distribution of a complex cation is spherical can be made, a test of this model is based on the calculation of relaxation rates. Unfortunately, such a procedure cannot be carried out in practice since the parameters governing this model are experimentally unavailable.

A third model developed by Deverell (2.53-2.54) postulates that the origin of the relaxation of a quadrupolar ion is due to instantaneous distortion of the electric field gradient produced by the overlap of the

intermolecular repulsive potential (S) of the interacting pair during a collision process, i.e., an electronic distortion model. Under such a condition, the quadrupole coupling constant can be written as

$$\left(e^2qQ\right) = \frac{8}{5} e^2Q\left\langle \frac{1}{r^3} \right\rangle_p \sum_i S_i^2$$

where $\sum S^2$ is the sum of the squares of the overlap integral S between the outer orbitals of the ions and the outer orbitals of the i neighbouring molecules and $\left\langle r^{-3} \right\rangle_p$ is the expectation value of r^{-3} in the outermost p orbital of the ion considered. This approach has not been entirely accepted in the literature. Although this effect may be more applicable for larger (softer) polarizable ions it has been found experimentally that the paramagnetic shielding of Li^+ is not dominated by the repulsive overlap integral (2.55).

Finally, covalent or weakly covalent interactions between the observed ion and the electron pair from the solvent have been proposed by Mishustin and Kessler (2.56-2.58) in an attempt to understand the solvent dependences of $^7Li^+$ relaxation behaviour. Three pieces of evidence have been cited to support this type of "electronic" effect;

i) I.R. studies on the interaction of Li^+ with acetone, acetonitrile, pyridine and substituted amines revealed definitive frequency shifts of characteristic functional groups (2.59, 2.60),

ii) quantum mechanical calculations have shown that charge transfer takes place from solvent molecules in the solvation shell to Li^+ in both aqueous and non-aqueous solution (2.61-2.64).

iii) neutron and x-ray diffraction of aqueous LiCl solution firmly establish a well-oriented hydration shell about Li^+ and that the lone pair provided by the solvent molecule directly interacts with Li^+ (2.65).

This type of behaviour is incompatible with a pure electrostatic theory. The inconsistency points to interaction of a non-electrostatic nature, namely donor-acceptor interaction. As pointed out by these authors, direct quantitative application of the effect of charge transfer on quadrupole relaxation time is not possible since a comprehensive treatment of the theory is unavailable. Other empirical parameters can be employed to characterize donor-acceptor interactions. In the following section, the donor-acceptor concept of Gutmann (2.66) is examined. Before closing this survey, a few review articles dealing with both the theoretical aspects as well as experimental results have appeared (2.67, 2.68). The reader is referred to them for detailed discussion.

2.5.2 Donor-Acceptor Interaction and the Donor Number (DN)

The basic foundation of the donor-acceptor theory is based on the Lewis concept (2.69). The most fundamental result of the Lewis concept is the formation of a coordinate covalent bond upon interaction of a Lewis acid (electron pair acceptor or acceptor) and a Lewis base (electron pair donor or donor) leading to a charge density rearrangement in the resulting adduct.

Charge density rearrangement due to actual charge transfer and/or polarization effects which results from the interaction between donor and

acceptor species generally manifests itself through measurable quantities such as bond lengths, thermodynamic and kinetic quantities. Of these, the availability of precise structural data in recent years has allowed formulation of simple rules - the bond length variation rules (2.70-2.72) accounting for bond length variation within a molecule in different donor solvents.

The first bond length variation rule states that "the smaller the intermolecular distance D→A, where D stands for donor and A for acceptor, the greater the induced lengthening of the adjacent intra-molecular bonds both in the donor and acceptor component of the charge transfer complex." The second bond length variation rule relates the effect of σ-bond distortion for the remaining part of the molecule upon formation of D→A complex. "As a result of donor-acceptor interaction, charge density rearrangement takes place. A σ-bond is lengthened when the electron shift occurs from a nucleus carrying a positive to one carrying a negative fractional charge whereas the σ-bond is shortened when the electron shift is induced in the opposite direction." Since precise local nuclear charge is unknown, the idea of electronegativity has been used to carry through the argument. Thus, a σ-bond is lengthened when the electron shift takes place from the more electropositive to the more electronegative atom in the uncomplexed species and a σ-bond is shortened when the reverse takes place in the uncomplexed species. The third bond length variation rule (2.73) states "When an adduct is formed, the coordination number is increased at both the donor and the acceptor atom and according to the first bond length variation rule, the bonds originating from these atoms

are lengthened irrespective of the state of the aggregation". Thus, as the coordination number increases, the lengths of the bonds originating from the coordination center increases (2.74-2.76). An illustrative example of the bond length variation rules is provided by Keitaibl et. al (2.77) in the study of the interaction of tetrachloroethylene carbonate with $SbCl_5$. The induced charges in bond distances are shown on the extreme right of Figure 2.1 (reproduced from reference 2.66). The agreement between changes in experimental bond lengths with the bond length variation rules is self-evident.

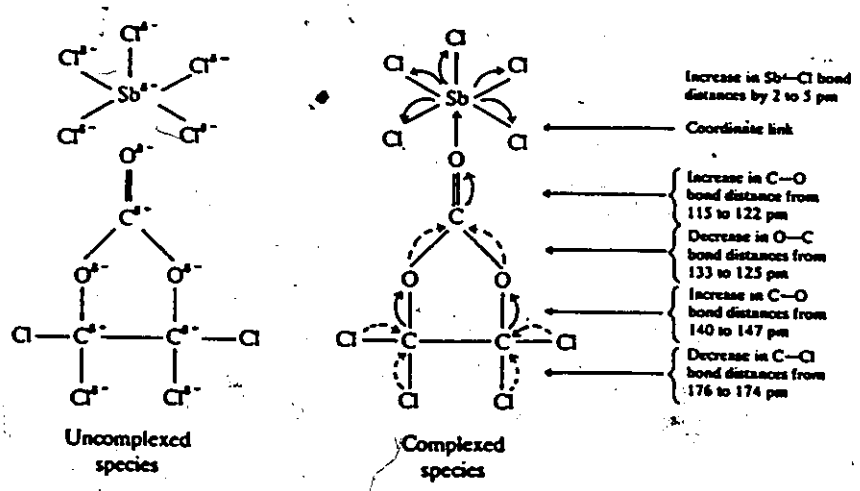

Figure 2.1 Donor-Acceptor Analysis of Bond Length Data of $(C_2Cl_4CO_3)SbCl_5$(2.66)

A direct consequence of changes in bond length are bond polarity changes due to changes in charge separation. These changes are related to the finite changes in charge density at both the donor and acceptor atoms leading to an electronic "pile up" or "spill-over" effect. "Upon interaction of a neutral donor and acceptor pair, a net gain in positive charges results at the acceptor atom due to the transfer of negative charges including part of those originally situated at the acceptor atom to other parts of the acceptor molecule. This leads to an overall increase in negative char-

ges in the acceptor component, in particular, those terminating the acceptor molecule." This is known as the "spill-over" effect of negative charge at the acceptor atom (2.78). Similarily, the "pile-up" effect of negative charges at the donor atom is due to a net gain in negative charges from the components of the donor molecule resulting in an overall decrease in negative charges throughout the donor molecule." This is schematically represented below;

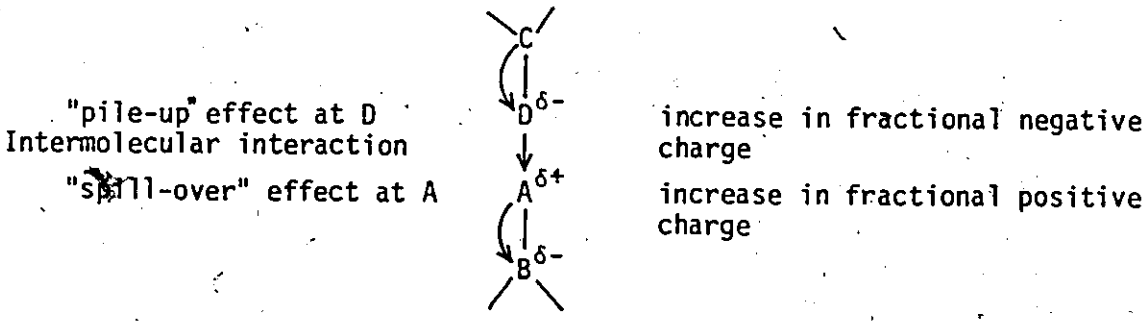

The "spill-over" and "pile-up" effects have been successfully applied to systems of which molecular association takes place in the liquid state. For example, calculations for the interaction between water and chlorine shows a total of 0.003 electron transfered (2.79, 2.80). The "spill-over" and "pile-up" effects are apparent at the chlorine and oxygen atoms, respectively.

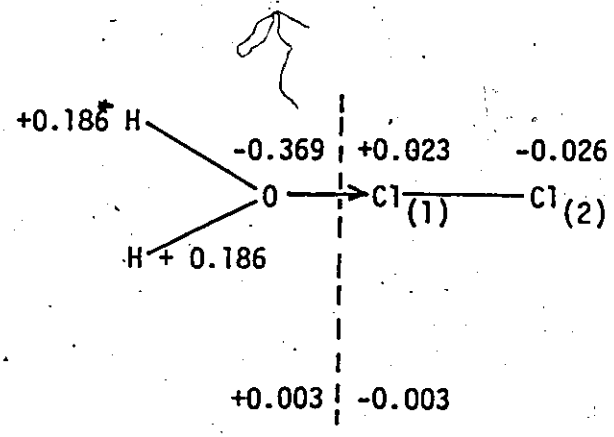

In the aforegoing discussion, the basic idea of the donor-acceptor approach to molecular interaction was examined. The reader is referred to the excellent text by Gutmann (2.66) for further detail. It has become obvious that ion solvation can be rationalized in much the same way but with caution since the so called "pile-up" and "spill-over" effect does not necessarily follow the same trend. A final example serves to illustrate these concepts. In the solvation of $^{7}Li^{+}$ in formic acid, Raman results (2.81) indicate four molecules of formic acid are coordinated to Li^{+}. Frequency shifts led to the conclusion that the C=O and C-H bonds are lengthened whereas the C-O bond is shortened. In addition, an ab-initio calculation (2.82)

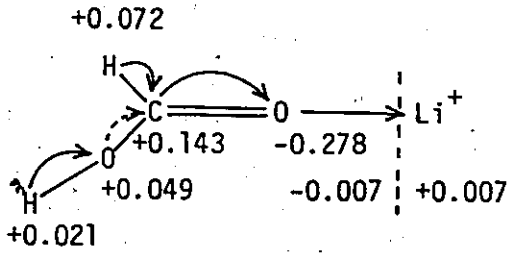

indicates that $^{7}Li^{+}$ gains a total of $0.007e^{-}$. The same calculation show that a considerable "pile-up" of charge density is located at the oxygen donor atom. The important feature of this example is that there is no "spill-over" at $^{7}Li^{+}$ leading to an overall decrease in the positive charge at $^{7}Li^{+}$. In addition, solvent-dependence studies of $^{7}Li^{+}$ and $^{23}Na^{+}$ relaxation rates provide further support for these ideas (2.56, 2.57). The conclusion that can be drawn from the last example is that cation solvation in different protic/aprotic solvents is directly related to the strength of the solvent in its ability to interact with the ion. It remains, therefore, a problem of seeking a proper characterization of the solvent with which

such properties of the solvent are directly reflected.

Various attempts have been made in solvent characterization by empirical parameters, notably Grunwald and Winstein's Y-values (2.83), Kosower's Z-values (2.84-2.88) and Dimroth and Reichardt's E_T-values (2.89). These empirical parameters have all proven successful, in limited applications. From calorimetric data on $SbCl_5$, Lindqvist (2.90) derived a qualitative order of solvent donor strength. This is the first solvent scale derived with emphasis on direct changes in bond properties. This idea has been expressed quantitatively by the donor number concept proposed by Gutmann and Wycheri (2.58). Gutmann sought solvent independent representation for the donor ability of a molecule. The "donor number (DN)" or "donicity" is defined as the molar enthalpy value for the reaction of the donor (D) with $SbCl_5$ as a reference acceptor in a 10^{-3}M solution of dichloroethane. Thus,

$$D + SbCl_5 \rightleftharpoons D\cdot SbCl_5 \quad , \quad -\Delta H_{D\text{-}SbCl_5} \equiv DN$$

the molar enthalpy of 1:1 molecular adduct formation in dichloroethane is taken as an approximate measure of the energy of the coordinate bond between the donor and Sb atoms of $SbCl_5$ (2.58). Therefore, the ΔH values can be used as a guide to the relative complex stabilities. A list of the donor numbers is given in Table 5.14. The importance of this definition is that ΔH is a direct function of changes in bond properties upon chemical interaction. Consequently, cation solvation can be characterized quantitatively by the DN and upon application of the bond length variation rules together with the "pile-up" and "spill-over" effect, much of the observed solvation phenomena can be explained qualitatively.

In magnetic resonance, chemical shifts are directly related to the so called "pile-up" and "spill-over" effect because charge density build up at nuclei adjacent to the observing nucleus induces shielding effects leading to a change in chemical shift. Therefore, chemical shift measuements serve as one method of measuring solvation power using magnetic resonance methods. For a quadrupolar nucleus, the quadrupole interaction dominates the relaxation mechanism and is sensitive to extranuclear fluctuating charge density about the quadrupole nucleus. Relaxation time measurements provide an alternative magnetic resonance method for probing solvation power. Examples of the former effect are known for the dependences of $^{23}Na^{+}$ chemical shifts with DN (2.57, 2.91) and the latter the solvation of $^{7}Li^{+}$ (2.56). A chemical shift correlation for $Coen_3^{3+}$ with DN has been reported (2.92), but relaxation time measurements of complexed ions in different solvents have not been reported.

CHAPTER THREE

EXPERIMENTAL

SECTION 3.1 Sources of Compounds and Synthetic Procedures

The synthesis of the complexes studied in this thesis have all been reported in the literature. The relevant references are compiled in Table 3.1.

Preparation of $Co(N_3)_6^{3-}$

In a typical preparation, 100mls of NaN_3 solution is allowed to react with $CoCl_2.6H_2O$ in the presence of 30% H_2O_2 (10mls) and activated charcoal. The NaN_3 is slightly in excess of the 6:1 stoichiometric ratio. The mixture is warmed to 60°C. Effervescence ceased 15-20 minutes after mixing. The pH of the solution containing $Co(N_3)_6^{3-}$ anion is then adjusted to 7, and the solution stored in the refrigerator.

SECTION 3.2 NMR T_1 and T_2 Measurements

General

^{59}Co NMR measurements were carried out on Bruker WH-90, WM-250 and WH-400 high resolution FT-spectrometers operating at 21.252, 59.035 and 94.457 MHz respectively. The latter two instruments use a super-conducting magnet and a field frequency lock was not necessary. All measurements were done on resonance except where multiline spectra were involved. The temperature of the probe was usually 295±1°, 295 ±0.5°, 293±1°K respectively for the instruments and was found to be the same within 1°C on different

Table 3.1

References to the Synthesis of Cobalt(III) Complexes

Complex	Reference	Complex	Reference
$K_3[Co(CN)_6]$	3.1	cis-$[Co(NH_3)_4(CN)_2]Cl.H_2O$	3.13, 3.21
$[Coen_3]Cl_3.3H_2O$	3.2	trans-$[Co(NH_3)_4(CN)_2]Cl$	3.13, 3.21
$[Co(NH_3)_6]Cl_3$	3.3	cis-$[Coen_2CO_3]Cl.H_2O$	3.5, 3.16
$Co(N_3)_6^{3-}$	This work	cis-$[Coen(NH_3)_4]Cl_3$	3.25
$Na_3[Co(CO_3)_3].3H_2O$	3.4, 3.5	cis-$K[Coen(CN)_4]$	3.21, 3.26
$[Co(NH_3)_5Cl]Cl_2$	3.6	cis-$[Co(NH_3)_4(N_3)_2]N_3$	3.27
$[Co(NH_3)_5Br]Br_2$	3.7	cis-$[Co(NH_3)_4CO_3]Cl$	3.5, 3.16
$[Co(NH_3)_5CO_3]NO_3$	3.8	trans-$[Co(dien)_2]Br_3$	This work
$[Co(NH_3)_5N_3]Cl_2$	3.9	trans-$[Co(dmgH)_2(NH_3)_2]Cl$	3.28
$[Co(NH_3)_5NCS]Cl_2$	3.10	fac,mer-$Co(NH_3)_3(CN)_3$	3.13, 3.21
$[Co(NH_3)_5SCN]Cl_2$	3.10	fac-$Co(NH_3)_3(N_3)_3$	3.29
$[Co(NH_3)_5NO]Cl_2$	3.11	mer-$Co(dien)(NO_2)_3$	3.30
$[Co(NH_3)_5NO_2](NO_3)_2$	3.8	mer-$Co(dien)Cl_3$	3.30
$[Co(NH_3)_5CN](ClO_4)_2.\frac{1}{2}H_2O$	3.12, 3.13	mer-$Co(NH_3)_3(NO_2)_3$	3.31
$[Co(NH_3)(CN)_5]^{2-}$	3.14	mer-$Co(dien)(CN)_3$	3.21
$[Co(NO_2)(CN)_5]^{3-}$	3.5, 3.14	ε-$[Co(en)(dien)Cl]Cl_2$	3.32
cis,trans-$[Coen_2Cl_2]Cl$	3.15, 3.16		
cis,trans-$[Coen_2Br_2]Br$	3.17	$[(Co(NH_3)_5)_2O_2](NO_3)_4$	3.33
cis,trans-$[Coen_2(N_3)_2]N_3$	3.18	$[(Coendien)_2O_2](ClO_4)_4.2H_2O$	↑
cis,trans-$[Coen_2(NO_2)_2]NO_3$	3.16, 3.19, 3.20	$[(Co(trien)(NH_3))_2O_2](ClO_4)_4.2H_2O$	3.34
cis,trans-$[Coen_2(CN)_2]Cl$	3.13, 3.21	$[(Co(tetraen))_2O_2](ClO_4)_4.2H_2O$	↓
cis,trans-$[Co(NH_3)_4Cl_2]Cl$	3.22	$(Co(salen))_2O_2(DMSO)_2$	↑
cis,trans-$[Co(NH_3)_4(NO_2)_2]NO_3$	3.23	$(Co(salen))_2O_2(DMF)_2$	3.35
cis,trans-$K[Co(NH_3)_2(CO_3)_2]$	3.24	$[(Co(salen))_2O_2(H_2O)]_2$	↓

days. Saturated samples in the pH range of 5-6 were examined to ensure that amine proton exchange does not take place. ^{14}N NMR spectra were obtained on Bruker WM-250 and WH-400 FT-spectrometers operating at 18.059 and 28.894 MHz respectively. ^{1}H NMR spectra were recorded on a WP-80 Bruker FT-spectrometer operating at 80.00 MHz. ^{13}C NMR spectrum was obtained on a WH-400 FT-spectrometer operating at 100.577 MHz.

Chemical shifts were measured by exact frequency method relative to external $Co(CN)_6^{3-}$. Bulk susceptibility corrections are of the order of 1-2ppm and were neglected.

SECTION 3.2.1 Linewidth Measurements

The transverse relaxation time T_2 is obtained from the full width at half height of the absorption signal. Instrumental broadening is of a few Hz and is therefore neglected. Peaks may be fitted to a Lorentzian shape function defined by equation 2.6. Examples of linefitting are shown in Figure 3.1 for the conventional mid-range standard $Coen_3^{3+}$(χ^2/df=0.008) and Figure 3.2 for the complex trans-$[Coen_2Cl_2]Cl$(χ^2/df=0.003). For complex spectra, a non-linear least square program was developed where the spectra were fitted to a sum of Lorentzians with a sixth order polynomial baseline function as well as options for sinewave baseline correction. Examples of complex spectra are given in Figure 7.4 and 7.5. The criteria for best fit is determined by the value of χ^2/df($\sim$1.0). The standard errors were calculated in the usual way from the estimated variance-covariance matrix of the fitted parameters(3.36).

SECTION 3.2.2 Longitudinal Relaxation Time (T_1) Measurements

(i) T_1 Measurements

Longitudinal relaxation time measurements were carried out on Bruker WM-250 (5.8749T) and WH-400 (9.3950T) FT-superconducting NMR spectrometers. M_z ($\tau = \infty$) was measured from the intensity $g(\omega_o)$ of the absorption signal.

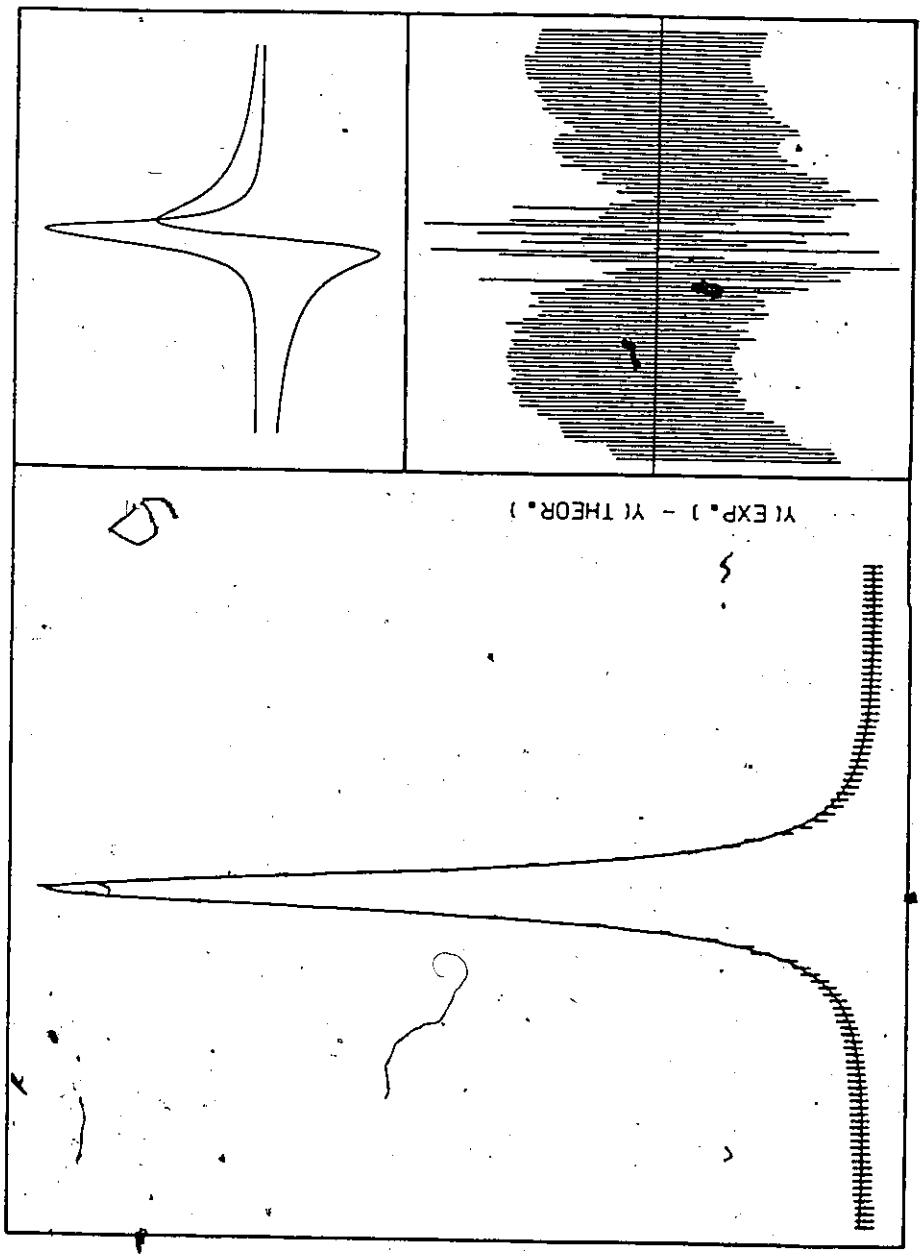

Figure 3.1 Experimental and fitted ^{59}Co NMR spectrum of $Coen_3^{3+}$ (59.035 MHz)

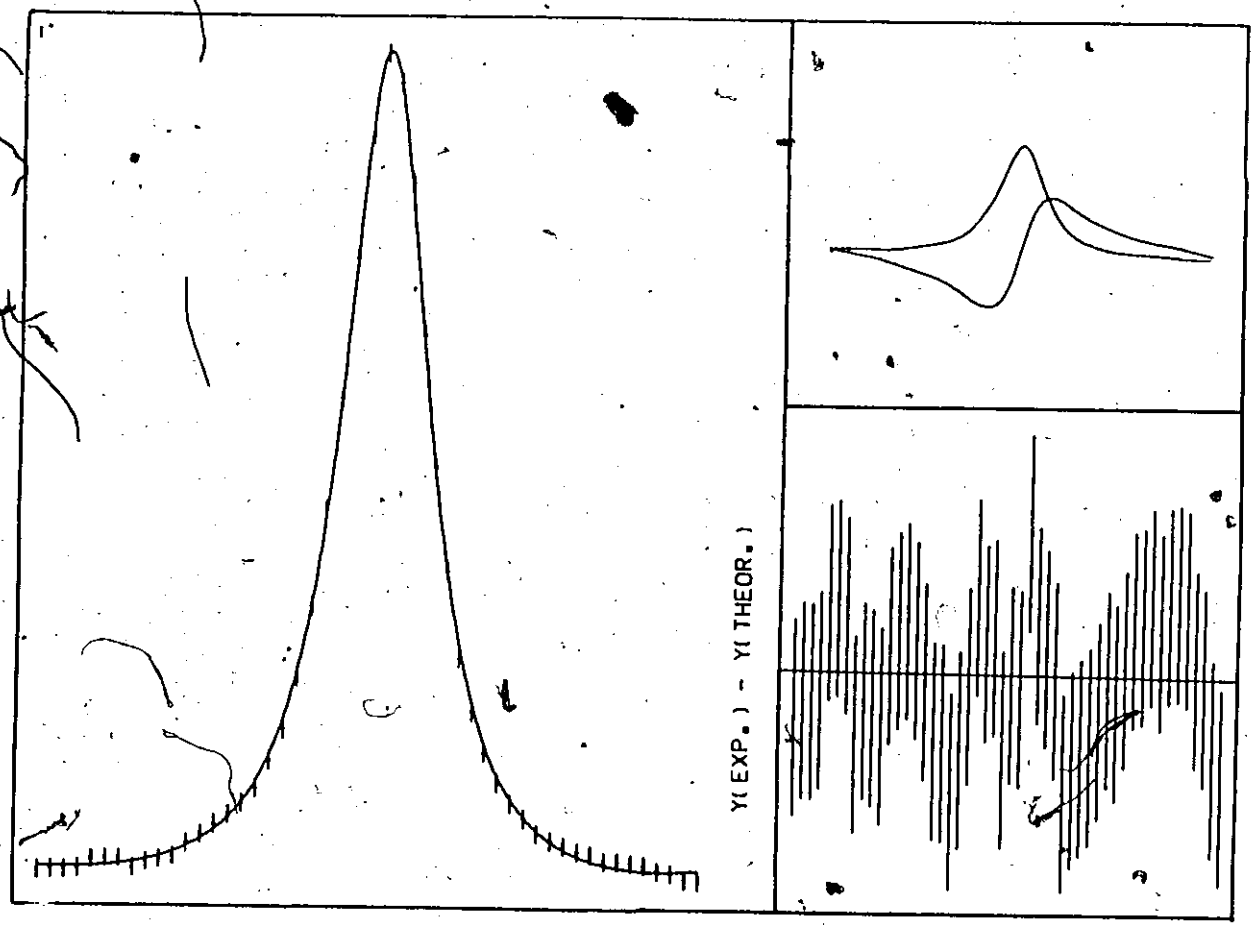

Figure 3.2 Experimental and fitted ^{59}Co NMR spectrum of trans-$Coen_2Cl_2^+$ (59.035 MHz)

In general, the signal/noise (S/N) ratio was at least 25 and on the average more than 100. For cases where the S/N ratio was low, exponential multiplication of the FID (Free Induction Decay) was used to improve its value. Instrumental drift in sensitivity can be neglected since most T_1 experiments were completed in a fairly short time ($\leq$ 2 hrs.).

The standard inversion-recovery pulse sequence $(180°-\tau-90°-T)_n$ was used where T is the relaxation delay and is always greater than 5 x T_1 (3.37). The pulse lengths for 90° and 180° pulses were determined by searching for a maximum or minimum, respectively, in the intensity of the FT-signal. The determined pulse widths for ^{59}Co T_1 measurements on the WM-250 ranged from 32 to 42μsec, and 64 to 95μsec on the WH-400, depending on the sample used.

Additional measures were undertaken to determine the effect of probe mis-tuning on T_1 such that the resulting 90° pulse length was 52μsec on the WM-250. The resulting T_1 value determined under these conditions compares well with that of the T_1 value determined under optimum probe tuning conditions and exact 180° and 90° pulse lengths. The results in Table 3.2 clearly demonstrate that this procedure only results in a loss of dynamic range through inefficient inversion and detection.

An attempt was made to increase the dynamic range for the inversion-recovery experiment by shortening the detection pulse lengths. T_1's on trans-$[Coen_2(NO_2)_2]NO_3$ in dimethylsulfoxide were determined using 56° and 14° for the detection pulse instead of the 90° pulse (Table 3.3). The T_1's obtained were in good agreement with those obtained using the normal 90° detection pulse. However, S/N is drastically reduced for shorter detection

Table 3.2

Dependence of ^{59}Co T_1 on Pulse Widths[1,2]

$M_z(t = \infty)$	$\frac{M_z\ (t = 0)}{(t = \infty)}$	T_1 (msec)	Standard error	Preparation Pulse length µsec	Preparation Pulse length deg	Detection Pulse length µsec	Detection Pulse length deg
14.2	0.83	8.50	±0.06	64	180	32	90
6.6	0.82	8.53	±0.10	105	180	52	90
5.4	0.31	8.55	±0.19	64	110	32	55

[1] Sample $[Co(en)_3]Cl_3$ in water.

[2] WM-250 Bruker-FT instrument

Table 3.3

Dependence of ^{59}Co T_1 on Detection Pulse Angle[1,2]

PW (µsec)	PW (degrees)	T_1 (msec)
32	90°	0.0767
32	90°	0.0774
20	56°	0.0767
5	14°	0.0790

[1] Sample [trans-$Coen_2(NO_2)_2]NO_3$ in dimethylsulfoxide

[2] WM-250 Bruker-FT instrument

pulse lengths. For this reason, the normal 90° detection pulse was used since it is obvious that it is more efficient. Thus, more efficient inversion was obtained by shorter detection pulse lengths but this gain was offset by loss in S/N ratio.

The 90° pulse width used for ^{14}N T_1 measurements on the WH-400 (28.894 MHz) was 100μsec. A number of independent determinations were carried out for each sample and the resulting T_1 values were found to be reproducible to ± 5% for ^{59}Co T_1's. The random errors obtained from a single set of data are considerably smaller than this value. The quality of the ^{14}N spectra were lower than those of ^{59}Co spectra, the T_1 values therefore involve a larger error (~ ± 10%).

The inversion of the NMR signal was far less than complete for all the complexes examined. This may have been due to the following reasons:

i) Inexact 180° pulse lengths,

ii) inhomogeneity in the H_1 field

iii) relaxation during the 180° pulse,

iv) relaxation during the 90° pulse, and

v) relaxation during the computer delay, DE, where

DE = (4 x sweep width)$^{-1}$ (minimum of 2.5μsec).

Reason (i) has already been dealt with. The combined effect of (ii) and (iii) is to cause $M_z(\tau=o) < -M_z(\tau)$ as well as x-y components of magnetization after the 180° pulse. These effects were easily corrected by the use

of quadruature phase detection or simple phase cycling of the detection pulse as suggested by Pegg et. al. (3.38). The effect of (iv) is uncertain and there is little known in the literature (3.39). In all practical consideration, (v) can be neglected.

(ii) Data Analysis

T_1 was calculated by a non-linear three parameter fit of the data to an equation of the form

$$M_z(\tau) = M_z(\infty) - [M_z(o) - M_z(\infty)] \exp(-\frac{\tau}{T_1})$$

The criteria for best fit was unweighted least squares and the calculations were carried out on an Osborne microcomputer using a BASIC program (GRAPTECH-non-iterative) developed in this laboratory (3.40) after the pattern of a solution presented in Draper and Smith (3.41) as well as a program developed by another group (3.42) (NMR T_1-iterative). The two programs are given in Appendix I. The standard errors for both GRAPTECH and NMR T_1 were calculated as described earlier. Figure 3.3 illustrates a fit of the T_1 experimental data and also indicates the signal to noise ratio of the spectra used to measure the linewidths for T_2 calculations.

SECTION 3.3 Miscellaneous

SECTION 3.3.1 Kinetic Measurements

All kinetic runs were performed on a Durrum D-110 glass/lucite Stopped-flow spectrophotometer with conventional Deuterium and Tungsten light sources covering the entire UV/VIS spectral range. The reagents were mixed in a

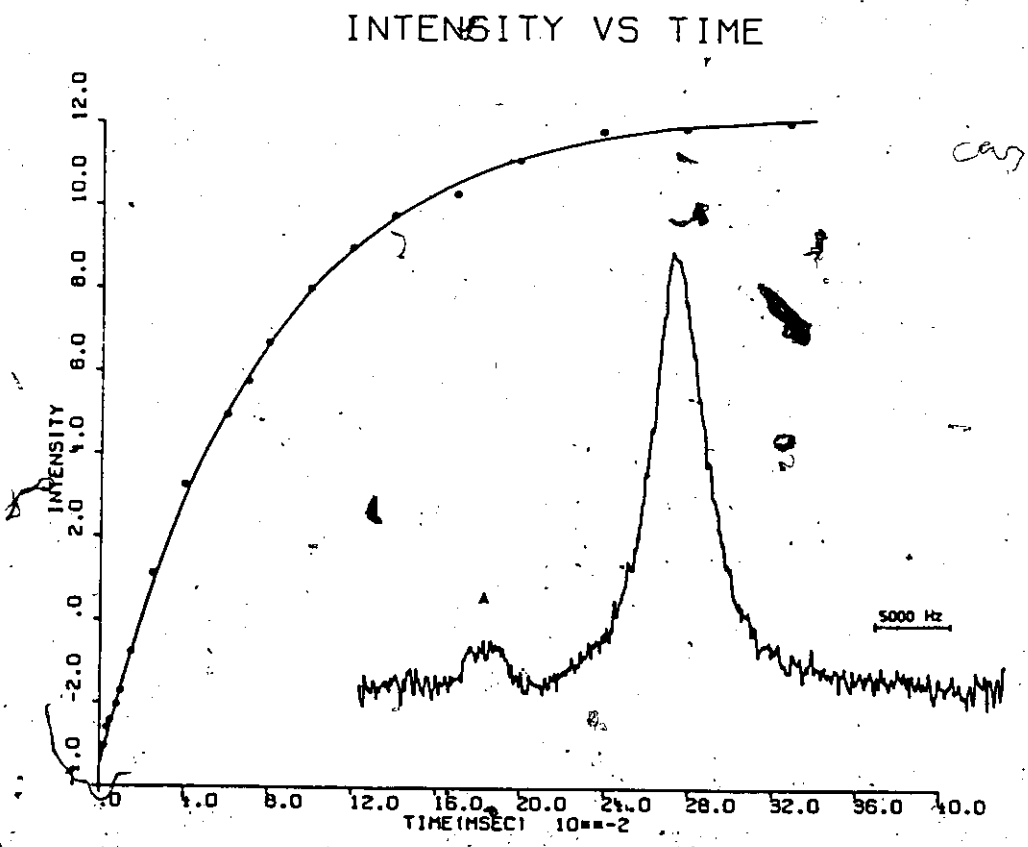

Figure 3.3 Experimental T_1 data (⊙)(59 MHz) for the complex trans-$Coen_2(NO_2)_2^+$/dimethyl sulfoxide. Solid line three parameter fit as described in Sec. 3.2(ii) T_1=.076 msec. A-traces of cis-$Coen_2(NO_2)_2^+$.

mixing jet and observation was carried out in an optical cell (2cm optical path length) via a 2mm diameter observation window. The syringe drive rate was ~30mls/sec operating at a pressure of 70 psi. The dead time for mixing was 2-5msec. The signals were digitized and fed into a Nicolet-1170 signal averaging system and the kinetic trace was recorded on a Hewlett Packard 7045A x-y recorder. The optical scale was calibrated by the standard reaction of 0.01M $Fe(NO_3)_3$ and 0.01M KSCN in 0.1N H_2SO_4 (0.5 Absorbance Unit.) All reactions were buffered with appropriate buffers (3.43) and were at constant ionic strength.

SECTION 3.3.2 Mössbauer Measurements

Mössbauer spectra were recorded by Dr. G. Dénès using an experimental set-up similar to that previously described by Birchall and Johnson (3.44) and the results are discussed in Appendix II.

SECTION 3.3.3 D.T.A./T.G.A. Measurements

Thermal analysis of $Fe(OH)_3$ samples were carried out on a Netysch STA-40g simulteneous D.T.A./T.G.A. instrument by Mr. Frank Gibbs of the Institution for Materials Research of McMaster University. The results are discussed in Appendix II.

SECTION 3.3.4 Solution Molecular Weight Measurements

Solution molecular weights were measured using an Hitachi-Perkin-Elmer (Model 115) Molecular Weight Apparatus. This apparatus utilizes the vapour pressure method and was calibrated with Imidazole.

CHAPTER FOUR

THE DEPENDENCE OF THE LINEWIDTHS OF COBALT(III) COMPLEXES IN AQUEOUS SOLUTION ON MAGNETIC FIELD STRENGTH

SECTION 4.1 Introduction

As treated in Chapter 2, the most important relaxation mechanism of a quadrupolar nucleus is due to modulation of the electric field gradient. This gives rise to the NMR line broadening. Broadening due to other mechanisms is usually neglected. In aqueous solution the NMR linewidths of $^{59}Co(III)$ complexes vary from a few Hz for $Co(CN)_6^{3-}$ to more than 9 kHz for trans-$Coen_2Cl_2^+$. This drastic change in the NMR linewidth is associated with a change in the quadrupole coupling constant, more precisely, $(e^2qQ/h)^2$. In the former case, the electric field gradient at the Cobalt nucleus is zero as expected for O_h symmetry. A value of 60.14MHz for (e^2qQ/h) has been reported for the latter complex and accounts for the much broader linewidth. For the complex cis-$Coen_2Cl_2^+$, the measured linewidth of 5kHz parallels a quadrupole coupling constant of 36MHz. The line width ratio for these geometric isomers is useful as an aid in structural assignments in cases for which the chemical shift differences are small.

Recent advances in High Field NMR instrumentation have led to the following significant improvements: (i) Enhancement of resolution due to the larger separations of the Nuclear Zeeman levels, and since (ii) the sensitivity of the NMR experiment varies as the square* of the magnetic field

---

* In practice only a power of 3/2 is achieved.

strength, it is therefore possible to study molecules containing nuclei of low natural abundance or compounds with limited solubility. In the case of Cobalt complexes, this latter aspect is particularly useful. In addition, variable magnetic field measurements allow investigation of shielding anisotropy. This is a sensitive probe of the electronic structure of a complex and is related to the electronic spectrum. Since quadrupolar relaxation is independent of the magnetic field strength, B_o, both the chemical shielding anisotropy ($\Delta\sigma$) and the quadrupole coupling constant ($e^2qQ/\hbar$) can be evaluated from the linewidth data if the correlation time can be estimated.

4.2 Results

The chemical shifts and linewidths for 22 octahedrally coordinated Cobalt(III) complexes have been measured at field strengths of 2.114T, 5.872T and 9.395T in aqueous solution. These data are tabulated in Table 4.1. For the purpose of comparison, low field data from the literature (4.1, 4.2, 4.3, 4.4) obtained at 1.005T, 1.348T and 2.349T are also collected and presented in Table 4.2. A few comments are in order with respect to Tables 4.1 and 4.2. Generally, the chemical shifts are reproducible at different fields and agree with literature values (4.5) with the exception of the complex trans-$Coen_2Cl_2^+$ for which the chemical shifts are apparently field dependent. This complex was also examined in methanol and acetonitrile and the chemical shifts were found to be satisfactorily constant (Sec. 5.2, Table 5.6). At this time, no explanation can be given for the apparent variation of the chemical shift in water. Recent articles

Table 4.1

Chemical Shifts and Line Widths of Co(III) Complexes

Complex	21.252 MHz		59.035 MHz		94.457 MHz	
	δ(ppm)	$\Delta\nu_{\frac{1}{2}}$(Hz)	δ(ppm)	$\Delta\nu_{\frac{1}{2}}$(Hz)	δ(ppm)	$\Delta\nu_{\frac{1}{2}}$(Hz)
1. $Co(CN)_6^{3-}$	0	5 ± 1.5	0	5 ± 1.5	0	6 ± 1.5
2. $Co(NH_3)_6^{3+}$	8175	172 ± 10	8174	183 ± 10	8176	183 ± 10
3. $Coen_3^{3+}$ [a]	7146	90 ± 10	7148	98 ± 5	7145	117 ± 10
4. $Co(CN)_5NO_2^{3-}$	609 ± 10	3767 ± 300	598 ± 10	4200 ± 400	599 ± 5	5100 ± 500
5. $Co(CN)_5NH_3^{2-}$	1162 ± 100	3131 ± 300	1174 ± 10	3747 ± 300	1169 ± 5	4470 ± 400
6. $Co(NH_3)_5Cl^{2+}$	8887 ± 5	1460 ± 100	8890 ± 5	1815 ± 150	8890 ± 5	1883 ± 150
7. $Co(NH_3)_5CO_3^{+}$	9062 ± 5	1947 ± 150	9090 ± 5	3383 ± 300	9084 ± 5	5395 ± 500
8. $Co(NH_3)_5NO^{2+}$	7867 ± 2	141 ± 10	7869 ± 2	162 ± 15	7865 ± 2	188 ± 15
9. trans-$Coen_2Cl_2^{+}/H_2O$	9333 ± 20	8597 ± 500	9163 ± 30	13400 ± 1000	8960 ± 30	16783 ± 1000
10. trans-$Coen_2(NO_2)_2^{+}$	6323 ± 5	1366 ± 150	6329 ± 5	1430 ± 150	6319 ± 5	1579 ± 150
11. trans-$Co(dmgH)_2(NH_3)_2^{3+}$	5386 ± 20	6123 ± 450	5370 ± 20	7299 ± 500	5382 ± 20	9189 ± 800
12. trans-$Co(CN)_2en_2^{+}$	4736 ± 20	8089 ± 600	4718 ± 20	12025 ± 1500	4726 ± 20	16690 ± 1500
13. aed,cbf-$Co(dien)_2^{3+}$ [a,b]	6836 ± 5	423 ± 30	6850 ± 5	428 ± 30	6846 ± 5	438 ± 30
14. cae,dfb-$Co(dien)_2^{3+}$ [c]	7031 ± 5	3021 ± 300	7032 ± 5	3384 ± 300	7032 ± 5	3468 ± 300
15. bfc,dae-$Co(dien)_2^{3+}$	6968 ± 5	395 ± 30	6985 ± 5	420 ± 30	6981 ± 5	427 ± 30
16. fac-$Co(NH_3)_3(CN)_3$	3317 ± 5	618 ± 50	3312 ± 5	720 ± 50	3313 ± 5	750 ± 50
17. mer-$Co(NH_3)_3(CN)_3$	3991 ± 25	4542 ± 400	3976 ± 20	10808 ± 1000	3947 ± 40	14078 ± 1500
18. cis-$Coen_2Cl_2^{2+}$	8966 ± 20	5126 ± 300	8968 ± 20	8483 ± 600	8987 ± 20	9218 ± 800
19. cis-$Coen_2(CN)_2^{+}$	4384 ± 20	3700 ± 300	4388 ± 20	5408 ± 400	4364 ± 5	5513 ± 400
20. $Coen(CN)_4^{-}$	2013 ± 25	5410 ± 300	1998 ± 25	5479 ± 300	2006 ± 20	5438 ± 300
21. cis-$Co(NH_3)_4CO_3^{+}$	9732 ± 20	3291 ± 300	9735 ± 20	5173 ± 400	9729 ± 20	5476 ± 400
22. cis-$Co(NH_3)_4(CN)_2^{+}$	5132 ± 20	2489 ± 200	5164 ± 20	7059 ± 600	5173 ± 200	9656 ± 800

[a] Ligand abbreviations: en = ethylene diamine, dien = diethylene triamine, dmgH = dimethyl glyoxime

[b] Structures in Figure 4.2.

[c] Assignment is tentative, there is evidence that this is a dimeric Co species involving bridging diethylenetriamine.

Table 4.2

Low Field Chemical Shifts and Linewidths of Co(III) Complexes Compiled from Literature Sources[a]

Complex	10.103 MHz		13.555 MHz		22.6 MHz	
	δ(ppm)	$\Delta\nu_{1/2}$(Hz)	δ(ppm)	$\Delta\nu_{1/2}$(Hz)	δ(ppm)	$\Delta\nu_{1/2}$(Hz)
1. $Co(CN)_6^{3-}$					0	200
2. $Co(NH_3)_6^{3+}$				87	8100	200
3. $Coen_3^{3+}$				86	7114	200
6. $Co(NH_3)_5Cl^{2+}$	8840	1645 ± 175	8905	1732		
9. trans-$Coen_2Cl_2^+/H_2O$		13509 ± 1000		13856		
10. trans-$Coen_2(NO_2)_2^+$	6570	1108 ± 90		1905	6555	601
16. fac-$Co(NH_3)_3(CN)_3$					3325	1002
17. mer-$Co(NH_3)_3(CN)_3$					4045	2503
18. cis-$Coen_2Cl_2^+$		8833		7794		
21. $Co(NH_3)_4CO_3^+$	9730	1350 ± 175		1925		
22. cis-$Co(NH_3)_4(CN)_2^+$					5065	2804

[a] Reference 4.1 - 4.4

by Doddrell (2.28, 2.29) report small variations of chemical shift with field for Cobalt complexes, namely $Co(CN)_6^{3-}$ and $Co(^{15}NH_3)_6^{3+}$ in water, and $Co(acac)_3$ in chloroform. Shielding differences of approximately 10Hz measured at field strengths of 0.34T and 2.10T were found for the complexes $Co(^{15}NH_3)_6^{3+}/H_2O$ and $Co(acac)_3/CHCl_3$. These differences are far too small to be significant considering that the chemical shift scale of Cobalt complexes is of the order of 15,000 ppm. In addition, the shielding differences are in the opposite direction to that predicted by fourth-order perturbation theory based on the paramagnetic contribution (2.28). These authors offered no explanation for this discrepancy. In short, the present treatment of field dependent chemical shifts, if they exist, is not well understood. The complexes $Co(CN)_6^{3-}$ and $Co(NH_3)_6^{3+}$ possess O_h site symmetry at the Cobalt nucleus and the linewidths are expected to be field independent. For the complex $Coen_3^{3+}$, the site symmetry at the Cobalt nucleus is close to O_h symmetry. Within experimental error, the measured linewidths for these three complexes are independent of field strength. In the case of $Co(CN)_6^{3-}$, instrumental contributions to the linewidth may be significant as pointed out in Section 3.2.1.

For the remaining complexes in Table 4.1, this source of error is negligible. Figure 4.1 shows the only spectrum from which computer deconvolution was necessary due to significant overlap of the resonances at low field strength (2.114T). Other spectra were all obtained on resonance. The structures for the isomers of $Co(dien)_2^{3+}$ are shown in Figure 4.2. The nomenclature used is that recommended by the Commission on the Nomen-

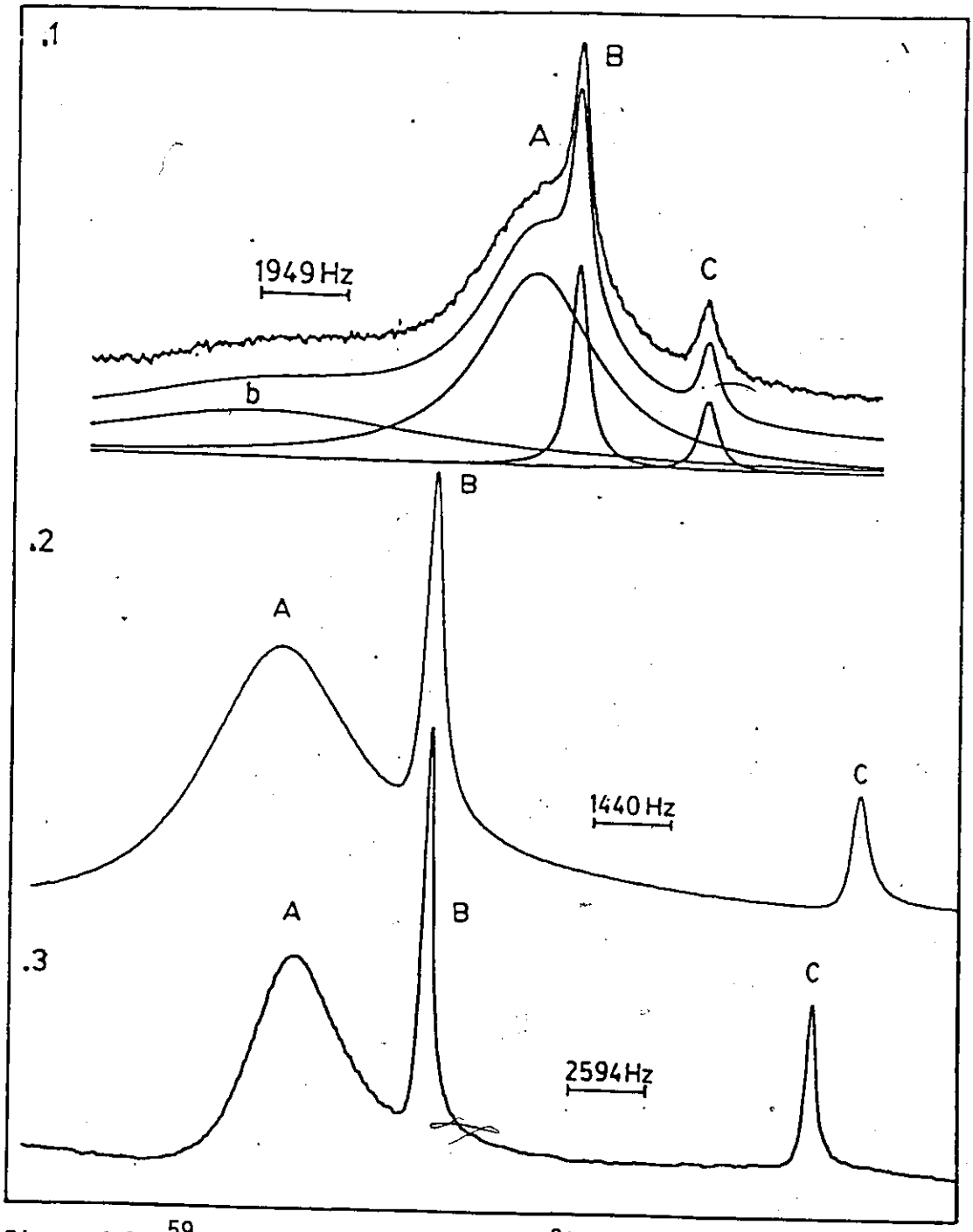

Figure 4.1 ^{59}Co NMR spectra of $Co(dien)_2^{3+}$ in H_2O. 4.1.1. Field strength 2.114T - experimental and simulated spectra. The curve b is background correction. 4.1.2. Field strength 5.872T. 4.1.3. Field strength 9.395T. (A) cae,dfb-$Co(dien)_2^{3+}$(tentative) (B) bfc,dae-$Co(dien)_2^{3+}$ (C) aed,cbf-$Co(dien)_2^{3+}$

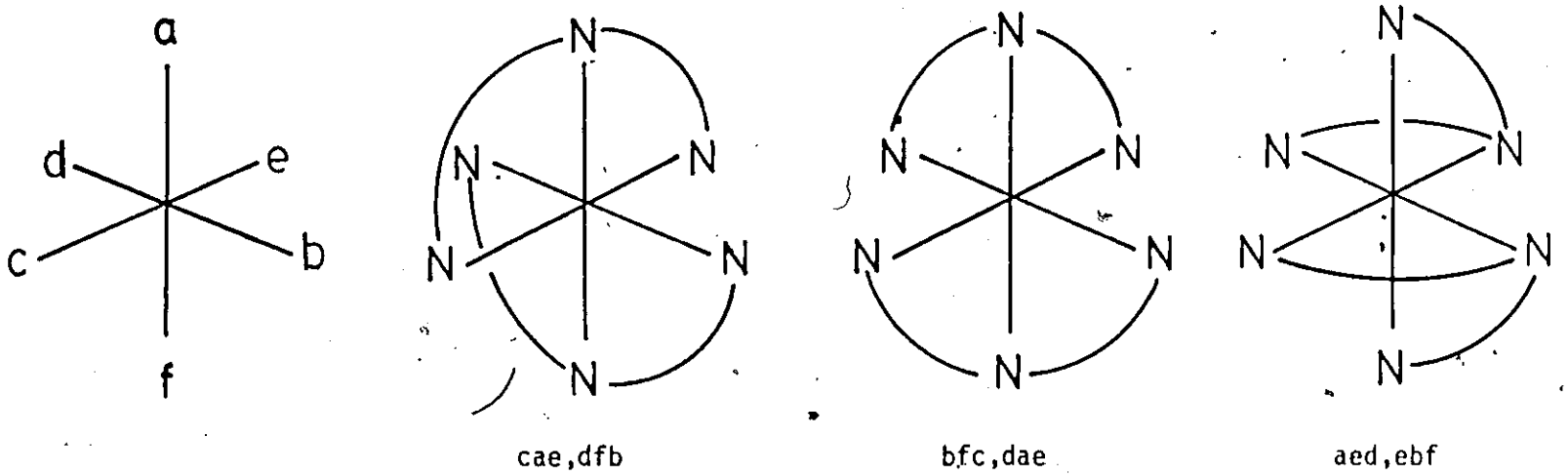

Figure 4.2 IUPAC labelling of the isomeric structures of $Co(dien)_2^{3+}$

clature of Inorganic Chemistry (4.6). For compounds 3-22, increases in linewidths varying from 30Hz to more than 9KHz were observed on increasing the field strength from 2.114T to 9.395T. These increases are listed in Table 4.3.

If the field dependence of linewidth indeed arises from relaxation due to chemical shielding anisotropy, in the limit of the white spectrum (extreme narrowing) approximation ($(\omega_0\tau_2)^2<<1$), a linear plot of linewidth versus the square of the field strength is anticipated. Formally, the intercept at $B_0=0$ gives the quadrupolar contribution and the slope the chemical shielding anisotropy. For compounds 4-14 in Table 4.1, the correlation coefficients for such plots are greater than 0.99, as is shown in Table 4.3. This is a satisfactory linear fit. The intercepts and slopes for these compounds are also given in Table 4.3. These compounds are generally of the types CoA_5B or trans-CoA_4B_2 giving site symmetries at the Co of C_{4v} or D_{4h}. For compounds 15-22, plots of line width versus field squared are not linear as shown by the much smaller correlation coefficients in Table 4.3. The broadening at the highest field is less than would have been expected for a B_0^2 correlation. Selected examples of such a non-linear dependence are shown in Figure 4.3. All of these compounds have lower site symmetry at Co. Most are of the type cis-CoA_4B_2 with C_{2v} symmetry or lower.

Another potential source of error is the use of D_2O as the solvent. Since most of the complexes are amines, exchange between N-H protons and solvent deuterons can occur. Such isotopic substitution can lead to sig-

Table 4.3

Linewidth Variation with Magnetic Field

Complex	Point Group	$\Delta\nu_{\frac{1}{2}}$ 94.457 / $\Delta\nu_{\frac{1}{2}}$ 21.252 (Hz)	$\Delta\nu_{\frac{1}{2}} / (\frac{\gamma B_o}{2\pi})^2$ x 10^{+12} (Hz^{-1})	$\Delta\nu_{\frac{1}{2}}$ at B_o=0 (Hz) a	b	r Corr. Coeff.[c]
1. $Co(CN)_6^{3-}$	O_h	1	0	-	5	-
2. $Co(NH_3)_6^{3+}$	O_h	11	0	-	183	-
3. $Coen_3^{3+}$	$D_3(O_h)$	27	0.0032		88	0.998
4. $Co(CN)_5NO_2^{3-}$	C_{4v}	1333	0.1583	3677	3677	0.999
5. $Co(CN)_5(NH_3)^{2-}$	C_{4v}	1238	0.1359	3113	3210	0.996
6. $Co(NH_3)_5Cl^{2+}$	C_{4v}	423		905	1092	
7. $Co(NH_3)_5CO_3^{+}$	C_{4v}	3448	0.4027	1682	1849	0.998
8. $Co(NH_3)_5NO^{2+}$	C_{4v}	47	0.0055	140	140	0.995
9. trans-$Coen_2Cl_2^{+}/H_2O$	D_{4h}	8156	1.0708	7587	7923	0.999
10. trans-$Coen_2(NO_2)_2^{+}$	D_{4h}	213	0.0254	600	1349	0.998
11. trans-$Co(dmgH)_2(NH_3)_2^{+}$	D_{4h}	3066	0.3625	5920	5920	0.999
12. trans-$Co(CN)_2en_2^{+}$	D_{4h}	8601	0.9968	7386	7995	0.994
13. aed,cbf-$Co(dien)_2^{3+}$	$C_{2h}(D_{4h})$	12	0.0014	404	423	0.998
14. cae,dfb-$Co(dien)_2^{3+}$[d]	$D_{2d}(D_{4h})$	447	0.0500	2655	3023	0.999
15. bfc,dae-$Co(dien)_2^{3+}$	$C_2(C_{2v})$	32		346	385	0.887
16. fac-$Co(NH_3)_3(CN)_3$	C_{3v}	132		519	566	0.893
17. mer-$Co(NH_3)_3(CN)_3$	C_{2v}	9536		2065	2750	0.942
18. cis-$Coen_2Cl_2^{+}$	C_{2v}	407		1820	1813	0.869
19. cis-$Coen_2(CN)_2^{+}$	C_{2v}	1813		1987	2622	0.805
20. $Coen(CN)_4^{-}$	C_{2v}	28			5331	0.250
21. $Co(NH_3)_4CO_3^{+}$	C_{2v}	2185		1558	1500	0.849
22. cis-$Co(NH_3)_4(CN)_2^{+}$	C_{2v}	7167		1156	1250	0.949

[a] Obtained by fitting to equations 2.15 and 2.18

[b] Obtained by extrapolation of plot versus B_o^2

[c] Correlation coefficient for B_o^2 plot.

[d] See footnote C Table 4.1

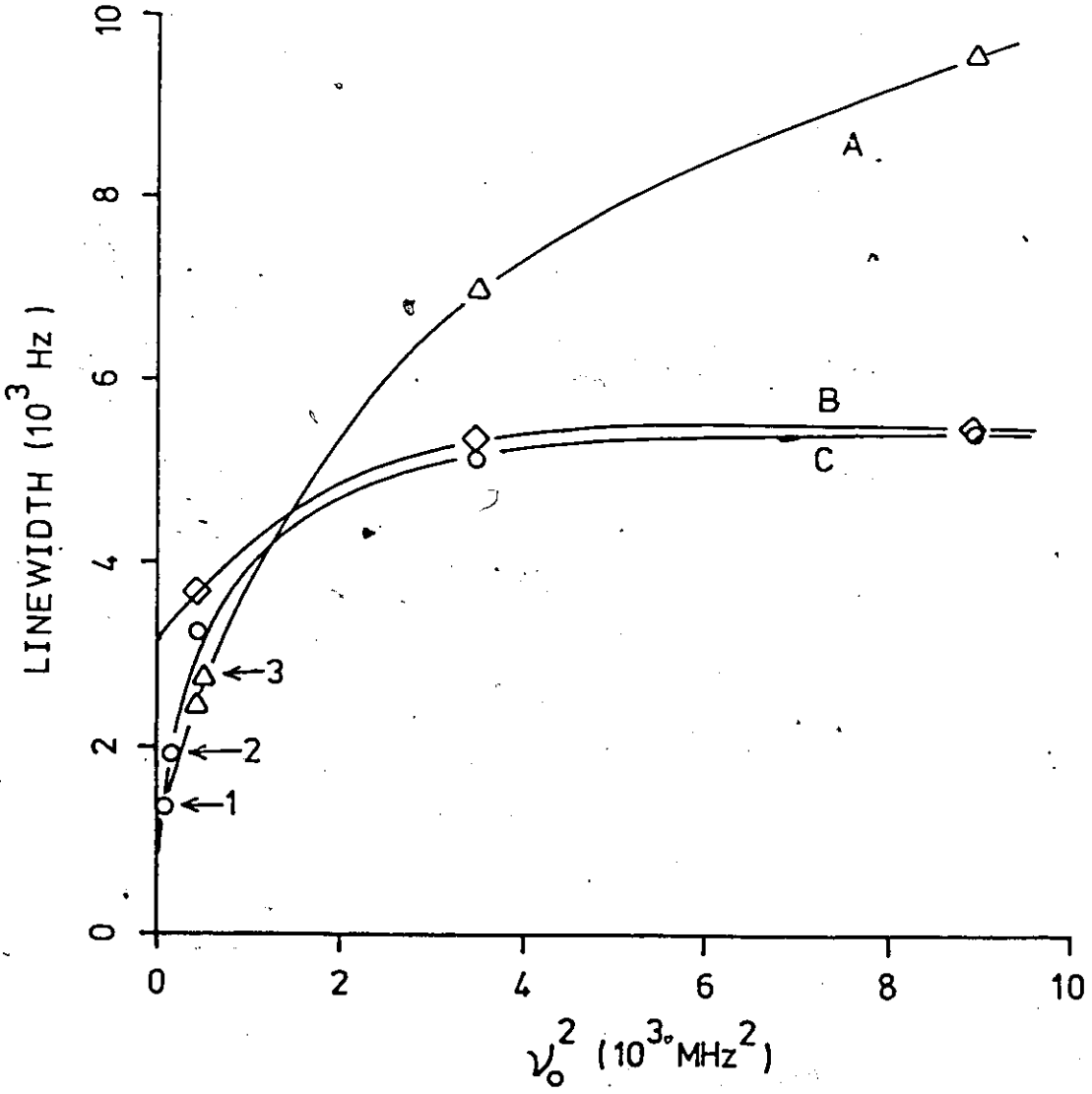

Figure 4.3 Plot of Linewidth versus ν_o^2 for (A) cis-$Co(NH_3)_4(CN)_2^+$ (B) cis-$Coen_2(CN)_2^+$ (C) $Co(NH_3)_4CO_3^+$. Data taken from reference 4.1(1), reference 4.3(2), and reference 4.4(3).

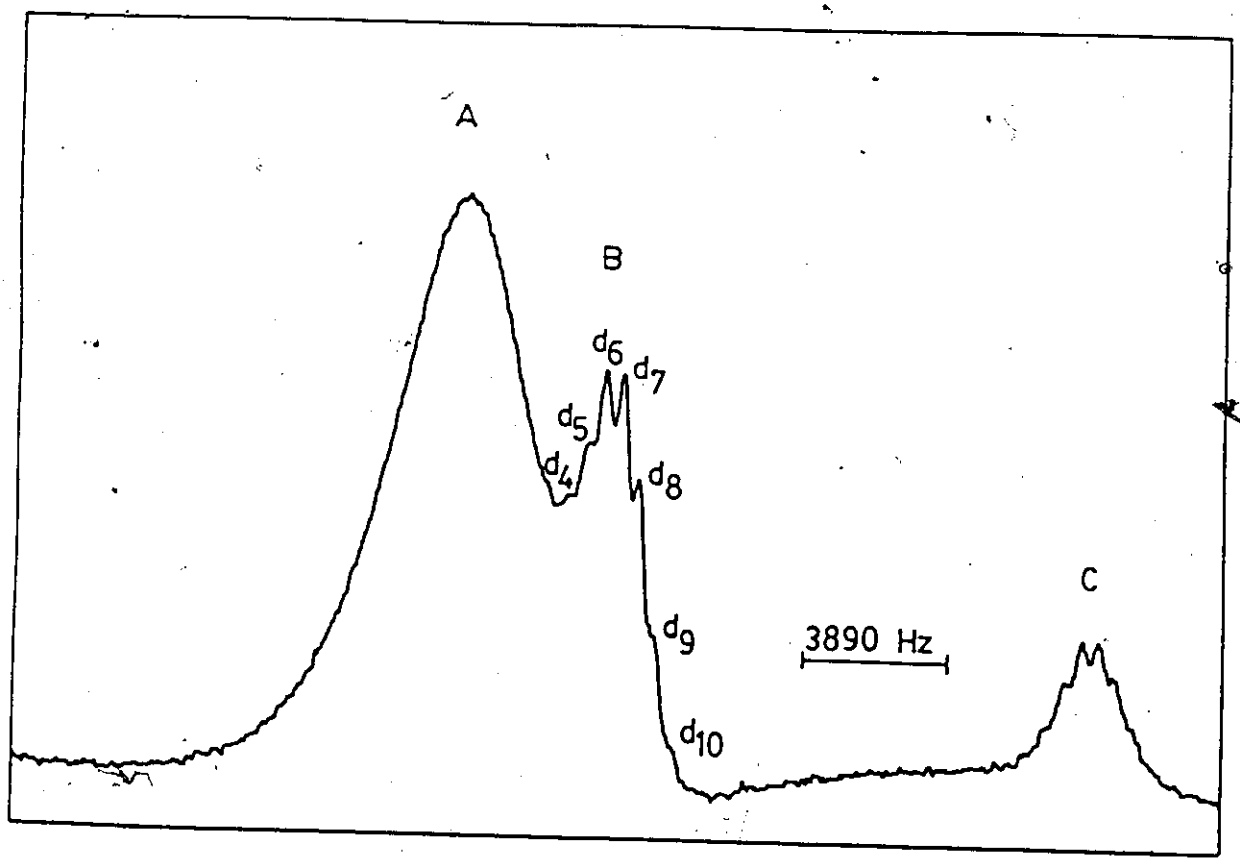

Figure 4.4 9.395T ^{59}Co NMR spectrum of $Co(dien)_2^{3+}$ after standing in D_2O.

nificant changes in ^{59}Co chemical shifts, as reported by Doddrell et al. (4.7). The results of such exchange are shown in Figure 4.4 for the system $Co(dien)_2^{3+}$. At the pH values of the present experiments, the exchange is slow, taking several hours to reach completion. If such an isotopic structure was unresolved due to inherently broad lines, it could lead to spurious additional broadening which would be field dependent. For this reason, the data of Table 4.1 were obtained from H_2O solutions in the pH range of 4-6.

4.3 Discussion

Of the various relaxation mechanisms outlined in Chapter 2, chemical shielding anisotropy is most likely to account for the observed field dependences of linewidth. The theory for this broadening mechanism was first presented by McConell and Holm (4.8) for I=1/2 nuclei, based on the general relaxation theory of Bloembergen, Purcell and Pound (2.1). The more generalized derivation is given by Spiess (Sec. 2.4.3). The contribution to T_2 from this mechanism, under extreme narrowing condition, i.e., $(\omega_o\tau_2)^2<<1$, is given by equation 2.18. When the contribution from the antisymmetric terms in the chemical shielding tensor has been neglected, evaluation of the contribution of shielding anisotropy to T_2 simply requires independent knowledge of $\Delta\sigma$ and τ_{CSA}.

There are two methods of obtaining shielding anisotropies. The first of the two is from direct single crystal NMR measurements. Spiess, Hass and Hartmann (4.9) have measured the chemical shielding anisotropy of the

complexes trans-$[Coen_2Cl_2]Cl \cdot HCl \cdot 2H_2O$, $[Co(NH_3)_5CN]Cl_2$, $[Co(NH_3)_4CO_3]Br$ and trans-$[Coen_2(NO_2)_2]NO_3$. With the exception of $[Co(NH_3)_4CO_3]Br$, plots of linewidth versus B_o^2 generate correlation coefficients of greater than 0.99 (Tables 4.3 and 5.11) for these complexes, therefore, $(\pi T_2)^{-1}$ is proportional to B_o^2.

The second method is calculation using Crystal Field Theory. It has been pointed out in Sec.2.2 that ^{59}Co chemical shift is dominated by the paramagnetic shielding term (σ^P) in the Ramsey (2.12-2.14) equation and that σ^P is directly proportional to the inverse of the energies of the first d-d electronic transitions observed in the visible spectrum. Simple Crystal Field theory can therefore be employed to estimate chemical shielding anisotropies. To illustrate the simplicity of the Crystal Field treatment of Yamatera (4.10) the calculations of the anisotropies for the complexes cis-trans $Coen_2Cl_2^+$, mer-fac $Co(NH_3)_3(CN)_3$, $Co(NH_3)_5Cl^{2+}$ and trans-$Coen_2(NO_2)_2^+$ serve as examples to the $\Delta\sigma_{cal}$ values listed in Table 4.6. For the following calculations, electronic absorption data were obtained from Wentworth and Piper (4.11) and Matsumoto et al. (4.12). The values for the radial factors $\langle r^{-3} \rangle (k')^2$ are those given by Fujiwara and co-workers (2.20). For a tetragonal D_{4h} complex;

$$\sigma_{zz} = \frac{-9.29 \times 10^3 \langle r^{-3} \rangle (k_1')^2}{\Delta E_z}$$

$$\sigma_{xx} = \sigma_{yy} = \frac{-9.29 \times 10^3 \langle r^{-3} \rangle (k_2')^2}{\Delta E_{x,y}}$$

The anisotropy is defined as

$$\Delta\sigma(\%) = \sigma_{zz} - 1/2\ (\sigma_{xx}+\sigma_{yy}) \text{ and}$$

$$\Delta\sigma = \frac{(\Delta\sigma(\%))\ x\ 10{,}000}{10^6}$$

For C_{2v} systems, the anisotropies can be calculated using equations from Sec.2.2 and the predicted first absorption band shifts of Yamatera (Table 4.4). As is shown in Table 4.4, the splitting of the first absorption band of a trans complex is twice as great as that of a cis complex, and that their level order is inverted. Appropriate electronic transitions and $\left\langle r^{-3}\right\rangle_c (k')^2$ together with calculated δ_1 values are collected in Table 4.5 and the calculated $\Delta\sigma_{cal}$ are collected in Table 4.6.

Table 4.4

Predicted Shifts and Splitting of First Absorption Band in Low Symmetry Co(III) Complexes (4.10)

Electronic Transition	MA_5B (+z)[a]	trans-MA_4B_2 (+z,-z)	cis-MA_4B_2 (+x,+y)	trans-MA_3B_3 (+x,-x,+z)	cis-MA_3B_3 (+x,+y,-z)
$d_{xy}\rightarrow d_{x^2-y^2}$	0 (A_2)	0 (A_{2g})	$2\delta_1$ (B_1)	$2\delta_1$ (A_2)	$2\delta_1$
$d_{yz}\rightarrow d_{y^2-z^2}$	δ_1[b] (E)	$2\delta_1$ (E_g)	δ_1 (A_2,B_2)	δ_1 (B_2)	$2\delta_1$ (A_2,B_2)
$d_{zx}\rightarrow d_{z^2-x^2}$	δ_1	$2\delta_1$	δ_1	$3\delta_1$ (B_1)	$2\delta_1$

[a] (+z), (+z,-z), etc., indicate the position of substitution

[b] $\delta_1 = 35/4\ D_t$

Table 4.5

Electronic Transitions and Band Shift Parameter δ_1

Complex	Electronic transitions[a,b] (cm^{-1})	$\left\langle \frac{1}{r^3} \right\rangle_c (k')^2$	δ_1 (cm^{-1})
fac-$Co(NH_3)_3(CN)_3$[c]	24916(A_2E) $\Delta E_{x,y,z}$	3.84	
mer-$Co(NH_3)_3(CN)_3$[c]	24916(A_2) ΔE_x	3.96	3869
	21047(B_2) ΔE_y	3.96	
	28785(B_1) ΔE_z	3.96	
trans-$Coen_2Cl_2^+$	16120(E_g) $\Delta E_{x,y}$	4.30	
	22490(A_{2g}) ΔE_z	4.30	
cis-$Coen_2Cl_2^+$	19305(A_2) ΔE_x	4.30	3185
	19305(B_2) ΔE_y	4.30	
	16120(B_1) ΔE_z	4.30	
$Co(NH_3)_5Cl^{2+}$	18720 (E) $\Delta E_{x,y}$	4.30	2630
	21350 (A_2) ΔE_z	4.30	
trans-$Coen_2(NO_2)_2^+$[d]	21000(E_g) $\Delta E_{x,y}$	4.30	1600
	24200(A_{2g}) ΔE_z	4.30	

[a] Ref. 4.11

[b] Ref. 4.13

[c] Ref. 4.12

[d] This work. The assymmetric band at 440nm was deconvoluted by fitting to two Gaussian forms.

A check on the validity of these calculations is provided by a comparison of the differences in the isotropic chemical shifts of isomer pairs calculated by this method with the experimental values. The agreement between the calculated value of 386 ppm and the observed value of 363 ppm for "cis"and "trans" $Coen_2Cl_2^+$, and the calculated value of 691 ppm and the observed value of 674 ppm for "mer" and "fac" $Co(NH_3)_3(CN)_3$ indicates that the calculations are relatively reliable.

If the assumption is made that the correlation times of these complexes are approximately the same, the broadenings due to chemical shielding anisotropy can be predicted. Qualitatively, the line broadening parallels the δ_1 values in Table 4.5. No field dependent broadening is expected for O_h complexes as observed. A complex such as $Coen_3^{3+}$, which approximates to O_h symmetry,has the anticipated small broadening of 27Hz between field strengths of 2.114T and 9.395T. A fac-CoA_3B_3 complex should have zero chemical shielding anisotropy based on the Crystal Field approximation, and this is consistent with the small field dependent broadening shown in Table 4.3 (130Hz). The mer-isomer on the other hand should have a large anisotropy, and this is paralleled by a large broadening of 9536Hz observed for mer-$Co(NH_3)_3(CN)_3$. The Crystal Field theory predicts that the trans isomer will have a larger chemical shielding anisotropy than that of the cis isomers, and this is reflected in the data for the complexes of cis and trans $Coen_2Cl_2^+$ with broadenings of 4072Hz and 8156Hz respectively. Similarly, the cis and trans isomers of $Coen_2(CN)_2^+$ show broadenings of 1813Hz and 8601Hz respectively. In general, the larger the δ_1 values of Table

4.5, the larger the chemical shielding anisotropies and the larger the increases in linewidths shown in Table 4.3.

It is important to point out that chemical shielding anisotropies in the solid state and in solution are not necessarily identical, and that there are inadequacies in any Crystal Field treatment. Within these limitations, the chemical shielding anisotropies in Table 4.6 have only order of magnitude reliability.

There are three ways to estimate the correlation time. The first is to use the linewidths at zero field obtained from the experimental data as a measure of the quadrupolar coupling relaxation and combine this information with quadrupole coupling constants from NQR data in the literature. The second is to calculate the correlation times from the modified Debye equation (4.14).

$$\tau_c = \frac{4\pi n a^3}{3kT} f, \qquad f = \frac{a_{solute}}{6a_{solvent}} \quad (\tau_c = \tau_2)$$

The factor "f" is known as the Gierer-Wirtz correction factor. Both sets of correlation times are shown in Table 4.6. The former is listed under τ_Q and the latter $\tau_{Deb\text{-}solv}$. In the Debye calculations, a value of the radius (a) corresponding to a solvated complex has been used. If the calculations were carried out with a free complex ion radius, the τ_Q and $\tau_{DEB\text{-}free\ ion}$ would be off by an order of magnitude. The most simple-minded rationalization is an implication of a second solvent shell having some finite life time at the complex, i.e., rotating as a kinetic unit within the isotropic model.

Table 4.6

Correlation Times and Chemical Shift Anisotropies

Complex	$\tau_Q \times 10^{11}$ sec	$\tau_{Deb\text{-}solv} \times 10^{11}$ sec	$\Delta\sigma_{x\text{-}tal}$ [a]	$\Delta\sigma_{cal}$ [b]	$\tau_{CSA} \times 10^{8}$ sec		$\Delta\nu_{1/2}$ [c] calc (Hz)
					$\Delta\sigma_{x\text{-}tal}$	$\Delta\sigma_{cal}$	
Tr-$Coen_2Cl_2^+$	1.652	1.716	0.00465	0.007105	2.517	1.112	13.8
Tr-$Coen_2(NO_2)_2^+$	2.275	2.585	0.00025	0.000252	20.790	4.567	0.1
$Co(NH_3)_5Cl^{2+}$	0.686	0.800		0.002630		1.599	0.83
$Co(NH_3)_5CN^{2+}$			0.00225	0.003907	13.092	1.733	15.3
$Co(NH_3)_4CO_3^+$	2.918	3.080					
cis-$Coen_2Cl_2^{2+}$	1.082	1.292		0.004158			

[a] Anisotropies obtained from single crystal NMR, Hartmann and Spiess(4.9)

[b] Anisotropies calculated from spectroscopic data.(4.11 - 4.13)

[c] Calculated contribution to $\Delta\nu_{1/2}$ at 94.457MHz assuming τ_Q and $\Delta\sigma_{cal}$.

Experimental justification for this point is given in Chapter 5. Finally, if the assumption that the correlation time responsible for quadrupolar relaxation (rotational re-orienting correlation time) is the same as that modulating the relaxation due to chemical shielding anisotropy, then τ_{CSA} obtained from using experimental linewidth and both crystal shielding anisotropies and calculated anisotropies for complexes showing a B_o^2 dependence would parallel or agree with τ_Q's. τ_{CSA} calculated from $\Delta\sigma_{x\text{-}tal}$ and $\Delta\sigma_{cal}$ are also listed in Table 4.6. Precaution must be taken since $\Delta\sigma$ values have only order of magnitude reliability, thus, the same is true for correlation times derived from them.

It is clear from Table 4.6 that the values obtained for τ_{CSA} ($\sim 10^{-8}$sec) are much longer than anticipated and are three orders of magnitude larger than τ_Q. The correlation times obtained from quadrupolar coupling constant and from the Debye relation are in reasonable agreement and are of a magnitude (10-30psec) consistent with accepted values in the literature for this size molecule. To demonstrate the discrepancy, the last column of Table 4.6 lists the increases in linewidths between 2.114T and 9.395T calculated from $\Delta\sigma_{cal}$ obtained from spectral data and correlation time (τ_Q) obtained from quadrupole coupling constants. When compared with the experimental values of Table 4.3, the disagreement is well outside experimental error.

There are, therefore, two problems in the interpretation of the field dependence of the linewidths of these Co(III) complexes in terms of relaxation due to chemical shielding anisotropy:

i) The broadening observed are two to three orders of magnitude greater than predicted from the estimated anisotropies and correlation times.

ii) Low symmetry complexes do not show a linear dependence of line widths with B_o^2.

At the same time, the qualitative variation from compound to compound is that expected of the anisotropies. It is, therefore, appropriate to consider possible deviations from equation 2.18.

In general, the rate of spin-spin relaxation, R_2 observed for a quadrupolar nucleus can be expressed as a sum of various relaxation rates and non-relaxation line broadening mechanisms as expressed in equation 4.1;

$$\frac{1}{T_{2obs}} = \frac{1}{T_{2Q}} + \frac{1}{T_{2SC}} + \frac{1}{T_{2CSA}} + \frac{1}{T_{2DD}} + \frac{1}{T_{2SR}} + \Delta\nu_{\Delta\chi} \qquad [4.1]$$

where T_{2Q}^{-1} (quadrupolar interaction); T_{2SC}^{-1} (scalar coupling); T_{2CSA}^{-1} (chemical shielding anisotropy); T_{2SR}^{-1} (spin rotation); $\Delta\nu_{\Delta\chi}$ (anisotropic susceptibility) and T_{2DD}^{-1} (dipolar-dipolar). In the following sections, it will be shown systematically that contributions from T_{2DD}^{-1}, $\Delta\nu_{\Delta\chi}$ and T_{2SR}^{-1} are negligible. The T_{2SC}^{-1} contribution to Cobalt linewidths is less than 10 per cent of the total, effectively leading to the interpretation that line broadening is due to T_{2CSA}^{-1} and T_{2Q}^{-1}. T_{2Q}^{-1} is independent of B_o^2 within the extreme narrowing condition; however, outside the extreme narrowing condition T_{2Q}^{-1} decreases with B_o^2, which is opposite to the experimentally observed effect.

SECTION 4.3.1 Dipolar Relaxation, $\frac{1}{T_{2dd}}$

It is extremely common in the literature to neglect dipolar relaxation contribution in studying relaxation rates of quadrupolar nuclei in spite of their relatively larger magnetic dipole moment (μ) in comparison to that of a proton. For example, the magnetic dipole moment of $^{93}Nb(I=9/2)$ and ^{99}Tc (I=9/2) is +6.167 and +5.68 respectively (4.15) in units of nuclear magnetons ($e\hbar/Mp$). These values are much larger than the proton magnetic moment of +2.79278 ($e\hbar/Mp$). It is, perhaps, instructive to examine the relative effectiveness of the two relaxation effects of different origin, namely the magnetic dipole-dipole interaction (magnetic) and the electric quadrupole interaction (electric).

For simplicity, consider an isolated Cobalt nucleus in the presence of a fluctuating electric field produced by the motion of a proton; for example, translational diffusion as would be the case in solution, at a separation r, the magnetic interaction of the Cobalt nucleus with the proton is given by (2.31).

$$\hat{H}_m \alpha \mu_{Co} \cdot \frac{\mu_{H^+}}{r^3}$$

the electric interaction is given by (2.31)

$$\hat{H}_e \alpha (eQ)_{Co} \cdot \frac{e_{H^+}}{r^3}$$

The dependence on the distance r is thus constant and at time t

$$\frac{\hat{H}_e}{\hat{H}_m} \alpha \frac{e_{H^+}(eQ)_{Co}}{\mu_{Co}\ \mu_{H^+}}$$

The transition probability W, i.e., the nucleus flips its spin direction under the influence of time-dependent interaction, is proportional to $\hat{H}^2$ and the relaxation time governing the transition can be approximated by W^{-1}, therefore,

$$\frac{W_e}{W_m} \alpha \frac{(e_{H^+}(eQ)_{Co})^2}{\mu^2_{H^+}\ \mu^2_{Co}}$$

For the case of Cobalt (I=7/2), μ= + 4.62 (eħ/Mp) and Q = + 0.4 x $10^{-24}cm^2$.

$$\frac{W_e}{W_m} \alpha\ 5 \times 10^3$$

Since $T_1 \alpha W^{-1}$, the relaxation time arising from quadrupolar effects may easily be 3 or 4 orders of magnitude smaller than that of relaxation via magnetic dipole-dipole interactions. In short, the relaxation effect of electric origin is 3 or 4 orders of magnitude larger than that of magnetic origin. The above consideration, of course, is an over-simplified approach since distortion of the ion core surrounding the nucleus also contributes to the field gradient. Thus, the discussion given above can be reasonably assumed to be the lower limit of the electric relaxation effect. This type of analysis is supported by experimental T_1 values of Cobalt complexes which are in the sub-millisecond range in comparison to those of protons which are usually in the range of secs - a change of 4 or 5 orders of magnitude.

In general, the total dipolar-dipolar relaxation rates consist of contributions from both inter and intra molecular dipole-dipole relaxation. The motion primarily responsible for intra-molecular relaxation has been well documented and is generally attributed to that of rotational re-orientation. On the other hand, the origin of inter-molecular dipole-dipole relaxation is due to that of translational motion. The total relaxation rate is given by equation 4.2, i.e.,

$$\frac{1}{T}_{1D\text{-}D} = \frac{1}{T}_{1\ intra} + \frac{1}{T}_{1\ inter} \qquad [4.2]$$

For I = 1/2, coupling of magnetic dipole moments dominates the relaxation. For protic solvents of small size, the inter-molecular relaxation contribution becomes significant. Most often, it has the same order of magnitude as intra-molecular relaxation (2.37).

The intra-molecular dipole-dipole relaxation is well understood and numerical estimation is straightforward by application of equation 2.8. A general calculation of the intra-molecular relaxation rate is extremely complex and the interested reader is referred to the excellent articles by Hertz (2.51, 2.52) for detailed discussion. In the presence of quadrupolar relaxation, the inter-molecular dipole-dipole contribution to the Cobalt relaxation rate can reasonably be assumed to be negligible. $T_{2Cod\text{-}d}^{-1}$ is calculated as a function of τ_c at a field strength of 9.395T for the complexes $Coen_3^{3+}$ and $Co(NH_3)_6^{3+}$ and the results are tabulated in Table 4.7. In the range of τ_Q values listed in Table 4.6, the dipole-dipole contribution to the total Cobalt relaxation rate is clearly negligible as reflected by the values in Table 4.7.

Table 4.7≠

Calculated contribution of intra-molecular dipole-dipole relaxation rates to Cobalt relaxation rates.

$\tau_2 \times 10^{11}$ sec	$T_2^{-1}(sec^{-1})$	
	$Coen_3^{3+}$	$Co(NH_3)_6^{3+}$
1	1.40	1.87
5	7.00	9.27
10	13.46	17.87
50	40.08	53.21
100	55.17	73.23
1000	289.40	384.19

≠ $r_{Co-N-H} = 2.7963 \times 10^{-10}_m$

$r_{Co-N-C-H} = 3.9290 \times 10^{-10}_m$

$\gamma_{Co} = 6.2928 \times 10^{7}$ rad-sec^{-1} T^{-1}

$\gamma_H = 26.7519 \times 10^{-7}$ rad-sec^{-1} T^{-1}

SECTION 4.3.2 Magnetic Field Alignment. $\Delta\nu_{\Delta\chi}$

The formal theory for the alignment of anisotropic magnetic susceptibility with the magnetic field has been treated in Sec. 2.4.6. As pointed out earlier, this is a broadening mechanism not involving relaxation. In sufficiently high magnetic field strengths, the molecule tends to align itself with the magnetic field, B_0. For a quadrupole nucleus this results in a non-zero time average of the electric field gradient at the nucleus. The interaction of the quadrupole moment with the electric field gradient acts as a small perturbation to the degenerate Zeeman levels, thus lifting the degeneracy. Under favourable circumstances, this would split the degeneracy of a nuclei of spin I into 2I + 1 energy levels giving rise to 2I transitions in a magnetic field. In the case of Cobalt (I=7/2), seven transitions are anticipated and the separation between adjacent energy levels is given by equation 2.19. In the limit of high field, first order approximation (2.31), first order perturbation treatment showed that for nuclei of half-integral spin, the splitting of the 2I lines is symmetrical about the centre resonance corresponding to the transition $-1/2 \leftrightarrow 1/2$. Furthermore, the first order shift vanishes for $I_z(m) = 1/2$ and the intensities of the various lines are proportional to $|\langle M|I_x|M-1\rangle|^2$ (2.31). For I = 3/2 the intensity ratio for the three transitions $-3/2 \leftrightarrow -1/2$: $-1/2 \leftrightarrow 1/2$: $1/2 \leftrightarrow 3/2$ is 3:4:3. Similarily, for I=5/2 the ratio are 5:8:9:8:5. If the individual lines are unresolved, this will appear as an additional broadening. Under the strong field treatment, the separation between the extreme lines for Cobalt complexes is simplified from equation 2.19. For complexes with higher than C_{3v} (axial) symmetry:

$$\Delta\nu_{\Delta\chi}(\text{Hz}) = 1.6470 \times 10^{27} \left(\frac{e^2qQ}{h}\right)\left(1+\frac{\eta_Q^2}{3}\right) \Delta\chi \frac{B_o^2}{T} \qquad [4.3]$$

For complexes with less than axial symmetry:

$$\Delta\nu_{\Delta\chi}(\text{Hz}) = 1.6470 \times 10^{27} \left(\frac{e^2qQ}{h}\right)\left(1+\frac{\eta_Q^2}{3}\right) \left(\Delta\chi + \eta_Q \frac{(\chi_{xx}-\chi_{yy})}{2}\right) \frac{B_o^2}{T} \qquad [4.4]$$

$\Delta\chi$ may be estimated from the absorption spectral data of Wentworth and Piper (Table 4.5) using the theory of Griffith and Orgel (4.16). This theory predicts that the magnetic susceptibility anisotropy will exactly parallel the chemical shielding anisotropy so that the trend from compound to compound would be that observed. With known quadrupolar coupling constants (4.9, 4.17) as well as equations 4.3 and 4.4, $\Delta\nu_{\Delta\chi}$ is estimated at B_o = 5.8719, 9.3950T at a probe temperature of 24°C and the results are collected in Table 4.8.

Table 4.8

Estimation of Anisotropic Susceptibility Broadening ($\Delta\nu$) at RT (24°) and B_o = 5.8719 and 9.3950T

Complex	e^2qQ/h[a] (MHz)	η_Q[b]	$\Delta\chi$ ($10^{-33}m^3$)	$\Delta\nu$(Hz) 5.8719T	$\Delta\nu$(Hz) 9.3950T
trans-$Coen_2Cl_2^+$	60.14	0.225	0.5366	6.3	16.0
cis-$Coen_2Cl_2^+$	36.05	0.173	0.8721[c]	6.1	15.5
$Co(NH_3)_5Cl^{2+}$	31.74	0.251	0.5607	3.5	8.9
$Co(NH_3)_5CN^{2+}$	26.57	0.185	0.6512	3.3	8.6
trans-$Coen_2(NO_2)_2^+$	13.22	0.727	0.0665	0.2	0.5

a = References (4.1 and 4.9) b $\frac{V_{xx}-V_{yy}}{V_{zz}}$

c the value is $\Delta\chi + \frac{\eta_Q(\chi_{xx}-\chi_{yy})}{2}$ as defined in equation 4.4.

It is important to point out that in this calculation, solid state quadrupole coupling constants were employed thus maximizing the field gradient effect. The estimation of χ values from solution spectral data can be safely assumed to have an inherent error of about 20%, thus the $\Delta\nu_{\Delta\chi}$ values in Table 4.8 can be regarded as the upper limit for this mechanism. In other words, the $\Delta\nu_{\Delta\chi}$ values can be considered as the maximum contribution to Cobalt linewidth as specified by the conditions in Table 4.8. In general, the agreement between $\Delta\chi$ values and the shielding anisotropy values listed in Table 4.6 is poor, which could be the result of an over simplification of the Griffith and Orgel approach to susceptibility. It is, however, clear that within this crude approximation the $\Delta\nu_{\Delta\chi}$ values are well outside experimental errors when compared with the broadening listed in Table 4.3, therefore, orientation effects are too small to cause the observed broadening.

SECTION 4.3.3 Spin-Rotation Relaxation, $\frac{1}{T_{2SR}}$

The origin of spin-rotation relaxation is due to local magnetic fields generated by circulating electron currents at the nucleus modulated by rotation of the molecule. Since the effect is directly proportional to the molecular rotational (angular) velocity, we may therefore expect this mechanism to be important for small molecules. For molecules with considerable inter-molecular interactions, for example hydrogen bonding, the angular velocities are affected by the strength of the interaction and the residence life time at a particular position due to these interactions.

For the complexes considered in this work, anisotropies obtained from single crystal NMR measurements as well as those calculated from solution spectral data can equally be employed for the estimation of the spin-rotation constant using the relationship proposed by Rigny and Virlet (4.18)

$$\vec{\vec{C}} = -\left(\frac{\mu_N}{\mu_\beta}\right)\left(\frac{\hbar}{\theta}\right)\vec{\vec{\sigma}} \qquad [4.5]$$

In equation 4.5, μ_N is the nuclear magneton, μ_β is the Bohr magneton, $\hbar$ is Planck's constant, θ is the moment of inertia. $\vec{\vec{\sigma}}$ is the shielding tensor and $\vec{\vec{C}}$ is the spin-rotation tensor. This relationship has been successfully applied by Deverell (4.19) in estimating spin-rotation constants for fluorine and phosphorous compounds. The agreement between values estimated from NMR paramagnetic shielding constants and molecular beam experiments are generally within 10%. In constrast, estimation of spin-rotation constants from spin-lattice relaxation times, in general, gave extremely poor results. This has been argued to be due to an incorrect estimation of the τ_{SR} from the Hubbard relationship relating the rotational re-orientation correlation time. Although Green and Powles (2.37) have experimentally confirmed the Hubbard relationship; the numerical factor of "1/6"

$$\tau_{SR}\tau_Q = \frac{\theta}{6kT}$$

has been questioned (2.37). With the spin-rotation constant estimated from equation 4.5, and the general equations of Sec. 2.4.2, contributions to Cobalt relaxation rates are calculated at a probe temperature of 24°C. The appropriate values of C, σ, τ and T_{2SR}^{-1} are collected in Table 4.9. τ_Q is given

Table 4.9

Estimated Line Broadening Contribution From Spin-Rotational Relaxation Mechanism

$\sigma, C, \tau, \theta, T_2$	Complex			
	trans-$Coen_2Cl_2^+$	trans-$Coen_2(NO_2)_2^+$	$Co(NH_3)_5CN^{2+}$	$Co(NH_3)_4CO_3^+$
σ_{iso}		0.006323		0.009732
σ_{xx}	0.010600	0.006200	0.006000	0.009900
σ_{yy}	0.010900	0.006500	0.005900	0.010400
$\sigma_{zz}(\sigma_{\parallel})$	0.006100	0.006100	0.008200	0.008900
$\sigma_{\perp}$	0.010750	0.006350	0.005950	0.010150
C_{xx} (KHz)	47.050	26.102	53.537	62.045
C_{yy} (KHz)	50.377	27.365	52.645	68.776
$C_{zz}(C_{\parallel})$ (KHz)	26.378	20.642	101.935	119.829
$C_{\perp}$ (KHz)	48.714	26.734	53.091	65.411
$\theta_{xx}(10^{-37}gmcm^2)$	1.306	1.364	0.644	0.916
$\theta_{yy}(10^{-37}gmcm^2)$	1.306	1.304	0.644	0.868
$\theta_{zz}(\theta_{\parallel})(10^{-37}gmcm^2)$	1.328	1.395	0.462	0.427
$\theta_{\perp}(10^{-37}gmcm^2)$	1.306	1.364	0.644	0.892
τ_{xx} $(10^{-14}sec)$	7.254	62.363	2.082	4.061
τ_{yy} $(10^{-14}sec)$	7.254	62.363	2.082	3.848
$\tau_{zz}(\tau_{\parallel})(10^{-14}sec)$	7.376	12.932	1.456	1.890
$\tau_{\perp}$ $(10^{-14}sec)$	7.254	62.363	2.082	3.955
τ (sec)	0.837	0.316	2.857	1.575
$\Delta\nu_{\frac{1}{2}}$ (Hz)	0.4	1	0.1	0.2

in Table 4.6. The contribution listed in the last row of Table 4.9 clearly demonstrates that spin-rotation is negligible at 24°C for complexes of this size - a generally valid assumption. Before closing this discussion, it is appropriate to point out that the approach that has been taken to calculate the spin-rotation relaxation contribution to the Cobalt relaxation rate is self-justified in that the results are in good agreement with the experimental work of Adler and Loewenstein (4.20). By studying the temperature dependence of ^{59}Co T_1 of the complexes $Coen_3Cl_3$ and $Co(NH_3)_6Cl_3$, these authors were able to show that at room temperature the spin rotation relaxation mechanism can be conclusively eliminated. However, above 60°C, the spin-rotation mechansim dominates the relaxation of $Co(NH_3)_6Cl_3$. Finally, since solid state shielding anisotropies agreed within a half order of magnitude with solution anisotropies calculated from absorption spectral data, the estimated contribution from solid state shielding values is relatively reliable.

SECTION 4.3.4 Chemical Exchange and Scalar Relaxation

The details of scalar relaxation have been treated in Sec. 2.4.3. In this section, the discussion will deal with scalar relaxation of the first kind, i.e., chemical exchange. For reasons which will become apparent later, a discussion of scalar relaxation of the second kind is deferred to Sec.5.3.2.

It has been stated in the general remarks of Sec. 2.3 that any mechanism which gives rise to a fluctuating local magnetic field causes relaxation. In the case of scalar (spin-spin) coupling between I and S spins,

when the coupling tensor A is time-dependent, a relaxation mechanism results (scalar relaxation of the first kind). This situation arises when chemical exchange is present. Two possible origins can be suggested for chemical exchange for the complexes studied in this work. The first is proton exchange between an ammine group of the first coordination sphere and the solvent. The rate for this exchange has been estimated by Wilinski and Kurland (4.21) for the case of $Coen_3^{3+}$. At pH=5, a lifetime $\tau_o \sim 10^5$ sec is predicted which is consistent with the deuterium exchange illustrated in Figure 4.5. Therefore, this process is too slow to cause any broadening. It is for this reason that all studies were carried out in this pH range. A second chemical process is the formation and breaking of hydrogen bonds between a first coordination sphere ligand and the solvent. If the rate of H-bonding exchange is much larger than the coupling A or the spin lattice relaxation rate R_1 for either I or S spin and if the time the two nuclei are coupled is much longer than the time they are uncoupled, τ_S or τ_I in equation 2.12 and 2.13 can be replaced by τ exchange. Using an upper value of $A \sim 10Hz$ a value of τ exchange $>>10^{-3}$ is required to produce any observable broadening, and as such, scalar relaxation of the first kind becomes irrelevant.

For the purpose of conclusion, the results of Sec. 5.3.2 will be stated here as less than 10% contribution to the total relaxation rate of Cobalt.

4.3.5 Quadrupolar and Chemical Shielding Anisotropy Relaxation

From the discussion presented in Sec. 4.3.1-4.3.4, equation 4.1 effectively reduces to equation 4.6;

$$\frac{1}{T_{2obs}} = \frac{1}{T_{2CSA}} + \frac{1}{T_{2Q}} + \frac{1}{T_{2SC}} \qquad [4.6]$$

From Sec. 5.3.2, scalar relaxation of the second kind contributes no more than 10% in aqueous solution for low symmetry Co(III) complexes. The exact expression for chemical shielding anisotropy is given in Sec. 2.4.5. This expression removes all approximations except the assumption of anisotropic rotation of the molecule. Before a complete evaluation of equation 2.12, the aspect of asymmetric rotation deserves some attention. It must be pointed out that a detailed discussion of the theory of anisotropic rotational diffusion is far beyond the scope of this thesis, it is therefore desirable to examine the general results of the treatment governing relaxation rates. The interested reader is referred to the original articles by Spiess (2.35) and Huntress (4.22). General expressions for spin-spin and spin-lattice relaxation rates allowing for different rotational motions about different axes have been derived by Spiess (2.35). A few point are to be noted: -

i) $\tau = \frac{1}{6D_S} \cdot \frac{1}{C}$ where

C is the correction factor due to asymmetric rotational diffusion - a function of $\eta_D = \frac{D_{yy}-D_{xx}}{D^*}$ $D^* = D_{zz}-D_S$, and $A = (1 + \eta_D^2/3)^{\frac{1}{2}}$, $D_S = \frac{1}{3}(D_{xx} + D_{yy} + D_{zz})$

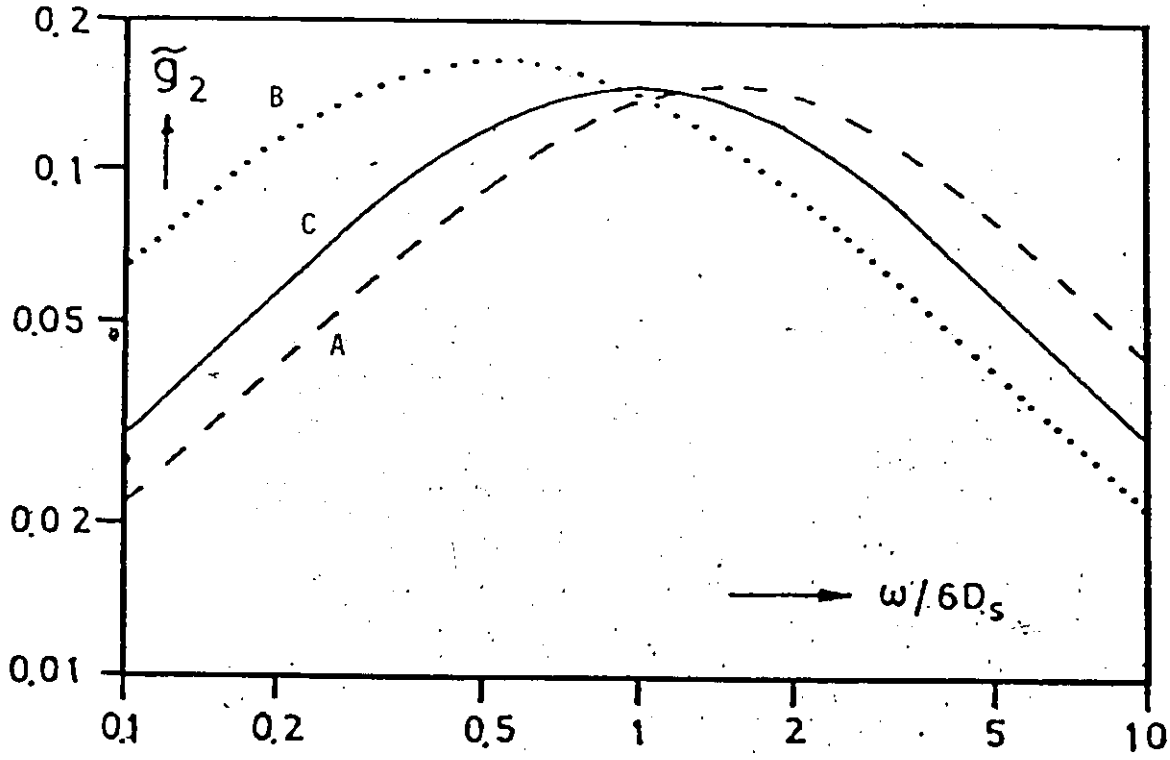

Figure 4.5 Reduced $g_2(\omega)$ for anisotropic rotational diffusion for a benzene derivative (Reference 2.35 page 135).

$Z_\lambda \| y_D$, $Y_\lambda \| x_D$ (case A)

$Z_\lambda \| z_D$, $X_\lambda \| x_D$ (case B)

isotropic motion (case C)

$\frac{D_s}{D^*} = 1$, $D^* = D_{zz} - D_s$

$D_{zz} = 2D_s$, $D_{yy} = \frac{5}{8}D_s$, $D_{xx} = \frac{3}{8}D_s$

$\eta_D = \frac{1}{4}$, $\eta_\lambda = 0.5$

ii) $R_{1,2} \alpha$ Re $G_\ell(\omega)$

$\simeq \tilde{G}_\ell(\omega)$ (reduced fourier transform of the correlation function)

iii) $G_\ell(\omega)$ involves coupling parameters of the Hamiltonian of interest, it is therefore not the usual spectral density encountered for isotropic diffusion motion.

A complete evaluation of c and $\tilde{G}_\ell(\omega)$ requires complete knowledge of (i) the Eulerian angles α, β, γ relating the principal axis system (X,Y,Z) of the interaction (λ) tensor and that of the principal axis system (x,y,z) of the diffusion (D) tensor, (ii) the different diffusion constants about the different axes, which are neither experimentally readily available nor is there any simple method of estimating these parameters; as such, numerical analysis is necessary. Figure 4.5 reproduced from Spiess (2.35) illustrates diagramatically the effect of the reduced fourier transform of the correlation function, $\tilde{G}_\ell(\omega)$, as a function of $\omega/6D_s$ ($\sim \omega\tau_{\ell k}$) of asymmetric rotational diffusion corresponding to a highly asymmetric rotor. The most important features of Figure 4.6 are as follows:

i) when $\omega/6D_s \simeq 1$, $\tilde{g}_2(A) \simeq \tilde{g}_2(B) \simeq \tilde{g}_2(C)$

ii) when $\omega/6D_s < 1$, $\tilde{g}_2(B) \simeq 2\tilde{g}_2(C)$

$\tilde{g}_2(A) \simeq 2/3\tilde{g}_2(C)$

iii) when $\omega/6D_s > 1$, $\tilde{g}_2(A) \simeq 3/2\tilde{g}_2(C)$

$\tilde{g}_2(B) \simeq 2/3\tilde{g}_2(C)$

If the origin of the field dependences which arises from anisotropic rotational diffusion is in the limit described by (ii) above (since $\tau_{Q's}$ of Table 4.6 are of the order of 10 psec), a maximum broadening factor of $\sim 2\tilde{g}_{iso}$ is anticipated at constant field strength. Since $\tilde{g}_{\ell}(\omega) \alpha R_{1,2}$, the last column in Table 4.6, which is a calculation of $\tilde{g}_{iso}$ for chemical shielding anisotropy at 94.457 MHz, serves to demonstrate that anisotropic diffusion cannot be responsible for the large discrepancies observed.

Returning to equation 2.12, the first term gives the contribution to the linewidth from rapid chemical exchange processes. If the lifetime in a given site is $\tau_o << \pi\Delta\nu/2$, where $\Delta\nu$ is the chemical shift difference, the standard approximate solution of the modified Bloch equation predicts an additional broadening proportional to B_o^2. The origin for such a term has been suggested in the last section. Since there is no proton exchange, the first of the two processes can be eliminated. Recently, it has been shown that second sphere hydrogen bonding in Cobalt complexes causes chemical shift changes by several hundred parts per million (4.23). At 94.457 MHz, this corresponds to a frequency separation of 10^4Hz. Such a frequency separation would require hydrogen bond lifetimes of 10^{-6} - 10^{-7} sec to produce the observed broadening. Lifetimes of this magnitude are much longer than those reported for uncomplexed amines (4.24) 10^{-10} - 10^{-12} sec but perhaps not entirely unreasonable for strong hydrogen bonds. If this were the origin of the field dependent broadening, it should be equally applicable to symmetric complexes such as $Co(NH_3)_6^{3+}$ and there is no simple reason to expect the trends for chemical shielding anisotropy, i.e., trans > cis, mer. > fac. to be obeyed. In addition, it cannot account for the lack of

B_o^2 dependence for the lower symmetry complexes such as cis-$Coen_2Cl_2^+$ and $Co(NH_3)_4CO_3^+$.

The second term in equation 2.12 arises from the antisymmetric term in the chemical shielding tensor. Buckingham and Malm (2.41) have calculated the point groups for which such terms are non-vanishing using group theoretical treatment and their results are reproduced in Table 4.10.

It is particularly important to note that symmetries as high as C_{4h}, C_{6h}, etc. possess non-vanishing components in the paramagnetic shielding term. Initially, it would appear that contribution from this term could be neglected for the complexes under consideration. However, if the first sphere ligands indeed hydrogen bond to solvent molecules, an effective site symmetry lowering takes place at the Cobalt, thus the point symmetry listed in Table 4.3 is no longer valid since it only considers the atoms directly bonded to Cobalt.

The theory of asymmetry in the general magnetic second rank shielding tensor has been treated first by Schneider (2.38) and later by Haeberlen (2.40). In order that non-zero antisymmetric components occur, it is necessary that the magnetic susceptibility tensor be anisotropic as it is in the present case. In favourable cases, the antisymmetric part of the chemical shielding tensor may have elements of the same order of magnitude as the symmetric anisotropic part, i.e., $\Delta_a\sigma \sim \Delta\sigma$ in equation 2.18. The correlation time τ_1 associated with $\Delta_a\sigma$ is predicted to be $3\tau_2$ within the isotropic diffusion model so that the effect on the linewidth could become large. It is extremely important to point out that $\Delta_a\sigma$ has neither been

Table 4.10[a]

Group Theoretical Analysis of the Contribution of Components of the Shielding Tensor

Point group appropriate to the shielded nucleus	Number of independent components $\sigma_{z\beta}^{(d)}$	$\sigma_{\alpha\beta}^{(p)}$	Non-vanishing components
C_1, C_i ($\equiv S_2$)	6	9	σ_{zz}, σ_{xx}, σ_{yy}, $\sigma_{xy}^{(s)}$, $\sigma_{xz}^{(s)}$, $\sigma_{yz}^{(s)}$ $\sigma_{xy}^{(a)}$, $\sigma_{xz}^{(a)}$, $\sigma_{yz}^{(a)}$
C_2, C_s ($\equiv C_{1h}$), C_{2h}	4	5	σ_{zz}, σ_{xx}, σ_{yy}, $\sigma_{xy}^{(s)}$; $\sigma_{xy}^{(a)}$
C_{2v}, D_2, D_{2h}	3	3	σ_{zz}, σ_{xx}, σ_{yy}
C_4, S_4, C_{4h}	2	3	σ_{zz}, $\sigma_{xx} = \sigma_{yy}$; $\sigma_{xy}^{(a)}$
C_3, S_6, C_{3h}, C_6, C_{6h} C_{4v}, D_{2d}, D_4, D_{4h}	2	3	σ_{zz}, $\sigma_{xx} = \sigma_{yy}$; $\sigma_{xy}^{(a)}$
C_{3v}, D_3, D_{3d}, D_{3h} C_{6v}, D_6, D_{6h}	2	2	σ_{zz}, $\sigma_{xx} = \sigma_{yy}$
$C_{\infty v}$, $D_{\infty h}$	2	1	σ_{zz}, $\sigma_{xx} = \sigma_{yy}$, ($\sigma_{zz}^{(p)} = 0$)
T, T_h, T_d, O, O_h	1	1	$\sigma_{xx} = \sigma_{yy} = \sigma_{zz}$

Table 4.10[a] The number of independent components of the diamagnetic (symmetric) and paramagnetic (non-symmetric) shielding constants for various point-group symmetries of the nuclear site. The final column shows the non-vanishing components, the z axis being the principal axis of symmetry, and for C_{2v}, D_2 and D_{2h}, the xz and yz planes are planes of symmetry; the components after the semicolon apply to $\sigma_{\alpha\beta}^{(p)}$ only.

[a] Reference 2.41.

experimentally measured nor calculated theoretically. Hence, its general magnitude remains unknown.

In the extreme narrowing condition ($\omega^2\tau_2^2 << 1$), the spectral density governing the final term in equation 2.18 reduces to 7/3 τ_2. Under conditions where the extreme narrowing condition is not met, the linewidths are no longer proportional to B_o^2. The quadrupolar contribution to the line widths also becomes field dependent because the full expression governing $1/T_2$ can no longer be approximated. For a field strength of 9.395T, the operating frequency of Cobalt is 94.457MHz so that $\omega^2\tau_2^2 \sim 1$ corresponds to a correlation time of $\sim 1.67 \times 10^{-9}$ sec. Both the chemical shielding anisotropy contribution and the quadrupolar contribution to the linewidths are reduced at high field. If τ_2 has values in the range of 10^{-9}- 10^{-10}sec and the term involving $\Delta_a\sigma$ is included, all of the data in Table 4.1 can be fitted to equations 2.15 and 2.18. An example of such a fit is shown in Figure 4.6 and the derived parameters for complexes where solid state quadrupole coupling constants are available are presented in Table 4.11. The observed curvature of the plots versus B_o^2 can only be obtained with a correlation time of this order of magnitude. The intercept at zero field formally gives the quadrupolar contribution and the effective quadrupolar coupling constants are generally one order of magnitude smaller than those obtained from solid state measurements with these long correlation times. The important feature is that $\Delta_a\sigma$ predominates and the effective correlation times are longer for lower symmetry complexes. An alternative way of fitting data to equations 2.15 and 2.18 is to remove the equality $\tau_1 = 3\tau_2$ resulting from the simple rotational diffusion model and allow τ_1 to vary freely. This results in derived parameters for quadrupole coupling compatible

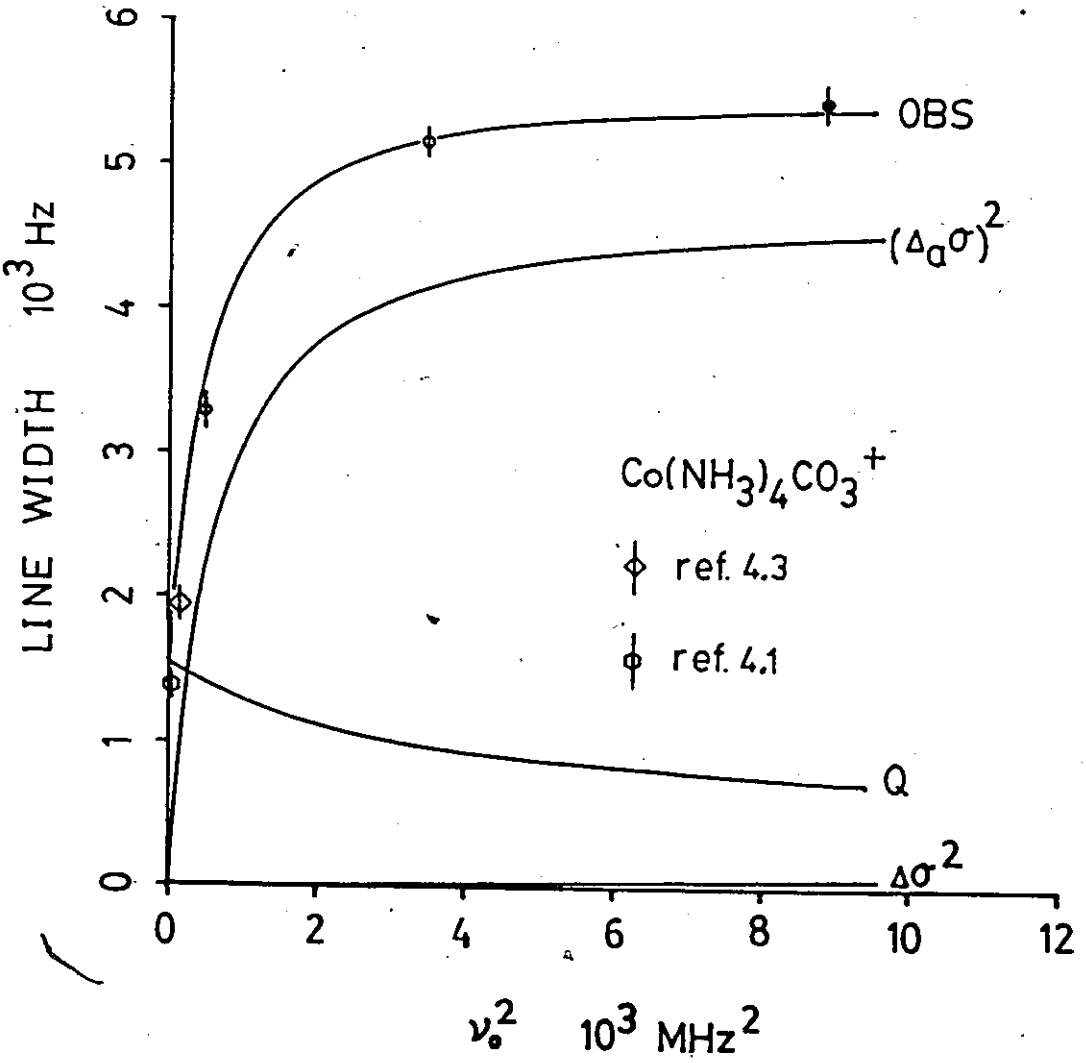

Figure 4.6 Observed and calculated field dependence of linewidths. The upper solid line shows the sum of the various contributions from the different terms of Equations 2.15 and 2.18.

Table 4.11

Effective Correlation Times and Couplings ($\tau_1=3\tau_2$)

Complex	$\tau_{eff} \times 10^{10}$ (sec)	$A(1 + \frac{\eta^2_Q}{3})_{eff}$ (MHz)	$\Delta\sigma(1 + \frac{\eta^2_{cs}}{3})_{eff}$	$\Delta\sigma_{a\ eff}$
trans-$Coen_2Cl_2^+/H_2O$	8.00	8.60	0.007	0.01549
trans-$Coen_2Cl_2^+$/MeOH	1.31	23.60	0.006	0.01816
cis-$Coen_2Cl_2^+$	21.00	2.60	0.006	0.02190
cis-$Co(NH_3)_4CO_3^+$	22.00	2.35	0.0013	0.01730
trans-$Coen_2(NO_2)_2^+$	27.00	1.62	0.00276	0.00854
$Co(NH_3)_5Cl^{2+}$	27.00	1.95	0.0026	0.00927

$A = (\frac{e^2qQ}{h})$ $\qquad \eta_Q = \frac{V_{xx} - V_{yy}}{V_{zz}}$

$\Delta\sigma = \sigma_{zz} - \frac{1}{2}(\sigma_{xx} + \sigma_{yy})$ $\qquad \eta_{cs} = \frac{\sigma_{xx} - \sigma_{yy}}{\sigma_{zz}}$

$\Delta\sigma_a = [(\rho^{cs}_{xy})^2 + (\rho^{cs}_{xz})^2 + (\rho^{cs}_{yz})^2]^{\frac{1}{2}}$

with solid state coupling constants, values of τ_2 of the expected magnitude of 10^{-11} sec and values of $\Delta\sigma$ corresponding to those from solid state measurements or calculated from optical data. This alternative however, requires τ_1 to be two orders of magnitude or more greater than τ_2 and $\Delta_a\sigma$ greater than $\Delta\sigma$. Examples of parameters derived on this basis are given in Table 4.12. A comparison of $\Delta_a\sigma_{eff}$ from Tables 4.11 and 4.12 suggest that either treatment of the data reflects the unambiguous importance of the anti-symmetric term. Quantitatively, the $\Delta_a\sigma_{eff}$ values do not change drastically in either treatment, and τ_1 from method two is compatible in order of magnitude to τ_{eff} of method one, again suggesting that this term dominates over all others. An interesting implication of this model involving the anti-symmetric term is that the unusual situation of $T_1<T_2$ is predicted and experimental results are presented in Chapter 5 to investigate this point.

The long correlation times of 10^{-9} sec are incompatible with the simple rotational diffusion model. A reasonable suggestion, which can be verified later in Chapter 5, would be that the second coordination sphere hydrogen bonding interactions are the dominant factor. For all of these complexes, two types of hydrogen bond formation are possible. The amine ligands can act as hydrogen bond donors whereas ligands such as CN^-, Cl^- and $CO_3^=$ can act as hydrogen bond acceptors to a solvent molecule. Formation of both types of bonds leads to closer charge neutrality and a second coordination sphere with a well-defined structure. For example, in the fragment

$$H_2O....H_3\overset{\delta+}{N} - Co - \overset{\delta-}{Cl} ..... HOH$$

Table 4.12

Effective Correlation Times and Couplings ($\tau_1 \& 3\tau_2$)

Complex	$\tau_2 \times 10^{11}$(sec)	$A(1 + \frac{\eta^2 Q}{3})$(MHz)	$\tau_1 \times 10^{11}$(sec)	$\Delta\sigma(1 + \frac{\eta^2_{cs}}{3})_{eff}$	$\Delta\sigma_{a\ eff}$
tr-$Coen_2Cl_2^+/H_2O$	1.652	61.155	193.1	0.0071	0.0172
tr-$Coen_2Cl_2^+$/MeOH	1.908	61.155	70.99	0.0071	0.0172
cis-$Coen_2Cl_2^+$	1.082	36.409	487	0.0041	0.020
cis-$Co(NH_3)_4CO_3^+$	2.918	22.129	621.5	0.0040	0.0158
trans-$Coen_2(NO_2)_2^+$	2.275	15.549	450.0	0.0020	0.009
$Co(NH_3)_5Cl^{2+}$	0.686	32.407	116.67	0.0020	0.0085

the donor interaction at the ammonia decreases the effective positive charge on the nitrogen and the acceptor interaction at the chlorine decreases the negative charge at the Cl^-. The electric field gradient at the Cobalt is altered. Cooperative effect of this type is more effective in complexes of the type $\overset{\delta+}{A} - M - \overset{\delta-}{B}$ than $\overset{\delta+}{A} - M - \overset{\delta+}{A}$ or $\overset{\delta-}{B} - M - \overset{\delta-}{B}$.

Consider a model in which two types of molecular rotation are allowed. The first is rotation of the whole complex, including both the first and second sphere ligands. This is presumed to correspond to a correlation time of 10^{-11} sec as estimated from quadrupolar relaxation and the calculations from viscosity data. The second type of motion would be rotation of the first coordination sphere complex within the second sphere involving the breaking of hydrogen bonds and would have a much longer correlation time of perhaps 10^{-9} - 10^{-10} sec consistent with known hydrogen bond lifetimes. By symmetry arguments, the changes in the electric field gradient at the Cobalt nucleus and in chemical shift for a symmetric complex such as $Co(NH_3)_6^{3+}$ produced by the second type of rotation are identical to those produced by rotation of the first type, i.e., the whole complex. Therefore, rotation of the inner sphere would not contribute to line broadening. For an unsymmetrical complex, rotation of the inner sphere produces a different chemical shielding tensor which cannot be accomplished by rotation of the whole complex. Inner sphere rotation which may involve a relatively longer correlation time could therefore contribute to line broadening. In short, a change in the hydrogen bonding arrangement via inner sphere rotation gives rise to line broadening.

For complexes with a fourfold axis of symmetry, rotation about the four fold rotation axis will not produce different hydrogen bonding arrangements. This is, of course, not true for rotation about axes perpendicular to the fourfold axis. For lower symmetries, rotation about any axis of rotation changes the hydrogen bonding. It may be significant that the effective correlation times for C_{4v} and D_{4h} molecules ($\sim 10^{-10}$sec) are intermediate between those for low symmetry complexes (10^{-9}sec) and the true correlation times ($\sim 10^{-11}$sec). This leads to a greater linearity in the B_o^2 plots for C_{4v} and D_{4h} molecules - a result predicted by the model.

The basis of the above model is somewhat a cross between the "Interstitial" (4.25, 4.26) and "Flickering Cluster" (4.27) models proposed in explaining the properties of water. The essential idea behind the interstitial model is that a fraction of water molecules are allowed to rotate in a cavity formed in the open hydrogen bonded tetrahedral network. In the flickering cluster model hydrogen bond making and breaking is co-operative due to partial covalent character as in donor-acceptor interaction of the hydrogen bond (4.26). In this context, short range interaction between the first and second spheres becomes important. If the lifetimes of the hydrogen bonds are long enough such that a pseudo-perturbing moment is created, the electronic arrangement of the complex is thus modulated by an additional time-dependent potential which may, in this case, manifest itself as the $\ell=1$, (i.e., τ_1) component of the general second rank shielding tensor in the course of field dependent measurements. Since interchanging of hydrogen bonds is a chemical exchange process, the relaxation of Cobalt necessarily becomes complex. In the analysis of the relaxation of quadrupolar halide

probe experiments, Marshall (4.28) has shown that the effective correlation times can only be obtained by summing rotational and exchange rates and that the necessary condition of $\omega_o t << 1$ must be imposed in particular for quadrupolar nuclei of half-integral spin in order that a Bloch-type equation can be applied. In the event that this condition is not met, terms proportional to I_z^3 result in the relaxation equation and the Bloch equation is invalid. This has been pointed out independently by Abragam (2.31) and Marshall (4.28). Until a more general theoretical treatment taking into account the combined effects of quadrupolar relaxation, chemical shielding anisotropy relaxation, and rapid chemical exchange on linewidth becomes available, together with the reasons cited above, little physical significance can be associated with the derived coupling parameters of Tables 4.11 and 4.12.

SECTION 4.4 Summary

The field dependent behaviour of Cobalt complexes has been investigated at field strengths of 2.114T, 5.872T and 9.395T. Linewidth measurements revealed that:

i) symmetric complexes show no field dependence,

ii) low symmetry complexes show changes in line widths of as much as 10KHz between the highest and the lowest field and the expected trend with shielding anisotropy is observed,

iii) plots of linewidths versus B_o^2 show deviation from expected linearity, this non-linearity becomes particularly pronounced for extremely low symmetry complexes,

iv) τ_c derived from quadrupolar contributions indicates the existence of a second coordination solvent shell reorientation as an entity at

a time scale of 10^{-11} sec,

v) τ_{CSA} ($\sim 10^{-9}$ - 10^{-10}) derived from field dependent measurements is associated with the lifetimes of hydrogen bonds between the first and second coordination spheres, and

vi) (tentatively), the anti-symmetric part of the chemical shielding tensor cannot be neglected.

These results suggest that calculation of the relaxation parameter, τ_c, employing solid state quadrupole coupling constants for quadrupolar nuclei yields incorrect results if hydrogen bonding with the solvent can occur. In Chapter 5, further evidence is given to support the idea of a second coordination solvent shell and the involvement of $\Delta_a\sigma$.

Before closing this chapter, the present experimental results provide an indication of the validity of the common assumption that ^{59}Co relaxation is dominated by electric quadrupolar interaction. At low field, eg. 2.114T, the error introduced by assuming complete quadrupolar relaxation is less than 5% for complexes of C_{4v} or D_{4h} point groups. For lower symmetry complexes, e.g., C_{2v}, an error of 50% could result. The ratio of the linewidths for trans to cis isomers obtained by extrapolation to zero field approaches 4, the value predicted by simple Crystal Field theory.

CHAPTER FIVE

SOLVENT AND FIELD DEPENDENCES OF RELAXATION TIME FOR LOW SYMMETRY COBALT (III) COMPLEXES

SECTION 5.1 Introduction

In the previous chapter, it was shown that T_2^{-1} for Co(III) complexes varied with magnetic field and that this variation could be either linear or non-linear. Within the framework of the isotropic diffusion model, the origin of the anomalous field dependent behaviour is attributed to hydrogen bonding effects between the first sphere ligands and solvent molecules. In this chapter, additional evidence is given for inter-molecular hydrogen bonding based on the solvent dependence of T_2^{-1} as a function of B_0^2. The proposed model involving the anti-symmetric term of the chemical shielding tensor is re-examined on the basis of both spin-lattice and spin-spin relaxation time. The resulting T_1/T_2 ratio is consistent with the earlier interpretation.

SECTION 5.2 Results

The chemical shifts and linewidths of nine Co(III) complexes have been measured at fields of 2.114, 5.872 and 9.395T in a variety of solvents and the results are presented in Tables 5.1-5.9. All of the complexes have less than octahedral symmetry and contain ligands such as amine, nitro, chloro, carbonate and cyano groups. All of the solvents can function as either proton donors or proton acceptors. For example, dimethyl sulfoxide can form strong hydrogen bonds by proton acceptance. Acetone and acetonitrile are much weaker hydrogen bond acceptors. Water and methanol can function as both hydrogen bond donors or acceptors. In strong acids, (good hydrogen donors), a limited amount of data was collected due to chemical instability.

Table 5.1

Chemical Shifts and Linewidths of mer-$Co(NH_3)_3(NO_2)_3$

Solvent	21.252 MHz		59.035 MHz		94.457 MHz	
	δ/ppm	$\Delta\nu_{\frac{1}{2}}$/Hz	δ/ppm	$\Delta\nu_{\frac{1}{2}}$/Hz	δ/ppm	$\Delta\nu_{\frac{1}{2}}$/Hz
$(CH_3)_2SO$	7007 ± 10	2231 ± 50	7000 ± 20	2907 ± 50	7000 ± 20	3336 ± 100
H_2O	6981 ± 10	782 ± 30	6982 ± 10	956 ± 20	6983 ± 10	970 ± 30
CH_3OH	6992 ± 10	595 ± 30	7005 ± 20	832 ± 50	6998 ± 20	1068 ± 50
CH_3CN	7026 ± 10	131 ± 15	7038 ± 5	182 ± 10	7033 ± 10	314 ± 30
$(CH_3)_2CO$	7012 ± 10	363 ± 30	7029 ± 5	376 ± 10	7023 ± 10	450 ± 30

Table 5.2

Chemical Shifts and Linewidths of mer-$Co(dien)(NO_2)_3$

Solvent	21.252 MHz		59.035 MHz		94.457 MHz	
	δ/ppm	$\Delta\nu_{\frac{1}{2}}$/Hz	δ/ppm	$\Delta\nu_{\frac{1}{2}}$/Hz	δ/ppm	$\Delta\nu_{\frac{1}{2}}$/Hz
$(CH_3)_2SO$	6471 ± 20	3853 ± 200	6476 ± 20	5491 ± 300	6463 ± 20	7130 ± 300
H_2O	6394 ± 10	1620 ± 50	6397 ± 20	2127 ± 200	6399 ± 20	3204 ± 100
CH_3OH	6418 ± 30	1826 ± 150	6428 ± 20	1969 ± 150	6431 ± 20	2400 ± 100
CH_3CN	6425 ± 10	610 ± 25	6451 ± 10	857 ± 40	6435 ± 10	1000 ± 50
$(CH_3)_2CO$	6435 ± 5	956 ± 100	6439 ± 10	926 ± 40	6449 ± 10	1000 ± 50

Table 5.3

Chemical Shifts and Linewidths of trans-$Coen_2(NO_2)_2^+$

Solvent	21.252 MHz		59.035 MHz		94.457 MHz	
	δ/ppm	$\Delta\nu_{\frac{1}{2}}$/Hz	δ/ppm	$\Delta\nu_{\frac{1}{2}}$/Hz	δ/ppm	$\Delta\nu_{\frac{1}{2}}$/Hz
$(CH_3)_2SO$	6387 ± 20	2963 ± 150	6401 ± 20	3642 ± 150	6396 ± 20	4400 ± 150
H_2O	6323 ± 5	1366 ± 50	6329 ± 5	1430 ± 50	6319 ± 5	1579 ± 50
CH_3OH	6374 ± 5	716 ± 50	6387 ± 10	751 ± 50	6383 ± 10	800 ± 20
CH_3CN	6361 ± 5	155 ± 20	6372 ± 5	163 ± 15	6366 ± 5	240 ± 20

Table 5.4

Chemical Shifts and Linewidths of trans-$Co(NH_3)_4(NO_2)_2^+$

Solvent	21.252		59.035 MHz		94.457 MHz	
	δ/ppm	$\Delta\nu_{\frac{1}{2}}$/Hz	δ/ppm	$\Delta\nu_{\frac{1}{2}}$/Hz	δ/ppm	$\Delta\nu_{\frac{1}{2}}$/Hz
$(CH_3)_2SO$	7225 ± 5	888 ± 50	7234 ± 10	1085 ± 20	7235 ± 20	1283 ± 50
H_2O	7207 ± 5	355 ± 20	7206 ± 5	356 ± 10	7208 ± 10	390 ± 30
CH_3OH	7224 ± 10	439 ± 50	7241 ± 5	487 ± 50	7236 ± 10	495 ± 50
CH_3CN	7228 ± 5	253 ± 50	7233 ± 5	260 ± 50	7238 ± 5	280 ± 50
CF_3COOH					7215 ± 20	2588 ± 100

Table 5.5

Chemical Shifts and Linewidths of cis-$Co(NH_3)_4(NO_2)_2^+$

Solvent	21.252 MHz		59.035 MHz		94.457 MHz	
	δ/ppm	$\Delta\nu_{\frac{1}{2}}$/Hz	δ/ppm	$\Delta\nu_{\frac{1}{2}}$/Hz	δ/ppm	$\Delta\nu_{\frac{1}{2}}$/Hz
$(CH_3)_2SO$	7274 ± 20	1181 ± 50	7288 ± 10	1648 ± 20	7290 ± 20	2310 ± 50
H_2O	7277 ± 10	331 ± 20	7272 ± 5	356 ± 10	7276 ± 10	440 ± 30
CH_3OH	7300 ± 10	326 ± 20	7316 ± 10	404 ± 30	7311 ± 10	700 ± 20
gla.CH_3COOH					7279 ± 20	1595 ± 50
CH_3CN	7305 ± 5	180 ± 20	7301 ± 5	230 ± 20	7305 ± 5	320 ± 30

Table 5.6

Chemical Shifts and Linewidths of trans-$Coen_2Cl_2^+$

Solvent	21.252 MHz		59.035 MHz		94.457 MHz	
	δ/ppm	$\Delta\nu_{\frac{1}{2}}$/Hz	δ/ppm	$\Delta\nu_{\frac{1}{2}}$/Hz	δ/ppm	$\Delta\nu_{\frac{1}{2}}$/Hz
$(CH_3)_2SO$			8897 ± 100	14180 ± 1500	8841 ± 100	17660 ± 1000
H_2O	9333 ± 20	8597 ± 300	9163 ± 30	13400 ± 500	8960 ± 30	16783 ± 500
CH_3OH	8873 ± 30	9375 ± 300	8850 ± 30	10209 ± 500	8821 ± 30	12920 ± 500
CH_3CN	8754 ± 30	3672 ± 300	8797 ± 30	4000 ± 300	8788 ± 30	5100 ± 300

Table 5.7

Chemical Shifts and Linewidths of cis-$Coen_2Cl_2^+$

Solvent	21.252 MHz		59.035 MHz		94.457 MHz	
	δ/ppm	$\Delta\nu_{\frac{1}{2}}$/Hz	δ/ppm	$\Delta\nu_{\frac{1}{2}}$/Hz	δ/ppm	$\Delta\nu_{\frac{1}{2}}$/Hz
$(CH_3)_2SO$	8867 ± 30	8686 ± 800	8871 ± 50	11660 ± 1500	9044 ± 50	11837 ± 1500
H_2O	8966 ± 20	5126 ± 300	8968 ± 30	8483 ± 600	8987 ± 20	9218 ± 800
CH_3OH	8814 ± 20	4700 ± 500	9028 ± 30	6540 ± 600	8787 ± 30	7661 ± 700

Table 5.8

Chemical Shifts and Linewidths of $Co(NH_3)_5CN^{2+}$

Solvent	21.252 MHz		59.035 MHz		94.457 MHz	
	δ/ppm	$\Delta\nu_{\frac{1}{2}}$/Hz	δ/ppm	$\Delta\nu_{\frac{1}{2}}$/Hz	δ/ppm	$\Delta\nu_{\frac{1}{2}}$/Hz
$(CH_3)_2SO$	6728 ± 30	7600 ± 500	6782 ± 30	9280 ± 1000	6731 ± 30	12526 ± 1500
H_2O	6669 ± 20	2370 ± 200	6674 ± 20	2577 ± 250	6683 ± 20	2799 ± 250
CH_3OH	6775 ± 20	3555 ± 300	6770 ± 20	6040 ± 500	6744 ± 30	7898 ± 800

Table 5.9

Chemical Shifts and Linewidths of $Co(NH_3)_4CO_3^+$

Solvent	21.252 MHz		59.035 MHz		94.457 MHz	
	δ/ppm	$\Delta\nu_{\frac{1}{2}}$/Hz	δ/ppm	$\Delta\nu_{\frac{1}{2}}$/Hz	δ/ppm	$\Delta\nu_{\frac{1}{2}}$/Hz
$(CH_3)_2SO$	9716 ± 30	5649 ± 500	9680 ± 30	5710 ± 500	9681 ± 30	5939 ± 500
H_2O	9732 ± 20	3291 ± 300	9735 ± 20	5773 ± 400	9729 ± 20	5476 ± 400
CH_3OH	9797 ± 30	2122 ± 300	9731 ± 20	2733 ± 300	9738 ± 20	3843 ± 350
CH_3CN	9753 ± 10	495 ± 150	9735 ± 10	835 ± [illegible]	[illegible]0 ± 10	1216 ± 150

Table 5.10

Viscosities of Saturated Solutions of Co(III) Complexes in Different Solvents

Complex	η(c p)				
	$(CH_3)_2SO$	CH_3OH	H_2O	$(CH_3)_2CO$	CH_3CN
tran-$[Coen_2Cl_2]Cl$	-	0.608	0.974	-	0.262
trans-$[Coen_2(NO_2(NO_2)_2]NO_3$	1.932	0.604	0.954	-	0.457
$[Co(NH_3)_5CN](ClO_4)_2$	1.953	0.606	0.973	-	-
$[Co(NH_3)_4CO_3]NO_3$	1.922	0.601	0.961	-	0.353
cis-$[Coen_2Cl_2]Cl$	-	0.608	0.975	-	-

The linewidths in different solvents are expected to vary due to the different viscosities of the solutions. The viscosities of saturated solutions of trans-$[Coen_2Cl_2]Cl$, trans-$[Coen_2(NO_2)_2]NO_3$, cis-$[Coen_2Cl_2]Cl$, $[Co(NH_3)_5CN](ClO_4)_2$ and $[Co(NH_3)_4CO_3]NO_3$ were measured in several solvents. These data are given in Table 5.10. The larger linewidths are found in the solvents with higher viscosity but the percentage change in the linewidth compared to the percentage change in the viscosity is much larger than one.

Table 5.11 and 5.12 summarize the spin-spin (T_2) and spin-lattice (T_1) relaxation times for both ^{59}Co and ^{14}N of low symmetry Cobalt(III) complexes at field strengths of 5.872 and 9.395T. Experimental details for T_1 measurements have been described in Chapter 3. Due to experimental difficulties only a limited number of complexes can be examined, particularly for ^{14}N T_1 measurements. The results of Table 5.11 clearly indicate that $T_1 \neq T_2$ at both field strengths with the exception of the complexes $[Co(NH_3)_5Cl]Cl_2$ and mer-$Co(NH_3)_3(NO_2)_3$ for which the ratio $T_1/T_2 \simeq 1$. For the symmetric complexes $Coen_3Cl_3$ and $Na_3[Co(NO_2)_6]$, the T_1/T_2 ratio is much larger than one. These discrepancies are attributed to scalar relaxation of the second kind and will be discussed in detail in Section 5.3.2. Another important feature of these results is that ^{59}Co T_1's are definitively field dependent indicating that chemical shielding anisotropy is important. The values reported in Table 5.11 are the average values for several determinations. Table 5.12 presents some T_1 values for ^{14}N. The most noticeable feature is that ^{14}N $T_1 \simeq T_2$ and that T_2 is field independent within experimental error. This is at least true for the two field strengths examined. An interesting observation is the detection of the coordinated NO_2^- group in the complex

Table 5.11

^{59}Co Relaxation Time for Low Symmetry Cobalt(III) Complexes

COMPLEX	59.035 MHz			94.457 MHz		
	T_1/msec	T_2/msec	T_1/T_2	T_1/msec	T_2/msec	T_1/T_2
1. trans-$[Coen_2(NO_2)_2]NO_3$/DMSO*	0.076±0.004(3)+	0.082±0.003(3)	0.93	0.062±0.005(3)	0.073±0.003(3)	0.85
" /H_2O	0.224±0.003(3)	0.241±0.030(3)	0.93	0.200±0.003(3)	0.221±0.012(4)	0.91
" /CH_3CN	2.137±0.150(2)	1.483±0.250(2)	1.44	2.105±0.118(3)	1.426±0.260(3)	1.48
2. ε-[CoendienCl]Cl_2/H_2O	0.079±0.006(2)	0.098±0.010(2)	0.81	0.050±0.002(2)	0.065±0.006(2)	0.77
3. $[Co(NH_3)_5Cl]Cl_2/H_2O$	0.174±0.009(1)	0.172±0.012(2)	1.01	0.167±0.006(1)	0.169±0.020(2)	0.99
4. cis-$[Coen_2(NO_2)_2]NO_3/H_2O$	0.271±0.003(1)	0.288±0.030(2)	0.94	0.257±0.005(1)	0.271±0.030(2)	0.95
5. mer-$Co(NH_3)_3(NO_2)_3/H_2O$	0.367±0.018(1)	0.360±0.040(1)	1.02	0.333±0.008(1)	0.328±0.030(1)	1.02
6. $[Coen_3]Cl_3/H_2O$	8.710±0.003(1)	4.00 ±0.300(1)	2.18			
7. $Na_3[Co(NO_2)_6]/H_2O$	38.45 ±0.000(1)	5.60 ±0.060(1)	6.87			

+ number in parenthesis indicates the number of determinations

* dimethyl sulfoxide

Table 5.12

^{14}N Relaxation Time for Low Symmetry Cobalt(III) Complexes

Complex[a]	Assignment	δ/ppm[b]	18.059 MHz		28.894 MHz		
			$T_{2_{obs}}$/msec	$T_{2_{corr}}$/msec	T_1/msec	$T_{2_{obs}}$/msec	$T_{2_{corr}}$/msec
trans-$[Coen_2(NO_2)_2]NO_3$	$-NH_2C$	-376±3	0.656±0.060	0.670	0.706±0.032	0.658±0.061	0.701
	$-NO_2$	121±10				0.055±0.005	0.055
ε-[CoendienCl]Cl_2	$-NHC_2$		0.315±0.030	0.318		0.307±0.030	0.309
	$-NH_2C$	-376±2	0.357±0.020	0.361		0.359±0.030	0.362
$[Co(NH_3)_5Cl]Cl_2$	$-NH_3$	-417±2	1.349±0.050	1.496		1.135±0.100	1.233
	$-NH_3$ (trans-Cl)	-433±2	1.168±0.050	1.277		1.065±0.100	1.151
cis-$[Coen_2(NO_2)_2]NO_3$	$-NH_2C$						
	$-NH_2C$ (trans-NO_2)	-377±5			0.592±0.012	0.335±0.025	.365
	$-NO_2$						
mer-$Co(NH_3)_3(NO_2)_3$	$-NH_3$ (trans-NO_2)	-393±3				1.011±0.080	1.177
	$-NH_2$ (trans-NH_3)	-412±3				1.360±0.140	1.679
$Coen_3Cl_3$	$-NH_2C$	-376±3			0.445±0.012	0.350±0.025	.445
$Na_3[Co(NO_2)_6]$	$-NO_2$	89±3			0.304±0.010	0.245±0.020	
$NaNO_2$	$-NO_2$	227±1				1.109±0.010	

[a] in saturated aqueous solution

[b] NH_4NO_3 external reference, NO_3^-(δ=0ppm)

[c] T_2 corrected for scalar coupling contribution from cobalt

[d] $J(^{59}Co-^{15}NR_3)$ = 45Hz, $J(^{59}Co-^{14}NO_2) \simeq$ 56.4Hz

trans-$[Coen_2(NO_2)_2]NO_3$. The assignment of ^{14}N signals follows that of the literature in most cases (5.1-5.5).

SECTION 5.3 Discussion

Consistent with the results of Section 4.2, not all of the plots versus B_o^2 are linear. Again, the slopes, intercepts, and correlation coefficients have been extracted and are summarized in Table 5.13. In cases where pronounced curvature is observed, only the intercept is given. A general trend of these results is that both the line widths and their field dependences are strongly solvent dependent. In some cases, the line widths vary by more than a factor of twenty in different solvents with the broader lines and the larger field dependences being associated with the stronger hydrogen bonding solvents.

Figure 5.1 shows a set of plots of linewidths versus B_o^2 for mer-Co(dien)$(NO_2)_3$ in the different solvents. These plots are reasonably linear. Figure 5.2 shows a set of plots for the complex cis-$Coen_2Cl_2^+$. Deviation from linearity is observed in strongly hydrogen bonding solvents. In methanol, a weaker hydrogen bonding solvent, less curvature is found and the anisotropy is smaller. Evidently, the data in Table 5.13 show that there is a difference of a factor of more than 60 between the slopes of the B_o^2 plots in acetone and in dimethylsulfoxide for the complex mer-Co(dien)$(NO_2)_3$. The linewidths at zero field show parallel changes. For example, the zero field linewidth of the complex trans-$Coen_2(NO_2)_2^+$ changes by a factor of $\sim$ 20 going from acetonitrile to dimethylsulfoxide. These observations show that the line-

Table 5.13

Slopes, Intercepts and Correlation Coefficient of $\Delta\nu_{\frac{1}{2}}$ vs B_0^2 Plots for Low Symmetry Co(III) Complexes in Different Solvents

Solvent		Mer-$Co(NH_3)_3(NO_2)_3$	Mer-Co(Dien)$(NO_2)_3$	Trans-$Coen_2(NO_2)_2^+$	Trans-$Co(NH_3)_4(NO_2)_2^+$	Cis-$Co(NH_3)_4(NO_2)_2^+$	Trans-$Coen_2Cl_2^+$	Cis-$Coen_2Cl_2^+$	$Co(NH_3)_5CN^{2+}$	$Co(NH_3)_4CO_3^+$
CH_3CN	A	0.0219	0.0437	0.01053	0.00325	0.0165	0.1726	-	-	0.083
(14.1)[a]	B	115	635	141	250	172	3517	-	-	492
	C	0.996	0.951	0.962	0.994	0.999	0.991	-	-	0.992
$(CH_3)_2CO$	A	-	0.0062	-	-	-	-	-	-	-
(17.0)	B	364	934	-	-	-	-	-	-	-
	C	-	0.713	-	-	-	-	-	-	-
H_2O	A	-	0.1883	-	0.00438	0.0132	-	-	0.0495	-
(18.0)	B	552	1510	600	348	319	7923	1820	2370	1558
	C	-	0.999	-	0.944	0.990	-	-	0.990	-
CH_3OH	A	0.0544	0.0692	0.00981	-	-	-	-	-	-
(19.0)	B	559	1769	714	420	350	9000	2549	2980	2030
	C	0.987	0.993	0.998	-	-	-	-	-	-
$(CH_3)_2SO$	A	0.1243	0.3768	0.1661	0.0454	0.1319	-	-	0.583	0.0352
(29.8)	B	2292	3877	2957	891	1418	-	4314	7301	5615
	C	0.958	0.987	0.991	0.987	0.998	-	-	0.999	0.987

[a] Donor number

[b] $\nu_0 = \frac{\gamma B_0}{2\pi}$

A = $\Delta\nu_{\frac{1}{2}}/\nu_0^{2b} \times 10^{12}$ (Hz^{-1})

B = $\Delta\nu_{\frac{1}{2}}/(B_0=0)$ (Hz)

C = correlation coefficient

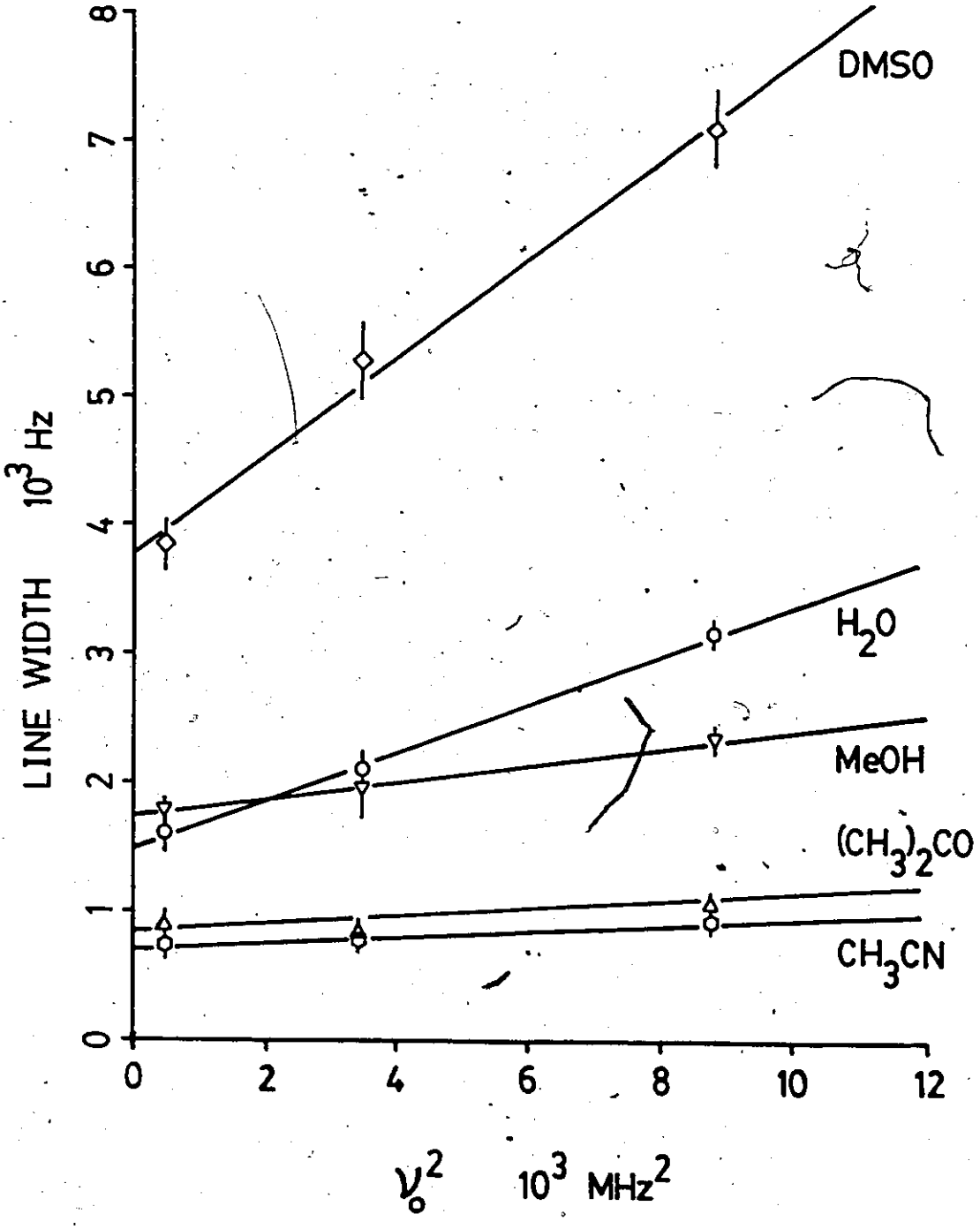

Figure 5.1 Field dependence of the ^{59}Co NMR linewidths of mer-Co(dien)$(NO_2)_3$ in different solvents.

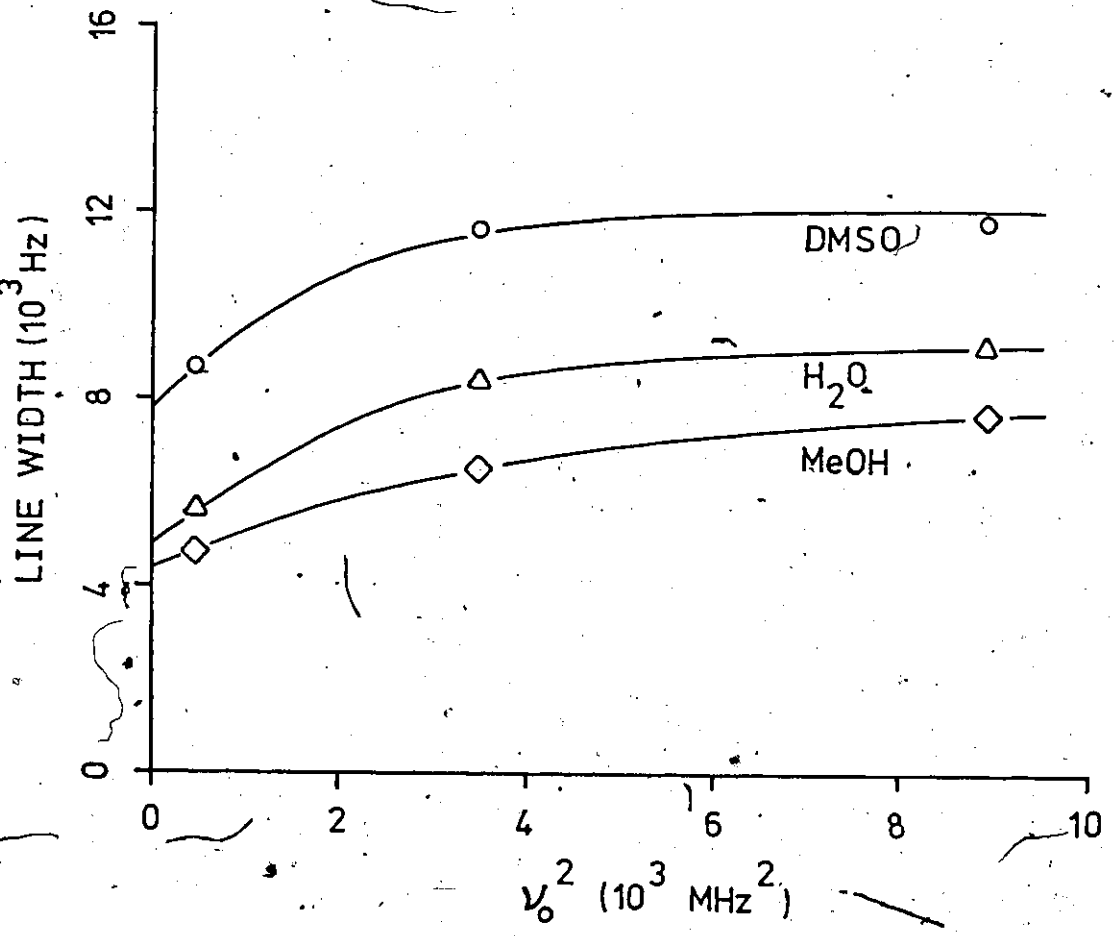

Figure 5.2 Plot of Linewidth versus ν_o^2 for the complex cis-$Coen_2Cl_2^+$ in different solvents.

width changes are directly associated with the properties of the solvent.

SECTION 5.3.1 Trends of Relaxation and the Donor-Acceptor Interaction

The solvent and field dependence linewidth results can be separated into the field dependent and the zero field parts. The field dependent part is not well understood. From the plots of Figures 5.1 and 5.2 it is evident that the trend is tending to decreasing curvature where non-linear plots with B_o^2 are obtained and the smaller slope for linear plots with B_o^2 going from the strongly hydrogen bonding solvent (dimethyl sulfoxide) to the weakly hydrogen bonding solvent (acetonitrile). This is an expected behaviour from the model proposed in Chapter 4.

The zero field part contains potentially more information and can be treated as follows:

i) The differences in linewidths obtained by extrapolation to zero field reflects directly the solvation effects towards quadrupolar relaxation of these complexed ions. A correlation of $(\pi T_2)^{-1}_{B_o=0}$ with the donor number is expected. Figure 5.3 gives representative plots of these results. The good correlation with Gutmann's donor number reinforces the suspected origin of the large linewidth differences.

ii) In Chapter Four, τ_2 has been ascribed as being responsible for the modulation of the quadrupole interactions. Therefore, from the linewidth obtained by extrapolation to zero field, $\tau_2(\tau_Q)$ can be obtained if it can be assumed that the solid state quadrupole coupling constant can be used as an upper limit to bracket the quadrupole interaction. The comparison with τ_2 values estimated from the modified Debye equation for different types of intermolecular interaction reflect the effect of the various solvents. These values are tabulated in Table 5.15 together with the appropriate f-factors and

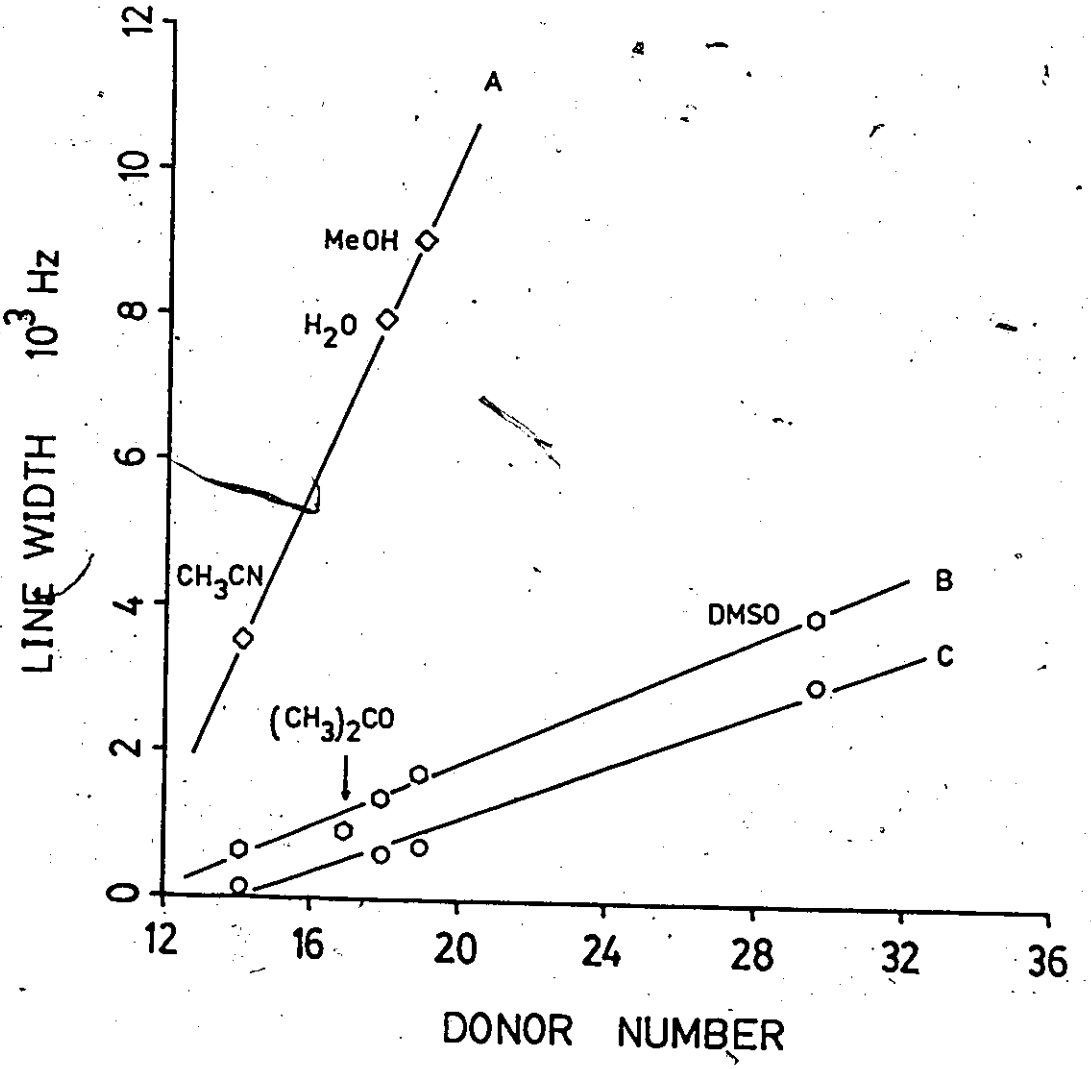

Figure 5.3 Variation of linewidth with Gutmann donor number (Table 5.14).

(A) trans-$Coen_2Cl_2^+$

(B) mer-$Co(NH_3)_3(NO_2)_3$

(C) mer-Co(dien)$(NO_2)_3$

Table 5.14 (2.66)

Donor Numbers (DN) for Various Solvents Obtained from Calorimetric Measurements in 10^{-3}M Solutions of Dichloroethane with $SbCl_5$ as a Reference Acceptor

Solvent	DN	Solvent	DN
1,2-Dichloroethane(DCE)	-	Ethylene carbonate(EC)	16.4
Benzene	0.1	Phenylphosphonic difluoride	16.4
Thionyl chloride	0.4	Methylacetate	16.5
Acetyl chloride	0.7	n-Butyronitrile	16.6
Tetrachloroethylene carbonate (TCEC)	0.8	Acetone(AC)	17.0
Benzoyl fluoride(BF)	2.3	Ethylacetate	17.1
Benzoyl chloride	2.3	Water	18.0
Nitromethane(NM)	2.6	Phenylphosphoric dichloride	18.5
Nitrobenzene(NB)	4.4	Diethylether	19.2
Acetic anhydride	10.5	Tetrahydrofuran(THF)	20.0
Phosphorous oxychloride	11.7	Diphenylphosphoric chloride	22.4
Benzonitrile(BN)	11.9	Trimethyl phosphate(TMP)	23.0
Selenium oxychloride	12.2	Tributyl phosphate(TBP)	23.7
Acetonitrile	14.1	Dimethylformamide(DMF)	26.6
Tetramethylenesulfone(TMS)	14.8	N-Methylpyrolidinone(NMP)	27.3
Dioxane	14.8	N-Dimethylacetamide(DMA)	27.8
Propandiol-(1,2)-carbonate (PDC)	15.1	Dimethylsulfoxide(DMSO)	29.8
Benzylcyanide	15.1	N-Diethylformamide(DEF)	30.9
Ethylene sulphite(ES)	15.3	N-Diethylacetamide(DEA)	32.2
iso-Butyronitrile	15.4	Pyridine(PY)	33.1
Propionitrile	16.1	Hexamethylphosphoric triamide (HMPA)	38.8

Table 5.15

Calculated and Experimental Correlation Times for Co(III) Complexes

Complex	trans-$[Coen_2Cl_2]Cl$[a]			trans-$[Coen_2(NO_2)_2]NO_3$[b]			
Solvent	CH_3OH	H_2O	CH_3CN	$(CH_3)_2SO$	CH_3OH	H_2O	CH_3CN
a solvent(Å)[c]	2.817	2.100	3.080	3.262	2.817	2.10	3.080
a free-ion(Å)	2.874	2.874	2.874	3.025	3.025	3.025	3.025
a solvated-ion(Å)	6.508	3.227	5.394	5.666	6.449	3.593	5.545
a ion-pair(Å)	4.080	4.080	4.080	5.765	5.765	5.765	5.765
f free-ion	0.340	0.456	0.311	0.309	0.358	0.480	0.327
f solvated-ion	0.77	0.512	0.584	0.579	0.763	0.570	0.600
f ion-pair	0.483	0.647	0.442	0.589	0.682	0.915	0.624
τ free-ion(10^{11}sec)	0.502	1.079	0.197	1.692	0.613	1.298	0.424
τ_0(10^{11}sec)	1.877	1.652	0.734	11.056	2.706	2.275	0.535
τ solvated ion(10^{11}sec)	13.131	1.716	4.290	20.839	12.66	2.585	4.788
τ ion-pair(10^{11}sec)	2.039	4.383	0.804	22.321	8.081	17.122	5.593

[a] 60.14 MHz, η = .225

[b] 13.22 MHz, η = .727

[c] $a = 1/3\ (a_x + a_y + a_z)$

ratio required for calculation for the two selected complexes. The trend reviewed by these calculation demonstrated that the τ value obtained experimentally (τ_Q) is always more than the τ calculated for the free ion but less than that calculated for the solvated ion. For the strongly hydrogen bonding solvents, it is closer to the solvated ion values and for the weakly hydrogen bonding solvents it is closer to the free ion values. For the complex trans-$[Coen_2Cl_2]Cl$ the variation in τ_Q in different solvents is comparable to the variation in the calculated τ values. For trans-$[Coen_2(NO_2)_2]NO_3$, the variation in τ_Q is clearly larger implying that the linewidth variation with solvent reflects changes in both correlation time and quadrupole coupling constant with hydrogen bond formation. For trans-$[Coen_2(NO_2)_2]NO_3$, with a smaller quadrupole coupling constant (13.22 MHz), a small additional field gradient produced by hydrogen bonding will give rise to a proportionately greater effect on the linewidth whereas such effects are less revealing for trans-$[Coen_2Cl_2]Cl$ since it has a much larger quadrupole coupling constant (60.14 MHz).

Similar changes in linewidth have been reported for alkali metal ions (2.56, 2.57, 2.91) with different solvents. In general, the exact nature of solute-solvent interactions is not well understood although the experimental literature in this area is vast; (2.67, 2.68, 5.6). There have been some advances in the theory of the solvent dependence of the relaxation rate of simple ions (Sec. 2.5). Although the nature of the problem is similar for complex ions, the mathematical treatment will be more complicated.

Consider the following scheme:

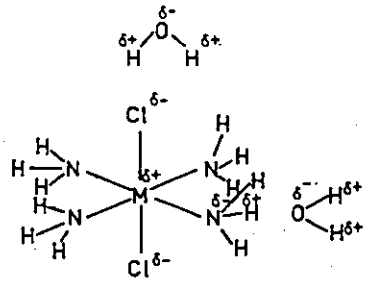

(I)

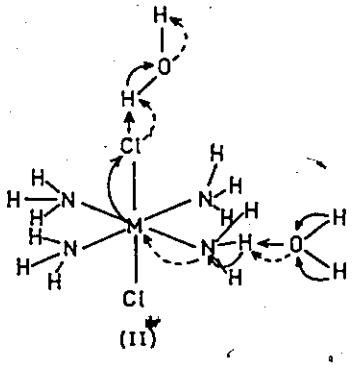

(II)

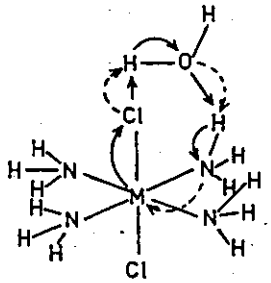

(III)

Structure (I) gives the electronegativity of the uncomplexed species and structures (II,III) illustrate the effect of second sphere interactions. According to the first bond length variation rule, Co-Cl and N-H bonds are lengthened as indicated by the solid arrows. By the second bond length variation rule, the Co-N bonds are shortened as indicated by the broken arrows. There will be an electronic "pile-up" effect at Cl^- and a "spill-over" effect towards the N atoms. These changes give rise to the following:

i) assuming symmetrical hydrogen bonding takes place the shape of the field gradient about Co does not alter drastically upon adduct formation, however its magnitude changes.

ii) The shape of the field gradient about Co changes only if the strength of the intermolecular interaction involving the chloride and the amine are significantly different. This will happen with a large donor number.

iii) The donor number characterizes the "donicity" or "ability in the charge transfer process" of the solvent, therefore, an increase in relaxation rate is expected with donor number. Therefore, a high donor number leads to a larger field gradient resulting in a shorter T_2.

iv) The relaxation of this modified field gradient is principally modulated by the rotational reorientation time of the complexed adduct because τ_2 is usually much shorter than τ_H, i.e., $\tau_2 << \tau_H$ where τ_H is the average hydrogen bond lifetime.

v) A correlation between linewidths at zero field with AN (acceptor number) is not found, implying that the donor properties of ligands such as Cl^-, NO_2^-, etc., are poor in spite of the large value (54) of the acceptor number for a solvent such as water. In this context, these ligands effectively are terminating atoms in the acceptor complex. Together with the "pile-up" effects at the nitrogen atoms, it is rather clear that the principal contribution to the quadrupole linewidths is due to fluctuation of charge densities in the first coordination shell.

SECTION 5.3.2 Relaxation in Hydrogen Bonding Solvents and Scalar Relaxation of the Second Kind

In the conclusion of Chapter Four, the field dependence behaviour of cobalt relaxation rates in aqueous solution has been attributed to non-vanishing components of the anti-symmetric term of the chemical shielding tensor. The origin of this term has been associated with second sphere

interaction as discussed in Section 5.3.1. The unique feature of this model is that T_1 is predicted to be less than T_2 if the antisymmetric term makes a dominant contribution to the overall field dependent relaxation. The primary objective of this section is to identify the origin of this term by measurement of T_1 and T_2. In addition, these relaxation measurements allow conclusive determination of the possibility of chemical exchange because such a mechanism also leads to $T_1 > T_2$.

Experimental difficulties limited the determination of T_1 to two field strengths. These results are presented in Table 5.11. An immediate conclusion that can be drawn from this data is that T_1 and T_2 are both field dependent and that shielding anisotropy contributes to the overall relaxation. The complex trans-$Coen_2(NO_2)_2^+$ was examined in three different solvents and in accord with Section 5.3.1, T_1's lengthened with decreasing DN. A second conclusion can be reached in that three types of behaviour are observed at both field strengths by the ratio T_1/T_2.

The complexes ε-$CoendienCl^{2+}$ and trans-$Coen_2(NO_2)^+$ in water and trans-$Coen_2(NO_2)_2^+$ in dimethyl sulfoxide exhibit the expected behaviour predicted by the model, i.e., $T_1/T_2 < 1$. The increase of 63% between the T_1 values at the two superconducting fields for ε-$CoendienCl^{2+}$ is significant and clearly demonstrates that the field dependence of the line widths does not arise from a chemical exchange process. For the complex trans-$Coen_2(NO_2)_2^+$ in water and dimethylsulfoxide, although the percentage increase in T_1 is smaller, the same conclusion is valid. For the complexes $Co(NH_3)_5Cl^{2+}$ and mer-$Co(NO_2)_3(NH_3)_3$ in water $T_1/T_2 \simeq 1$, both chemical exchange and $\Delta_a\sigma$ con-

tribution to the overall relaxation can be eliminated initially. A similar argument would lead to the conclusion that since $T_1 > T_2$, the relaxation for the complexes $Coen_3^{3+}$ and $Co(NO_2)_6^{3-}$ in water and the complex trans-$Coen_2(NO_2)_2^+$ in acetonitrile is dominated by chemical exchange or by scalar relaxation of the second kind. In fact, correction for scalar relaxation would yield results compatible with the above model. It is, therefore, necessary to assess scalar relaxation of the second kind in some detail.

The formal theory for scalar relaxation has been treated in Section 2.4.3. Because all of the complexes studied have directly bonded nitrogen, relaxation contribution due to scalar coupling with nitrogen are anticipated. The solutions to the Bloch equations are given by equation 2.12 and 2.13. Since $T_2^{-1} \neq T_1^{-1}$, the contribution to $1/T_2$ is larger than to $1/T_1$ (of the observed nucleus). For the Cobalt-nitrogen system, the ^{14}N and ^{59}Co resonance frequencies are well separated, the term $(\omega_I - \omega_S)^2 T_2^{S^2}$ is large ($\sim 10^{10}$) and the contribution of scalar spin-spin coupling to $1/T_1$ for the observing nucleus is negligible. The contribution to $1/T_2$ becomes

$$\frac{1}{T_2 I} = \frac{1}{3} S(S+1)\, J_{iso}^2 T_1^S \qquad [5.1]$$

leading to the equation

$$\frac{1}{T_2 Co} = \frac{8\pi^2}{3} (J_{Co-N})^2 T_1^N \qquad [5.2]$$

per Co-N bond pair. If additive properties can be assumed(2.31, 5.6), the total scalar contribution can be estimated as the sum of the individual scalar relaxation rates. Inspection of Cobalt T_1 values indicates that

the reverse relaxation process also takes place, i.e., the nitrogen is being relaxed by cobalt with the appropriate expression given by

$$\frac{1}{T_2^N} = \frac{21\pi^2}{3} (J_{Co-N})^2 T_1(Co) \qquad [5.3]$$

In order to carry out correction for scalar relaxation for both the ^{14}N and ^{59}Co relaxation rates, it is necessary to know (i) the coupling constant $J_{(Co-N)}$ (ii) ^{59}Co T_1 and (iii) ^{14}N T_1.

From known $J_{(Co-^{15}NR_3)}$ values measured by ^{15}N NMR on similar amine complexes (5.1-5.4), the coupling constant of $J_{(Co-^{14}NR_3)}$ was estimated to be $\sim$ 45Hz and $J_{(Co-^{14}NO_2)}$ is obtained from Cobalt T_1 and T_2 data of $Co(NO_2)_6^{3-}$ since the ^{14}N T_1 for $Co(^{14}NO_2)_6^{3-}$ was experimentally determined. This procedure gave a value of 56.4Hz which is comparable to the value of 60Hz obtained by estimation from a simple hybridization relationship (5.7) The measurements of ^{59}Co T_1 values present some difficulties and experimental access to ^{14}N T_1's are limited by its low sensitivity. Since ^{14}N T_2's can be determined more readily, it is more desirable to substitute ^{14}N T_2 for ^{14}N T_1 in equation 5.2. Prior to substitution, it is necessary to establish that $T_1 \simeq T_2$ for ^{14}N relaxation.

From the results of Table 5.12, the following conclusions can be drawn;

i) the observed T_2 values are, within experimental error, independent of the magnetic field strength. Relaxation due to chemical shielding anisotropy for ^{14}N is therefore negligible. This is a

great advantage since measurement at high field can be employed in the calculation at low field as well.

ii) At 28.894 MHz, $T_1 > T_2$ where data are available. By the argument presented in Section 4.3.4, this cannot be due to chemical exchange. ^{14}N relaxation is dominated by quadrupolar relaxation, and the field gradient about ^{14}N is modulated by the re-orientation rotational correlation time of the solvated complex as suggested in Section 5.3.1 under conditions of extreme narrowing, $1/T_{1Q} = 1/T_{2Q}$. The difference in T_1 and T_2 can safely be attributed to scalar coupling of ^{14}N with ^{59}Co.

This conclusion is checked by application of equation 5.3 together with estimated coupling constants and ^{59}Co T_1 values from Table 5.11. The results are listed in Table 5.12 under $T_{2\ corr}$. For the low symmetry complexes, $T_1 = T_{2\ corr}$ for ^{14}N. For the high symmetry complexes such as $Coen_3^{3+}$ and $Co(NO_2)_6^{3-}$, such a procedure for correction for ^{14}N is no longer valid since the condition for the derivation of equation 2.12 and 2.13 is no longer obeyed. In other words, the ^{14}N spin system no longer "sees" the Cobalt spins as being part of the lattice, i.e., the condition $T_1^S \ll T_1^I$ is violated. For the complex cis-$Coen_2(NO_2)_2^+$, the value of T_2 is inaccurate because the cis and trans NH_2 resonances are unresolved. For these reasons, corrected T_2 values are not listed. Upon establishing $T_1^N \simeq T_{2\ corr}^N$, equation 5.2 can be rewritten as;

$$\frac{1}{T_2}_{Co} = \frac{8\pi^2}{3} (J_{Co-N})^2\ T_{2\ corr}^N \qquad [5.4]$$

Scalar contributions towards the overall relaxation rate of Cobalt can be evaluated in this manner. In the correction for the two complexes, ε-$CoendienCl^{2+}$ and $Co(NH_3)_5Cl^{2+}$, the contribution from Co-Cl is not known because the coupling constant is unknown and there is no means of making an estimation. Therefore, in this discussion, contribution due to Co-Cl is neglected. The results are given in Table 5.16. The corrected Cobalt T_2 is listed in the first column, the ratio T_1/T_{2obs} in the second column and T_1/T_{2corr} in the third column under the appropriate operating frequency. Comparison of T_1/T_{2obs} with T_1/T_{2corr} shows that the correction is negligibly small for short T_2's but could be as much as 10% for the longer T_2's obtained for these low symmetry complexes in aqueous solution. For complexes with O_h symmetry, scalar relaxation dominates the relaxation mechanism. This is evident for both $Coen_3^{3+}$ and $Co(NO_2)_6^{3-}$ with corrections of 56% and 85% respectively. The shorter relaxation time for $Coen_3^{3+}$ simply reflects the fact that the symmetry of this complex is D_3 rather than O_h. Since the ^{14}N results were obtained in aqueous solution, and correction employing these results to trans-$Coen_2(NO_2)_2^+$ in acetonitrile or dimethylsulfoxide is strictly invalid. It does however, indicate the overall consistency of this method.

Relaxation due to the $\Delta\sigma$ term of the shielding anisotropy gives rise to $T_1/T_2 = 7/6$ under the condition of extreme narrowing. This value is comparable with the values of T_1/T_{2corr} for trans-$Coen_2(NO_2)_2^+$ in acetonitrile. From Section 5.3.1, and 5.3.2 intermolecular interaction has been demonstrated to be negligible in this solvent, leading to $\Delta_a\sigma = 0$. The ratio of $T_1/T_{2corr} = 1.113$ may then be compared with that of the value $7/6 \simeq 1.16$.

Table 5.16

^{59}Co Spin-Spin (T_2) Relaxation Time Corrected for Scalar Contribution of the Second Kind

Complex	59.035 MHz			94.457 MHz		
	T_2 corr/msec	T_1/T_2 obs	T_1/T_2 corr	T_2 corr/msec	T_1/T_2 obs	T_1/T_2 corr
trans[$Coen_2(NO_2)_2$]NO_3/DMSO	0.083	0.93	0.92	0.074	0.85	0.84
trans[$Coen_2(NO_2)_2$]NO_3/H_2O	0.250	0.93	0.90	0.229	0.91	0.87
trans[$Coen_2(NO_2)_2$]NO_3/CH_3CN	1.915	1.44	1.12	1.847	1.48	1.14
df,abe,c-[CoendienCl]Cl_2/H_2O	0.099	0.81	0.80	0.065	0.77	0.77
$[Co(NH_3)_5Cl]Cl/H_2O$	0.184	1.01	0.95	0.179	0.99	0.93
Cis-[$Coen_2(NO_2)_2$]NO_3/H_2O	0.300	0.94	0.90	0.281	0.95	0.91
mer-$Co(NH_3)_3(NO_2)_3/H_2O$	0.396	1.02	0.93	0.358	1.02	0.93
$[Coen_3]Cl_3/H_2O$	9.28	2.18	~ 1			
$Na_3[Co(NO_2)_6]/H_2O$	38.65	6.87	1			

predicted by relaxation due to the symmetric part of the shielding anisotropy tensor under the condition of extreme narrowing.

The $T_1/T_{2\ corr}$ ratio uniquely demonstrates that $T_1 < T_2$, consistent with the prediction of this model. Within this context in the extreme narrowing condition, plots of $1/T_1$ and $1/T_2$ versus B_o^2 should be linear with a common intercept (giving the quadrupolar and scalar contribution) and with the slopes for the $1/T_1$ plot being twice that for the $1/T_2$ plot. Figure 5.4 shows such a plot and Table 5.17 summarizes the slopes and intercepts for these complexes. The ratio of the slopes M_1/M_2 in aqueous solution has a value less than 2 supporting the idea that the condition $(\omega\tau)^2 << 1$ is not necessarily met. The exact decrease from 2 cannot be calculated but a consistent ratio of $\sim$ 1.5 strongly favours the solvent effect argument.

In the case of trans-$Coen_2(NO_2)_2^+$ in dimethyl sulfoxide, the value of $M_1/M_2 = 2.09$ implying that the extreme narrowing condition is met and indicating that the hydrogen bond lifetimes (in so far as hydrogen bonding is important) are shorter than those in water. Careful consideration would suggest that although dimethyl sulfoxide has a larger DN, it does not necessarily have an "average" hydrogen bonding lifetime longer than those of water since the cooperative effect is much less efficient in the former solvent. As such, the DN concept is not violated.

SECTION 5.3.3. Relaxa[illegible]of Co(III) Complexes in Weakly/Non-Hydro[illegible]ing Solvent

In Section 5.3.1 it has been established that the anamalous change in relaxation rate (at zero field) with respect to changes in solvent is

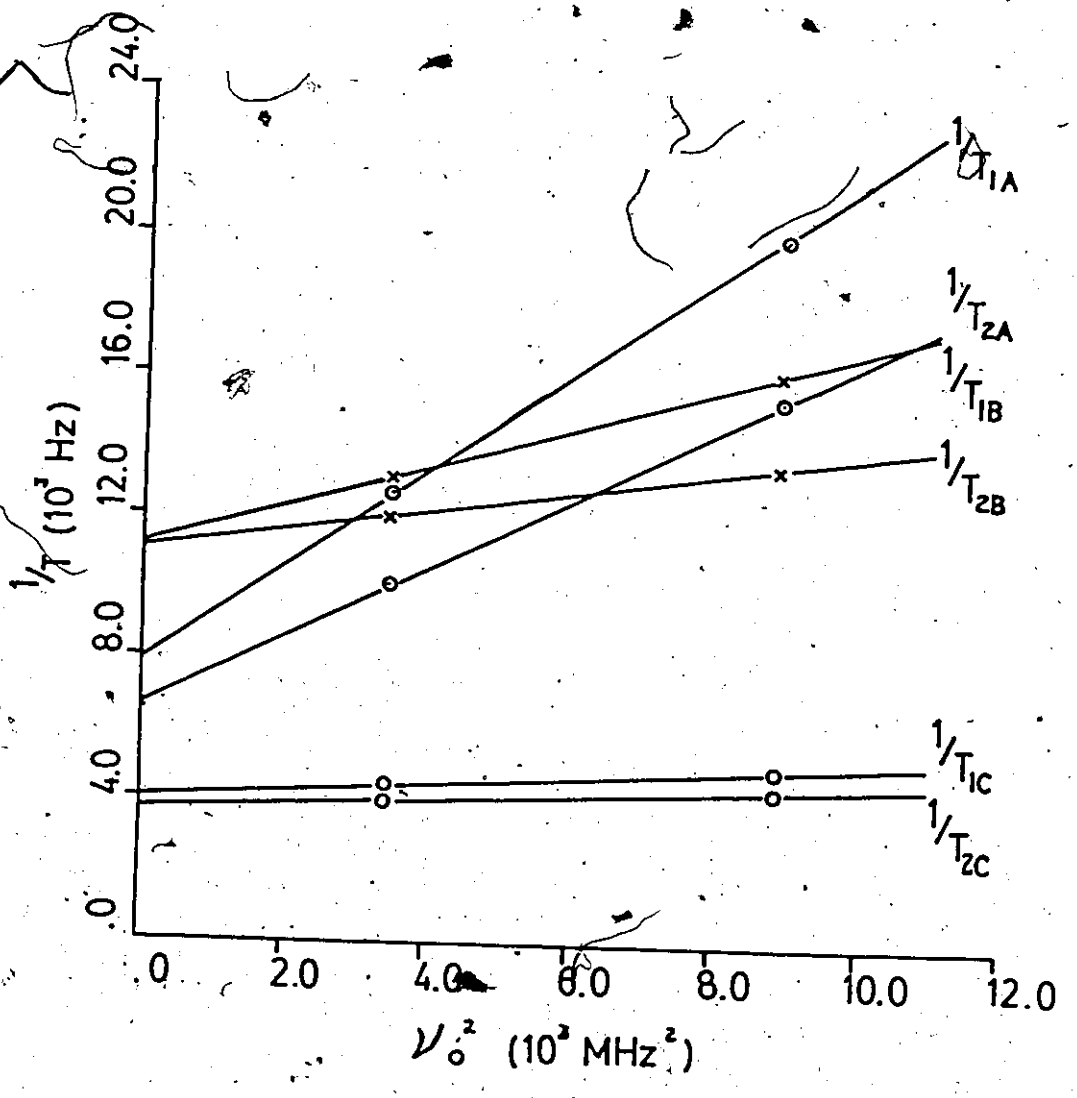

Figure 5.4 Plot of $1/T_{1,2}$ versus B_o^2

A trans-$Coen_2(NO_2)_2^+$/dimethyl sulfoxide

B ε-$CoendienCl^{2+}$/H_2O

C trans-$Coen_2(NO_2)_2^+$/H_2O

Table 5.17

Field Dependence of Relaxation in Hydrogen Bonding Solvents

Complex	$1/T_1$		$1/T_2$		$\frac{M_1}{M_2}$
	Slope(M_1)x10^{14} Hz^{-1}	Intercept/Hz	slope(M_2)x10^{14} Hz^{-1}	Intercept/Hz	
1. trans-$[Coen_2(NO_2)_2]NO_3$/DMSO	56.228	11112	26.951	11108	2.09
" /H_2O	9.851	4121	6.747	3765	1.46
2. ε-[CoendienCl]Cl_2/H_2O	138.749	7823	97.178	6714	1.43
3. $[Co(NH_3)_5Cl]Cl_2$/H_2O	4.431	5593	2.792	5337	1.59
4. cis-$[Coen_2(NO_2)_2]NO_3$/H_2O	3.697	3561	2.526	3333	1.46
5. mer-$Co(NH_3)_3(NO_3)_3$/H_2O	5.117	2547	4.930	2353	1.04

due to intermolecular interaction between complex ion and solvent. The results presented in Section 5.2 were conveniently characterized by the Donor Number. Correlation times estimated from the modified Debye equation employing solid state quadrupole coupling constants and crystal structure bond lengths suggest that:

i) the line width in acetonitrile approaches that of a freely tumbling complex ion,

ii) the extreme narrowing condition is met in the solvent acetonitrile,

iii) the relaxation mechanism for Co(III) complexes is dominated by the quadrupole interaction.

Observations (i) - (iii) strongly favour a model where second sphere interactions are negligible. This is an underlying result of the DN concept. The consequence of (i) - (iii) is that the linearity between $(\pi T_{2obs})^{-1}_{B_o=0}$ and $(\frac{e^2qQ}{h})(1+\frac{\eta^2}{3})$ for low symmetry Co(III) complexes is expected to hold in the solvent acetonitrile providing that the quadrupole coupling constant is the same in solution as in the solid state and that the rotational reorientation correlation time τ_2 is approximately constant.

Based on the results presented in Chapter 4, and Section 5.3.2, the observed relaxation rates for Cobalt amine complexes in non-hydrogen bonding solvents is the sum of the contributions from both the quadrupolar relaxation and relaxation due to scalar coupling of the second kind, i.e.,

$$\frac{1}{T_{2obs}} = \frac{1}{T_{2Q}} + \frac{1}{T_{2sc}} \qquad [5.5]$$

Under the condition $(\omega\tau_2)^2 << 1$, equation 2.10 reduces to the standard form. Substitution into equation 5.5 yields

$$\frac{1}{T_{2obs}\ (B_o=0)} = \frac{2\pi^2}{49}\left(\frac{e^2qQ}{h}\right)\left(1+\frac{\eta^2}{3}\right)\tau_2 + \frac{1}{T_{2sc}} \qquad [5.6]$$

where $\frac{e^2qQ}{h}$ is the solid state quadrupole coupling constant and η is the asymmetry parameter. As has been stated in Chapter 3, solubility limitations have prevented the measurement of linewidths in acetonitrile for the complexes $Co(NH_3)_5CN^{2+}$ and cis-$Coen_2Cl_2^+$. Therefore, their linewidths require estimation by indirect methods. It has been shown in Section 5.3.1, that the linewidths at zero field are linearly related to Gutmann's donor number for the solvents, thus this proportionality may be used to obtain an estimate of linewidths. This is done by extrapolation of plots of linewidths versus donor number to DN=14.1 (corresponding to the solvent acetonitrile). The linewidths obtained by this procedure together with those determined experimentally are collected in Table 5.18. Also listed in Table 5.18 are the solid state quadrupole coupling constants, τ_Q, determined from experimental linewidths at zero field as well as those calculated from estimated linewidths and the average radii of the free complex ion. A plot of $\frac{1}{T_{2\ obs\ (B_o=0)}}$ versus $\left(\frac{e^2qQ}{h}\right)^2\left(1+\frac{\eta^2}{3}\right)$ is shown in Figure 5.5. The slope of this plot yields a τ_2 value of 7.45 psec and an intercept of 73 Hz.

The τ_2 extracted from this plot is closely comparable to the average τ_Q of 7.82 psec from Table 5.18. The significance of Figure 5.5 is that τ_2 can only be constant when the ions are of approximately the same effective size and relaxation is not affected by intermolecular interaction. From

Table 5.18

Zero Field Linewidth and Quadrupole Coupling Constants for Cobalt(III) Complexes

Complex	$\Delta\nu_{\frac{1}{2}}(B_o=0)$ at DN = 14.1 (Hz)	$(\frac{e^2qQ}{h})^2(1+\frac{n^2}{3})(MHz)^2$	[a]free complex ion(ppm)[d]	τ_Q (10^{12}sec) in CH_3CN
trans-$[Coen_2Cl_2]Cl$	3517	3675[b]	288	7.34[a]
Cis-$[Coen_2Cl_2]Cl$	1330[a]	1331[c]	285	7.79
$[Co(NH_3)_5CN](ClO_4)_2$	863[a]	714[b]	284	9.43
$[Co(NH_3)_4CO_3]NO_3$	491	416[b]	305	9.20
trans-$[Coen_2(NO_2)_2]NO_3$	141	206[b]	303	5.35
			ave.	7.82

[a] by extrapolation procedure

[b] Ref. 4.9

[c] Ref. 4.17

[d] $a = 1/3\ (a_x + a_y + a_z)$

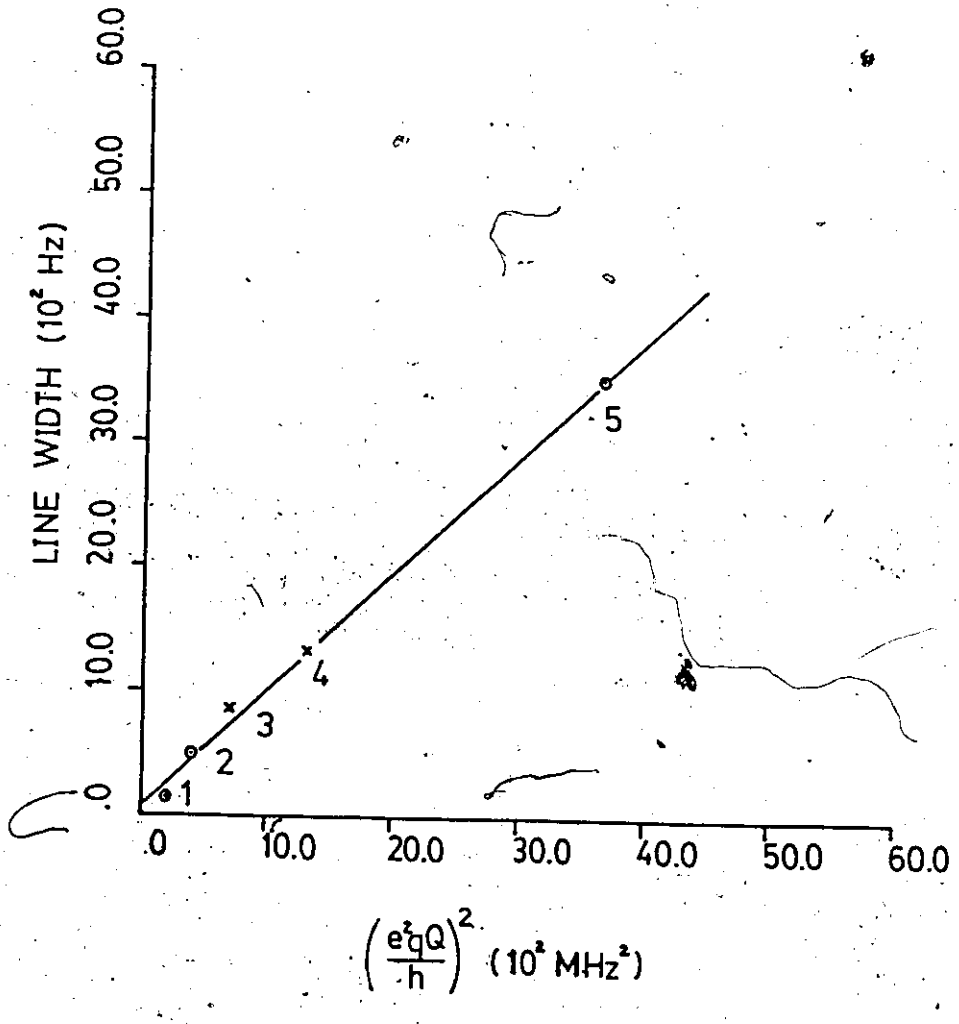

Figure 5.5 Plot of Zero field linewidths in acetonitrile versus $(\frac{e^2qQ}{h})^{2'} = (\frac{e^2qQ}{h})^2(1+\frac{\eta^2}{3})$

1 trans-$[Coen_2(NO_2)_2]NO_3$

2 $[Co(NH_3)_4CO_3]NO_3$

3 $[Co(NH_3)_5CN](ClO_4)_2$

4 cis-$[Coen_2Cl_2]Cl$

5 trans-$[Coen_2Cl_2]Cl$

the "a" values of Table 5.18 and the result of the DN concept, this is undoubtedly true. A second comment is that τ_Q can be bracketed by values obtained from both the Debye and modified Debye equation. Using an"a" value of 300 pm, η = 0.35cp, f = 0.16233 at 296.16°K;

$$\tau_{Debye}(9.67psec) > \tau_Q(7.82psec) > \tau_{Debye\ modified}(15.7psec)$$

suggesting that in acetonitrile, the traditional Debye equation gave a much closer estimation of τ_Q within the rigid sphere approximation. This is an expected result since intermolecular interaction between the ion and acetonitrile is almost negligible. Finally, the intercept of 73Hz reflects the average contribution from scalar relaxation of the second kind for these complexes. This value is in agreement with the values obtained in Section 5.3.2 for $Co(NO_2)_6^{3-}$ of $\sim$ 50Hz due to scalar relaxation of the second kind but is smaller than the value of $\sim$ 167Hz (^1H decoupled) for $Co(NH_3)_6^{3+}$ scalar spin-spin coupling with ^{14}N. The differences are clearly a reflection of the differences in both the ^{14}N T_1 as well as J_{Co-N}. Nevertheless, in view of the errors associated with relaxation time measurement the value of 73Hz lies reasonably well in the range expected for scalar relaxation of the second kind for Cobalt amine complexes.

SECTION 5.4 Summary

The solvent and field dependence of linewidth with B_o^2 was measured for nine complexes. The results of these investigations confirm the following;

i) Intermolecular interaction between ion and solvent is extremely

important and this effect accounts for as much as 80% of the line-width for a quadrupole complexed ion in a hydrogen bonding solvents.

ii) Good correlation with DN implies that the interaction with amine groups is more important than the acceptor interaction with nitro, chloro, cyano, and carbanato-type ligands.

iii) The major contribution to quadrupolar relaxation is due to charge density fluctuation in the first coordinated ligand shell resulting from intermolecular interaction.

iv) In solvents where intermolecular interaction is negligible, τ_C, the rotational reorientation time estimated by the classical Debye equation gave better agreement with experimental values.

v) $(\pi T_2)^{-1}_{B_0=0}$ versus $(\frac{e^2qQ}{h})^2 (1+\frac{\eta^2}{3})$ is linear implying that the solid state quadrupole coupling constant is a good approximation for solution quadrupole interaction. An implication is that ion-pairing may be important under these conditions.

vi) In weakly hydrogen bonding solvents, the relaxation of low symmetry Cobalt complexes is dominated by quadrupolar interaction whereas scalar spin-spin interaction with ^{14}N dominates high symmetry Cobalt amine complexes. In hydrogen bonding solvents scalar relaxation contributes no more than 10% to the overall relaxation of low symmetry cobalt complexes.

vii) The principal axis system which diagonalizes the field gradient tensor likewise diagonalizes the symmetric part of the shielding tensor, and a trend characteristic of shielding anisotropy is expected, i.e., trans > cis, mer > fac etc..

viii) The variation in the Chemical Shielding Tensor is modulated by the hydrogen bonding lifetimes whereas the relaxation of the quadrupolar interaction is modulated by the rotational reorientational motion of the solvated complex.

Spin-lattice and spin-spin relaxation time measurements agree with a model in which the antisymmetric term of the shielding tensor is non-zero. This has been attributed to site symmetry lowering at Cobalt upon interaction with solvent molecules. The magnitude of $\Delta_a\sigma$ term is determined by τ_h, the average lifetime of the hydrogen bond and the overall solvent and field dependence results compliment those of relaxation time measurements.

CHAPTER SIX

AN EMPIRICAL MODEL FOR FACILE ESTIMATION OF CHEMICAL SHIFTS AND LINEWIDTHS OF Co(III) COMPLEXES

SECTION 6.1 Introduction

Two important points emerged from the results of Chapters Four and Five, they are:

i) the chemical shift is independent of magnetic field strength, at least from 2.113T to 9.395T, and

ii) the linewidth when extrapolated to zero field for mixed ligand cobalt complexes follows simple Crystal Field (electrostatic point charge) Theory.

i.e., $\Delta\nu_{\frac{1}{2}}$ (trans-MA_2B_4) $\sim 4\Delta\nu_{\frac{1}{2}}$ (cis-MA_2B_4)

$\Delta\nu_{\frac{1}{2}}$ (mer-MA_3B_3) $\sim 12\Delta\nu_{\frac{1}{2}}$ (fac-MA_3B_3)

These findings create the possibility of forming an empirical model to assign structures of cobalt complexes containing mixed ligands in solution based on the combination of chemical shift and linewidth data. It is the purpose of this chapter to exploit this possibility.

SECTION 6.2 Theory

SECTION 6.2.1 Chemical Shift Correlations

In the literature survey of Chapter Two, it was shown that ^{59}Co NMR chemical shift is dominated by the paramagnetic term in the Ramsey equation (2.13-2.14, 2.19-2.20) and that this paramagnetic shielding term correlates

with the inverse of the first spin allowed d-d transition. This approximation was further advanced by Yamasaki et. al. (2.20) to include an orbital reduction factor k' and a radial factor $\langle r^{-3} \rangle$ to account for the covalency of the varying types of metal-ligand interaction. This type of approach generally leads to shielding tensors of the form given in Table 2.4. The isotropic chemical shift is given by the average over the three principal components of the shielding tensor.

Various authors have shown that ^{59}Co chemical shifts correlate well with

i) the sum of the electronegativities of the first-sphere ligands (6.1),

ii) $\delta = 360(X) + \sum_{i=1}^{y} \delta_i(L)$ for complexes of the type $Coen_x(NH_3)_{6-2x-y}L_y$, where $\delta_i(L)$ is a constant for a given ligand (4.3), and

iii) the rule of average environment (6.2).

Yoneda et. al. (6.2) have shown that ^{59}Co chemical shifts obey an additivity rule: "... the ^{59}Co chemical shift value in solution can roughly be given by the sum of contributions from each ligand". This additivity rule is based on M.O. calculations(6.2) as well as experimental solid state shielding values of cobalt (4.9). Thus, the additivity rule translates mathematically to equation 6.1.

$$\sigma_{iso}^{(p)} = \sum_{i} \sigma_{ii}^{p}(^{59}Co)/3 \qquad i=x,y,z \qquad [6.1]$$

This additivity treatment of the ^{59}Co chemical shift makes the same assumptions to that of the Crystal Field treatment of the splittings of the absorption spectra of diamagnetic cobalt complexes of Yamatera (4.10)

Juranic et. al. (2.27) have recently shown that for low symmetry complexes it is necessary to allow for the anisotropy of the shielding when correlating ^{59}Co chemical shifts with the inverse of the absorption band. For an octahedral complex, the lowest excited state is triply degenerate but this splits into a maximum of three states with energies of E_x, E_y, and E_z as the symmetry is lowered. In other words

$$\delta(\text{ppm}) = \frac{C}{3}\left(\frac{1}{\Delta E_x} + \frac{1}{\Delta E_y} + \frac{1}{\Delta E_z}\right) - 11{,}000 \qquad [6.2]$$

where C is a collection of various constants.

In fact, Juranic has demonstrated that ^{59}Co chemical shift correlates far better with the weighted average of wavelengths of the first absorption band for low symmetry complexes (2.27). On the basis of these findings, equation 6.2 can be modified, within the framework of the electrostatic Crystal Field Theory, to take the form of equation 6.3.

$$\delta(\text{ppm}) = \frac{1}{3}\left(\frac{1}{S_1+S_2} + \frac{1}{S_3+S_4} + \frac{1}{S_5+S_6}\right) - 11{,}000 \qquad [6.3]$$

where S_1 and S_2 are chemical shift parameters characteristic of the ligands on the x-axis, S_3 and S_4 of the ligands on the y-axis, and S_5 and S_6 of ligands on the z-axis. Equation 6.3 is justified by the fact that the electronic structure of a given complex is determined by the sum of the charges on each axis when all the distances are equal. This has been explicitly pointed out by Ballhausen (6.3). Successful application of this approach to the prediction of the splitting of the d-d electronic bands of complexes of different symmetry has been demonstrated independently by Yamatera (4.10) and Wentworth and Piper (4.11).

There are a number of approximations inherent in the use of equation 6.3 in addition to the assumption of unequal distances mentioned above:

i) The correct expressions for the electronic transition energies also include terms involving the inter-electronic repulsion (the Racah parameter) which may vary with the ligand in a different manner to the Crystal Field Splitting parameter, D_q,

ii) The orbital reduction factors (k') and the radial factor $\langle r^{-3} \rangle$ will vary from complex to complex, and

iii) The Crystal Field Splitting and hence the chemical shift parameter, S_L, for a given ligand may depend upon the presence of other ligands.

Thus given a set of chemical shift parameters S_L for all the different ligands encountered, equation 6.3 will provide a quick and simple calculation of the chemical shift of Cobalt complexes. In the light of (i) to (iii) above, equation 6.3 is only expected to give a fair fit to experimental values.

SECTION 6.2.2 Linewidth Correlations

^{59}Co has a spin of 7/2 and therefore possesses a quadrupole moment. It was demonstrated in Section 4.3.1, that quadrupole interaction dominates the relaxation mechanism at field strengths that are sufficiently low(2.11T). The linewidth $(\pi T_2)^{-1}$ will be given by equation 2.15. Assuming the condition of extreme narrowing ($\tau_2 \sim 10^{-11}$ sec) modulating the quadrupolar interaction, equation 2.15 reduces to 2.16. If the correlation times for a series of complexes are approximately the same, the differences in linewidths for different complexes will then depend on the quadrupole coupling constants, (e^2qQ/h) and the asymmetry parameters, η, of the complexes.

Linewidth variations of Co(III) complexes have been considered by various authors (6.1, 4.3). Yajima et.al. deduced from simple Crystal Field theory that the linewidths of the trans-MA_2B_4 isomer should show broader lines than the cis-MA_2B_4 isomers and that the mer isomer of the stiochiometry MA_3B_3 should show a broader line than the fac isomer of MA_3B_3. Qualitatively, this is supported by experimental results. Valiyev and Zripov (6.4) have treated the theory of quadrupolar relaxation on the basis of a point charge/point dipole approximation to rationalize the NMR linewidth. This latter theory has been applied to the ^{93}Nb linewidths of Niobium halides by Tarasov et. al (6.5) and to ^{27}Al linewidths of Aluminum halide complexes by Wehrli and Wehrli (6.6). Valiyev and Zripov's theoretical treatment of quadrupolar relaxation rates is sound and thorough, however, its main drawback is the requirement of a large number of insufficiently known parameters. For example, the expression for the relaxation rate of the $M(H_2O)_4X_2$ system is given by

$$\frac{1}{T_{1,2}} = \frac{6}{5}\left(\frac{eQ(1+\gamma_\infty)}{h}\right)^2\left[p\left(\frac{e_x}{b^3} - \frac{3d}{a^4}\right)\right]^2\tau_2 \qquad [6.4]$$

In equation 6.4, the ligand H_2O is treated as a point dipole whereas the halides are treated as two point charges. Neither the Sternheimer antishielding coefficient is readily available nor p(a measure of the field induced electronic polarization effect in the medium by the particle under consideration) can be estimated easily. In addition, all the parameters of interest require estimation, i.e., e_x-charge of the halide, d-dipole moment of coordinated H_2O, b and a are the distances of the halide and H_2O from the metal respectively and τ_2 the rotational correlation time. Therefore, although the theory is extremely sophisticated in detail, its

practical usefulness is rather limited.

An alternative approach is to adopt the point charge model for quadrupolar coupling developed by Bancroft and Platt (6.7, 6.8) which has been extensively and successfully applied to the interpretation of quadrupole coupling constants dervied from Mössbauer spectra. The simplicity of this model is that the components of the electric field gradient tensor are expressed in terms of the partial quadrupole splitting parameters (PQS-values) for the individual ligands. Thus, a single ligand gives rise to the field gradient.

$$\begin{aligned} V_{xx} &= Zer^{-3} \cdot (3\sin^2\theta\cos^2\phi - 1) \\ V_{yy} &= Zer^{-3} \cdot (3\sin^2\theta\sin^2\phi - 1) \\ V_{zz} &= Zer^{-3} \cdot (3\cos^2\theta - 1) \end{aligned} \qquad [6.5]$$

where Z is the charge on the ligand and e the charge of an electron. r, θ and ϕ have their usual definitions in the polar coordinate system. The field gradient for a complex is obtained by summing the contributions to V_{xx}, V_{yy} and V_{zz} from all six ligands with the θ and ϕ values being determined by the position of each ligand in the complex. Since it was found possible to parameterize ions and groups attached to a central metal ion, Zr^{-3} have characteristic values representing different ligands or groups. For example, in the case of a trans-CoA_4B_2 complex:

$$\begin{aligned} V'_{xx} = V_{yy} &= [-2(Zr^{-3})_A + 2(Zr^{-3})_B]e \\ V_{zz} &= [4(Zr^{-3})_A - 4(Zr^{-3})_B]e \end{aligned} \qquad [6.6]$$

where the subscripts A and B correspond to the appropriate ligands. Substituting equation 6.6 into equation 2.16 gives $\eta=0$ and

$$\Delta\nu_{\frac{1}{2}} = \frac{\pi}{98}\frac{e^4Q^2}{h^2}[4(Zr^{-3})_A - 4(Zr^{-3})_B]^2\tau_2 = [4\gamma_A - 4\gamma_B]^2$$

where $\gamma_A = \frac{\pi}{98}(\frac{e^4Q^2}{h^2})(Zr^{-3})_A\tau_2$ and $\gamma_B = \frac{\pi}{98}(\frac{e^4Q^2}{h^2})(Zr^{-3})_B\tau_2$

Following this procedure, the linewidth formula for various symmetries expressed in terms of the broadening parameter γ_L are derived and are collected in Table 6.1. The numerical values for γ_L are given in Table 6.2. The expressions of Table 6.1 agree with those given by Bancroft and Platt (6.7) for all cases where direct comparison is possible. A few numerical factors differ from those given by Tarasov et. al., (6.5). In deriving the line broadening parameters from linewidth data, only differences are obtained and there is ambiguity with respect to the sign since they appear as squares. It will be shown in Sec. 6.3 that absolute values can be obtained by comparison with Mössbauer data.

There are, however, four approximations inherent in the use of equation 2.11 for linewidth correlation;

i) The instrumental linewidth is neglected since this contribution is less than a few Hz, which is an insignificant error.

ii) In Chapters 4 and 5, it was demonstrated that chemical shielding anisotropy can be important for low symmetry complexes at low field strengths. However, the variation of the chemical shielding tensor with geometry mathematically parallels that of the field gradient tensor as demonstrated by Spiess, Haas and Hartmann(4.8) (these authors found that single crystal shielding anisotropies of Cobalt complexes are directly proportional to the quadrupolar coupling constants), therefore, the procedure developed for linewidth correlations based on quadrupolar relaxation is justified providing it is recognized that

Table 6.1

Linewidth Formula for Octahedral Complexes Derived from the Point Charge Model

Structural type*	n	Line Width Formula
MA_6	0	0
(a,bcdef)-MAB_5	0	$4(\gamma_A-\gamma_B)^2$
cis-(be,acdf)-MA_2B_4	0	$4(\gamma_B-\gamma_A)^2$
trans-(af,bcde)-MA_2B_4	0	$16(\gamma_A-\gamma_B)^2$
fac-(bef,acd)-MA_3B_3	0	0
mer-(abf,cde)-MA_3B_3	≠0	$9(\gamma_A-\gamma_B)^2 + 3(\gamma_B-\gamma_A)^2$
cis-(b,acdf,e)-MAB_4C	≠0	$(2\gamma_B-\gamma_A-\gamma_C)^2 + 3(\gamma_C-\gamma_A)^2$
trans-(a,bcde,f)-MAB_4C	0	$4(\gamma_A + \gamma_C-2\gamma_B)^2$
fac-(b,acd,ef)-MAB_3C_2	0	$4(\gamma_C-\gamma_A)^2$
mer,trans(b,adf,ce)-MAB_3C_2	≠0	$(3\gamma_B-2\gamma_C-\gamma_A)^2 + 3(2\gamma_C-\gamma_B-\gamma_A)^2$
mer,cis(b,aef,cd)-MAB_3C_2	≠0	$(3\gamma_B-2\gamma_C-\gamma_A)^2 + 3(\gamma_B-\gamma_A)^2$
cis,cis,cis(be,ad,cf)-$MA_2B_2C_2$	≠0	$(\gamma_B + \gamma_C-2\gamma_A)^2 + 3(\gamma_C-\gamma_B)^2$
trans,cis,cis(af,be,cd)-$MA_2B_2C_2$	0	$4(2\gamma_A-\gamma_B-\gamma_C)^2$
trans,trans,trans(bd,af,ce)-$MA_2B_2C_2$	≠0	$4(3\gamma_B-\gamma_C-\gamma_A)^2 + 12(\gamma_C-\gamma_A)^2$
mer(b,acf,d,e)-MAB_3CD	≠0	$2(\gamma_B-\gamma_A-\gamma_C-\gamma_D)^2 + 3(\gamma_B+\gamma_D-\gamma_A-\gamma_C)^2$
mer(b,adf,c,e)-MAB_3CD	≠0	$(3\gamma_B-\gamma_A-\gamma_C-\gamma_D)^2 + 3(\gamma_C+\gamma_D-\gamma_A-\gamma_B)^2$
trans,cis(b,af,de,c)-MAB_2C_2D	≠0	$(4\gamma_B-2\gamma_C-\gamma_A-\gamma_D)^2 + 3(\gamma_D-\gamma_A)^2$
cis,cis(b,ae,cf,d)-MAB_2C_2D	≠0	$4(\gamma_B+\gamma_C-\gamma_A-\gamma_D)^2$
trans,cis(b,ce,ad,f)-MAB_2C_2D	≠0	$(2\gamma_D-\gamma_C-2\gamma_B-\gamma_A)^2 + 3(2\gamma_B-\gamma_A-\gamma_C)^2$
cis,cis(b,ae,cd,f)-MAB_2C_2D	≠0	$(2\gamma_D+\gamma_B-2\gamma_C-\gamma_A)^2 + 3(\gamma_B-\gamma_A)^2$
cis,cis(b,ad,ef,c)-MAB_2C_2D	≠0	$(\gamma_B+\gamma_C-\gamma_A-\gamma_D)^2 + 3(\gamma_D+\gamma_C-\gamma_A-\gamma_B)^2$
trans,trans(b,ce,af,d)-MAB_2C_2D	≠0	$(4\gamma_C-2\gamma_B-\gamma_D-\gamma_A)^2 + 3(2\gamma_B-\gamma_A-\gamma_D)^2$

* the ligating atoms are arranged as indicated by the IUPAC convention reference 4.6

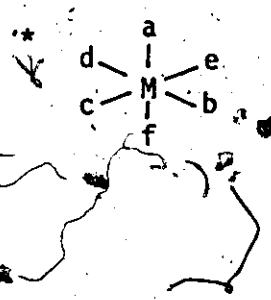

the derived γ_L values contain a contribution from chemical shielding anisotropy which will be field dependent

iii) As demonstrated in Chapters 4 and 5, scalar relaxation of the second kind also contributes to the resonance linewidth for Cobalt amine type complexes. The contribution is small when the quadrupole coupling constant is large but becomes important with complexes with high symmetry and small quadrupole coupling constants, i.e., narrow resonance linewidths. Therefore, it is expected that linewidth correlation will be quantitatively poor for the latter complexes.

iv) The imposition of the extreme narrowing condition ($\omega^2\tau_2^2<<1$) is probably valid for most complexes but may not be true for polymeric species.

Finally, it was demonstrated in Section 5.3, that $(\pi T_2)^{-1}$ is indeed proportional to $(\frac{e^2qQ}{h})^2(1+\frac{\eta^2}{3})$ in acetonitrile. This evidence therefore serves as direct justification for this linewidth correlation procedure.

SECTION 6.3 Results

Table 6.2 contains chemical shifts and linewidths for 44 Co(III) complexes. The complexes reported in this table are well characterized compounds of the types $CoA_6(O_h)$, $CoA_5B(C_{4v})$, cis-$CoA_2B_4(C_{2v})$, trans-CoA_2B_4 (D_{4h}), fac-CoA_3B_3 (C_{3v}) and mer-CoA_3B_3 (C_{2v}). This data will be used to test the model for calculating chemical shifts and linewidths described in Sec. 6.2. Data taken from the literature (4.5) is given in parentheses. ^{59}Co NMR for eleven of these compounds have not been reported previously. Of the remainder, all but five have been remeasured. Agreement with the literature chemical shift values is generally good with the exception of some of the values for the cis and trans CoA_2B_4 isomers. The present data give distinct chemical shifts for the different isomers in all cases.

Table 6.2

^{59}Co Chemical Shifts and Linewidths of Cobalt(III) Complexes

COMPLEX	δ/ppm			$\Delta\nu_{\frac{1}{2}}$/Hz		
	exp.[a]		cal.	exp.		cal.
CoA_6						
$Co(CN)_6^{3-}$	0		246	5±2	(-)	0
$Coen_3^{3+}$	7146±5	(7110)	7149	90±10	(87-120)	0
$Co(NH_3)_6^{3+}$	8175±5	(8160)	8172	172±10	(87-350)	0
$Co(N_3)_6^{3-}$	12532±5	(-)	12530	207±20	(-)	0
$Co(CO_3)_3^{3-}$/satd. $KHCO_3$	14070±5	(13975)	13789	513±20	(437)	0
CoA_5B						
$Co(NH_3)_5F^{2+}$	-	(9520)	9520	-	(1750)	10816
$Co(NH_3)_5Cl^{2+}$	8887±5	(8850)	8925	1460±100	(1750)	1311
$Co(NH_3)_5Br^{2+}$	8823±5	(8820)	8820	1317±100	(1750)	1032
$Co(NH_3)_5I^{2+}$	-	(8760)	8760	-	(2100)	484
$Co(NH_3)_5CO_3^{+}$	9062±15	(9000)	8988	1947±150	(-)	1089
$Co(NH_3)_5N_3^{+}$	8821±5	(8680)	8823	396±30	(350)	324
$Co(NH_3)_5NCS^{2+}$	8328±10	(8200)	8328	1317±100	(-)	196
$Co(NH_3)_5SCN^{2+}$	8600±10	(8760)	8545	1538±100	(-)	784
$Co(NH_3)_5H_2O^{3+}$	9147±10	(9147)	9143	4018±200	(5248)	4196

Cont....

Table 6.2 (Continuted)

Complex	δ/ppm			$\Delta\nu_{\frac{1}{2}}$/Hz		
	exp.[a]		cal.	exp.		cal
cis,trans-CoA_4B_2						
cis-$Coen_2Cl_2^+$	8974±30	(8970)	8901	5126±100	(7870)	2150
trans-$Coen_2Cl_2^+$	9333±50	(8970)	9198	8597±300	(14000)	8601
cis-$Coen_2Br_2^+$	8764±30	(8960)	8708	5420±300	(5250)	1788
trans-$Coen_2Br_2^+$	8982±20	(8960)	8939	7453±300	(9620)	7152
cis-$Co(NH_3)_4Cl_2^+$	9630±20	(9810)	9618	3400±150	(3500)	1311
trans-$Co(NH_3)_4Cl_2^+$	9808±20	(9810)	9880	5857±200	(7000)	5243
cis-$Co(CO_3)_2(NH_3)_2^-$	11626±20	(11647)	11678	820±100	(-)	1089
trans-$Co(CO_3)_2(NH_3)_2^-$	11933±20	(-)	11917	4274±100	(-)	4356
cis-$Coen_2(N_3)_2^+$	8763±10	(8400)	8711	986±100	(875)	793
trans-$Coen_2(N_3)_2^+$	9092±15	(-)	8942	3500±100	(-)	3172
cis-$Co(NH_3)_4(N_3)_2^+$	9448±5	(9400)	9476	385±20	(525)	324
trans-$Co(NH_3)_4(N_3)_2^+$	-	(9170)	9624	-	(875)	1296
cis-$Coen_2(NH_3)_2^{3+}$	-	(7400)	7480	-	(350)	103
trans-$Coen_2(NH_3)_2^{3+}$	-	(7510)	7490	-	(700)	413

Cont...

Table 6.2 (Continued)

Complex	δ/ppm exp.	δ/ppm (cal)	δ/ppm cal	$\Delta\nu_{\frac{1}{2}}$/Hz exp.	$\Delta\nu_{\frac{1}{2}}$/Hz (cal)	$\Delta\nu_{\frac{1}{2}}$/Hz cal.
cis,trans-CoA_4B_2(contd.)						
cae,bfd-$Co(dien)_2^{3+}$	6968±5	(-)	7003	395±30	(-)	30
bae,cfd-$Co(dien)_2^{3+}$	6836±5	(-)	6856	425±30	(-)	135
cis-$Coen(NH_3)_4^{3+}$	7843±5	(7790)	7822	325±30	(-)	103
cis-$Co(NH_3)_4CO_3^+$	9732±20	(9735)	9805	3291±300	(1925)	1089
cis-$Coen_2CO_3^+$	8888±20	(8880)	9020	2968±200	(3325)	1862
$Co(CN)_{6-x}(NH_3)_x$-						
$Co(NH_3)_5CN^{2+}$	6675±10	(6695)	6507	2370±200	(3005)	3025
cis-$Co(NH_3)_4(CN)_2^+$	5132±10	(5665)	4842	2489±200	(2804)	3025
trans-$Co(NH_3)_4(CN)_2^+$	5498±100	(6045)	5530	14810±2000	(4006)	12100
fac-$Co(NH_3)_3(CN)_3$	3314±5	(3325)	3176	618±50	(1002)	0
mer-$Co(NH_3)_3(CN)_3$	3991±10	(4045)	3865	4542±500	(2503)	9075
cis-$Co(NH_3)_2(CN)_4^{b-}$	2457±100	(-)	2200	2673±500	(-)	3025
trans-$Co(NH_3)_2(CN)_4^{-b}$	2744±200	(-)	2888	13096±2000	(-)	12100
$Co(NH_3)(CN)_5^{2-}$	1168±20	(-)	1223	3131±300	(-)	3025

Cont...

Table 6.2 (Continued)

Complex	δ/ppm			$\Delta\nu_{\frac{1}{2}}$/Hz		
	exp.[a]		cal	exp.		cal.
$Co(CN)_{6-2x}(en)_x^-$						
cis-$Coen_2(CN)_2^+$	4379±30	(-)	4308	3700±300	(-)	2010
trans-$Coen_2(CN)_2^+$	4727±50	(-)	4848	8089±600	(-)	8043
cis-$Coen(CN)_4^-$	2006±30	(-)	2026	5410±300	(-)	2010

[a] Values in bracket obtained from reference 4.5

[b] observed as transient in a satd. solution of $Co(NH_3)_5H_2O^{3+}$ containing 1M KCN.

In one or two cases, the present linewidths do not agree with the literature values obtained from broad line instruments. The ligands chosen range from the strong field CN^- to the weak field $CO_3^=$. The total range of chemical shifts is more than 14,000 ppm which is close to the maximum observed for Co(III) complexes. This data should therefore provide a fair and adequate test for the model.

Evaluation of S_L

To obtain the S_L values, the experimental chemical shifts for CoA_6 complexes were equated to equation 6.3 and an initial value of S_L was obtained. Following this procedure, S_L values for other ligands can be obtained via the chemical shifts of CoA_5B type complexes. The S_L values obtained in this manner were then employed to calculate the chemical shifts for other Cobalt complexes listed in Table 6.2. By iterative method, the best fit S_L values were found and are listed in Table 6.3.

Evaluation of γ_L

The calculation of the partial broadening factor γ_L is slightly more complex. According to the definition proposed above, the square root of the linewidth of a given complex, e.g., $Co(NH_3)_5Cl^{2+}$ gives the difference $(\gamma_{NH_3} - \gamma_{Cl^-})$. The signs of these differences were obtained by comparison with the analogous ^{57}Fe Mossbauer partial quadrupole coupling constants given by Bancroft and Platt (6.7,6.8). Figure 6.1 shows a plot of the differences in partial broadening constants ($\Delta\gamma_L$) versus the differences in ^{57}Fe partial quadrupole splitting constants (ΔPQS). There is a linear

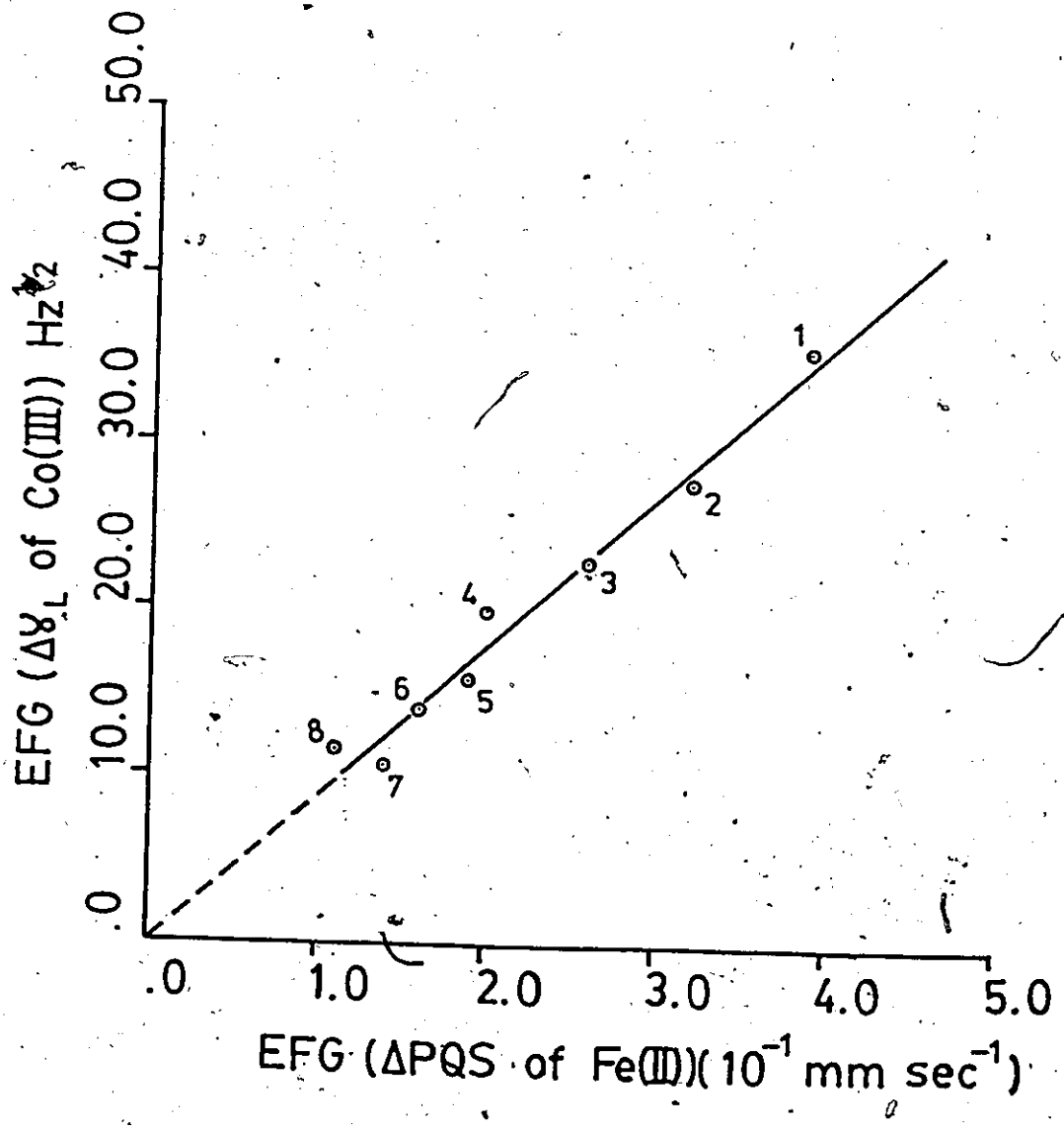

Figure 6.1 A plot of the differences in partial broadening factor ($\Delta\gamma_L$) versus the corresponding differences in the isoelectronic Fe(II) partial quadrupole splitting values for various ligand pairs.
1. CN^--H_2O 2. CN^--NH_3 3. en-Br^- 4. NH_3-Cl^- 5. en-N_3^- 6. en-NO_2^-
7. NH_3-N_3^- 8. NO_2^--NH_3

relationship with a correlation coefficient of 0.988. Since the absolute values of the quadrupole splitting constants are known, the absolute values of the partial broadening constants can be obtained from the slope of this plot. This leads to a set of γ_L values which were then adjusted to give the best fit to the linewidths of Table 6.2. The best fitted γ_L values are collected in Table 6.3. The implicit assumption made using this treatment is that since the Co(III) complexes and the Fe(II) complexes are isostructural and isoelectronic, there will be proportionality between the field gradient produced by a given ligand at the Cobalt nucleus and the electric field gradient produced by the same ligand at the Fe nucleus. The approximation involved in this assumption is probably less than the errors arising from assuming constant correlation times and neglecting relaxation mechanisms other than quadrupolar.

SECTION 6.4 Discussion

SECTION 6.4.1 Evaluation of the Model

Five of the complexes of the type $Co(NH_3)_5X^{2+}$ where x=F^-, I^-, NCS^-, SCN^- and H_2O have been included to provide the corresponding X parameters for application purposes in Chapter Seven. Since these ligands are only present in one compound, the calculated chemical shifts cannot constitute a test for the validity of the model. Of the remaining 39 complexes containing eight different ligands (NH_3, en, CN^-, Cl^-, Br^-, $CO_3^=$, N_3^- and dien), the terminal NH_2 of the dien ligand has been assigned the same parameters as the NH_2 of en. Two different parameters have been used for the central NH of dien depending on whether the three coordinate positions are planar or at right angles. The same parameters will be used for tetraen and the

Table 6.3

^{59}Co Chemical Shift (S_L) and Broadening (γ_L) Parameters for Cobalt(III) Complexes

Ligand	S_L (10^{-5} ppm^{-1})	γ_L ($Hz^{\frac{1}{2}}$)	f-factor[e]
$\overset{*}{C}N^-$	4.446	79.500	~1.7
$\overset{*}{N}O_2^-$	3.098	60.587	-
$\overset{*}{N}(CH_2CH_2NH_2)_3$	3.087	65.958	-
$\overset{*}{N}H(CH_2CH_2NH_2)_2$[a]	2.895	59.985	1.29
$\overset{*}{N}H_2CH$	2.858	59.210	1.30
$NH(CH_2CH_2\overset{*}{N}H_2)_2$[b]	2.823	58.488	1.29
$\overset{*}{N}H_2CH_2CH_2\overset{*}{N}H_2$	2.755[c]	57.080[c]	1.28
$\overset{*}{N}H_3$	2.608	52.000	1.25
$\overset{*}{N}CS^-$	2.476	45.000	1.02
$\overset{*}{S}CN^-$	2.320	38.000	0.73
$\overset{*}{O}_2^=$	2.169[c]	44.446[c]	-
$\overset{*}{I}^-$	2.168	41.000	-
$\overset{*}{N}_3^-$	2.125	43.000	0.83
$\overset{*}{B}r^-$	2.125	35.938	0.72
$\overset{*}{C}l^-$	2.058	33.895	0.78
$\overset{*}{C}O_3^=$[d]	2.017	35.500	-
$\overset{*}{O}H^-$	1.930	19.658	-
$H_2\overset{*}{O}$	1.920	19.613	1.00

* indicating ligating atom.

[a] terminal amine groups arranged 90° to each other.

[b] terminal amine groups arranged 180° to each other.

[c] per ligating atom.

[d] same value for bidentate and monodentate carbonate.

[e] References 6.9.

terminal NH_2 group of trien. The same parameters have been used for both monodentate and bidentate $CO_3^=$. Therefore, a total of nine parameters were used to fit 39 chemical shifts and a similar number to calculate the linewidths. The standard deviation of the calculated from the experimental shifts is 108 ppm. The total range of the shifts is 14,070 ppm and it would be anticipated that the fit is worst at the extreme ends of the chemical shift range. Of the four complexes for which the differences between the observed and calculated chemical shifts are greater than 200ppm, three of these four complexes are cyanide-amine compounds including $Co(CN)_6^{3-}$ and the fourth is the tris-carbonato complex. The assumption of a constant orbital reduction factor is least applicable for these compounds.

The calculations predict that cis-isomers have a smaller shift than the trans-isomer and that the fac-isomers have a smaller shift than the mer-isomers. The experimental data support these predictions in all cases. The agreement between observed and calculated linewidths is only qualitative. Thus it is predicted that trans-CoA_2B_4 will have a broader resonance linewidth than the cis-CoA_2B_4 isomers by a factor of four. This prediction is well reflected by the results of Table 6.2 although the factor is generally less than four. The discrepancies can be attributed to the chemical shielding anisotropy which was demonstrated in Chapter Four. Nevertheless, the correct prediction of the trends in the linewidths may be illustrated with the series of cis-$Coen_2X_2^+$ complexes with X^- = Cl^-, Br^-, CN^-, $CO_3^=$ and NH_3. The experimental linewidths are 5126, 5420, 3700, 2968, 986 and 350 Hz respectively compared to the calculated linewidths of 2150, 1788, 2010, 1862 793 and 103 Hz respectively. Similarly, the mer-isomers always showed broader lines than fac-isomers as predicted. The model predicts the fac-isom-

er to have a zero quadrupolar broadening. The observed residual width of a few hundred Hz probably arises from scalar relaxation of the second kind with the nitrogen ligands for the complexes considered. The above considerations, therefore, demonstrate the direct usefulness of this simple model.

SECTION 6.4.2 Quantitative Correlations

Since the point charge model used to calculate the linewidth parameters uses precisely the same assumptions as the familiar Crystal Field theory used to obtain the Crystal Field splitting parameter, Dq, from electronic spectra, a correlation of γ_L with the *f*-factor of Jorgensen (6.9) is expected. This is due to the fact that Dq is expressed in terms of ligand contributions and metal ion contributions, i.e.,

$$10\ Dq = f_{ligand} \times G_{ion}$$

The *f*-factors evaluated by Jorgensen are also tabulated in Table 6.3 and the resulting plot of *f*-factor versus γ_L for the same ligand is shown in Figure 6.2. An excellent linear correlation (0.98) is obtained with the plot passing through the origin.

Figure 6.3 gives a plot of the chemical shift parameter S_L versus the linewidth parameter γ_L. Although the plot is not linear, there is a smooth correlation. The deviation from linearity is believed to reflect that E and hence S depend on both Dq and the Nephelauxetic parameter, β, and that for strong field ligands change in the orbital reduction factor, k', cannot be neglected. This result is consistent with the progressive Crystal Field - Ligand Field treatment of electronic absorption by Yamatera (4.10). One other interesting point to note is that the intercept on the

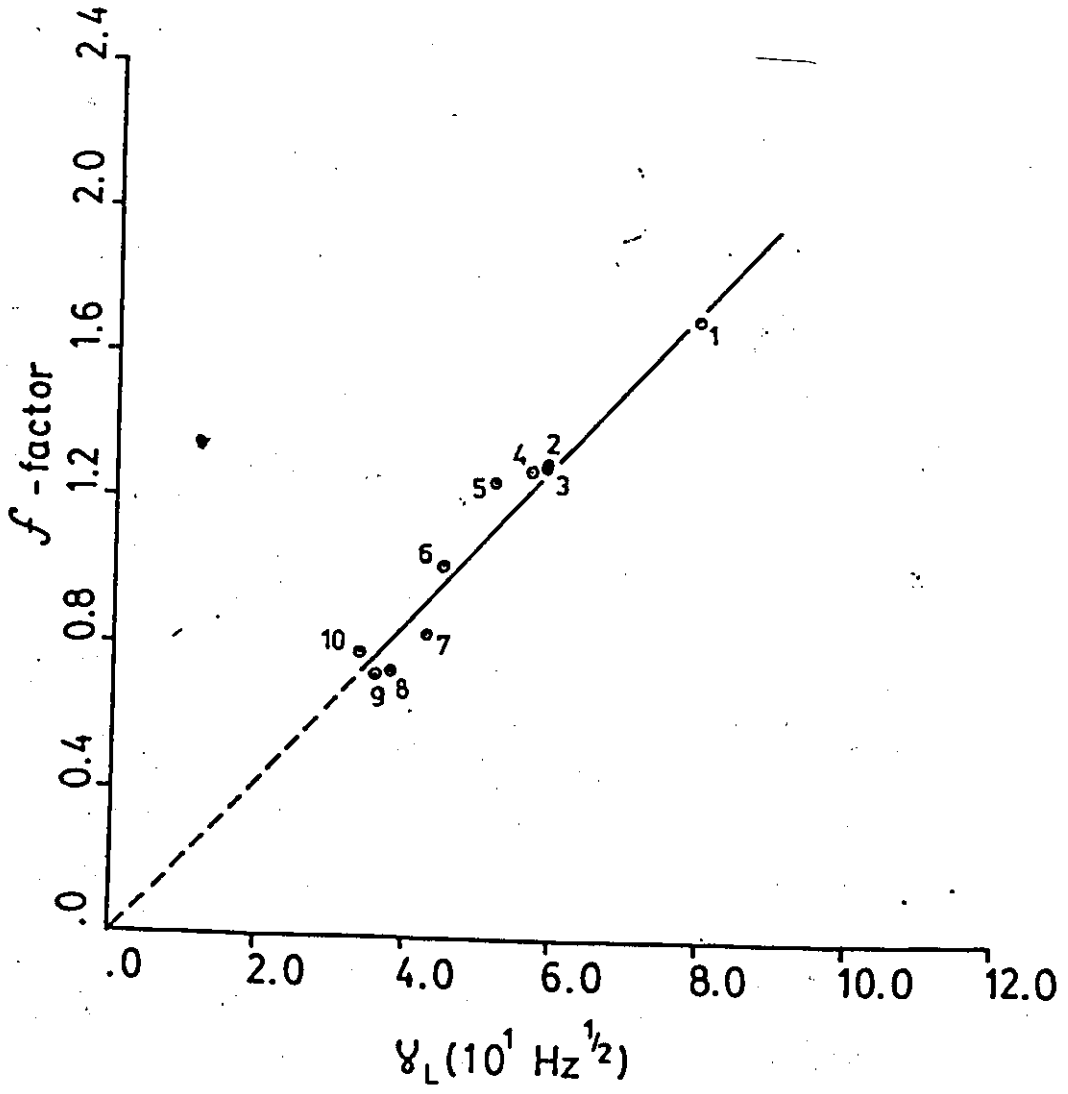

Figure 6.2 A plot of the ligand free field factor f versus the partial broadening factor γ_L.

1. CN^- 2. $NH(CH_2CH_2NH_2)_2$ 3. NH_2OH 4. $NH_2(CH_2)_2NH_2$
5. NH_3 6. NCS^- 7. N_3^- 8. SCN^- 9. Br^- 10. Cl^-

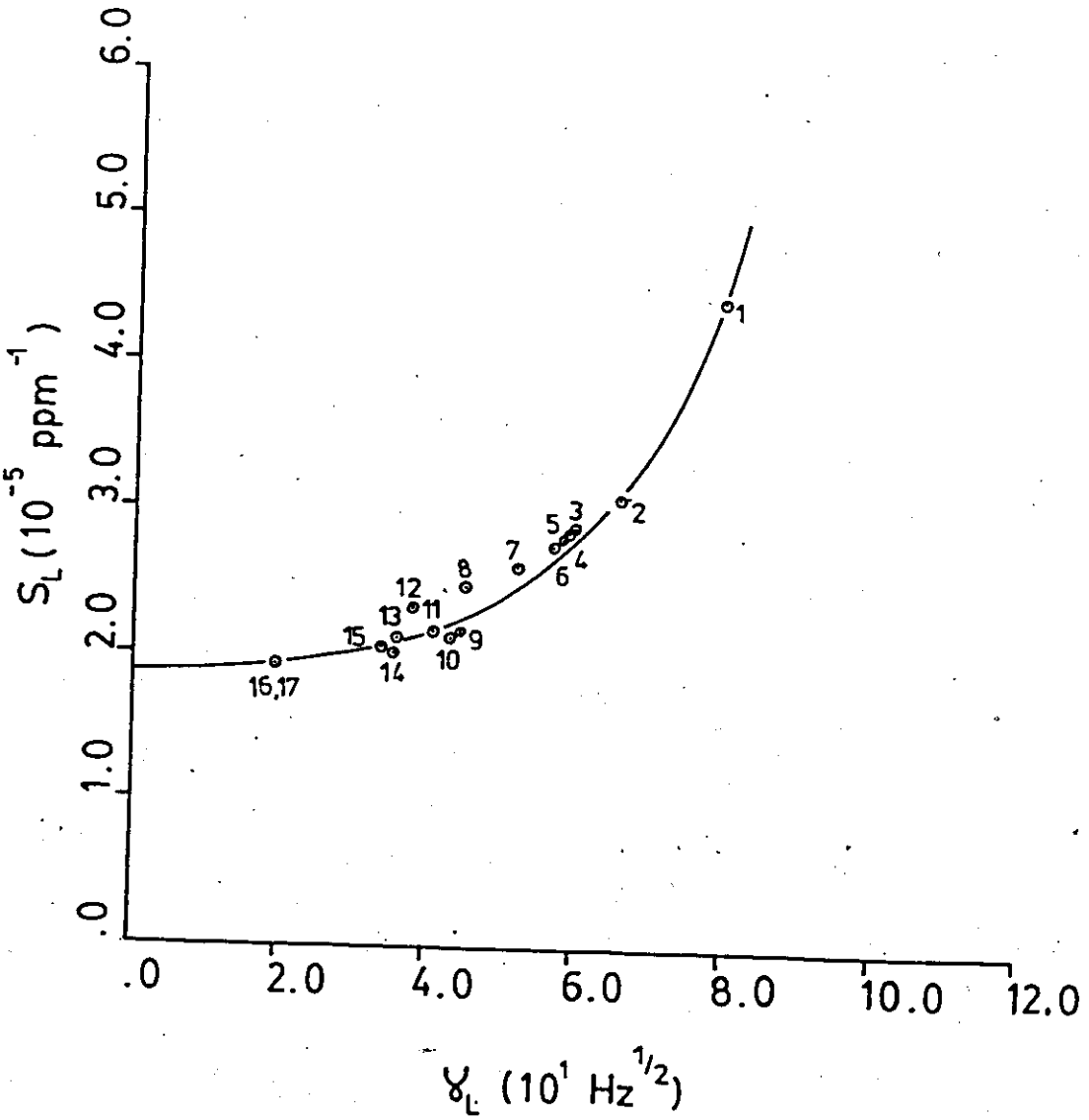

Figure 6.3 A plot of the Shift parameter S_L versus the Partial Broadening factor γ_L.

1. CN^- 2. $N(CH_2CH_2NH_2)_3$ 3. $NH(CH_2CH_2NH_2)_2$* 4. NH_2OH
5. $NH(CH_2CH_2NH_2)_2$ 6. $NH_2(CH_2)_2NH_2$* 7. NH_3 8. NCS 9. SCN^-
10. $O_2^=$ 11. I^- 12. N_3^- 13. Br^- 14. Cl^- 15. $CO_3^=$
16. OH^- 17. H_2O

S_L axis correspond to the S_L value for F^-(1.868×10^{-5} ppm^{-1}) with an approximately zero broadening factor. Low spin $Co(III)F_6^{3-}$ is not known.

It may be suggested that the combination of both Figures 6.2 and 6.3 provides some quantitative usefulness since both the linewidth parameter and the chemical shift parameter provide an indication of the position of a ligand in the spectrochemical series. ^{59}Co NMR spectra may therefore be used to obtain information in cases where assignments of electronic spectra are uncertain. In the case of the Cobalt di-oxygen complexes, the d-d electronic spectra are most often complicated by the charge transfer band corresponding to the transfer of an electron to the Cobalt d_z2 orbital from the $\pi^*_{2p}O_2$ orbital.

SECTION 6.4.3 Further Testing of the Point Charge Model

Table 6.4 presents chemical shifts and linewidths of fourteen low symmetry Co(III) complexes. Most of these complexes have three different ligands and offer a variety of isomeric possibilities. Most of this data is taken from the literature (4.5). None of this data appeared in Table 6.2 in the calculation of ligand parameters and therefore provides a further test for the model. For the fourteen complexes in this table, the standard deviation between observed and calculated chemical shifts is 57ppm. Most of the data is from older literature where accuracy is not comparable to modern F.T. instruments. Nevertheless, the model clearly demonstrates that it has predictive values for spectral parameters for complexes with mixed ligands.

Table 6.4

^{59}Co Chemical Shifts and Linewidths for Low Symmetry Cobalt(III) Complexes

Complex [a]	δ/ppm			$\Delta\nu_{\frac{1}{2}}$/Hz		
	exp		cal	exp		cal
cis, cis, cis-Coen$(NH_3)_2Cl_2^+$	-	(9320)		-	(5342)	1783
cis, cis, trans-Coen$(NH_3)_2Br_2^+$	-	(9310)	9270	-	(8584)	5537
cis-Coen$_2(NH_3)Cl^{2+}$	-	(8050)	9084	-	(3500)	1782
cis-Coen$_2(NH_3)Br^{2+}$	-	(8040)		-	(3500)	1462
df, abe, c-CoendienCl^{2+}	7758 ± 30	(-)	7875	2787 ± 100	(-)	2454
de, abf, c-Coendien Cl^{2+}	7964 ± 40	(-)	7951	3194 ± 200	(-)	2290
mer-Coen$(NO_3)_3Br^{2+}$	-	(8390)	8435	-	(4375)	809
mer-Co(dien)Cl_3	9988 ± 5	(-)	9977	2080 ± 200	(-)	6464
fac-Co$(NH_3)_3(N_3)_3$	9917 ± 2	(9970)[b]	9911	250 ± 10	(297)[d]	0
$Co(NH_3)_5NO_2^{2+}$	7652 ± 1	(7620)	7623	295 ± 30	(262)	295
cis-Coen$_2(NH_3)_5(H_2O)^{3+}$	-	(8350	8395	-	(12250)	4957
fac-Coen$(NH_3)_5NO_2^{2+}$	-	(7255)	7277	-	(295)	50
Coen$(NH_3)(OH)_3$	-	(10860)	10966	-	(-)	14626
tr-Co$(NH_3)_4(CN)(H_2O)^{2+}$	-	(6950)	7017	-	(-)	100

[a] values obtained from reference 4.5

[b] in dimethylsulfoxide

SECTION 6.5 Summary

A simple point charge model has been developed for calculating the chemical shifts and linewidths obtained from the ^{59}Co NMR spectra of Co(III) complexes. The chemical shift calculations assume the predominance of the paramagnetic term in the Ramsey equation and the relationship of this term to the energies of the d-d electronic transitions. The linewidth calculations assume the predominance of quadrupolar broadening and use a similar point charge model to calculate the electric field gradients in a manner used to interpret Mossbauer spectra. The model is tested by application to sixty known complexes. One chemical shift parameter, S_L, and one partial broadening parameter, T_L, are required for each different type of ligand. These parameters are related to each other and to the Crystal Field splitting parameters of the ligands. The calculation can be applied to complexes of any symmetry and can differentiate between geometrical isomers of the same stiochiometry. The entire range for Co(III) complexes was covered and the standard deviation between the calculated and experimental values is 108 ppm. Linewidth calculation is only qualitative due to the complication of chemical shielding anisotropy relaxation. It nevertheless provided additional information for aiding assignments.

The errors involved in other approximations are assumed to be small compared to the assumption of a constant correlation time for complexes given in Tables 6.2 and 6.4 and may be estimated to be ± 10%. Polymeric complexes will have significantly longer correlation times and the linewidths are likely to be significantly broader than those calculated by the above simple procedure.

Chemical shift calculations are applied to all field strengths whereas linewidth calculations are limited to low field.

CHAPTER SEVEN

CHARACTERIZATION OF μ-PEROXO-COBALT-DIOXYGEN COMPLEXES- AN APPLICATION OF THE POINT CHARGE MODEL

SECTION 7.1 Introduction

Since the discovery of the first Cobalt dioxygen complex, the physical characterization of the peroxo-Cobalt dioxygen complexes has usually relied on the observation of a characteristic CT (Charge Transfer) band in and slightly below the Soret region (330-400nm) of the electronic spectrum, or a stretching frequency of $\cong 900cm^{-1}$ in the vibrational spectrum (Raman spectroscopy). Although these characteristic frequencies serve as quick and simple "fingerprint" identification for di-oxygen complex, they do not provide information regarding the detailed arrangement of ligands about the metal center. This is particularly true for mixed ligand systems.

In Chapter Six, the Point Charge Model has been developed for this purpose. Since chemical shifts and linewidths are highly sensitive to the geometrical arrangements of the ligands about the Cobalt ion, this serves as a more sensitive probe for the geometric structure of dioxygen complexes. The significance of knowing the precise assignment will become apparent in Chapter Eight. In this chapter, the Point Charge Model for ^{59}Co chemical shifts and linewidths will be utilized to identify geometrical isomers of Cobalt di-oxygen complexes.

SECTION 7.2 Results.

A series of water soluble Cobalt dioxygen complexes was prepared and

the ^{59}Co NMR chemical shifts and linewidths were measured at three field strengths (21.252 MHz, 59.035 MHz and 94.457 MHz). These results are summarized in Table 7.1. Again, some complexes showed a linear and some a non-linear dependence of linewidth with B_o^2. This is evident from the results presented in the table. In general, there is a great tendency for $\Delta\nu_{\frac{1}{2}}$ versus B_o^2 plots to deviate from linearity. This is consistent with an expected longer correlation time for tumbling motion. For single bridged dioxygen complexes, the possibility of rotation about the O-O bond may be important.

For the complexes $(Co(salen))_2O_2(DMSO)_2$ and $(Co(salen))_2O_2(DMF)_2$, the observed chemical shifts and linewidths are identical within experimental error to that of the complex $[(Co(salen))_2O_2(H_2O)]_2$. Hydrolysis of the DMSO and DMF complexes is indicated. Solution molecular weight studies and ^1H NMR results are dealt with in Sec. 7.4.

The NMR spectrum of the complex $(Co(NH_3)(trien))_2O_2^{4+}$ has been measured at both high and low pH's to examine the possibility of μ-amine bridge formation. An anticipated linewidth increase of a factor of around ten would result from this behaviour. The observed small change in linewidth and chemical shift from pH 4.75 to 10.5 is therefore more consistent with broadening due to amine proton exchange.

SECTION 7.3 Discussion

The Cobalt di-oxygen complex with 2:1 $Co:O_2$ stoichiometry presented in Table 7.1 are usually regarded as Co(III) complexes of the peroxy anion. This formulation is consistent with the molecular structure of $(Co(NH_3)_5)_2O_2(SO_4)(HSO_4)_3$ determined by x-ray crystallography (7.2). The chemical shift of this

Table 7.1

^{59}Co Chemical Shift and Linewidth of Cobalt Di-Oxygen Complexes

Complex Assignment	21.252 MHz		59.035 MHz		94.457 MHz		Calculated
	δ/ppm	$\Delta\nu_{\frac{1}{2}}$/Hz	δ/ppm	$\Delta\nu_{\frac{1}{2}}$/Hz	δ/ppm	$\Delta\nu_{\frac{1}{2}}$/Hz	δ/ppm($\Delta\nu_{\frac{1}{2}}$/Hz)
$\{(Co(NH_3)_5)_2O_2^{4+}$/6MNH$_4$OH	8759±5	1172±25					8758(228)
sym[a]-ec(adf),b-$(Co(NH_3)(trien))_2O_2^{4+}$/pH=10.5	7655±10	1913±50					7680(830)
/pH=4.75	7672±10	1766±50					
sym-$(Co(salen))_2O_2(DMSO)_2$[b]	8369±100	12854±1500			8367±50	13207±1000	
sym-$(Co(salen))_2O_2(DMF)_2$[b]	8375±100	13264±2000					
sym-$((Co(salen))_2O_2(H_2O))_2$	8365±100	13249±1500			8381±50	13153±2000	
sym-edf,ac,b-$(Co(dien)(en))_2O_2^{4+}$	7555±5	760±30	7552±20	846±20	7554±10	1282±50	7681(379)
sym-def,ac,b-$(Co(dien)(en))_2O_2^{4+}$	7572±5	850±50	7569±10	924±20	7568±20	1661±50	7710(819)
sym-aef,cd,b-$(Co(dien)(en))_2O_2^{4+}$	7652±10	1453±50	7654±20	2231±50	7650±20	3560±100	7795(718)
sym-edacf,b-$(Co(tetraen))_2O_2^{4+}$	7447±5	777±50	7456±2	967±50	7455±1	958±30	7458(572)
sym-aedcf,b-$(Co(tetraen))_2O_2^{4+}$	7484±2	364	7483±1	553±50	7483±1	667±30	7484(408)
sym-deacf,b-$(Co(tetraen))_2O_2^{4+}$	7569±10	1311±50	7560		7576±2	2306±250	7575(985)
(dfcaa',ed'e'b'f'),bc'-$(Co(tetraen))_2O_2^{4+}$[c]	7516±10	970±100	7515±5	1721±200	7518±1	1621±50	7502(1113), 7556(772)
					7552±1	3858±400	
(fcdaa',f'bcde'),bc'-$(Co(tetraen))_2O_2^{4+}$[c]	7408±50	2354±200	7417±50	8500±1000	-	-	7381(638) , 7556(772)
(cfed'e',f'b'a'ad),bc'-$(Co(tetraen))_2O_2^{4+}$[c,d]					7494±1[d]	801±140	7498(1061), 7575(985)
					7594±3[d]	3932±600	
(acff'b',a'e'd'ed),bc'-$(Co(tetraen))_2O_2^{4+}$[c,d]	7614±30	2985±200	7632±30	4200±800	7640±2	6386±400	7612(960) , 7458(572)

[a] symmetric with respect to peroxo-bridge

[b] ^{1}H NMR indicated that DMSO, DMF is replaced by H_2O followed by dimerization to form sym-$(Co(salen))_2O_2(H_2O))_2$. Solution molecular weight studies support this assignment and the resonance is best assigned to the Cobalt center of the inner dimeric pair. The terminal Co(salen) groups do not conform to $Co^{III}O_2{}^*Co^{III}$ formalism(e). This is supported by kinetic results. see Sections 7.4, and 8.2.

[c]
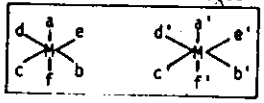

[d] assignment is less certain

[e] Reference 7.1

compound supports this electronic assignment. This chemical shift may be compared with those of several other complexes of the type $Co(NH_3)_5X^{n+}$ collected in Table 7.2. These data indicate that the position of the peroxy anion in the spectrochemical series is intermediate between N_3^- and Br^- with a Crystal Field splitting similar to I^-. This conclusion (i.e., they are normal Co(III) complexes) is supported by the chemical shifts of the remaining di-oxygen complexes containing amine and peroxy ligands. Employing the same strategy as in Chapter Six, chemical shift parameter and linewidth parameter were determined to be 2.17×10^{-5} ppm^{-1} and 44.446 $Hz^{\frac{1}{2}}$ respectively. These best fit values for the $O_2^=$ ligand quantitatively place the peroxy ligand in a

Table 7.2

^{59}Co Chemical Shifts and Linewidths of $Co(NH_3)_5X^{n+}$ Complexes

Complex	δ/ppm	$\Delta\nu_{\frac{1}{2}}$/Hz
$Co(NH_3)_5CN^{2+}$	6641±20	3260±200
$Co(NH_3)_5NO^{2+}$	7576±5	440±20
$Co(NH_3)_5N_3^{2+}$	8671±5	172±10
$(Co(NH_3)_5)_2O_2^{4+}$/6MNH_4OH	8759±5	1172±25
$Co(NH_3)_5I^{2+}$	8760*	
$Co(NH_3)_5Br^{2+}$	8820	1317±100
$Co(NH_3)_5Cl^{2+}$	8887±5	1460±100
$Co(NH_3)_5H_2O^{3+}$	9122±10	4005±200

*Reference 4.5

position closer to N_3^- than to I^- in the spectrochemical series. From the linear relationship of Figure 6.2, the f value for $O_2^=$ is determined to be 0.95.

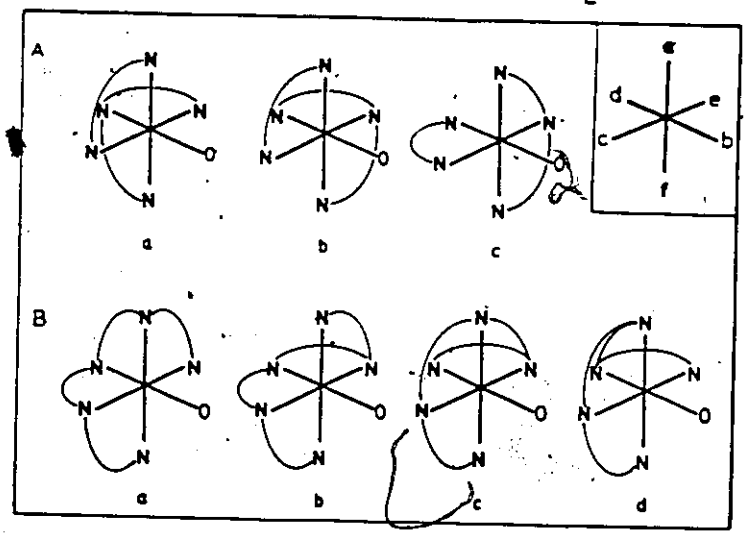

Figure 7.1 Isomeric Structures for (A) $(Co(en)(dien))_2O_2^{4+}$ and (B) $(Co(tetraen))_2O_2^{4+}$

For Cobalt dioxygen complexes containing mixed ligands, geometrical isomerism is expected. In principle, both ^{13}C and ^{59}Co NMR can be used to obtain information regarding the geometries of isomers of the complex $(Co(en)(dien))_2O_2^{4+}$. The three isomers expected for this complex are illustrated in Figure 7.1(A). The ^{13}C spectrum is expected to show four resonances for isomer (c), four resonances for isomer (b) and three resonances for isomer (a). The ^{13}C spectrum (Figure 7.2) at 100.577 MHz demonstrates that several isomers are present but is not useful in making assignments.

The spectra of Figure 7.3 illustrate the ^{59}Co NMR spectrum of the same complex at three different fields. In Figure 7.3(A), corresponding to the low field 21.252 MHz spectrum, only two resonances are immediately obvious. Upon going to higher fields (Figure 7.3(B) and (C)), the low field resonance is resolved into three components with distinctly different chemical shifts corresponding to the three isomers. The increased resolution obtained from the

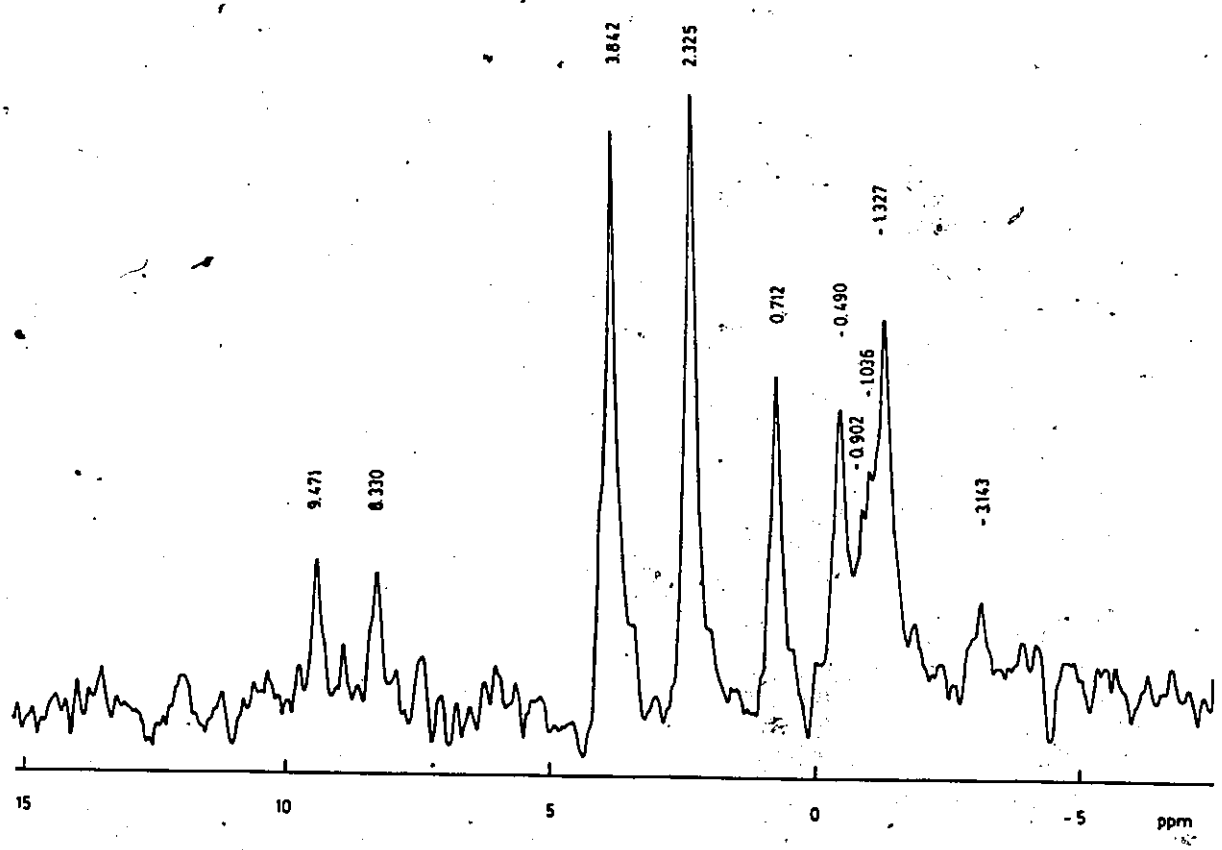

Figure 7.2 100.577 MHz ^{13}C NMR spectrum of $(Co(en)(dien))_2O_2^{4+}$ in H_2O (saturated, referenced to 0.1M $Coen_3^{3+}$).

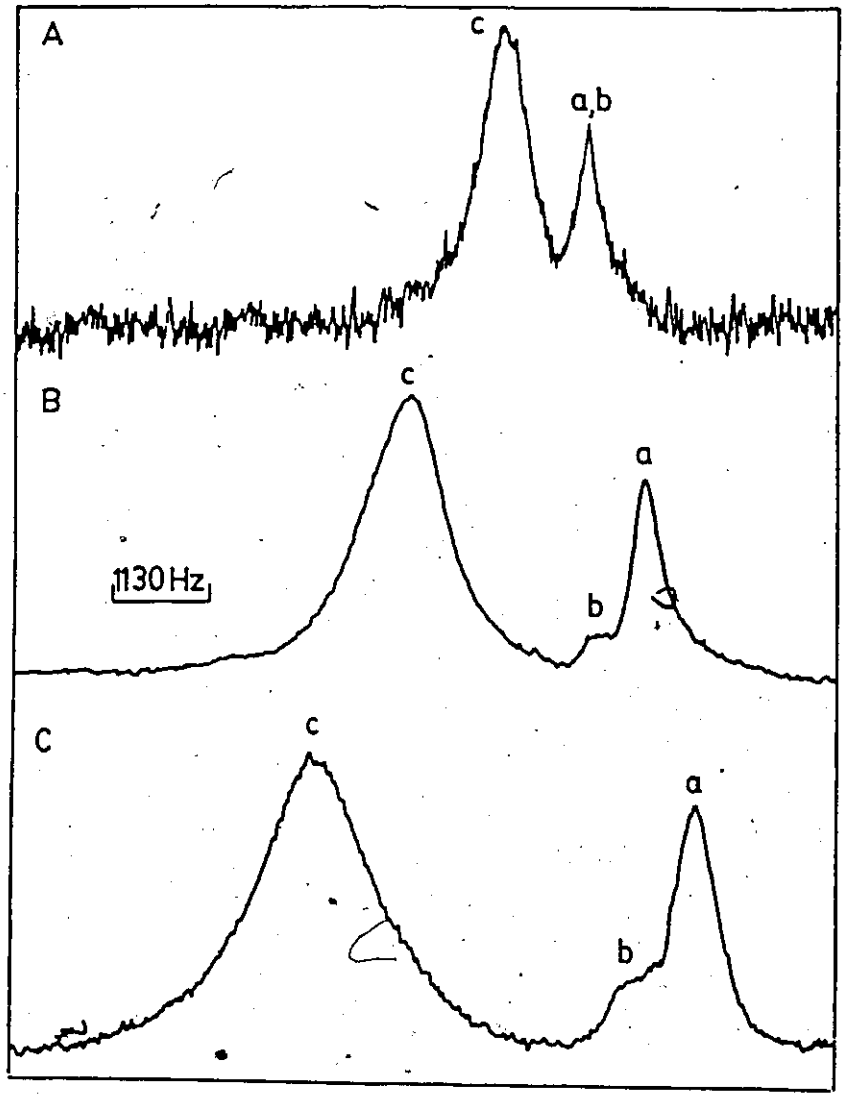

Figure 7.3 ^{59}Co NMR spectrum of $(Co(en)(dien))_2O_2^{4+}$ (A) 21.252MHz (B) 59.035MHz (C) 94.457MHz. The assignments correspond to the structures of Figure 7.1 and Table 7.1.

59.035 MHz spectrum (Figure 7.3(B)) tends to be offset by an increase in broadening due to shielding anisotropy at 94.457 MHz (Figure 7.3(C)). Nevertheless, these spectra clearly demonstrate the advantage of using high field ^{59}Co NMR over ^{13}C NMR in this particular application.

The assignment of the ^{59}Co resonances can be accomplished by application of the point charge model developed in Chapter Six. According to the model, a low field resonance at 77 ppm from the central line (observed 80 ppm) and a high field resonance of 37 ppm from the central line (observed 17 ppm) are predicted. The model also correctly predicts that the highest field component will have the smallest width. The linewidths for the remaining isomers are less satisfactory in comparison to calculated widths. This poor correlation may well be due to complication by CSA relaxation effects as demonstrated in Chapter Four. It is to be noted that the calculated chemical shifts for these isomers are all 130-140 ppm higher than the experimental values but the relative shifts and linewidths are well predicted. The assignments for the three isomers are given in Table 7.1. The possibility of cis/trans isomerism about the peroxo bridge is neglected. An interesting point is that the assignments of cis/trans isomers of a and b of Figure 7.1 (A) has the reverse order, i.e., the cis isomer has a larger chemical shift than the trans isomer. This type of behaviour has been observed in the ^{93}Nb (24.5 MHz) spectrum of $[NbCl_nBr_{6-n}]^-$ (n=0 to 6) in acetonitrile solution by Tarasov et al. (6.5), and is predicted by this model when ligands have similar shielding parameters or the complex has extremely low symmetry.

Four isomers are expected for $(Co(tetraen))_2O_2^{4+}$ as shown in Figure 7.1(B). This is consistent with the ^{59}Co spectrum at 21.252 MHz (Figure 7.4(B)). However, the 94.457 MHz spectrum (Figure 7.4(A)) shows a minimum of seven lines. Computer fitting requires eight components in order to obtain a satisfactory fit ($\chi^2/df=1.17$). The fitting in the region between δ = 7516 ppm and δ = 7494 ppm is less satisfactory. Both phasing errors and acoustic ringing cause distortion of the resonance shape resulting in poor fitting. The four symmetric* isomers have calculated shifts of 7381, 7458, 7484 and 7575 ppm and their calculated linewidths are 638, 571, 408 and 985 Hz respectively corresponding to structures a, d, b, c in Figure 7.1(B). From Figure 7.4(A) only the symmetric isomers of d, b and c are observed. For these resonances, the 21.252 MHz and 59.035 MHz spectra data are consistent reinforcing their assignments. Since aquated species resonate at much larger chemical shift values, the additional resonance can only be due to poly-bridged (tri)-meric complexes. The di-bridged μ-peroxo, μ-ethylenediamine complexes of Cobalt(III) have been identified by Nakon et. al (1.98) using ^{13}C NMR.

An obvious expectation in the distinction between the symmetric mono-bridged and asymmetric tri-bridged complexes would be an increase in the correlation time of the latter resulting in larger linewidths. Linewidth correlations for these latter complexes are much less reliable for reasons such as possibilities of asymmetric rotation as well as diffusion and the correlation time becomes a complicated function of the individual

---

* symmetric with respect to the $O_2^=$ bridge

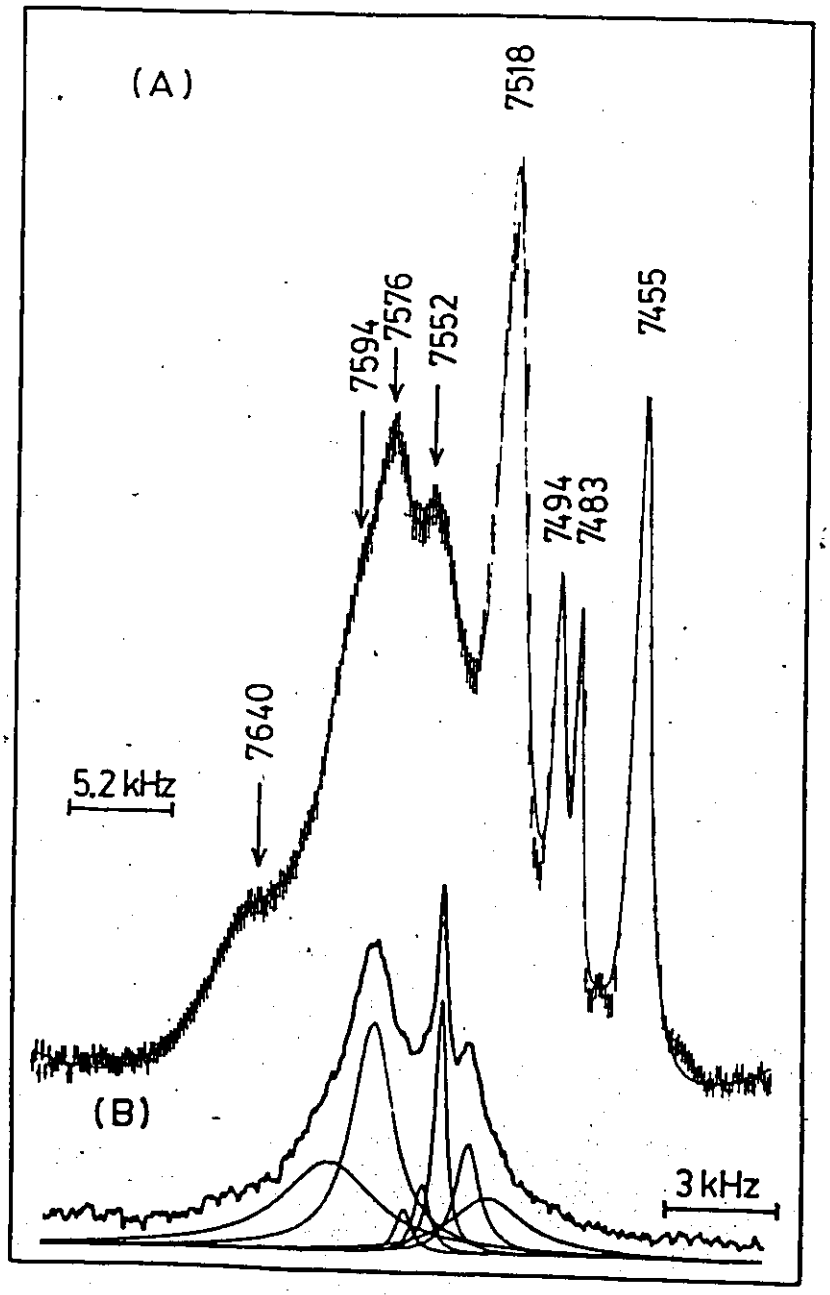

Figure 7.4 ^{59}Co NMR spectrum of $(Co(tetraen))_2O_2(ClO_4)_4$ in aqueous solution (A) 94.457MHz (9.395T) (B) 21.252MHz (2.1139T). In (A) the continuous line is the simulated spectrum.

τ's contributing to the molecular motion as illustrated by Spiess (2.35). The assignment therefore relies on the calculated chemical shift values only. From Figure 7.4(A) and Table 7.1 where 59.035 MHz data is available the resonances at 7518 and 7552 can be compared with the calculated chemical shift values of 7502 and 7556 ppm forming one dimeric tri-bridged isomeric pair. The resonances at 7417 and 7552 ppm arise from another dimeric tri-bridged complex. The assignments for all other resonances are indicated in Table 7.1. The signal corresponding to the calculated chemical shift of 7381 ppm was not observed on the 94.457 MHz spectrum but was observed on both the 21.252 MHz and 59.035 MHz spectra. The linewidth obtained from the 21.252 MHz spectrum ruled out the existence of the corresponding symmetrical mono-bridged possibility. Since the increase in linewidth from 21.252 MHz to 59.035 MHz is rather large, it is possible that the signal corresponding to this chemical shift value becomes extremely broad and is not observed on the 94.457 MHz spectrum. Thus, for complex spectra, data obtained at various field strengths is necessary for an overall analysis.

A final example of the direct application of the Point Charge Model involves an experiment in which a mixture in the ratio of one mole of $Co(SCN)_2$, two moles of ethylenediamine and four moles of KSCN was oxygenated in aqueous solution. The initial ^{59}Co NMR spectrum obtained at 21.252 MHz is shown in Figure 7.5(B). The time required to obtain this spectrum is one hour. The corresponding 94.457 MHz spectrum (Figure 7.5(A)) of the mid-range region, obtained in 15 minutes, shows additional transient lines. The spectrum was computer fitted ($x^2/df = 0.15$) giving a total of eight species. The observed and calculated chemical shifts and linewidths are

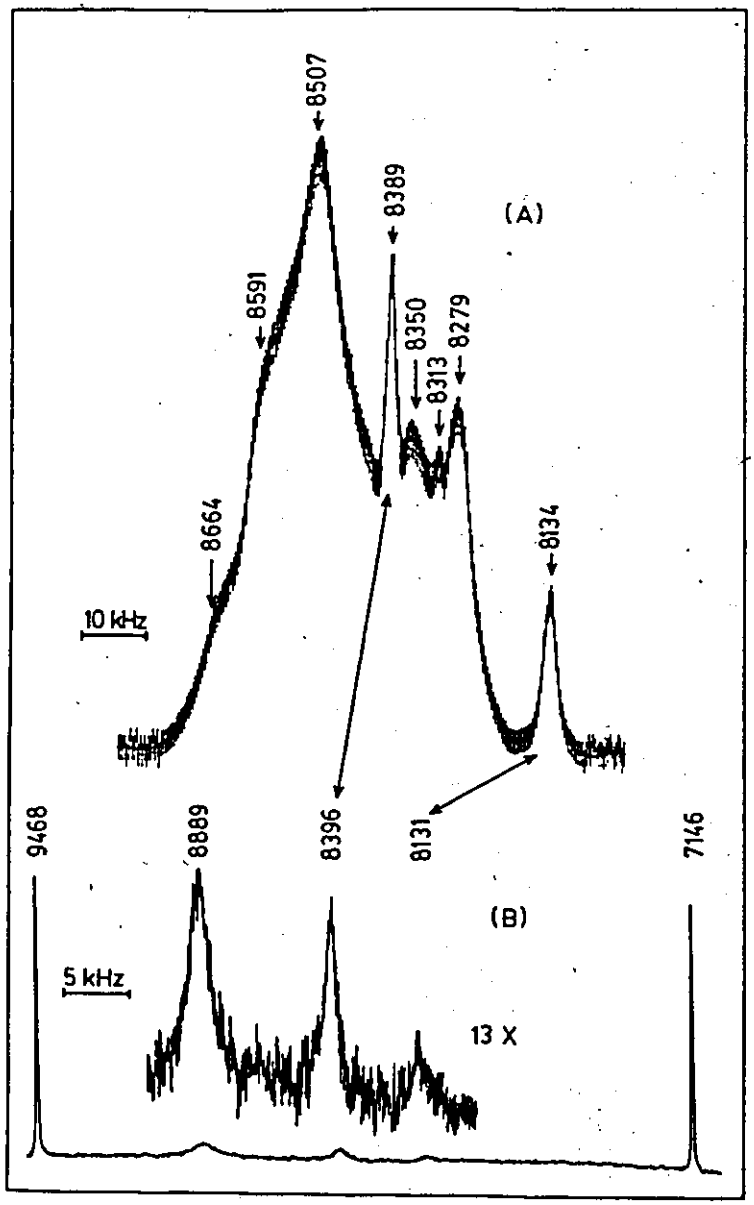

Eigure 7.5 ^{59}Co NMR spectrum of the oxygenation reaction of $Co(SCN)_2$+2en+4KSCN $\xrightarrow{O_2}$ product (A) 94.457MHz (9.395T) spectrum obtained after 15 minutes, (B) 21.252MHz (2.1139T) spectrum obtained after 1 hour. In(A) the continuous line is the simulated spectrum.

Table 7.3

Species observed after 15 mins. (94.457 MHz ^{59}Co) and after 1 hr. (21.252 MHz ^{59}Co) for the Reaction $Co(SCN)_2$ + 2en + 4KSCN $\xrightarrow{O_2}$ Products.

Complex Assignment	Experimental				Calculated	
	21.252 MHz		94.457 MHz			
	δ/ppm	$\Delta\nu_{\frac{1}{2}}$/Hz	δ/ppm	$\Delta\nu_{\frac{1}{2}}$/Hz	δ/ppm	$\Delta\nu_{\frac{1}{2}}$/Hz
$Coen_3^{3+}$	7146±2	97±10	7146±1	100±5	7146	0
sym[a]-ad,cf,e,b-$(Coen_2NCS)_2O_2^{2+}$	8131±2	839±150	8134±1	2522±213	8190	612
sym-ae,cf,d,b-$(Coen_2NCS)_2O_2^{2+}$	-	-	8279±1	4964±517	8275	2443
sym-ad,bc,f,e-$(Coen_2(NCS)_2SCN)_2en$	-	-	8313±1	871±128	8313	196
sym-cd,af,b,e-$(Coen(NCS)_2SCN)_2en$	-	-	8350±5	12064±2257	8349	1947
sym-ad,cf,e,b-$(Coen_2SCN)_2O_2^{2+}$	8396±5	1230±100	8389±1	1400±226	8387	1130
sym-ae,cf,d,b-$(Coen_2SCN)_2O_2^{2+}$	-	-	8501±1	13646±1003	8525	4023
sym-ac,df,e,b-$(Coen(NCS)_2)_2(en)(O_2)$	-	-	8591±3	6951±1132	8598	1833
sym-ad,c,f,e,b-$(Coen(NCS)(SCN))_2(en)(O_2)$	-	-	8664±5	7023±1266	8710	182
sym-cd,(a,e,f),b-$(Coen(NCS)_3)_2O_2^{2-}$	8889±5	2084±200	-	-	8873	558
sym-cf,(d,a,e),b-$(Coen(NCS)_3)_2O_2^{2-}$			-	-	8921	638
sym-(a,c,d,e,f),b-$(Co(NCS)_5)_2O_2^{6-}$	9468±2	219±20	-	-	9413	196

[a] See footnote of Table 7.1

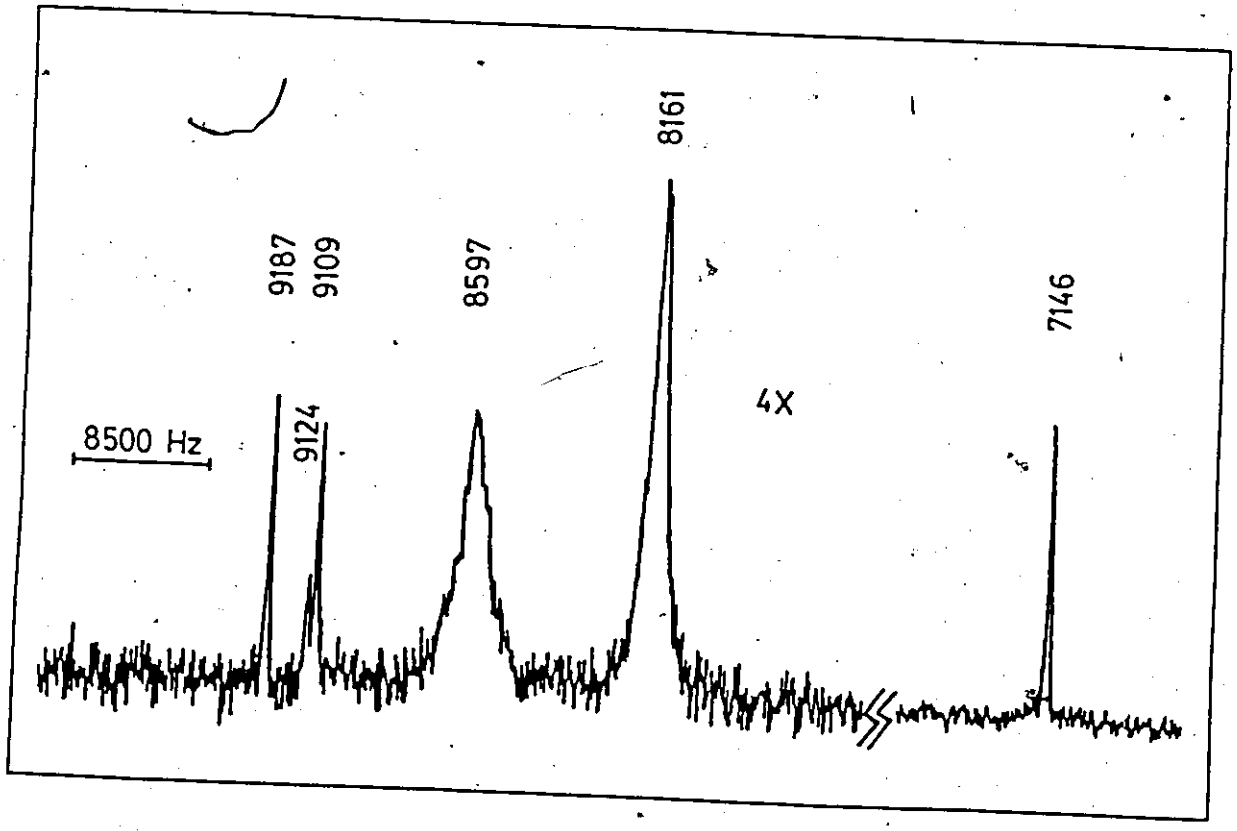

Figure 7.6 21.252MHz (2.1139T) ^{59}Co NMR spectrum of the oxygenation reaction $Co(SCN)_2$+2en+4KSCN $\xrightarrow{O_2}$ products after 2 hours showing the final products of the reaction.

Table 7.4

Species Observed After 2 hrs. for the Reaction $Co^{II}(SCN) + 2en + 4KSCN \xrightarrow{O_2}$ Product

Complex Assignment	Experimental (21.252 MHz)		Calculated	
	δ/ppm	$\Delta\nu_{\frac{1}{2}}$/Hz	δ/ppm	$\Delta\nu_{\frac{1}{2}}$/Hz
$Coen_3^{3+}$	7146±1	100±10	7146	0
ad,cf,b,e-$CoenNCS)_2)_2en(O_2)$	8161±2	1144±100	8186	1563
sym-ac,df,c,b-$(Coen(NCS)_2)_2en(O_2)$	8597±20	1742±150	8598	1833
sym-bcde,a,f-$(Co(NCS)_4(SCN))_2en^{4-}$	9101±2	180±10	9031	103
sym-acdf,b,e-$(Co(NCS)_4(SCN))_2en^{4-}$			9054	1117
cd, abe, f-$(Coen(SCH)_3NCS)^-$	9124±2	302±20	9087	584
$Co(NCS)_6^{3-}$	9187±2	158±10	9194	0

summarized in Table 7.3. The 21.252 MHz spectrum after two hours is presented in Figure 7.6 and the assignments are collected in Table 7.4. The oxygen complexes found are of the types $(Coen_2NCS)_2O_2^{2+}$, μ-ethylenediamine-μ-O_2-$((Coen(NSC)_2)_2$, $(Coen(NCS)_3)_2O_2^{2-}$ and $(Co(NCS)_5)_2O_2^{6-}$, i.e., the ethylene-diamine isothiocyanato complex series predominates and there are no thiocyanato/isothiocyanato mixed ligand complexes. The final product shows a mixture of $Coen_3^{3+}$, $Coen_2(SCN)_2^+$(cis-isomer) and $Co(NCS)_6^{3-}$. The latter complex can be assigned with some confidence to the line at 9194 ppm (linewidth 158 Hz) on the basis of the calculated shift of 9187 ppm (linewidth 0 Hz). This simple complex has apparently yet to be isolated. In addition to the above, the product mixture shows resonances at 9124 and 9101 ppm. These resonances can be assigned to the mer and fac isomers of $Coen(SCN)_3(NCS)^-$ on the basis of chemical shifts. The agreement between experimental and calculated linewidths is poor with the observed linewidths being too small. An alternative to these assignments involves bridged ethylenediamine complexes with four isothiocyanato and one thiocyanate ligands. These data are collected in Table 7.4. The assignments for the latter two resonances (i.e., 9124 and 9101 ppm) must be regarded as tentative. The occurrence of the dibridged μ-ethylenediamine-μ-O_2-$(Coen(NCS)_2)_2$ complex in the final product mixture is consistent with the known stability of μ-ligand-μ-peroxo bridged Cobalt di-oxygen complexes (1.2). The μ-ligand bridge tends to "lock in" the binuclear species thus enhancing its stability.

SECTION 7.4 Solution Molecular Weight Determination of $(Co(salen))_2O_2L_2$ where L=DMSO, H_2O

In Section 7.2, the chemical shift and linewidth data suggested that

the complexes $(Co(salen))_2O_2L_2$ (L=DMSO, DMF, H_2O) form the dimeric-μ-peroxo complex $[(Co(salen))_2O_2(H_2O)]_2$ in aqueous solution. It is therefore desirable to provide further supporting evidence for the structure in aqueous solution. The solution molecular weight of the complexes $(Co(slaen))_2O_2L_2$ (L=DMSO, H_2O) has been determined and the results are tabulated in Table 7.5. The agreement between the experimental values with the calculated value for the dimer is self evident. The determined solution molecular weight for $(Co(salen))_2O_2(DMSO)_2$ with respect to the molecular weight of a monomeric μ-peroxo unit clearly demonstrates that in aqueous solution this complex is best formulated as a dimeric μ-peroxo dioxygen complex. The lower value of 1321 gms/mole compared to the calculated value of 1521 gms/mole indicates that there is free DMSO, a result in agreement with ^1H NMR. Table 7.6 summarizes the ^1H NMR shifts for the di-oxygen complex $(Co(salen))_2O_2L_2$. Under

Table 7.5

Solution Molecular Weight of $(Co(salen))_2O_2L_2$

L	Exp.[a,b] (gms/mole)		Cal (gms/mole) (mono) $(Co(salen))_2O_2L_2$	(dimer) $((Co(salen))_2O_2L)_2$
DMSO	1350 ± 117 1347 ± 122 1267 ± 153	(ave. 1321)	839	1521
H_2O	1417 ± 60 1392 ± 60 1414 ± 85	(ave. 1408)	719	1401

[a] See Sec. 3.34

[b] Calibrant Range 0-22 (10^{-3}M)
Solvent H_2O
R.T. = 23°C

identical conditions, the shifts of the axial bases (DMSO and DMF) are identical to the free DMF and DMSO shifts, in accord with both ^{59}Co NMR and molecular weight results. The possibility of rapid ligand exchange has also been considered. The results show that neither complexed DMSO nor DMF is in exchange with bulk DMSO or DMF.

Table 7.6

Proton Resonance Signal of Coordinated and Free Axial Ligand for the System $(Co(salen))_2O_2L_2$ (L=DMSO,DMF)

Compound	τ(ppm)	Solvent
$(CH_3)_2NCHO$	7.159, 7.003, 2.081	D_2O
$(CH_3)_2SO$	7.275	D_2O
$(Co(salen))_2O_2(DMF)_2$	7.153, 6.991, 2.084	D_2O
$(Co(salen))_2O_2(DMSO)_2$	7.275	D_2O

SECTION 7.5 Summary

The $O_2^=$ ligand has been placed in the spectrochemical series in the region of weak ligand field strength (δ = 0.95). The di-oxygen complexes are best described as normal Cobalt(III)-peroxy type complexes. The stability of di-oxygen complexes with weak field ligands is questionable as demonstrated by the oxygenation reaction of $Co(SCN)_2$, en and KSCN mixture.

To summarize, the structure of the Cobalt dioxygen complexes $(Co(salen))_2O_2L_2$ (L = $(CH_3)_2SO$, $(CH_3)(NCHO)$) in aqueous solution is best described by equation 7.1.

$$(Co(salen))_2O_2L_2 \xrightarrow[\text{aqueous solution}]{\text{R.T.}} (Co(salen))_2O_2(H_2O)_2 + 2L$$

$$\downarrow \text{dimerization}$$

$$[(Co(salen))_2O_2(H_2O)]_2 \qquad [7.1]$$

L = $(CH_3)_2NCHO$, $(CH_3)_2SO$, H_2O

This conclusion is supported by the crystallographic results of the tetrameric complex Bis-(3-fluorosalicylaldehyde)ethylenediimine Cobalt(III) (7.1).

The Point Charge Model has been successfully applied to identify ^{59}Co resonances in complex spectra. However, its predictive value is limited when polymeric species are involved. This is particularly true for linewidth calculations since the errors involved in the assumption of a constant correlation time are substantial. It does, however, provide a reasonable starting point for the assignment of complex spsctra.

CHAPTER EIGHT

REACTIONS OF COBALT DIOXYGEN COMPLEXES

SECTION 8.1 Introduction

In the literature survey of Chapter One, it was demonstrated that oxidation-reduction reactions for Cobalt dioxygen complexes are relatively well characterized. Substitution reactions for dioxygen complexes were demonstrated to take place following intramolecular reduction of the Co(III) by the peroxy bridge (1.124, 1.125). In other words, substitution takes place at Co(II) intermediates. Direct substitution reactions at the Cobalt (III) center on the other hand, for Cobalt dioxygen complexes are less well understood. In this chapter, some results relating to the mechanism of substitution and oxidation/reduction reactions will be presented.

SECTION 8.2 Substitution Reaction

In Chapter Seven, the type A Cobalt-Schiff base (salen) dioxygen complexes, $(Co(salen))_2O_2L_2$ (L=DMSO, DMF, H_2O) in aqueous solution were shown to have tetrameric structures with two water molecules occupying the coordination sites trans to the dioxygen bridge in the terminal Co(salen) units. This solution structure presents a favourable case for studying substitution reactions since:

i) the intermediate is constrained to have a five coordinate square pyramidal geometry, and

ii) the reactions involve replacement of water which is present in large excess.

SECTION 8.2.1 Results

The following reactions were studied.

$$[(Co(salen))_2O_2(H_2O)]_2 + 2X^- \xrightarrow{R.T.} [(Co(salen))_2O_2(X)_2]^{2-}$$

$$X^- = CN^-, NCS^-$$

The reactions were examined at 24°C. Added ligand concentrations varied from 0.1 to 2.0M at a total ionic strength of 4.5M ($NaClO_4$). The reaction was carried out in a pH=7.0 buffer (Na_2HPO_4 -NaH_2PO_4). The kinetics of the initial reactions were studied by means of stopped-flow spectrophotometry. The solubility of the cobalt complex is limited and a concentration of 0.11 mM (assuming the molecular weight of the bis-(μ-peroxo complex)) was used throughout. The reactions were followed at 448 nm and at 470 nm corresponding to the formation of $[(Co(salen))_2O_2(CN)]^{2-}$ and $[(Co(salen))_2O_2(NCS)]^{2-}$ anions respectively. Good exponential formation curves were observed indicating a pseudo first order reaction. The pseudo first order rate constants are summarized in Table 8.1 for the two reactions. Two points may be noted:

i) evolution of molecular oxygen was observed for both reactions

ii) the substitution involving NCS^- ligand showed a second step on the stopped-flow trace.

Considerable light scattering was observed (indicating O_2 evolution). For the CN^- substitution reaction only a single reaction step was observed.

Table 8.1

Pseudo First Order Rate Constants for Substitution Reaction of $[(Co(salen))_2O_2(H_2O)]_2$ with CN^- and NCS^-

X^-	$[X^-]$ (M)	$k_{obs}(sec^{-1})$
$CN^{-a,b,c,e,f}$	0.10	0.0200 ± 0.0085
	0.25	0.0439 ± 0.0072
	0.50	0.0620 ± 0.0113
	0.75	0.0925 ± 0.0056
	1.00	0.1104 ± 0.0060
	1.50	0.1246 ± 0.0040
	2.00	0.1385 ± 0.0040
$NCS^{-a,b,d,e,f}$	0.15	0.0127 ± 0.0080
	0.20	0.0170 ± 0.0064
	0.33	0.0303 ± 0.0091
	0.50	0.0353 ± 0.0064
	0.75	0.0572 ± 0.0100
	1.00	0.0611 ± 0.0050
	1.25	0.0810 ± 0.0064
	1.50	0.0833 ± 0.0050
	1.75	0.0840 ± 0.0064

a $[(Co(salen))_2O_2(H_2O)]_2$ = 0.11mM 460nm (ε=8.9 x $10^2 M^{-1}cm^{-1}$) shoulder

b I = 4.5 M ($NaClO_4$)

c reaction followed at λ_{max} = 448nm (ε=1x10^3 $M^{-1}cm^{-1}$)

d reaction followed at λ_{max} = 470nm (ε=725 $M^{-1}cm^{-1}$)

e 24°C

f pH =7.0 (0.2M Na_2HPO_4-0.2MNaH_2PO_4)

Bubbles due to oxygen evolution produced only modest disruption of the stopped flow traces and it appears that formation of oxygen does not occur in the first step of the reaction. Since a second step can be observed for the thiocyanate reaction, it is likely that this second reaction step is faster with the cyanide ion which is consistent with markedly more interference from bubbles in the first step.

SECTION 8.2.2 Discussion

Plots of k_{obs} vs $[X^-]$ for the results of Table 8.1 are shown in Figure 8.1. It is evident that the deviation from linearity occurs at high concentrations of both anions. This behaviour conclusively rules out the operation of an S_N2 (lim) or A-type mechanism since for such a mechanism a linear plot of k_{obs} against $[X^-]$ over the entire concentration range of X^- is predicted. That is, the rate should be first order in X^- at all concentration of X^- as shown below:

$$ML_6^{n+} + X^- \underset{k_{-1}}{\overset{k_1}{\rightleftharpoons}} [X^-..ML_6^{n+}] \xrightarrow{k_2} ML_5X^{(n-1)+} + L$$

$$\frac{d}{dt}[ML_5X^{(n-1)+}] = k_2[X^-..ML_6^{n+}] \qquad [8.1]$$

assuming steady-state approximation for $[X^-...ML_6^{n+}]$,

$$\frac{d}{dt}[X^-..ML_6^{n+}]=0=k_1[ML_6^{n+}][X^-]-k_{-1}[X..ML_6^{n+}]-k_2[X^-..ML_6^{n+}]$$

$$[X^-..ML_6^{n+}] = \left(\frac{k_1}{k_{-1}+k_2}\right)[ML_6^{n+}][X^-] \qquad [8.2]$$

Substituting into equation 8.1

$$\frac{d}{dt}[ML_5X^{(n-1)+}] = \left(\frac{k_1k_2}{k_{-1}+k_2}\right)[ML_6^{n+}][X^-] \qquad [8.3]$$

Under pseudo first order conditions

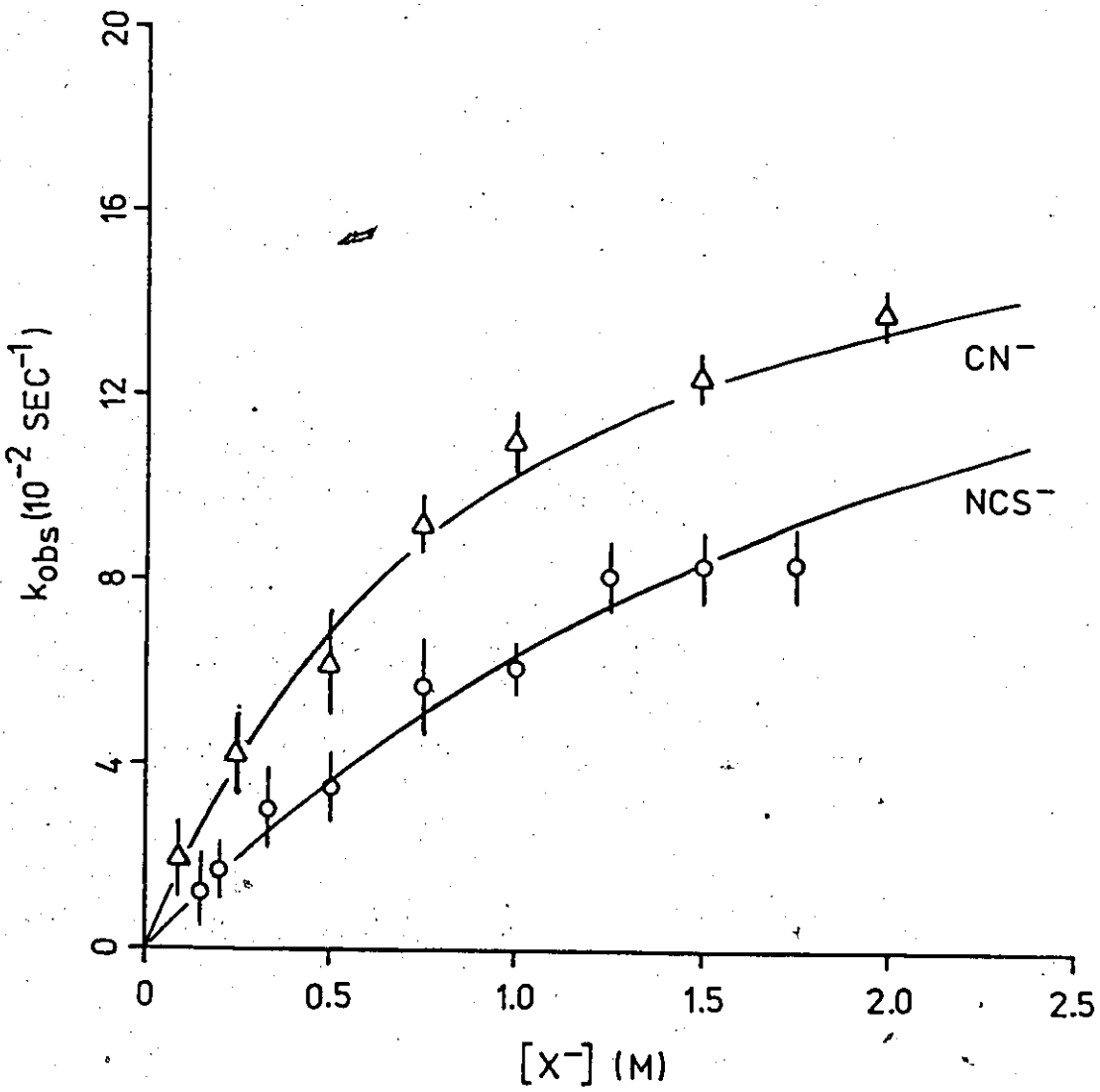

Figure 8.1 Plot of k_{obs} versus $[X^-]$ where $X=CN^-$, NCS^-. Solid line calculated from equation 8.6.

$$k_{obs} = \left(\frac{k_1 k_2}{k_{-1} + k_2}\right) [X^-] \qquad [8.4]$$

When $k_2 >> k_{-1}$, equation 8.4 further simplifies to

$$k_{obs} = k_1[X^-] \qquad [8.5]$$

Equations 8.4 and 8.5 predict linear plots of k_{obs} against $[X^-]$.

Three reasonable mechanisms could account for the present results.

i) An S_N1 (lim) or D-type mechanism,

ii) An I_d (dissociative interchange of outer-sphere complex) mechanism,

iii) An I_a (associative interchange of outer-sphere complex) mechanism.

Mechanism (i), S_N1 (lim) or D-type

$$L_5M\text{-}OH_2^{n+} \underset{k_{-1}}{\overset{k_1}{\rightleftharpoons}} L_5M^{n+} \cdot + H_2O$$

$$L_5M^{n+} + X^- \xrightarrow{k_2} L_5M\text{-}X^{(n-1)+}$$

Mechanism (ii) I_d (dissocative interchange) and (iii) I_a (associative interchange) at the Outer-sphere Complex

$$L_5M\text{-}OH_2^{n+} + X^- \overset{K_o}{\rightleftharpoons} [L_5M\text{-}OH_2^{n+}, X^-]$$

(outer-sphere(ion-pair) complex)

$$[L_5M\text{-}OH_2^{n+}, X^-] \xrightarrow{k} L_5M\text{-}X^{(n-1)+} + H_2O$$

If the following assumptions can be made;

i) the concentration of the intermediate L_5M^{n+} in mechanism (i) can be approximated by steady state treatment,

ii) substitution can be treated as a one site problem since the two identical reaction centers are remote from each other (this approximation is supported by crystallographic data (7.1)). such that simultaneous substitution takes place at both sites obeying the same kinetics, and

iii) the second reaction is irreversible.

The dependence of the observed rate constant, k_{obs}, for mechanism (i) is given by equation 8.6.

$$k_{obs} = \frac{k_1}{(k_{-1}/k_2) + [X^-]} \qquad [8.6]$$

$$\frac{1}{k_{obs}} = \left(\frac{k_{-1}}{k_1 k_2}\right) \frac{1}{[X^-]} + \frac{1}{k_1} \qquad [8.7]$$

A plot of $1/k_{obs}$ versus $1/[X^-]$ is linear with a slope (k_{-1}/k_1k_2) and an intercept $(1/k_1)$. Similarly for mechanisms (ii) and (iii)

$$k_{obs} = \frac{kK_o[X^-]}{1+K_o[X^-]} \qquad [8.8]$$

$$\frac{1}{k_{obs}} = \left(\frac{1}{kK_o}\right) \frac{1}{[X^-]} + \frac{1}{k} \qquad [8.9]$$

Equation 8.9 again gives a linear plot with slope $(\frac{1}{kK_o})$ and intercept $(1/k)$ (1.69, 1.70).

The distinction between mechanisms (ii) and (iii) is that the rate in the first case is controlled by the dissociated step in the interchange of the coordinated H_2O and X^- within the outer-sphere (ion-pair) complex. This process does not involve bond making in the interchanging process between the metal center and the incoming ligand X^-. It is expected that (kK_o) would be fairly constant for similarly charged ions. The value of

kK_o for mechanism (iii) is not expected to remain constant since k is dependent on the direct ligating strength of the incoming ligand X^-. In the outer-sphere complex, a bond making process between the metal center and X^-, i.e., an increase in coordination number at the transition state, preceeds the formation of the product. For mechanism (i), the rate determining step is dissociation of coordinated water. This condition requires that k_1 (rate of H_2O exchange) is identical for a series of similarly charged ligands. In other words, a plot of k/k_{obs} versus $1/[X^-]$ for different ligands should converge at $1/k_1$ - a distinct feature of this mechanism. To summarize the salient features of the three mechanisms obtained from the $1/k_{obs}$ versus $1/[X^-]$ plots

i) For S_N1 (lim) and I_d mechanisms a common intercept and different slopes for a series of ligands are expected.

ii) For the I_a mechanism, the same slope but different intercepts are expected for the same series of ligands.

Having established empirical criteria for differentiating between the various mechanisms, the data of Figure 8.1 can be treated accordingly for a best fit mechanism. Figure 8.2 gives the plot of $1/k_{obs}$ versus $1/[X^-]$ and the results (slopes and intercepts) were treated according to the three mechanisms for comparison. This is summarized in Table 8.2. From Table 8.2, it is immediately clear that mechanism (iii) (I_a) is not likely to be operating since its rates of product formation k are almost identical. This is contrary to the expected behaviour since by definition bond forming influences k. The outer-sphere complexation constant can be

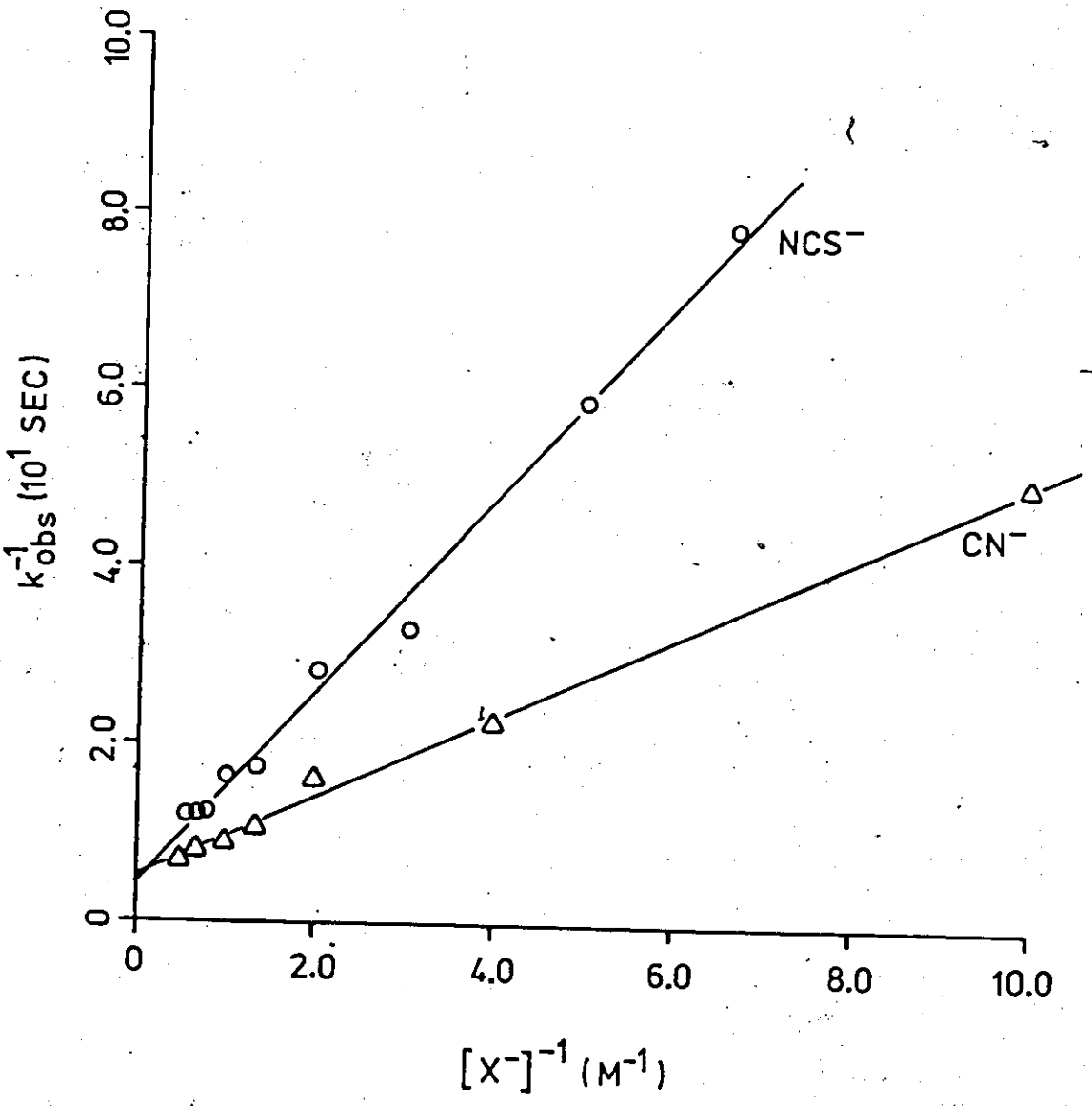

Figure 8.2 Plot of $1/k_{obs}$ versus $1/[X^-]$ for the ligands NCS^- and CN^-.

Table 8.2

Slopes and Intercepts of $1/k_{obs}$ versus $1/[X^-]$ Plot Fitted to Mechanisms (i) to (iii)

Ligand	S_N1 (lim)		I_d or I_a		
	k_2/k_{-1}	$k_1(sec^{-1})$	$kK_o(M^{-1}sec^{-1})$	$k(sec^{-1})$	$K_o(M^{-1})$
CN^-	1.163	0.192	4.877	0.192	23.42
NCS	0.443	0.208	10.857	0.208	52.27

estimated from the modified Fuoss relationship (8.1).

$$K_o = \frac{4\pi N_A a^3}{3000} e^{-\nu(a)/kT} \qquad [8.10]$$

where

$$\nu(a) = \frac{Z_1 Z_2 e_o^2}{aD} - \frac{Z_1 Z_2 e_o^2 \alpha}{D(1+\alpha a)}$$

and

$$\alpha^2 = \frac{8\pi N_A e_o^2 \mu}{1000\ DkT}$$

with

N_A = Arogadro's number

a = center-to-center distance (in cm) between the two reacting partners at the point of closest approach

Z_1 and Z_2 are formal charges on the reacting species.

e_o = electronic charge in (esu)

D = bulk dielectric constant

k = Boltzmann constant in (ergs)

T = absolute temperature

When one of the species is uncharged, in this case the metal complex, equation 8.10 simplifies to

$$K_o = \frac{4\pi N_A a^3}{3000}$$

$$K_0 = (2.52 \times 10^{21})\ a^3\ (M^{-1}) \qquad [8.11]$$

Equation 8.11 has been employed by various authors to estimate K_o as an aid to mechanistic assignments (8.2,8.3,8.4). It has been argued (8.5) that for aquated metal complexes, the "a" value is between 3.5 to 5Å depending on the extent to which the incoming ligand penetrates the first coordination shell. If it can be assumed that the average value of 4.25Å is the most probable value for "a", K_o is estimated to be $0.20M^{-1}$. It is necessary to stress that this complexation constant is difficult to estimate for $[(Co(salen))_2O_2(H_2O)]_2$ but it would probably be larger than this value due to the large size of the molecule. K_o calculated as a function of "a" is listed in Table 8.3. The K_o values in Table 8.2 are much larger than those of Table 8.3. For a radius of 10Å, a K_o of $2.52M^{-1}$ is calculated. This is considerably less than the values of 20 to 50 obtained in Table 8.2. It can be concluded that the data are inconsistent with an I_d mechanism and that a S_N1 (lim) or D mechanism is indicated.

The results of Figure 8.2 best fit that of mechanism (i), i.e., D-type. This is immediately apparent from the plot in Figure 8.2, the unique feature of a common k_1 is very apparent. Using values obtained from Table 8.2, the smooth curves in Figure 8.1 were back calculated. The differences in the ratio of k_2/k_{-1} and their magnitude is consistent with

Table 8.3

Estimated Outer-Sphere Complexation Constant K_o

a (Å)	K_o (M^{-1})
3	0.068
4	0.163
5	0.315
6	0.544
7	0.864
8	1.290
9	1.837
10	2.520

known literature results for the substitution of Co(III) complexes. Notable are those of the substitution of $Co(CN)_5H_2O^{2-}$ by Haim and Wilmarth (8.6), Co(Hematoporphyrin)$(H_2O)_2^{3+}$ by Mestichelli and co-workers (8.7) and the substitution of trans-$Co(NH_3)_4(SO_3)X$ by Halpern et. al., (8.8), which operate under the same mechanism. The k_2/k_{-1} values from different systems are summarized in Table 8.4.

Structurally, a five coordinate "square" pyramidal intermediate with the peroxo group occupying the apical position is reasonable with Co(salen) system since the strict planar arrangement of the salen ligand does not allow any stereo-transformation at the transition state. A simple inter-

Table 8.4

Discrimination Factors for Intermediates in Reactions of Co(III) Complexes

Reaction	Intermediate	Y	Relative reactivity of nucleophile towards intermediate	Reference
trans-$Co(NH_3)_4SO_3X$ + Y	$Co(NH_3)_4SO_3$	NH_3	1	
		SCN^-	30	8.8
		CN^-	43	
		NO_2^-	70	
$Co(CN)_5H_2O^{2-}$ + Y	$Co(CN)_5^{2-}$	H_2O[a]	1	
		Br^-	0.10	
		NH_3	0.15	8.6
		N_3^-	0.53	
$[(Co(salen))_2O_2(H_2O)]$ + Y	$[(Co(salen))_2O_2]_2$	NCS^-	1	This work
		CN^-	2.63	

[a] assuming H_2O = 55M

pretation of the results is as follows:

i) If an I_a mechanism were operative, the transition state would have an increased coordination for the Cobalt. In cases where monodentate ligands are involved this is possible since the entire coordination sphere is capable of undergoing some rearrangement to minimize both steric and electronic repulsion between neighbouring groups. This type of mechanism has been found for Cr compounds (8.9). This is clearly not reasonable for the present complex.

ii) If an I_d mechanism were operative, the incoming anion is likely to experience large electronic repulsion from the extensive π-cloud of the salen ligand. This effect tends to destabilize the outer-sphere complex and decrease the probability of ligand exchange within the outer-sphere complex.

The above considerations are consistent with the D-type mechanism indicated by the kinetic results.

The value of k_1 is expected to be close to the rate of $k_{exchange}$ of co-ordinated water and bulk water (1.69). The value of k_1 observed for these reactions (2×10^{-1} sec^{-1}) is much higher than $k_{exchange}$ for classically inert Co(III) complexes. It is not entirely unreasonable on the basis of electronic considerations discussed below. Table 8.5 summarizes $k_{ex(H_2O)}$ for various Cobalt (III) complexes. From Table 8.5 the obvious feature is that the k_1 obtained for these reactions is much smaller than $k_{exchange}$ for Co(II). The value found lies between those of $Co(CN)_5H_2O^{2-}$ and trans-$Co(NH_3)_4SO_3(H_2O)^+$. The bonding in $Co(CN)_5H_2O^{2-}$ and trans-$Co(NH_3)_4SO_3(H_2O)^+$ has been extensively discussed (8.6,8.8). The large k_{ex} for these complexes reflects the trans-labelizing effect due to the $d\pi$-$p\pi^*$ and $d\pi$-$d\pi$ interactions for the former and latter respectively. In large macrocyclic Co(III) complexes where the Co(III) ion becomes extensively involved in delocalized

Table 8.5

$k_{ex}^{\circ}(H_2O)$ for Cobalt Complexes

Complex	$k_{ex}(sec^{-1})$	T(°C)	pH	Reference
$Co(H_2O)_6^{2+}$	1.10×10^{6}	25		1.69
$Co(HP)(H_2O)_2^{3+a}$	1.70×10^{1}	25	7.2	8.7
trans-$Co(NH_3)_4SO_3(H_2O)^{+}$	1.34×10^{1}	25		8.8
$[(Co(salen))_2O_2(H_2O)]_2$	2.00×10^{-1}	24	7.1	This work
$Co(CN)_5(H_2O)^{2-}$	1.00×10^{-3}	40		8.6
$Co(NH_3)_5(H_2O)^{3+}$	6.00×10^{-6}	25		1.69

a HP = hematoporphyrin

bonding with its ligands, the formal oxidation state formalism breaks down leading to kinetic lability (8.7, 8.10). An example of this is $Co(HP)(H_2O)^{3+}$ (8.7). The crystal structure of the tetrameric Bis(3-fluorosalicylaldehyde) ethylenediamine Cobalt-oxygen complex has been determined by Wang and Schaefer (7.1). Both bond length and bond angle data indicate that the bonding description of this tetramer does not satisfy either one of the two extreme formal oxidation state assignments, i.e., neither $Co(III)O_2^{=}Co(III)$ nor $Co(II)O_2^{\circ}Co(II)$. Bayer and Schretzman (1.23) have considered the bonding in detail and have concluded that this type of complex is best described as a weak π-bonding complex where the bonding involves partial charge transfer

from the filled $3d_{xz}$ or $3d_{yz}$ orbitals of Co(II) to the π^* orbital of O_2. This description is consistent with the present results, in that, upon substitution by good π-ligands, the coordination of oxygen is destabilized due to the effective competition of the axial ligands trans to it, decreasing the available charge transferred to the π^* orbital of O_2 from the metal $3d_{xz}$ or $3d_{yz}$ orbitals. It follows that the five co-ordinated intermediate is stabilized as the trans ligand departs from the complex. This type of bonding picture also rationalizes the observation of two reaction steps in the stopped flow results for NCS^- and one for CN^-. The latter competes much more effectively than the former in its π-bonding ability causing immediate destabilization of the Cobalt-oxygen bond.

Finally, it is interesting to compare the mechanism for ligand exchange found in the present study to those reported by Sasaki et. al. (1.125). The implication is that for amine/dioxygen complexes, intramolecular electron transfer is faster than axial ligand dissociation but for the schiff base (salen)/dioxygen complexes, the converse is true. The first order rate constant found by Sasaki ($5 \times 10^{-3} sec^{-1}$) is almost two orders of magnitude less than the dissociation rate ($2 \times 10^{-1} sec^{-1}$) reported here. With a planar π-ligand, stabilization of the five coordinate intermediate is enhanced and axial dissociation of the ligand trans to the oxygen bridge is rate determining. Without a planar π-ligand, electron transfer is rate determining. Either case leads to "anomously rapid" ligand exchange.

SECTION 8.3 Redox Reactions in Aqueous Solution

The following reactions were studied:

sym-edf, ac, b
sym-aef, cd, b
sym-def, ac, b
} $(Coendien)_2O_2^{4+} + FeSO_4 \cdot 7H_2O \rightarrow$ Products.

The primary objective was to detect reaction intermediates using ^{59}Co NMR technique to verify the reaction mechanism suggested by Sykes (Scheme 1.2).

SECTION 8.3.1 Results

(A) Kinetic Measurements

The reduction reaction was followed by stopped-flow spectrophotometry at the wavelength of 420nm corresponding to the absorption by the Fe^{3+} product. Two different rate processes were observed. The two processes were studied concurrently using the dual time base provided on the Nicolet-1170 signal averaging system. The pH dependence of the reaction was examined in the range 3.46-4.55. The reactions were examined at 24°C. Added reducing agent, Fe^{2+}, concentrations varied from 4 to 50mM at a total ionic strength of 1.2M ($NaClO_4$). The reaction was carried out in a pH = 4.5 buffer (0.1M - KH phthalate - 0.1M NaOH). Good exponential formation curves were observed indicating a pseudo first order reaction. The kinetic data are collected in Table 8.6 and the corresponding plots for k_{obs} versus $[Fe^{2+}]$ are shown in Figure 8.3. In both cases, k_{obs} is proportional to $[Fe^{2+}]$, the two second order rate constants obtained from the linear least

Table 8.6

Kinetic Data* For the Reduction of $(Coendien)_2O_2^{4+}$ by $FeSO_4 \cdot 7H_2O$

$[FeSO_4 \cdot 7H_2O]$ (mM)	pH	k_{obs} (sec^{-1})	$k_{obs}/[FeSO_4 \cdot 7H_2O]$ ($M^{-1}sec^{-1}$)	k_{obs} (sec^{-1})	$k_{obs}/[FeSO_4 \cdot 7H_2O]$ ($M^{-1}sec^{-1}$)
		1st reaction		2nd reaction	
3.91	4.5	0.0108±0.0021	2.7621		
7.81	4.5	0.0265±0.0015	3.3931		
15.62	4.5	0.0396±0.0015	2.5352	0.0103±0.0039	1.3188
23.43	4.5	0.0817±0.0007	3.4869	0.0175±0.0025	1.1204
31.24	4.5	0.0910±0.008	2.9129	0.0232±0.0011	0.9902
39.05	4.5	0.1077±0.0019	2.7580	0.0338±0.0016	1.0819
47.31	4.5	0.1506±0.0013	3.1828	0.0418±0.0013	1.0704
			ave.(3.0044±0.3568)	0.0523±0.0021	1.1055
			least square (3.0403±0.0496)		ave.(1.1145±0.1098)
39.05	3.46[a]	0.1033±0.015	2.6451		least square(1.0655±0.0158)
39.05	3.89	0.100 ±0.021	2.5653	0.0403±0.0012	1.0322
39.05	4.22	0.094 ±0.010	2.4072	0.0420±0.0008	1.0756
39.05	4.42	0.113 ±0.008	2.8948	0.0365±0.0010	0.9347
39.05	4.55	0.103 ±0.018	2.6385	0.0405±0.0009	1.0627
			ave.(2.6302±0.1762)	0.0385±0.0009	0.9859
					ave.(1.0186±0.0572)

* $[(Co(en)(dien))_2O_2](ClO_4)_4]$ = 0.781 mM
Buffer = 0.2M NaOAc - 0.2M HOAc
μ = 1.2M ($NaClO_4$)
[a] Buffer = 0.1M KH phthalate /0.1M NaOH

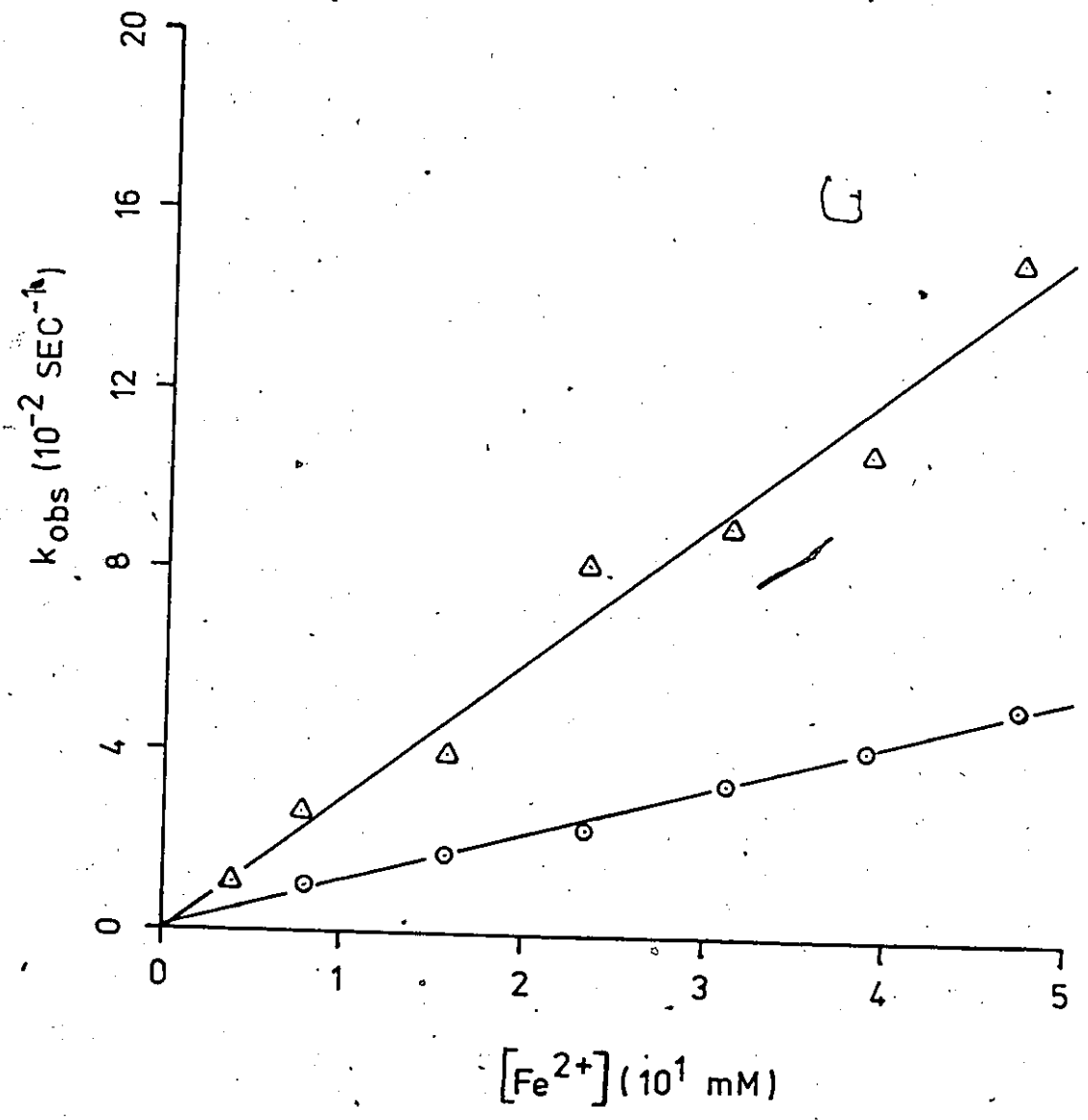

Figure 8.3 Plot of k_{obs} versus $[Fe^{2+}]$
(A) sym-edf,ac,b-$(Co(en)(dien))_2O_2^{4+}$
(B) sym-aef,cd,b-$(Co(en)(dien))_2O_2^{4+}$
Solid line is linear least squares fit.

squares method gave k_2 = 3.0403 $M^{-1}sec^{-1}$ and k_2 = 1.0655 M^{-1} sec^{-1} for the faster and slower rate processes respectively. For the concentration range studied, the linear plots of Figure 8.3 demonstrate that the rate law 8.12 applies to both processes.

$$\frac{d}{dt}[\text{Product}] = k_2[Co_2O_2^{4+}][Fe^{2+}] \qquad [8.12]$$

where $Co_2O_2^{4+} = (Coendien)_2O_2^{4+}$

(B) The Nature of the Reaction Product

For preparative purposes, the reaction was done with a stoichiometric ratio of 1:1 for Co:Fe. Under these conditions, a solid precipitate (light brown in colour) characterized as $FeO_{3/2-x}(OH)_{2x}(\frac{3}{2}-x)\ H_2O$, x = o (see Appendix II) was obtained. From the Mössbauer results of Appendix II, the above solid contains two Fe^{3+} sites with the same chemical isomer shift (δ = 0.38 mm sec^{-1}) but different quadrupole splitting constants. The contribution of the two sites are 38% and 62% with corresponding quadrupole splittings of 0.47 mm sec^{-1} and linewidth Γ = 0.31 mm sec^{-1} for the first Fe^{3+} site and 0.74 mm sec^{-1} and linewidth Γ = 0.47 mm sec^{-1} for the second Fe^{3+} site. The total yield of $FeO_{3/2-x}(OH)_{2x}\ (\frac{3}{2}-x)H_2O$ is approximately 85% based on Cobalt.

The resulting solution, after filtration, was examined by ^{59}Co NMR. 16% of the sym-edf, ac, b-$(Coendien)_2O_2^{4+}$ isomer had not reacted whereas approximately 30% of the sym-aef, cd, b-$(Coendien)_2O_2^{4+}$ isomer remained.

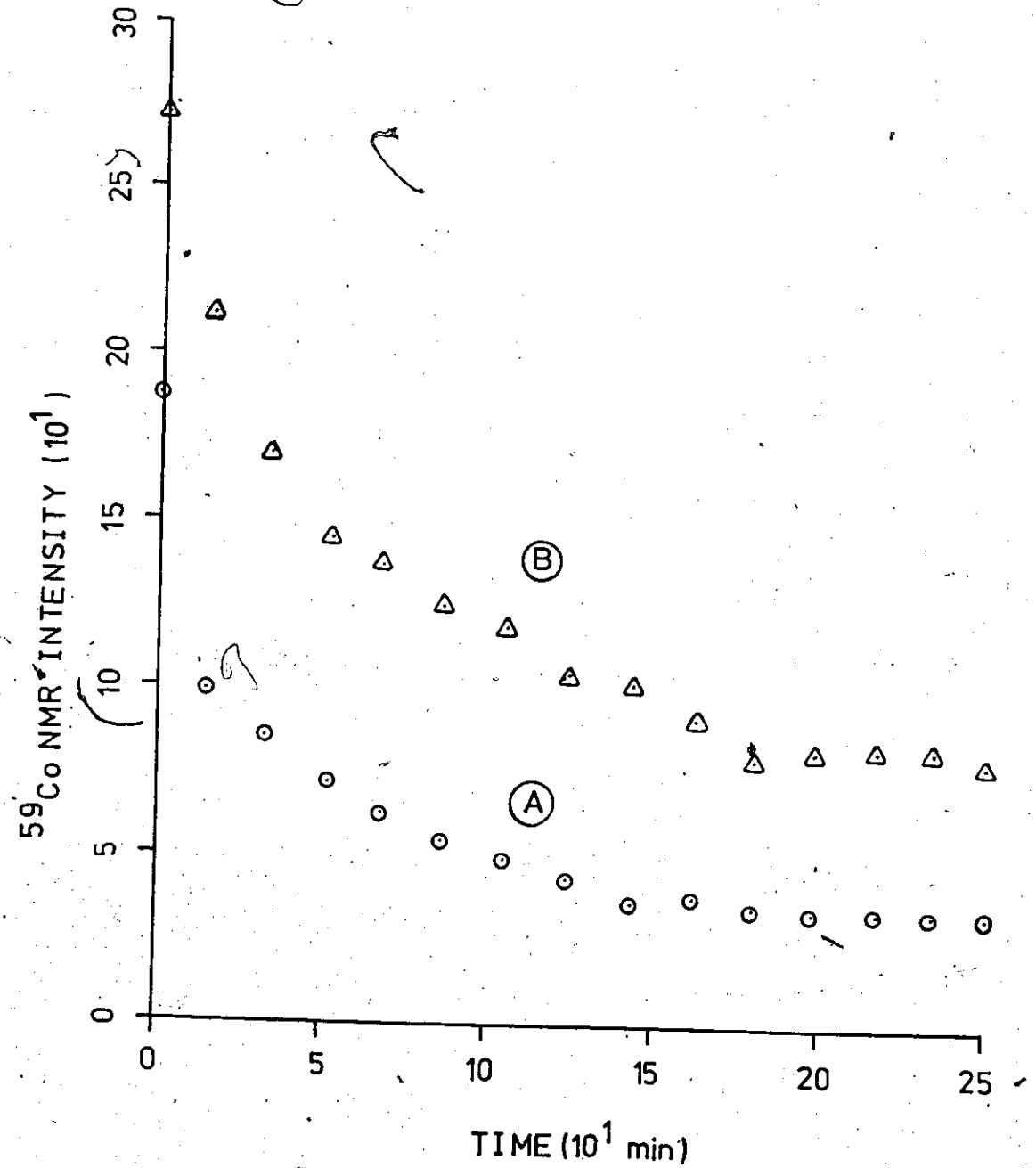

Figure 8.4 ^{59}Co NMR intensity versus time plot of the reduction reaction of $(Co(en)(dien))_2O_2^{4+}$ by $FeSO_4\ 7H_2O$

(A) sym-edf,ac,b-$(Co(en)(dien))_2O_2^{4+}$

(B) sym-aef,cd,b-$(Co(en)(dien))_2O_2^{4+}$

The sym-def, ac, b-$(Coendien)_2O_2^{4+}$ isomer which contributes 3.5% to the total original isomeric mixture remained unreacted. One additional resonance was observed at δ = 6972 ppm ($\Delta\nu_{1/2}$ = 358 Hz). This was present in less than 2% abundance relative to the original mixture and was assigned to cae,bf,d-$Co(dien)_2^{3+}$ by the model calculations of the type described in Chapter Six. Visible spectroscopy confirmed the formation of Co^{2+} ($\sim$ 500nm). The pH of the filtrate is acidic (pH $\sim$ 5). ^{13}C NMR shows two broad resonances at δ = 43.384 and 54.205 ppm and δ = 46.601 ppm relative to TMS consistent with the presence of free diethylenetriamines and ethylenediamines. The low field shift of 2 ppm and line broadening of the ^{13}C resonance is due to relaxation by paramagnetic Co^{2+}.

SECTION 8.3.2 Discussion

From the kinetic plots of Figure 8.3, it is apparent that two independent reduction processes take place. Therefore, it is necessary to identify the two rate processes. This was accomplished by direct monitoring of the rate of loss of Cobalt. The reaction was followed directly by ^{59}Co NMR at 6°C with $Coen_3^{3+}$ as the internal standard. The stoichiometry of the mixture was 1Fe: 1Co. The resulting intensity versus time plot is shown in Figure 8.4. For the two curves corresponding to the isomers of interest, there is also evidence of a much slower reaction occuring after the initial rapid loss of intensity. Thus, the slower rate process can be assigned to ferrous ion reduction of the isomer (c) sym-aef, cd, b-$(Co(dien)(en))_2O_2^{4+}$ and the faster rate process to reduction of isomer (a) sym-edf, ac, b-$(Co(dien)(en))_2O_2^{4+}$ with some confidence.

The observed second order rate constants for the initial reduction step, $k_2 = 3.04\ M^{-1}\ sec^{-1}$ for isomer (a) and $k_2 = 1.07\ M^{-1}\ sec^{-1}$ for isomer (c), are well within the range for an inner-sphere electron transfer process.* In the mechanism proposed by Sykes, it was suggested that the approach (coordination) of the ferrous ion labilizes the Cobalt-oxygen bond and that the rate of oxygen bond cleavage is then rapid ($k_1 \simeq 0.01\ sec^{-1}$ for $L = (en)_2$) (1.118-1.119) This lability is a direct effect of the electron transfer process. The intermediate spectrum for the species $Co^{III}-O-O-Fe^{III}$ has been observed by Sykes (1.118) and Martell (1.119). These kinetic results obtained by ^{59}Co NMR are consistent with the presence of this intermediate. The second step of the reaction is clearly associated with another electron transfer step since it involves the loss of Co(III) signal intensity.

Going back to the original mechanism proposed by Sykes (Scheme 1.2), reaction (1) is unambigious while reactions (2), (3) and (4), are difficult to distinguish. From the ^{59}Co NMR point of view, the rearrangement step described by (2) generating the species $L_5Co^{III}\underset{OH}{O}-Fe^{3+}$ could in principle be detected since the character of the trivalent oxygen is less peroxy in nature. This would require the ^{59}Co resonance frequency to increase, thus δ(ppm) becomes more +ve (in this case increasing to $\sim$ 8000-7800 ppm). This was clearly not observed during the ^{59}Co NMR kinetic run. Although it could be argued that the relaxation effect of the high spin Fe^{3+} could effectively relax Co(III) to the extent that it becomes too broad (extremely short T_2) to be observed. This effect was shown to be minimal by two experiments as follows:

*See Table 1.2

i) the relaxation effect of 0.05M Fe^{3+} in natural abundance $^{17}OH_2$. The result shows that T_2 of $^{17}OH_2$ decreases by a factor of 20 (3.9 msec to 0.3 msec). The $^{17}OH_2$ signal can be detected easily despite the fact that ^{17}O is quadrupolar (I = 5/2). This experiment therefore demonstrates that an intermediate of the type $L_5Co^{III}-\underset{OH}{O}-Fe^{3+}$ is not likely to affect the ^{59}Co resonances.

ii) The relaxation effect of 0.1M Fe^{3+} gives no broadening of the ^{59}Co NMR signal of $Coen_3^{3+}$.

Thus, on the basis of (i) and (ii), Fe^{3+} should not prevent detection of the intermediate of the type described in (i). However, if the intermediates exhibit strong peroxy character, a slight shift on the ^{59}Co resonance is expected and would very likely be indistinguishable from the original ^{59}Co resonance of the di-oxygen complex. Since step (2) and step (3) of Scheme 1.2 are rapid for Cr^{2+} reduction of the μ-peroxo-complex studied by Sykes, it is unlikely that the second-stage of reduction observed in this experiment using ^{59}Co NMR corresponds to step (2) (an outer-sphere process). It is more consistent with step (3) via a second inner-sphere electron transfer process rather than an outer-sphere electron transfer ($k_{2} \geq 10^2\ M^{-1}\ sec^{-1}$). In other words, if step (2) were to take place, the second reduction step is more likely to be consistent with a scheme described by equations 8.13 to 8.15 as suggested by Martell (1.119).

$$L_5Co^{III}-O-O-Fe^{III} \underset{fast}{\overset{H^+}{\rightleftharpoons}} LCo^{III}-\underset{OH}{O}-Fe^{III} \text{ (isomerism)} \qquad [8.13]$$

$$L_5Co^{III}-\underset{O\text{-}Fe^{II}}{O}-Fe^{III} \xrightarrow[slow]{H^+} L_5Co^{III}-\underset{HO\text{-}Fe^{II}}{\overset{H}{O}}-Fe^{III} \qquad [8.14]$$

$$L_5Co^{III}-\underset{HO\text{-}Fe^{II}}{\overset{H}{O}}-Fe^{III} \xrightarrow[slow]{} L_5Co^{II} + 2Fe^{III} \qquad [8.15]$$

That is, bond scission takes place with reduction. Such a mechanism is quite plausible under conditions with excess reducing agent as well as strongly acidic solutions (1.115).

Going back to Figure 8.4, the time scale in which Cobalt intensities reach a constant value far exceeds that of the stopped-flow experiment. Secondly, substantial NMR intensities remained at t_∞ (~4hrs.), implying that the amount of Fe^{2+} present is insufficient to complete the reduction of the Cobalt dioxygen complexes. From reduction studies of similar systems by other workers (1.118 - 1.120) it has been established that four equivalents of a one electron reducing agent are required to completely reduce the peroxo complexes to Co(II) and water. Two electrons for the reduction of the peroxo complex to Co(II) and two electrons for the reduction of the peroxide ($O_2^=$) to water.

$$Co^{III}O_2^=Co^{III} + 2\tilde{R}^{n+} \longrightarrow 2Co^{II} + O_2^= + 2\tilde{R}^{(n+1)+} \qquad [8.16]$$

$$4H^+ + O_2^= + 2\tilde{R}^{n+} \longrightarrow 2H_2O + 2\tilde{R}^{(n+1)+} \qquad [8.17]$$

With a stoichiometric amount of Fe:Co and when both equations 8.16 and 8.17 are operative, it is not likely that all the original $Co^{III}O_2^=Co^{III}$ complex would be reduced. In the case of strong reducing agents such as Cr^{2+} the reduction of peroxide to water may occur by direct reaction with the metal ion. In the case of Fe^{2+}, a relatively milder reducing agent, a likely sequence is decomposition of free peroxide to molecular oxygen and water (probably catalyzed by the metal ions present) followed by reoxygenation to reform Cobalt dioxygen complex. The presence of a small but detectable

amount of $Co(dien)_2^{3+}$ in the final solution is consistent with this sequence, since it is well known that the intermediate in the formation of Co(III) complexes takes place via the superoxide-peroxide oxygenation pathway.

Finally, it should be noted that at the end of this sequence half of the Co^{3+} has been reduced to Co^{2+} and half of the peroxide has been reduced to water. Reaction with more Fe^{2+} will eventually complete the reduction. The results of the NMR kinetic experiment shown in Figure 8.4 are consistent with this scheme. The reactions studied by Stopped-flow are complete before the first NMR spectrum has been acquired. There is therefore a sharp initial decrease in ^{59}Co intensity followed by a much slower decay. The intensity does not fall to zero even after several hours showing that some of the Fe^{2+} has been used to reduce peroxide rather than Co. This experiment was performed at 6°C in the hope of identifying intermediates of the type postulated by Sykes and McClendon and Martell. There is no indication of species other than the starting complexes and it is inferred that all the reactions in the sequence described by equations 8.13-8.15 were not observed in the NMR spectra. The important observation is that the relative intensities of the resonances arising from the different isomers are significantly different after the initial stage of the reaction is finished. Thus the ratio of the aef,cd,b isomer to the edf,ac,b isomer is 0.68 initially and .47 on the first NMR run on the reacting solution. Clearly one isomer is consumed faster than the other confirming the interpretation of the Stopped flow data.

SECTION 8.4 Summary

The kinetics of substitution for $[(Co(salen))_2O_2(H_2O)]_2$ are consistent with the bonding description suggested by known X-ray crystallographic data. From these results, it is inferred that if the formal oxidation state assignment is valid, the rates of substitution would most likely be similar to normal Co(III) complexes.

On the question of the redox mechanism of the μ-peroxo Cobalt dioxygen complex, it was demonstrated that when isomeric mixtures occurs, the various isomers can react at different rates. The most reactive isomer has the ligand with the highest point charge (or Crystal Field splitting) parameter trans to the peroxo group. This is consistent with findings of substitution reactions that groups such as CN^- and NCS^- activate peroxide in a trans position.

CHAPTER NINE

CONCLUSIONS AND FURTHER WORK

A central theme in the discussion presented in Chapters Four and Five is the possible importance of the antisymmetric term, $\Delta_a\sigma$, in the chemical shielding tensor. The origin of the antisymmetric chemical shielding is uncertain but is tentatively attributed to site symmetry lowering at the Cobalt nucleus by inter-molecular interaction with solvent molecules. The rotational reorientation correlation time τ_2 is one order of magnitude larger in hydrogen bonding solvents than in solvents where inter-molecular interactions are weak (CH_3CN). The correlation time τ_1 is associated with the lifetimes of the inter molecular interactions. In the present case, this is thought to be H-bonding.

It would be of interest to extend the investigation of the field dependence of linewidths to complexes of other metal ions. There is no reason to expect that the effects observed are peculiar to Co. Both quadrupolar nuclei (e.g., ^{51}V, ^{139}Ca) and non-quadrupolar nuclei (e.g., ^{89}Y, ^{199}Hg) should be examined. The measurements on T_1 should be confirmed and extended to shorter relaxation times by using a high power instrument when one becomes available.

One of the more surprising results demonstrated in Chapter Five is that Gutmann's donor numbers correlate well with the linewidths at zero fields in different solvents. It would be expected that such solvent dependence would be largest for systems where the donor-acceptor bond is at one bond separation as it is for $^{23}Na^+$ (2.57, 2.91) and $^{7}Li^+$ (2.56). The changes

in relaxation rates exhibited by the complexes studied in this thesis are surprisingly large and further investigation of their origin is warranted.

Combining literature information, an alternative model described below may equally account for the very large relaxation rates for quadrupolar nuclei.

i) For low symmetry complexes, the quadrupole coupling constant is best described by equation 9.1.

$$e^2qQ = (eQ)e\langle q \rangle \qquad [9.1]$$

where $q = f(q,n,r,t)$

n = number of inter-molecular bonds

r = bond distance of the intermolecular bond

t = lifetime of the intermolecular bond

In other words, the quadrupole coupling is determined by the time average of the effective electronic charges located in the first coordination shell. A proposal of the form described may be tested by field gradient calculations.

ii) As a result of charge density fluctuations in the first coordination shell, induced by intermolecular interactions, the ligand field potential also fluctuates with time. The paramagnetic electronic currents are modified as a function of time and intermolecular bonding arrangements. Therefore, the matrix elements governing the paramagnetic term in the Ramsey equation is also time averaged. The shielding values are thus directly affected. This type of transient chemical shielding relaxation effect has been proposed for I=1/2 spherical heavy atoms(9.1). However, the fundamental differences between the collision model described above and that of the donor-acceptor model is that the former assumes an asymmetric electronic distribution whereas the latter involves fluctuation in the total electronic charges. Thus, a mathematical formalism of the latter is needed to test the model.

Several authors (2.38, 2.40) have dealt with the theoretical and experimental means for the detection of $\Delta_a\sigma$ in the solid state. However, the magnitude of $\Delta_a\sigma$ is at present unknown. Thus calculations of $\Delta_a\sigma$ for simple systems are needed to shed light on this particular area.

Chapter Six presents a simple and unique model for structural assignments for low symmetry complexes utilizing both chemical shifts and linewidths. Its direct application has been demonstrated in Chapter Seven. A few points deserve further work.

i) measurement of the orbital reduction factor, k', for a variety of low symmetry complexes. This procedure allows improvement on S_L values.

ii) extension of the model to incorporate the circulation removing ratio (9.2) proposed by Juranic for fine correction of metal-ligand covalency.

iii) extension of the model to other ligands particularly those of H_2O and OH^-.

APPENDIX I

BASIC PROGRAMS FOR CALCULATION OF T_1 DATA. (3.41, 3.42)

(i) "NMR T_1"

```
5 FOR I=1 TO 32:PRINT:NEXT I
10 PRINT "TO FIT THREE CONSTANTS TO A FUNCTION"
11 REM - THE METHOD IS GENERAL, THE PARTICULAR FUNCTION IS FOR
12 REM - T1 DETERMINATION IN NMR, AND LOCATED IN STATEMENTS 280 -330
13 REM -
20 DIM X(50),Y(50),R(50)
30 PRINT"INPUT X (TIME), Y(INTENSITY), NEGATIVE X &Y TO END LIST"
40 FOR G=1 TO 50
50 INPUT X(G),Y(G)
60 IF X(G)<0 GOTO 90
70 N=G
80 NEXT G
90 PRINT"INPUT INITIAL ESTIMATES OF A,B,C"
100 INPUT A1,B1,C1
110 PRINT "INPUT T, 0=CALCULATE, 1=FINAL TABLE, 2=DELETE 1 POINT,"
120 PRINT"3=ADD 1 POINT, 4=ABSOLUTE END, 5=DIFFERENT A,B,C"
130 INPUT T
140 IF T=0 THEN 200
150 IF T=1 THEN 751
160 IF T=2 THEN 880
170 IF T=3 THEN 1110
180 IF T=4 THEN 1150
190 IF T=5 THEN 90
200 H=1
205 IF H=6 GOTO 700
210 M1=0:M2=0:M3=0:M4=0:M5=0:M6=0:M7=0
220 M8=0:M9=0:S1=0
230 FOR G=1 TO N
240 IF (H=1) AND (G=1) THEN 280
250 GOTO 290
255 REM -
260 REM - T1=F'A, T2=F'B, T3=F'C, T4=R=Y-(F(A,B,C))
270 REM - SECTION FOR SPECIFIC FUNCTION FOLLOWS, NOTE JUMP INTO IT
280 PRINT"PARTICULAR FUNCTION IS Y=A-A EXP(-X/B)-AG EXP(-X/B)"
290 T5=EXP(-X(G)/B1)
300 T1=1-T5-C1*T5
310 T6=A1*X(G)*T5/(B1*B1)
320 T2=-T6-C1*T6
330 T3=-A1*T5
335 T4=Y(G)-(A1-A1*T5-A1*C1*T5)
339 REM-
340 REM - COMPLETE SECTION SPECIFIC FOR FUNCTION
350 R(G)=T4
```

```
360 REM - CALCULATION OF SUMS
370 M1=M1+T1*T1
380 M2=M2+T1*T2
390 M3=M3+T1*T3
400 M4=M4+T2*T2
410 M5=M5+T2*T3
420 M6=M6+T3*T3
430 M7=M7+T1*T4
440 M8=M8+T2*T4
450 M9=M9+T3*T4
460 S1=S1+T4*T4
470 NEXT G
475 REM -
480 REM - CALCULATIONS USING SUMS -- CRAMER'S RULE
485 REM - ALSO CALCULATION OF APPROPRIATE VARIANCE-
486 REM - COVARIANCE MATRIX ELEMENTS AND DETERMINANT
490 S3=2*M2*M3*M5-M3*M3*M4-M1*M5*M5+M1*M4*M6-M2*M2*M6
500 S3=1/S3
510 S4=M4*M6-M5*M5
520 A2=S3*(M3*M5*M8-M3*M4*M9+M2*M5*M9-M2*M6*M8+M7*S4)
530 Q3=S3*S4
540 S5=M1*M6-M3*M3
550 B2=S3*(M2*M3*M9+M8*S5+M3*M5*M7-M1*M5*M9-M2*M6*M7)
560 Q4=S3*S5
570 S6=M1*M4-M2*M2
580 C2=S3*(M2*M5*M7-M3*M4*M7+M2*M3*M8-M1*M5*M8+M9*S6)
590 Q5=S3*S6
600 A1=A1+A2
670 B1=B1+B2
680 C1=C1+C2
690 H=H+1:GOTO 205
700 S2=SQR(S1/(N-3))
710 PRINT"STD DEV OF Y = "S2;"FOR 5 REPEATS"
720 PRINT"NEW A = ";A1;"NEW B = ";B1;"NEW C = ";C1
730 PRINT
740 GOTO 110
747 REM -
748 REM - FINAL TABLE OF CALCULATED Y VALUES AND
749 REM - STANDARD ERRORS
751 PRINT "  X              Y          YCALC          Y-YCALC  "
752 FOR G=1 TO N
753 PRINT X(G),Y(G),Y(G)-R(G),R(G)
754 NEXT G
755 PRINT "TO CONTINUE TYPE RETURN"
756 INPUT K
800 A$="":GOSUB 2000
810 A$="A= "+STR$(A1)+"   STD ERROR= "+STR$(S2*SQR(Q3))
811 GOSUB 2000
820 A$="B= "+STR$(B1)+"   STD ERROR= "+STR$(S2*SQR(Q4))
821 GOSUB 2000
830 A$="C= "+STR$(C1)+"    STD ERROR= "+STR$(S2*SQR(Q5))
831 GOSUB 2000
```

```
840 A$="NUMBER OF POINTS= "+STR$(N)+"    STD ERROR OF Y= "+STR$(S2)
841 GOSUB 2000
850 A$="":GOSUB 2000:GOSUB 2000
870 GOTO 110
874 REM -
875 REM - SORT DATA SET AND DELETE WRONG X AND Y
880 PRINT"INPUT WRONG X AND Y"
890 INPUT T4,T5
900 FOR G=1 TO N
910 IF X(G)<>T4 OR Y(G)<>T5 THEN 930
920 X(G)=9999
930 NEXT G
940 FOR H=1 TO N
950 C=0
960 FOR G=1 TO N-1
970 IF X(G)<X(G+1) THEN 1050
980 T4=X(G)
990 T5=Y(G)
1000 X(G)=X(G+1)
1010 Y(G)=Y(G+1)
1020 X(G+1)=T4
1030 Y(G+1)=T5
1040 C=1
1050 NEXT G
1060 IF C=0 THEN 1090
1070 NEXT H
1080 IF X(N)<>9999 THEN 110
1090 N=N-1
1100 GOTO 110
1105 REM -
1110 PRINT"INPUT ADDITIONAL X & Y"
1120 INPUT X(N+1),Y(N+1)
1130 N=N+1
1140 GOTO 110
1150 END
1154 REM -
1155 REM - SUBROUTINE FOR OUTPUT
2000 A$=A$+CHR$(10)+CHR$(13)
2050 PRINT A$
2060 A$=""
2070 RETURN
```

(ii) "GRAPTECH"

```
10 PRINT "NONLINEAR REGRESSION BY GRAPHICAL TECHNIQUES"
20 PRINT
30 DIM X(35),Y(35),LY(35)
40 K=0
45 REM -
46 REM - INPUT DATA
50 PRINT "NUMBER OF KNOWN POINTS";
60 INPUT N
70 FOR I=1 TO N
80 PRINT "X,Y OF POINT ";I
90 INPUT X(I),Y(I)
100 NEXT I
105 REM -
106 REM - EXAMINE DATA AND MAKE ANY CHANGES AS NECESSARY
110 FOR I=1 TO N
120 PRINT "X,Y OF POINT ";I,"ARE";X(I),Y(I)
130 NEXT I
140 PRINT "IF SATISFIED TYPE '1'";
150 INPUT M
160 IF M=1 GOTO 530
170 PRINT "IF YOU WISH TO CHANGE A POINT,TYPE 1"
180 PRINT "OTHERWISE TYPE 2";
190 INPUT KIL
200 IF KIL=1 THEN GOTO 210 ELSE GOTO 300
210 PRINT "NO. OF POINT TO BE CHANGED IS";
220 INPUT LIK
230 IF LIK>N GOTO 210
240 PRINT "X,Y OF POINT";LIK;"IS";
250 INPUT X(LIK),Y(LIK)
260 PRINT "MORE POINTS TO BE CHANGED? TYPE 1";
270 INPUT AA
280 IF AA=1 GOTO 210
290 PRINT
300 PRINT "IF YOU WISH TO DELETE A POINT "
310 PRINT "TYPE THE NUMBER OF THE POINT TO BE DEL-"
320 PRINT "ETED, OTHERWISE TYPE 0";
330 INPUT BB
340 IF BB<=0 OR BB>N GOTO 450
350 IF B=N THEN N=N-1
360 FOR ILL=BB TO N
370 X(ILL)=X(ILL+1)
380 Y(ILL)=Y(ILL+1)
390 NEXT ILL
400 N=N-1
410 PRINT
420 PRINT "YOU NOW HAVE ";N;"POINTS"
430 PRINT
440 GOTO 300
450 PRINT "IF YOU WISH TO ADD MORE POINTS, TYPE 1"
460 PRINT "OTHERWISE TYPE A 3";
```

```
470 INPUT CC
480 IF CC=1 GOTO 490 ELSE GOTO 530
490 PRINT "X,Y OF POINT";N+1;"IS";
500 INPUT X(N+1),Y(N+1)
510 N=N+1
520 GOTO 450
521 REM -
522 REM - CALCULATE M(0) USING THE TWO DERIVED EQUATIONS
523 REM - AND A SELECTED RANGE OF T1 VALUES
524 REM -
530 PRINT "ESTIMATE T1 BY NULL POINT METHOD"
540 PRINT "CHOOSE T1MAX TO BE AT LEAST TWICE THAT"
550 PRINT "MAX. T1 VALUE IS ";
560 INPUT T1MAX
570 PRINT "MIN. T1 VALUE IS ";
580 INPUT T1MIN
590 T1S=(T1MAX-T1MIN)/10
600 PRINT " THE IDEA IS TO FIND T1 FOR WHICH MO(1)=MO(2)
610 PRINT "  T1          MO(1)       MO(2)         MO(1)-MO(2)
620 FOR T1=T1MIN TO T1MAX STEP T1S
630 RESTORE
640 READ A#,B#,C#,D#,E#,F#,G#,H#,O#
650 DATA 0,0,0,0,0,0,0,0#,0#
655 REM - CALCULATE SUMS
660 FOR I=1 TO N
670 A#=A#+Y(I)*EXP(-X(I)/T1)
680 B#=B#+EXP(-X(I)/T1)
690 C#=C#+Y(I)
700 D#=D#+EXP(-2*X(I)/T1)
710 E#=E#+X(I)/T1^2*EXP(-X(I)/T1)
720 F#=F#+X(I)/T1^2*EXP(-2*X(I)/T1)
730 G#=G#+X(I)/T1^2*Y(I)*EXP(-X(I)/T1)
740 H#=H#+X(I)^2*EXP(-2*X(I)/T1)
750 O#=O#+(1-EXP(-X(I)/T1))^2
760 NEXT I
770 MO1=(A#*B#-N*A#-C#*D#+C#*B#)/(B#^2-N*D#)
780 MO2=(C#*E#-C#*F#+B#*G#-N*G#)/(B#*E#-N*F#)
790 IF L=1 GOTO 980
800 PRINT T1,MO1,MO2,MO1-MO2
810 NEXT T1
820 PRINT "MO VALUES SHOULD BE CLOSE TO ESTIMATE"
830 PRINT "IF NOT, TRY DIFFERENT RANGE OF VALUES"
840 PRINT "IF THEY ARE, NARROW RANGE OF CALCULATION"
850 PRINT "IF SATISFIED TYPE '1'";
860 INPUT L
870 IF L=1 GOTO 930
880 PRINT "IF YOU WOULD LIKE TO RE-EXAMINE DATA"
890 PRINT "TYPE A '1'";
900 INPUT LL
910 IF LL=1 GOTO 110
914 REM -
915 REM - IF SATISFIED, CHOOSE BEST T1 AND CALCULATE
```

```
916 REM - M(0) AND M(00)
920 GOTO 550
930 PRINT "BEST VALUE OF T1 IS";
940 INPUT T1B
950 T1MIN=T1B
960 T1MAX=T1B+1
970 GOTO 620
980 MO=(MO1+MO2)/2
990 MOO1=(MO*B$-C$)/(B$-N)
1000 MOO2=(-MO*F$+G$)/(E$-F$)
1010 PRINT "ESTIMATES OF M(0) ARE ";MO1,MO2
1020 PRINT "ESTIMATES OF M(00) ARE ";MOO1,MOO2
1030 PRINT "AVE. M(00) IS ";(MOO1+MOO2)/2
1040 MOO=(MOO1+MOO2)/2
1050 PRINT "AVE, M(0) IS ";MO
1060 PRINT "ESTIMATE OF T1 IS ";T1B
1061 REM -
1062 PRINT "IF YOU WOULD LIKE CALCULATION OF Y* VALUES "
1063 PRINT "AND EST. OF STAND. ERRORS, TYPE A '1'";
1064 INPUT CAL
1065 IF CAL<>1 GOTO 1370
1070 EE=E$*T1^2*(MOO-MO)
1080 FF=F$*T1^2*(MOO-MO)
1090 HH=H$*(MOO-MO)^2
1100 P$=B$-D$
1110 S$=FF$/T1^2
1120 Q$=EE$/T1^2-S$
1130 T$=HH/T1^4
1140 ZZ=O$*(D$*H$-S$^2)-P$*(P$*H$-S$*Q$)+Q$*(P$*S$-Q$*D$)
1150 Z=N*(D$*HH-FF^2)-B$*(B$*HH-EE*FF)+EE*(B$*FF-EE*D$)
1160 PPMOO=(D$*HH-FF^2)/Z
1170 PPMO=(O$*H$-Q$^2)/ZZ
1180 PPT1=(N*D$-B$^2)/Z
1220 RSS=0
1240 PRINT "  I          X(I)          Y(I)          CALCULATED Y  "
1250 FOR JI=1 TO N
1260 YT=MOO+(MO-MOO)*EXP(-X(JI)/T1)
1270 RSS=RSS+(YT-Y(JI))^2
1280 PRINT JI,X(JI),Y(JI),YT
1290 NEXT JI
1300 PRINT "RESIDUAL SUM OF SQUARES IS ",RSS
1310 SMOO=SQR(RSS/(N-3)*PPMOO)
1320 SMO=SQR(RSS/(N-3)*PPMO)
1330 ST1=SQR(RSS/(N-3)*PPT1)
1340 PRINT "STANDARD ERROR IN M(00) IS ";SMOO
1350 PRINT "STAND. ERROR IN M(0) IS ";SMO
1360 PRINT "STAND. ERROR IN T1 IS ";ST1*T1^2
1365 REM -
1370 PRINT "IF SATISFIED WITH NON-LIN. ESTIMATION TYPE '1'";
1380 INPUT NOL
1390 IF NOL=1 GOTO 1420
1400 L=0
```

```
1410 GOTO 110
1415 REM -
1420 PRINT "IF YOU WISH TO CALCULATE T1 BY LINEAR REGRESSION "
1430 PRINT "OF LN(Y-M(OO)) VS TIME, TYPE '1'";
1440 INPUT D
1450 IF D<>1 GOTO 1850
1455 REM -
1460 PRINT "IF YOU WISH TO USE M(INFINITY) FROM 3-PARAMETER"
1470 PRINT "FIT, TYPE A "1", OTHERWISE TYPE RETURN"
1480 INPUT MINF
1490 IF MINF=1 GOTO 1520
1500 PRINT"ENTER A REASONABLE M(INFIN) VALUE"
1510 INPUT MOO
1520 A=0
1530 B=0
1540 C=0
1550 D=0
1560 E=0
1570 PRINT "HERE IS LINEARIZED DATA"
1580 PRINT "  I           X(I)        Y(I)"
1590 FOR I=1 TO N
1600 IF Y(I)>=MOO GOTO 1680
1610 LY(I)=LOG(MOO-Y(I))
1620 PRINT I,X(I),LY(I)
1630 A=A+LY(I)
1640 B=B+X(I)
1650 C=C+X(I)^2
1660 D=D+X(I)*LY(I)
1670 E=E+LY(I)^2
1680 NEXT I
1700 M=(A*B/N-D)/((B^2)/N-C)
1710 BB=A/N-M*B/N
1720 RSS=E-BB*A-M*D
1730 PRINT "RSS";RSS
1740 DM=SQR(N*RSS/(N-2)/(N*C-B^2))
1750 DB=SQR(DM^2*C/N)
1760 DT1=DM/M^2
1770 TI=-1/M
1780 PRINT "CALCULATED T1 IS ";TI
1790 PRINT "CALCULATED M(OO)-M(O) IS";EXP(BB)
1800 PRINT "STANDARD EST. OF ERROR IN T1 IS";DT1
1810 PRINT "STANDARD EST. OF ERROR IN LN(M(OO)-M(O)) IS";DB
1815 REM -
1820 PRINT "IF SATISFIED WITH LINEAR REGRESSION TYPE '1'";
1830 INPUT T
1840 IF T<>1 GOTO 1370
1850 END
```

APPENDIX II

"PREPARATION AND CHARACTERIZATION OF "$Fe(OH)_3$ POWDER"

A-II.1 Introduction

As part of an effort to understand the reduction of the Cobalt-dioxygen complex $(Co(en)(dien))_2O_2(ClO_4)_4$ by $FeSO_4 \cdot 7H_2O$, the Iron hydroxide powder obtained from this reaction ($Fe(OH)_3$) was isolated and characterized by Mössbauer spectroscopy. To date, all published preparations of $Fe(OH)_3$ involve base hydrolysis of ferric salts and give an amorphous (gelatinous) material. The nature of this material considerably restricts the investigation of its physical properties. Since little is known about $Fe(OH)_3$ in the powder form, this chapter presents some preliminary results on the physical properties of the compound prepared by the reaction of $FeSO_4 \cdot 7H_2O$ with Cobalt di-oxygen complexes.

A-II.2 Brief Survey

The literature on hydrated iron oxides is scattered. This reflects the complexity of these systems which are generally not well understood (A-II.1, A-II.2). Hydrated iron oxides Fe_2O_3 have been shown to exhibit various phases (A-II.2). Of these, α-Fe_2O_3 exhibits interesting magnetic properties which find application in both the magnetic tape and electronic devices industries (A-II.3). It has been shown that the dehydration of the hydrated oxides is mostly topotatic, i.e., the loss of water does not significantly affect the iron-oxygen skeletal framework suggesting that the structure and properties of Fe_2O_3 depend strongly on the parent hydrated oxide (A-II.4).

A-II.3 Preparation and Characterization of $Fe(OH)_3$ from Reduction Reactions of $(CoL_5)_2O_2^{4+}$ where L en, dien, tetraen and NH_3

A-II.3.1 Preparation

A typical preparation involves dissolving stoichiometric amounts (2:1 $FeSO_4 \cdot 7H_2O$: Co-dioxygen complex) in aqueous solution under argon. The mixture is typically stirred for three hours and light brown $Fe(OH)_3$ collected by filtration. A 70-75% yield is obtained. Prolonged stirring (overnight) usually improves the yield to 85-90%. The crude product usually contains some Co^{2+} and free amine ligands. It is essential to wash the product by completely suspending in water, stirring for 30 minutes and then re-filtering. The washing procedure is usually repeated three times. The weight of the product reaches a limiting value after drying by standing for two days under normal atmospheric conditions.

A-II.3.2 Characterization

(A) Chemical Analysis and Thermal Decomposition

The powder obtained after drying at room temperature until constant weight is reached is light brown. 100mg samples were analyzed for both Iron and Cobalt by atomic absorption spectroscopy. The quantity of water was determined by thermal decomposition of a known quantity of $Fe(OH)_3$ on a high vacuum line in a quartz tube. The sample was slowly heated (~4 hrs) to 920°C and the amount of water evolved was trapped in a preweighed pyrex vessel immersed in liquid nitrogen. When decomposition was complete, both the weight of the Iron residue and the water were recorded. The solid Iron

residue was checked by Mössbauer spectroscopy and was found to be α-Fe_2O_3. The water was analyzed by microboiling point and refractive index. The analysis results are tabulated in Table A-II.1. Table A-II.1 shows that Cobalt is present to approximately 5% in the crude product. Thorough washing of the $Fe(OH)_3$ powder by distilled water decreases the amount of Cobalt to less than 0.25%. It can be concluded that Cobalt co-precipitates as a soluble impurity. This is important since FeOOH ($Fe_2O_3 \cdot H_2O$) has been reported to incorporate large quantities of trivalent metal M^{3+} ions to form a solid solution of composition $Fe_{1-x}M_xOOH$ ($M^{3+} = Cr^{3+}$ (A-II.5) and Al^{3+} (A-II.6)) and that the presence of M^{3+} alters the physical and spectroscopic properties of the oxide hydrate.

The Iron analysis by atomic absorption gave results in good agreement with the calculated values for $Fe(OH)_3$ ($Fe_2O_3 \cdot 3H_2O$). Complimentary, the analytical result obtained for the product of thermal decomposition of $Fe_2O_3 \cdot 3H_2O$ gave reproducible and fairly accurate weight percents of Iron Oxide and water.

(B) Bulk Density

The bulk density (Archimedia method) was determined to be $\rho_{ave} = 2.79 \pm 0.21$ gm.cm^{-3} (results in Table A-II.2). Figure A-II.1 illustrates the variation of density with water content for various known Iron(III) oxide hydrates. For $Fe_2O_3 \cdot 2H_2O$ ($2FeOOH \cdot H_2O$) the density determined by various groups varies considerably and is not considered reliable. The value obtained for the $Fe(OH)_3$ of this study is the first reported value of its kind.

It is well known that large differences in the value of density can occur

Table A-II.1

Chemical Analysis of % wt. (Fe and Co by Atomic Absorption Method; Fe_2O_3 and H_2O by Thermal Decomposition)

Sample number	Fe	Co	Fe_2O_3	H_2O
Calculated	52.26	0	74.71	25.29
1	49.57	4.37		
2	54.34	0.25	74.25	25.46
3	49.51	2.35		
4	50.51	0.21	72.24	24.90
5	49.51	5.07		
6	54.09	0	71.01	23.71
7	52.15	0	71.07	23.26
8	49.15	0	70.02	27.27

1 from 5mM $(Coendien)_2O_2^{4+}$ (unwashed)
2 from 5mM $(Coendien)_2O_2^{4+}$ (washed)
3 from 2mM $(Co(tetraen))_2O_2^{4+}$ (unwashed)
4 from 2mM $(Co(tetraen))_2O_2^{4+}$ (washed)
5 from 50mM $(Co(NH_3)_5)_2O_2^{4+}$ (unwashed pH=8)
6 from 0.1M $Fe^{3+} + OH^-$
7 from 0.1M $FeSO_4 \cdot 7H_2O + H_2O_2$ (pH=10.86)
8 from 0.1M $FeSO_4 \cdot 7H_2O + H_2O_2$ (pH=4.5)

even for systems with well defined stoichiometries. For example, the transformations of γ-FeOOH→ γ-Fe_2O_3 (A-II.1) and β-FeOOH → δ-Fe_2O_3 (A-II.8) give structures with increasing vacancies leading to a lower density. The δ-α

Table A-II.2

Bulk Density of $Fe_2O_3 \cdot 3H_2O$ from Different Preparations

$Fe_2O_3 \cdot 3H_2O$ prepared from	$\rho(gmcm^{-3})$
$(Coendien)_2O_2^{4+}$	3.01 ± 0.03
$(Co(tetraen))_2O_2^{4+}$	2.78 ± 0.05
H_2O_2	2.60 ± 0.02

transition of Fe_2O_3 at high temperature gives the tightly packed hematite structure which lead to an increase in density from 4.4 to 5.25$gmcm^{-3}$(A-II.7, A-II.9). Therefore, both crystal packing and structural defects influence the density significantly. A few trends can be deduced from Figure A-II.1.

(i) the densities of various $Fe_2O_3 \cdot XH_2O$ compounds decrease as X increases

(ii) large variations of density are observed for a given composition, implying the significant role of structural effects such as packing and crystal defects, etc.

(iii) if the water is present due to absorption on the surface, the density should obey the following equation (A-II.18).

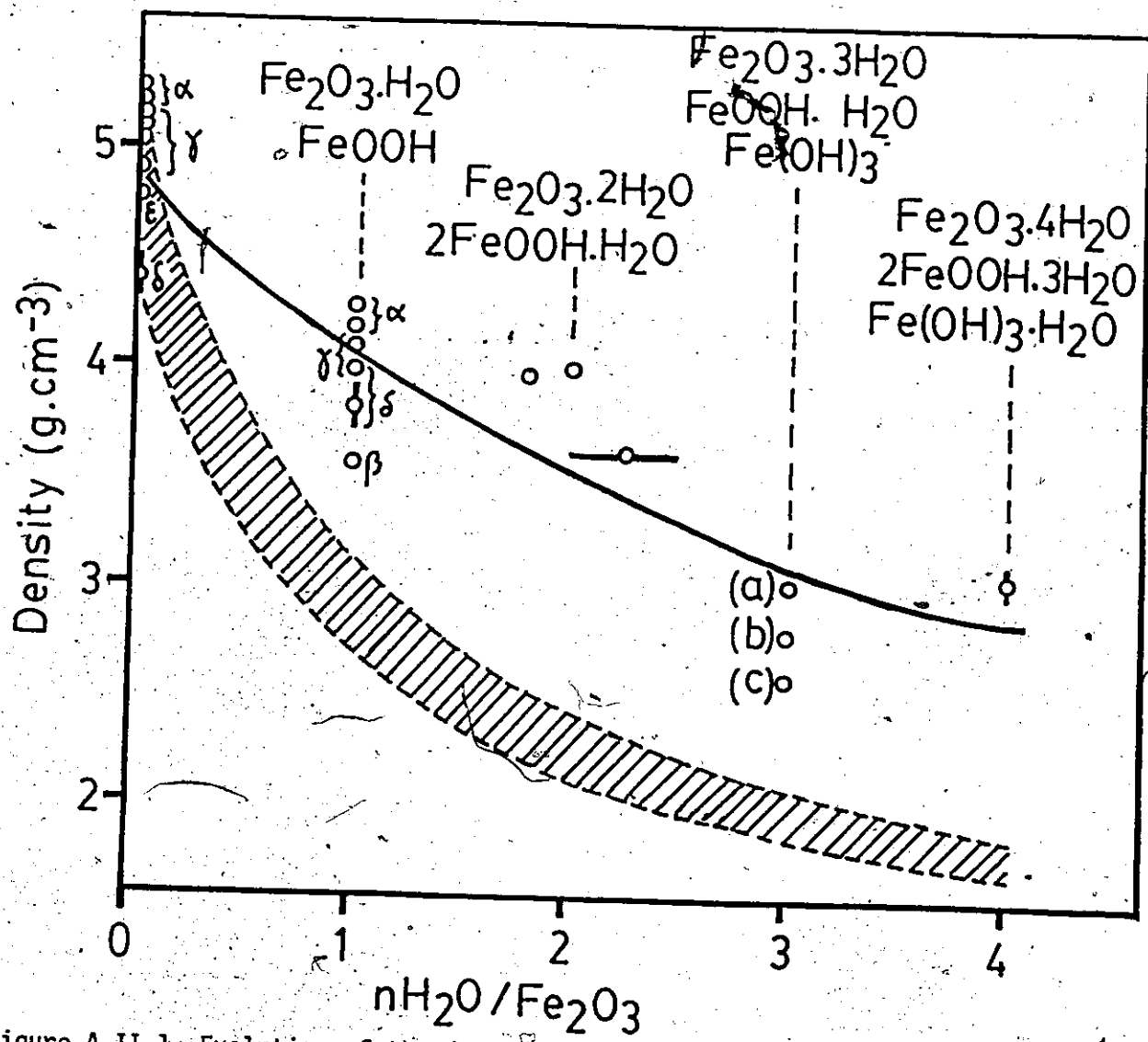

Figure A-II.1 Evolution of the density of hydrated iron oxides with the degree of hydration. The values of the measured density are taken from the literature for the following oxide-hydroxide α-Fe_2O_3(A-II.7, A-II.9), γ-Fe_2O_3 (A-II.10), δ-Fe_2O_3(A-II.9), ε-Fe_2O_3(A-II.11), α-FeOOH goethite(A-II.7, A-II.9, A-II.11), γ-FeOOH lepidocrocite(A-II.7, A-II.9, A-II.12), δ-FeOOH(A-II.9, A-II.13), unspecified phase of FeOOH(A-II.14), unspecified phase of $Fe_2O_3 \cdot H_2O$ (A-II.15), $Fe_2O_3 \cdot 1.8H_2O$(A-II.16), $Fe_2O_3 \cdot 2H_2O$(A-II.2), $Fe_2O_3 \cdot 2\text{-}2.5H_2O$(A-II.17) and $Fe_2O_3 \cdot 4H_2O$(A-II.15). The shaded area gives the range of calculated densities for a simple adsorption of water molecules by Fe_2O_3.

$$\rho_{Fe_2O_3 \cdot X_{H_2O}} = \frac{\rho_{Fe_2O_3} + \rho_{H_2O}}{x + 1} \qquad [A\text{-II.1}]$$

i.e., the average of the densities of the two components of the mixture is obtained. This is shown in the shaded region of Figure A-II.1. The upper and lower boundries of the shaded region reflect the maximum and minimum densities reported for α and δ Fe_2O_3 respectively. According to equation A-II.1 (A-II.19).

$$\rho_{Fe_2O_3 \cdot X_{H_2O}} = \frac{\rho_{Fe_2O_3} + x}{x + 1} \quad \rho_{H_2O} \simeq 1$$

The density of a physical mixture of $1Fe_2O_3$ and $x\ H_2O$ should be close to the density of Fe_2O_3 having xH_2O absorbed on its surface. From 0 to $2H_2O$, the calculated density for a physical mixture using equation A-II.1 falls far more rapidly than the experimental density implying that the water is most likely present in lattice positions rather than simply absorbed on the surface. Beyond $2H_2O$, experimental and calculated densities agree well. The third H_2O could be surface absorbed. However, after desorption, there is only partial rehydration (~50%). The absorption is most likely in pores and not on the surface.

(C) Thermal Analysis (Simultaneous D.T.A./T.G.A.) of Dehydration of $Fe(OH)_3$

[redacted] thermogravimetric curve is presented in Figure A-II.2 for the dehydration of $Fe(OH)_3$. The dehydration process starts at approximately 40°C and continues up to 170°C. There is a total weight loss of 8.5%; the solid has the formal composition of $Fe_2O_3 \cdot 2H_2O$ or $2FeOOH \cdot H_2O$. The loss of the second

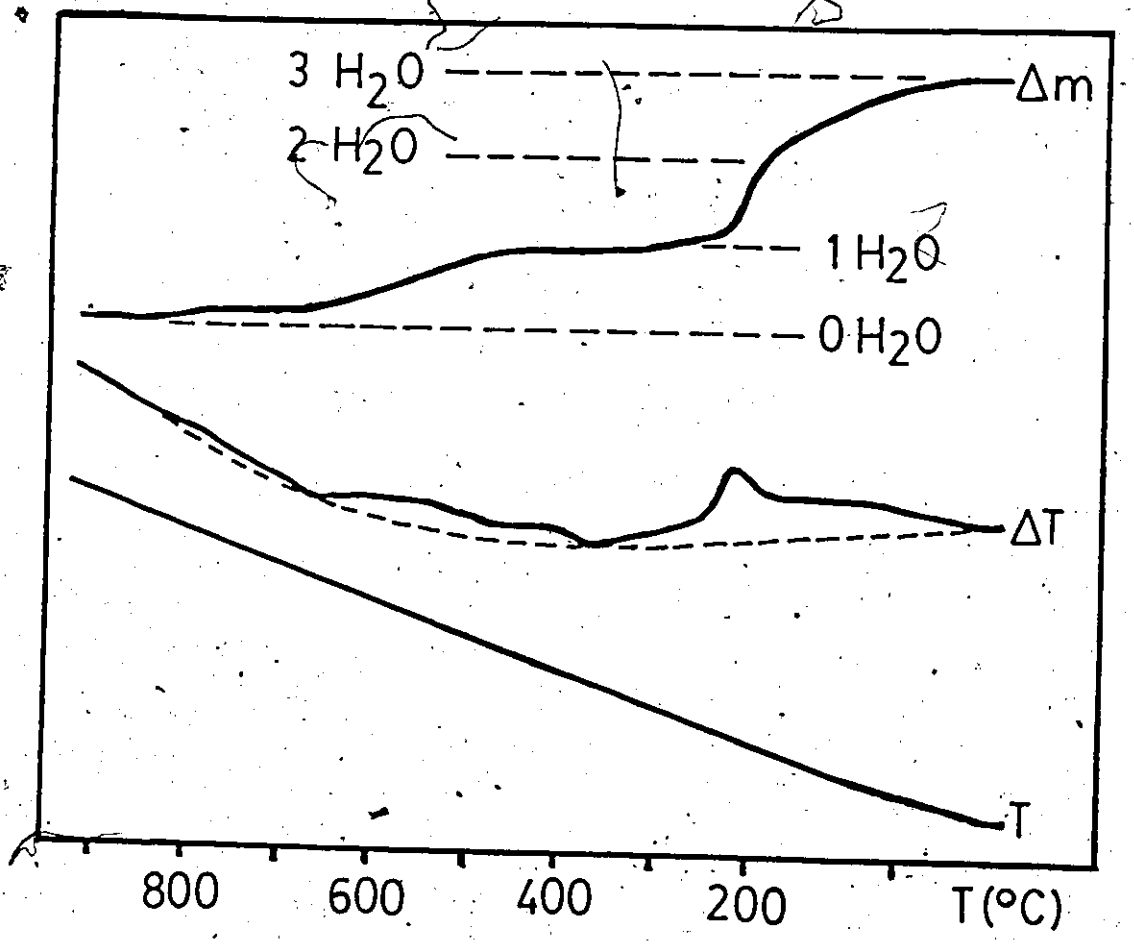

Figure A-II.2 D.T.A./T.G.A. curves for the dehydration of $Fe(OH)_3$ powder. FeOOH and $Fe_2O_3 \cdot XH_2O$ (hydrohematite) are intermediate products. Linear heating rate = 10°C/minute. The broken line is an interpolated estimate of the baseline for the D.T.A. Curve.

water molecule is characterized by a very sharp endothermic step followed by slower step trailing to ~350°C. A total of 16.9% of the total weight has been lost to this point. The solid now has the formal composition of $Fe_2O_3 \cdot H_2O$ or FeOOH. A third dehydration step starts at ~490°C and is completed at 690°C. At this point, the solid sample still retains 1.9% of water and is generally known as "hydrohematite".

It has been demonstrated by Wolska (A-II.19) that hydrohematite is made up of a close packed sublattice (O^{2-} and OH^-) with Fe^{3+} deficiencies in the cationic positions. Hydrohematite has the formula $Fe_{2-x/3}(OH)_xO_{3-x}$ and can contain up to 3-4.5% of tightly held water and requires a temperature in excess of 1000°C to complete dehydration. In the case of crystalline $Fe(OH)_3$, the removal of the remaining 2% of water to form the hematite α-Fe_2O_3 is completed at 900°C. The total amount of water loss is equivalent to 2.95 H_2O.

Each step of "water" loss is characterized by endothermic steps with the second "water" loss well defined on the T.G.A. curve. Similar changes are observed for $Fe(OH)_3$ samples obtained from preparations using other Cobalt dioxygen complexes. Their T.G.A. curves are presented in Figure A-II.3. Also included for comparison in Figure A-II.3 are the T.G.A. curves of $Fe(OH)_3$ prepared from the reaction of $FeSO_4 \cdot 7H_2O$ with H_2O_2 and the reaction of $FeCl_3$ with NH_4OH. The latter reaction gives a gel as reported in the literature (A-II.2). It is quite obvious from Figure A-II.3 that the gel loses most of its water (~ 90-95%) at 300°C whereas the crystalline powder loses only approximately 65% of its water at this temperature. The first two stages

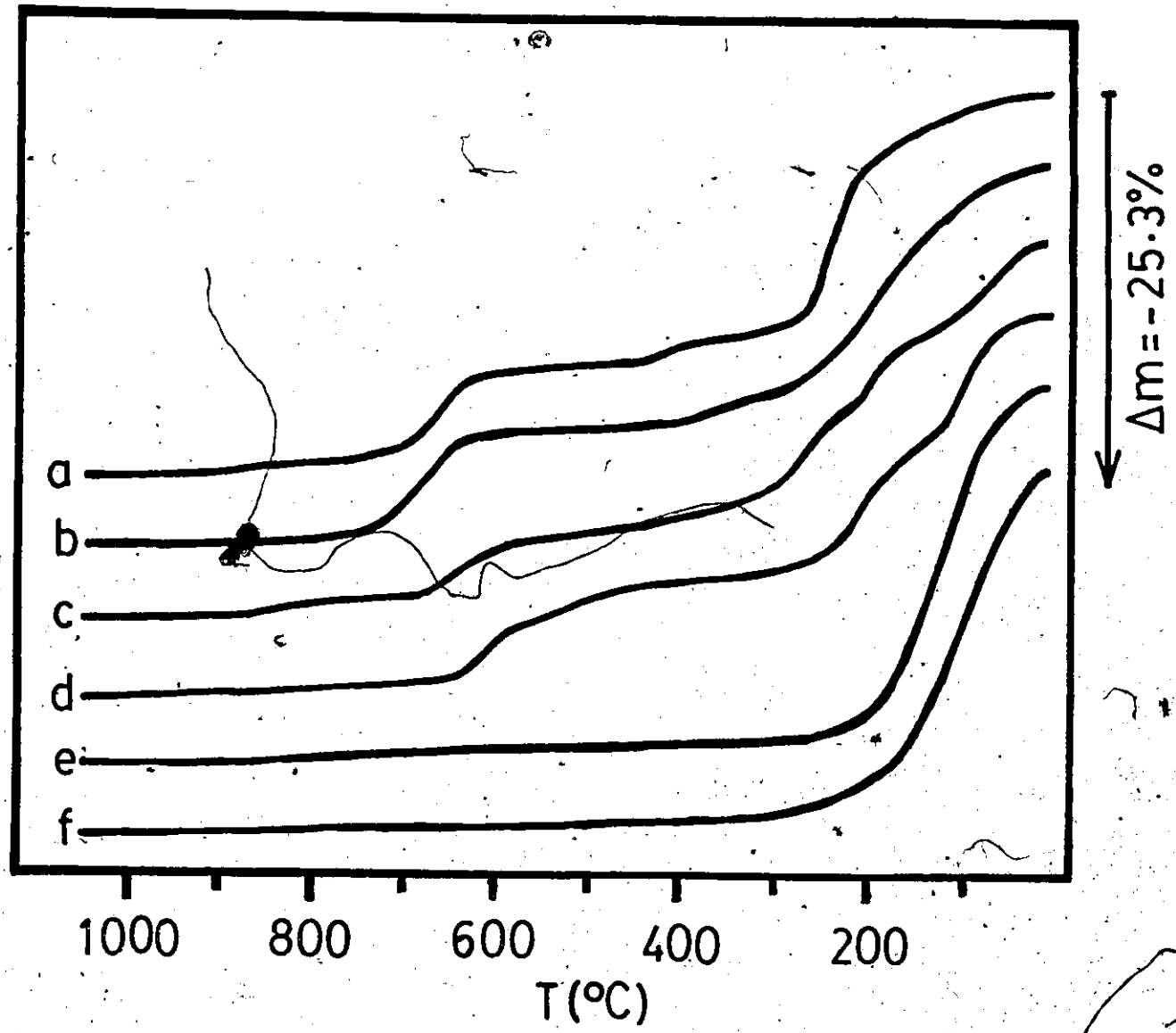

Figure A-II.3 Origin of Samples

(a)	Fe^{2+} + $(Co(en)(dien))_2O_2^{4+}$	5mM	(powder)
(b)	Fe^{2+} + H_2O_2 pH < 7		(powder)
(c)	Fe^{2+} + $(Co(tetraen))_2O_2^{4+}$		(powder)
(d)	Fe^{2+} + $(Co(NH_3))_5O_2^{4+}$		(powder)
(e)	Fe^{2+} + H_2O_2 pH = 10.9		gel
(f)	Fe^{3+} + NH_4OH		gel

of dehydration for $Fe(OH)_3$ obtained from the hydrogen peroxide reaction are not well resolved suggesting that the two types of water are probably structurally quite similar. This result may be compared with the T.G.A. curve of the $Fe(OH)_3$ powder obtained from the reaction of $[(Co(NH_3)_5)_2 O_2]^{4+}$ with $FeSO_4 \cdot 7H_2O$ in which the first and second dehydration step are clearly resolved. The third stage of dehydration covers a range of 250°C (~ 500-750°C) for both the gel and for crystalline $Fe(OH)_3$ obtained from the dioxygen complex reaction or by reaction with H_2O_2. These characteristic T.G.A. patterns can be considered as further evidence for the synthesis of a new form of synthetic crystalline $Fe(OH)_3$. Two additional points are to be noted;

i) After the T.G.A. analysis the samples were observed to reversibly absorb moisture but not all of the water was regained after 48 hours.

ii) Weight fluctuations are observed when the humidity of the environment fluctuates. These fluctuations were found to be less than 5%.

The process of dehydration is summarized in Scheme A-II.1.

From Scheme A-II.1, it is clear that a substantial amount of water is loosely bound in the lattice in both gel and powder forms of $Fe(OH)_3$. Since the stoichiometry of $3H_2O \cdot Fe_2O_3$ is not fully recovered in air of normal humidity after the T.G.A. experiment at room temperature, it is likely that simple absorption on the surface is an over-simplified explanation for the crystalline powder. This is contrary to the absorption behaviour proposed for the gels (A-II.2). The powder sample differs from the dried gels in that one molecule of water is retained up to ~500°C and the individual intermediate dehydration steps are resolved. It is

Scheme A-II.1

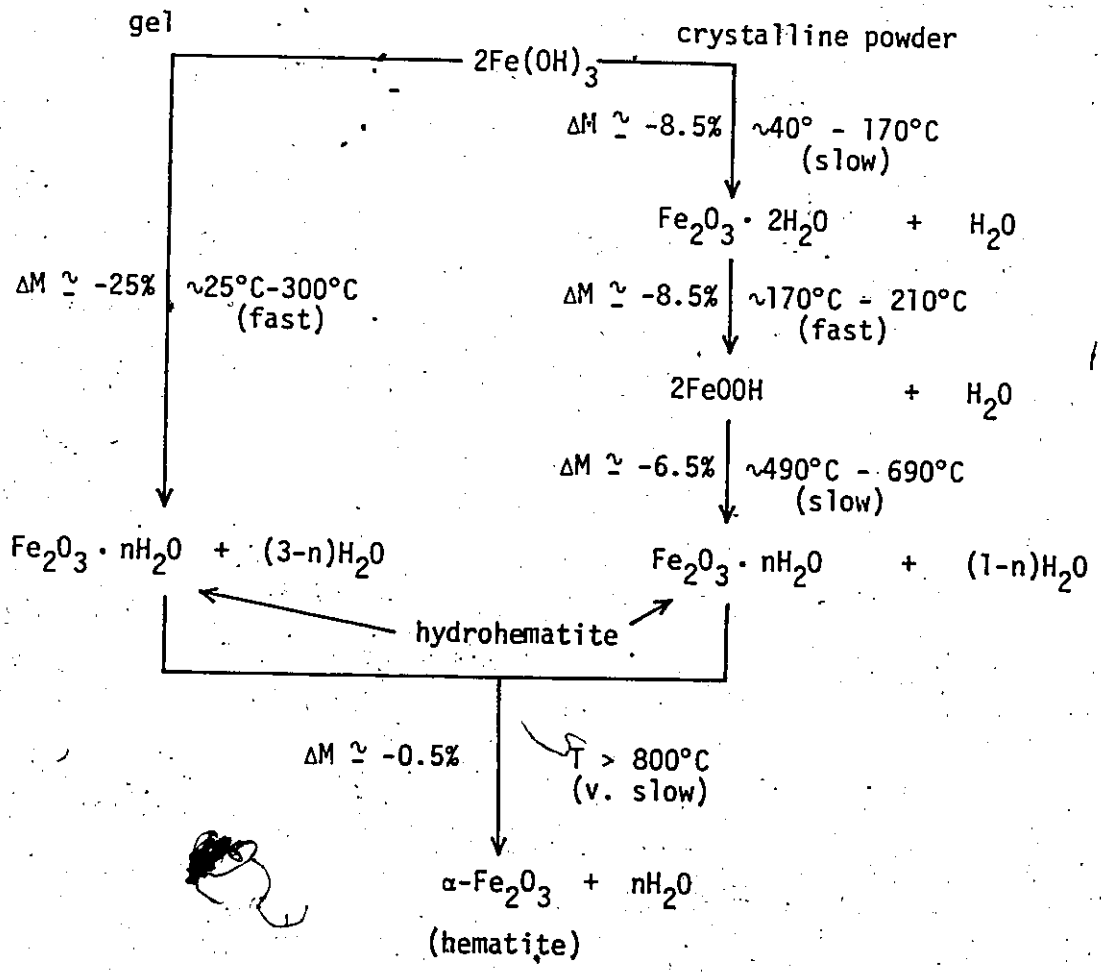

highly likely that the water lost above 500°C is not present as an actual water molecule in the sample, but is formed by the reaction, i.e.,

$$2OH^- \xrightarrow{\Delta} H_2O + O^{2-}$$

where the O^{2-} ion bridges two neighbouring iron atoms. This process will require a considerable input of energy since structural rearrangement takes place. As for the gels, there is no way of distinguishing the individual steps. Some low temperature evolution of water from the $Fe(OH)_3$ gel has been interpreted as originating from OH^- groups (A-II.2, A-II.20). Therefore, combining known literature results and the present study, neither

the formulation of $Fe(OH)_3$ (iron trihydroxide) nor that of $Fe_2O_3 \cdot 3H_2O$ (iron oxide trihydrate) is appropriate for this compound. It may be suggested that the formula $FeO_{3/2-x}(OH)_{2x}(\frac{3}{2}-x)\cdot H_2O$ where X=0 to 3/2 best describes the series of compounds listed in Figure A-II.1. The oxide hydroxide hydrate prepared in this work has a value of X=0 and a formal composition of $Fe_2O_3 \cdot 3H_2O$. For simplicity, "$Fe(OH)_3$ powder" will be used in further discussion.

(D) Mössbauer Spectroscopy

The room temperature Mössbauer spectrum of $Fe(OH)_3$ powder is similar to that of $Fe(OH)_3$ gel (A-II.2) and of the natural ferric gel $Fe(OH)_3 \cdot 0.9H_2O$ (A-II.2) in the paramagnetic phase. Spectral fitting to one iron site is unsatisfactory ($\chi^2/df = 2.153$) giving an unreasonable linewidth in comparison to the calibrant. This fit is shown in Figure A-II.4(a) together with the corresponding plot of the residual deviations. Both distribution of the isomer shift and/or quadrupole splitting was observed for the gel of $Fe(OH)_3 \cdot nH_2O$. This could result in large line broadening and lineshape distortion (A-II.21). Fitting the spectrum to one iron site with a distribution of quadrupolar splitting constraints improves the fit slightly but not perfectly. When the spectrum was fitted to two Iron sites with equal linewidths, the fitting improved to give ($\chi^2/df=1.011$), but remained poor particularly at the point of minimum absorption between the components of the observed doublet. Finally, releasing the equal linewidth constraint in the two site fitting gave a completely satisfactory fit for the entire spectrum. This is shown in Figure A-II.4 (b) and the chemical isomer shift and quadrupole splitting parameters are given in Table A-II.3. Also given

Table A-II.3

^{57}Fe Mossbauer Data for "$Fe(OH)_3$ Powder" and Related Materials

Compound	T (°K)	number of sites	δ	Δ(2ε)	Γ	H kOe	contribution of site(%)	χ^2/df
			mmsec^{-1}					
"$Fe(OH)_3$ powder"								
Sample 1	296	1	0.37	0.60	0.45			2.15
		2	0.38	0.47	0.31		38(10)	0.87
			0.38	0.74	0.47		62(10)	
	77							
	4.2	1	0.50		0.66	424(1)		1.18
Sample 2	296							
	77	1	0.47	0.63	0.45			1.69
		2	0.47	0.50	0.34		51(8)	0.98
			0.51	0.82	0.45		49(8)	
	4.2	1	0.52		0.56	432(1)		1.22
"$Fe(OH)_3$gel"[a]								
	290	1	0.385[b]	0.62				
	77	1	0.455[b]					
	4.2	1				~515[c]		
"$Fe(OH)_3 \cdot 0.9H_2O$"[d]								
	296	1	0.35[d]	0.72	0.48			
	77	1	0.47[d]	0.81	0.58			
	4.2	1	0.38[d]	0.03		458		
"β-FeOOH"[e]								
	295	2	0.374	0.546	0.274		60(2)	
			0.379	0.951	0.376		40(2)	
	77	3	0.51	-0.07	0.45	470	54	
			0.46	-0.34	0.27	462	15	
			0.48	-0.49	0.65	442	31	

[a] Reference (A-II.2)

[b] Isomer shifts are given relative to a ^{57}Co in Pd source in Reference (A-II.2) The numbers in the table are relative to α-Fe at room temperature; the correction is made using the value given in Reference (A-II.2).

[c] Value estimated from figure 4.4 of reference (A-II.2); no value of H_{eff} is given in reference (A-II.2).

[d] Reference (A-II.2).

[e] Isomer shifts are given in reference (A-II.2) relative to a ^{57}Co in Cr source they are converted to α-Fe reference using the value given in reference (A-II.2).

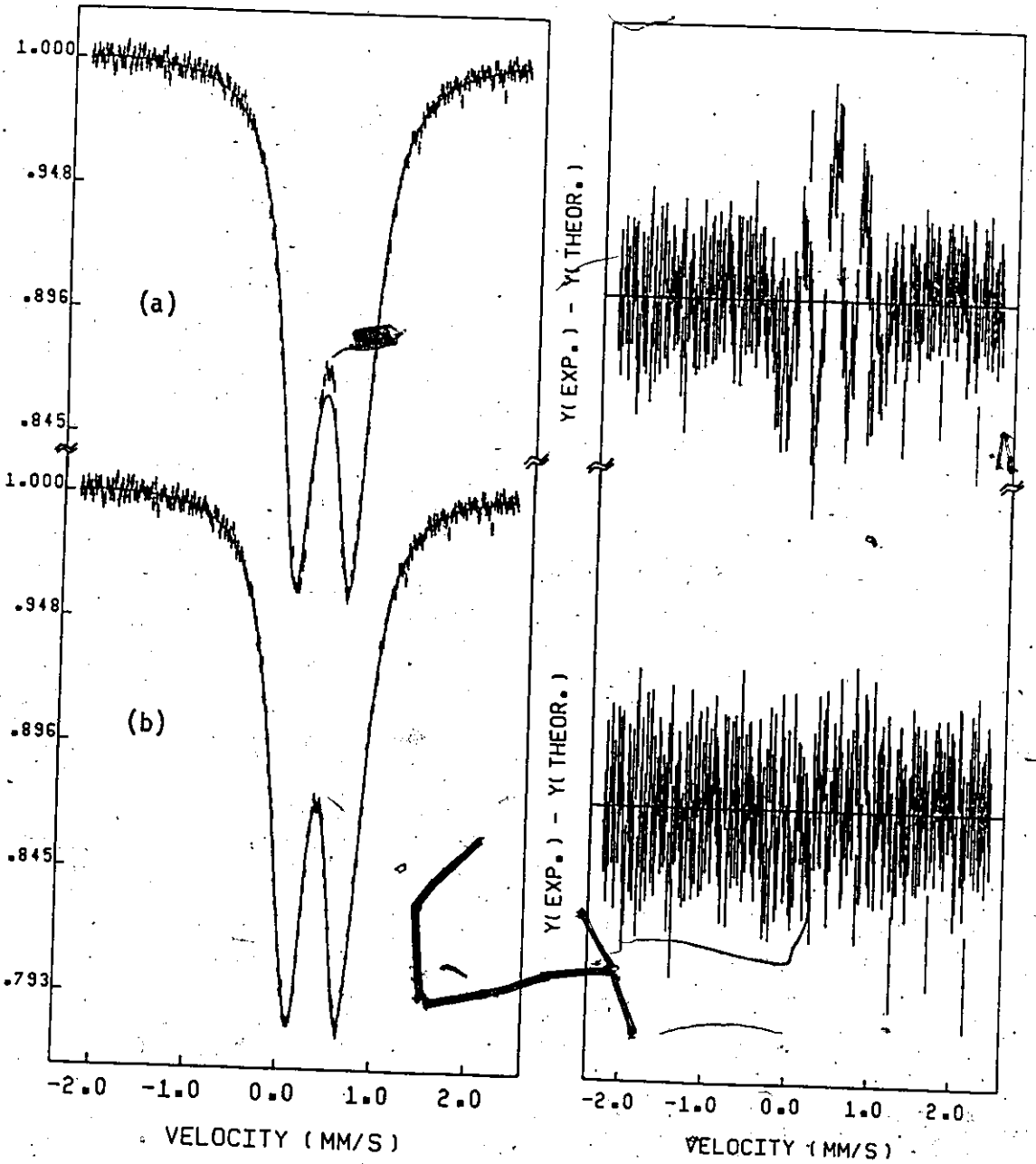

Figure A-II.4 Mossbauer spectrum of $Fe(OH)_3$ at room temperature (paramagnetic region) and their corresponding plot of the residual derivations.
(a) fitted as one quadrupole doublet ($\chi^2/df = 2.153$)
(b) fitted as two quadrupole doublet with unequal linewidth ($\chi^2/df = 0.87$).

in Table A-II.3 are literature parameters for $Fe(OH)_3$ gel, the natural ferric gel $Fe(OH)_3 \cdot 0.9H_2O$ and β-FeOOH (containing 3% Cl^-) for comparison. The results suggest that the $Fe(OH)_3$ powder, when compared to the various other materials in Table A-II.3, is most similar to β-FeOOH. The chemical isomer shift of δ_{ave} = 0.375 $mmsec^{-1}$ of the latter and also the values of the quadrupole splitting of the inner and outer doublet (0.546 and 0.951 $mmsec^{-1}$ respectively) can be compared to δ = 0.375 $mmsec^{-1}$ and 0.47 and 0.74 $mmsec^{-1}$ for the inner and outer doublet of $Fe(OH)_3$. Although the quadrupole splitting values are substantially different, they cannot be considered to provide conclusive evidence for identifying the material since surface effects as well as impurities affect the quadrupole splitting values. These effects may be particularly important for β-FeOOH since it contains ∿ 3% chloride. The chemical isomer shifts of the two materials offer no help in differentiating these materials since they have similar values.

Fortunately, low temperature Mössbauer spectroscopy provides additional information since β-FeOOH exhibits a magnetically ordered hyperfine splitting spectrum at 77°K (see Table A-II.3) whereas the $Fe(OH)_3$ crystalline powder obtained in this work shows no noticable change at 77°K (Figure A-II.5)(a) except that there is an increase in isomer shift by ∿ 0.1 $mmsec^{-1}$ which is due to the second order Doppler effect. This is a relativistic temperature - dependent effect which is due to the fact that the Fe^{3+} ions are vibrating in the solid and the mean value $\langle v^2 \rangle$ of the Doppler shift is non-zero. This type of behaviour has been observed for α-Fe_2O_3 over the same temperature range (A-II.22). The relative con-

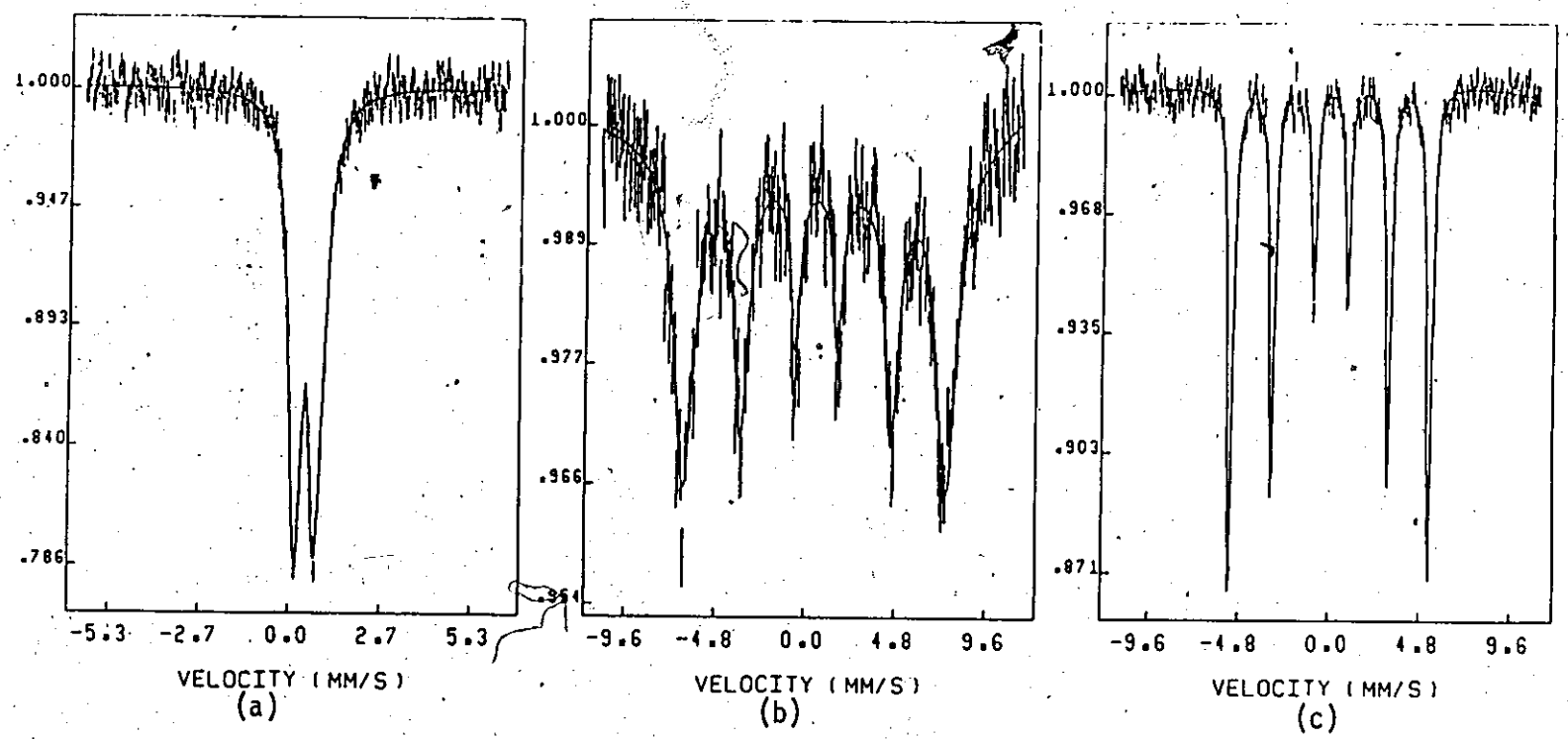

Figure A-II.5 Mossbauer spectrum of $Fe(OH)_3$ powder;

(a) "$Fe(OH)_3$ powder" at 77°K (superparamagnetic region)

(b) "$Fe(OH)_3$ powder" at 4.2°K (ordered state)

(c) α-Fe at room temperature. Note that the linewidth for α-Fe (no field distribution), the same for all the six lines, is much smaller than for $Fe(OH)_3$ powder (field distribution).

tribution of each iron site at 77°K is approximately the same as that at 296°K. The magnetically ordered spectrum of $Fe(OH)_3$ powder is observed at 4.2°K. This is shown in Figure A-II.5(b). The calibrant α-Fe at room temperature is shown in Figure A-II.5(c).

The spectrum of Figure A-II.5(b) consists of six symmetrically broadened lines ($\Gamma_3 = \Gamma_4 = 0.567(7)$, $\Gamma_2 = \Gamma_5 = 1.23(10)$, $\Gamma_1 = \Gamma_6 = 1.86(10)$ $mmsec^{-1}$, where Γ_1, to Γ_6 represent the linewidths of the lines 1 to 6 from negative to positive velocities). The broadened lines are characteristic of magnetic field distribution. The spectrum was fitted to a single hyperfine magnetic site including the magnetic field distribution parameters (A-II.21). The calibrant of α-Fe is shown to contrast the linewidth differences. Similar broadening by magnetic field distribution was also observed in synthetic and natural ferric gels. There is no evidence of more than one hyperfine site for the 4.2°K spectrum as a one site fit is satisfactory. Attempts to include two hyperfine sites resulted in divergence. This result clearly differs for that obtained for β-FeOOH. Three hyperfine sites were found for the latter at 77°K. The fitting of the 4.2°K spectrum to one site is not inconsistent with the fact that two iron sites are observed at higher temperatures due to:

i) the resolution is decreased and thus the distinction between two closely overlapping sites becomes more difficult.

ii) $2\varepsilon = \Delta\left(\frac{3\cos^2\theta-1}{2}\right)$, where θ is the angle between the axis of magnetization (internal magnetic field) and V_{zz}. Since θ and Δ can have a different value, 2ε can be similar for both sites in the magnetically ordered phase.

Therefore, low temperature Mössbauer data has definitively shown that the product "$Fe(OH)_3$ powder" is a different material to any of the known Iron oxide-hydroxide-hydrates.

A-II.4 Summary

The chemical isomer shift of the"$Fe(OH)_3$ powder" (δ = 0.375 $mmsec^{-1}$) is compatible with the values for the $Fe(OH)_3$ gel (δ = 0.385 $mmsec^{-1}$), the natural ferric gel $Fe(OH)_3 \cdot 0.9H_2O$ (δ = 0.35 $mmsec^{-1}$) and β-FeOOH (δ = 0.37 $mmsec^{-1}$) and shows that the iron is in the ferric state. Where the isomer shifts have the same values for two Fe^{3+}sites, as it is for the present case and that of β-FeOOH, it is suggestive that the "average" enviroment about the two Fe^{3+} sites is approximately similar. The differences in the quadrupole splitting between the two Fe^{3+} sites reflect differences in coordination and bonding about iron. The contribution of each site may reflect differences in the mechanisms of formation with different di-oxygen complexes.

In conclusion, from the magnetic point of view, the $Fe(OH)_3$ powder behaves in an entirely different manner to β-FeOOH and other related materials. These findings, together with density, T.G.A. and analysis results, warrants the description of this material as a new compound.

REFERENCES

CHAPTER ONE

1.1 G.L. Eichhorn, "Inorganic Biochemistry" ed. Vols. 1 and 2, American Elsevier, New York (1973).

1.2 G. McLendon and A.E. Martell Coord. Chem. Rev., 19, 3 (1976).

1.3 R.D. Jones, D.A. Summerville and F.Basolo, Chem. Rev., 79, 144 (1979).

1.4 T.E. King, M. Mason and M. Morrison, "Oxidases and Related Model Systems", Vols. 1 and 2, University Park Press, Baltimore, 1974.

1.5 A.E. Martell and M.M. Taqui Khan, in G.L. Eichhorn (Ed.), "Inorganic Biochemistry", Elsevier, New York, 1973, p. 654.

1.6 M. Calvin, Science, 184, 375 (1974).

1.7 M. Calvin and S.R. Cooper, Science, 185, 376 (1974).

1.8 M. Balnor, J. Biol. Chem., 245, 6125 (1970).

1.9 G.N. Schranzer and L.P. Lee, J. Amer. Chem. Soc. 92, 1551 (1970).

1.10 F. Antonini and M. Brunori, "Hemoglobin and Myoglobin and Their Reactions with Ligands", North-Holland, Amsterdam, 1971, and references therein.

1.11 J.S. Griffith, Proc. Roy. Soc., Ser. A, 235, 23 (1956).

1.12 A.A. Vleck, Trans. Faraday Soc., 56, 1137 (1970).

1.13 L. Pauling, Nature (London), 203, 182 (1964).

1.14 J.B. Wittenburg, B.A. Wittenburg, J. Peisach and W. Blumberg, Proc. Nat. Accord. Sci. (U.S.A.), 67, 1846 (1970).

1.15 J.J. Weiss, Nature (London), 203, 83 (1964).

1.16 D.M.P. Mingo, Nature (London), 230, 154 (1971).

1.17 E.I. Ochai, J. Inorg. Nucl. Chem., 35, 3375 (1974).

1.18 J.D. Dunitz and L. Orgel, J. Chem. Soc., 2594 (1953).

1.19 L.H. Vogt. Jr., H.M. Faigenbaum and S.E. Wiberly, Chem. Rev., 63 269 (1963).

1.20 M.J. Carter, P.P. Rillema and F. Basolo, J. Amer. Chem. Soc., 96 392 (1974).

1.21 L. Vaska, Acc. Chem. Res., 1, 335 (1968).

1.22 J.A. O'Connor and E.A.V. Ebsworth, Adv. Inorg. Chem. Radiochem., 6, 279 (1964).

1.23 E. Bayer and P. Stretzmann, Struct. Bonding (Berlin), 2, 181 (1967).

1.24 S. Fallab, Angew. Chem. Int. Ed. Engl., 6, 496 (1967).

1.25 A.G. Sykes and J.H. Weil, Prog. Inorg. Chem., 13, 1 (1970).

1.26 R.G. Wilkins, Adv. Chem. Ser., No. 100, 111 (1971).

1.27 V.J. Choy and C.J. O'Connor, Coord. Chem. Rev., 19, 145 (1972/73).

1.28 J.S. Valentine, Chem. Rev., 73, 235 (1973).

1.29 L. Kleran J. Peone and S.K. Madan, J. Chem. Educ., 50, 670 (1973).

1.30 F. Basolo, J. Indian Chem. Soc., 51, 1 (1974).

1.31 G. Henrici-Olivé and S. Olivé, Angew. Chem. Int. Ed. Engl., 13, 29 (1974).

1.32 F. Basolo, B.M. Hoffman and J.A. Ibers, Acc. Chem. Res., 8, 384 (1975).

1.33 V. Savitsky and V.I. Nelyubia, Russ. Chem. Rev., 44, 110 (1975).

1.34 E. Ochiai, J. Inorg. Nucl. Chem., 37, 1503 (1975).

1.35 R.W. Erskine and B.O. Field, Struct. Bonding (Berlin), 9 1 (1976).

1.36 L. Vaska, Acc. Chem. Res., 9, 175 (1976).

1.37 J.P. Collman, Acc. Chem. Res., 10, 265 (1977).

1.38 G. Speier, Magy. Kem. Lapja, 32, 381 (1977).

1.39 Y. Moriguchi, Dojin Nyusu, 7, 1 (1977).

1.40 A. Nishinaga, in O. Hayaishi and K. Asada (Eds.) "Biochemical and Medical Aspects of Activation of Oxygen", University Park Press, Baltimore, MD, (1977), p. 13.

1.41 T. Eishun, Kagakin Sosetsu, 20, 30 (1978).

1.42 F. Basolo, Chem. Aust., 45, 127 (1978).

1.43 A.B.P. Lever and H.B. Gray, Acc. Chem. Res., 11, 348 (1978).

1.44 D.A. Summerville, R.D. Jones, B.M. Hoffman and F. Basolo, J. Chem. Educ., 56, 157 (1979).

1.45 R.S. Drago, J.R. Stahlbush, D.J. Kitko and J. Bruse, J. Amer. Chem. Soc., 102, 1884 (1980).

1.46 R.S. Young., "Cobalt in Biology and Biochemistry" Academic Press, London, (1979).

1.47 T.G. Spiro "Metal Ion Activation of Dioxygen" Wiley, Chicester (1980).

1.48 E. Fendrich and M. Marko, Zb, Pedagog, Fak. Univ. Komenskeho Bratislave Sidlom Tynave (Ser.): Chem., 8, 3 (1977).

1.49 G.D. Lawrence and D.T. Sawyer, Coord. Chem. Rev., 27, 173 (1978).

1.50 W.E. Coleman and L.T. Taylor, Coord. Chem. Rev., 32,1 (1980).

1.51 C.A. McAuliffe, H. Al-Khateeb, M.H. Jones, W. Levanson, K. Minten and F.P. McCullough, J. Chem. Soc., Chem. Commun., 736 (1979).

1.52 C.K. Chang and D. Dolphin, Bioorg. Chem., 4, 37 (1978).

1.53 M. Nuzaki, Top. Curr. Chem., 78, 145 (1979).

1.54 R. Davis, Coord. Chem. Rev., 35, 31 (1981).

1.55 A.W. Adamson, M. Cairns, R.K. Dinello, N.P. Farell, B.R. James, D.R. Parson, C. Welborn and D. Dolphin, Int. J. Quantum Chem., 16, 311 (1979).

1.56 R. Davis, Coord. Chem. Rev., 41, 40 (1982) and reference therein.

1.57 H. Beinert, Coord. Chem. Rev., 33, 55 (1980).

1.58 R.S. Drago, Coord, Chem. Rev., 33, 251 (1980).

1.59 J. Ivan Legg, Coord. Chem. Rev., 25, 103 (1978).

1.60 R.A. Bulman, Coord. Chem. Rev., 31, 221 (1980).

1.61 T.N. Lockyer and R.L. Martin in S.J. Lippard (Ed.) "Progress in Inorganic Chemistry", Vol. 27 (1980) John Wiley, Chichester.

1.62 H. Yamasaki and Y. Wakasuki, Yuki Gosei Kagaku Kyokaishi, 37, 1065 (1979).

1.63 B.E. Donglas and Y. Saito (Eds.), "Stereochemistry of Optically Active Transition Metal Compounds", ACS Adv. Chem. Ser., 219 A.C.S. Washington.

1.64 N.M. Samus, O.N. Damaskina and T.S. Luk'yanets, "Substitution Reactions in Cobalt Coordination Compounds", Shtiintsa Kishinev, Mold. SSR, (1979).

1.65 E. Tsuchida and H. Nishide, Adv. Polym. Sci., 24, 1 (1977).

1.66 H.F. Klein, Angew. Chem., 92, 362 (1980).

1.67 R.W. Hay, Coord. Chem. Rev., 41, 191 (1982).

1.68 R.W. Hay, Coord, Chem. Rev., 35, 85-86 (1981).

1.69 F. Basolo and R.G. Pearson, "Mechanisms of Inorganic Reactions" 2nd Ed. John Wiley and Sons Inc. (1967).

1.70 R.G. Wilkins, "The Study of Kinetics and Mechanisms of Transition Metal Complexes", Publisher: Allyn and Bacon Inc., (1974).

1.71 D.A. House, Coord. Chem. Rev., 23, 223 (1977).

1.72 T.W. Swaddle, Coord. Chem. Rev., 14, 217 (1974).

1.73 I. Bodek and G. Davis, Coord. Chem. Rev., 14, 269 (1974).

1.74 G. Davis, Coord. Chem. Rev., 14, 287 (1974).

1.75 G.B. Kauffman, Coord. Chem. Rev., 15, 1 (1975).

1.76 F. Miller, J. Simiplicio, R.G. Wilkins, J. Amer. Chem. Soc., 91, 1962 (1969).

1.77 F. Miller Bogdansky, Ph.D. Dissertation, State University of New York, Buffalo (1971).

1.78 J. Simiplico and R.G. Wilkins, J. Amer. Chem. Soc. 89, 6092 (1967).

1.79 K. Watters, and R.G. Wilkins, Inorg. Chem., 13, 752 (1974).

1.80 J. Simiplicio, Ph.D. Dissertation, State University of New York, Buffalo (1969).

1.81 F. Miller and R.G. Wilkins, J. Amer. Chem. Soc., 92, 2687 (1970).

1.82 D. H. Huchital and A.E. Martell, Inorg. Chem., 13, 2966 (1974).

1.83 D.V. Stynes, H.C. Stynes, J.A. Ibers and B.R. James, J. Amer. Chem. Soc., 95, 1142 (1973).

1.84 E.I. Ochiai, J. Inorg. Nucl. Chem., 35, 1727 (1973).

1.85 A.B.P. Lever, E. Lee-Ruff and G.P. Kharl, Can.J.Chem., 54, 3432 (1976).

1.86 J.P. Collman, R.R. Gagne, T.H. Halbert, J.C. Marchon and C.A. Reed J. Amer. Chem. Soc, 95, 7868 (1973).

1.87 J.P. Collman, R.R. Gagne, J. Kouba and H. Ljusberg-Wahran J. Amer. Chem. Soc., 96, 6800 (1974).

1.88 M.F. Perutz, "The Harvey Lecture", Academic Press, New York-London 213 (1963).

1.89 M.F. Perutz, Nature (London), 228, 726 (1970).

1.90 M. Calvin, R.H. Bailes and W.K. Wilmouth, J. Amer. Chem. Soc., 68, 2254 (1946).

1.91 A.E. Martell and M. Calvin, "Chemistry of the Metal Chelate Compounds" Prentice-Hall. Inc., Englewood Cliffs, N.J. (1952).

1.92 M. Calvin and C.H. Berkelew, J. Amer. Chem. Soc., 68, 2267 (1946).

1.93 M. Calvin and C.H. Berkelew, J. Amer. Chem. Soc., 68, 2257 (1946)

1.94 W.K. Wilmarth, S. Aranoff and M. Calvin, J. Amer. Chem. Soc., 68, 2263 (1946).

1.95 D.L. Harle and M. Calvin, J. Amer. Chem. Soc., 68, 2612 (1946).

1.96 A.E. Martell and C. McLendon, J. Coord, Chem., 4, 235 (1974).

1.97 A.E. Martell, Acc. Chem. Res., 15, 155 (1982).

1.98 M. Crawford, S.A. Bedell, R.I. Patel, L.W.Young and R. Nakon, Inorg. Chem, 18, 2075 (1979).

1.99 L.D. Brown and K.N. Raymond, Inorg. Chem., 14, 2595 (1975).

1.100 J.H. Bayston and M.E. Winfield, J. Cat., 3, 123 (1964).

1.101 J.H. Bayston, R.N. Beale, N.K. King and M.E. Winfield, Aust. J. Chem., 16, 954 (1963).

1.102 A. Rossi - Fanelli, E. Antonini and A. Caputo, Adv. Protein Chem., 19, 74 (1964).

1.103 T. Yonetani, H. Yamamoto, F. Kayne and G. Woodrow, Biochem. Soc. Trans., 1, 44 (1973).

1.104 B.M. Hoffman and D.H. Petering, Proc. Natl. Acad. Sci. U.S.A. 63, 637 (1970).

1.105 T. Takayanagi, H. Yamamoto and T. Kwan, Bull. Chem. Soc. Jpn., 48, 2618 (1975).

1.106 D.V. Stynes, H.C. Stynes, B.R. James and J.A. Ibers, J. Amer. Chem. Soc., 95, 1796 (1973).

1.107 J.P. Collman, C.M. Elliott, T.R. Halbert and B.S. Tovroy, Proc. Natl. Acad. Sci. U.S.A.,74, 18 (1977).

1.108 C.K. Chang, J. Chem. Soc., Chem. Commun., 800 (1977).

1.109 T.D. Smith and J.R. Pilbrow, Coord, Chem. Rev., 39, 295 (1981).

1.110 B.S. Tovrog, D.J. Kitko, R.S. Drago, J. Amer. Chem. Soc., 98, 5144 (1976).

1.111 C.R. Krishnamoorthy, R. Van Eldik and G.M. Harris, J. Coord. Chem., 10, 195 (1980).

1.112 G. Navon and H. Shinar, Inorg. Chim. Acta., 46, 51 (1980).

1.113 M. Ferrer, T.D. Hand and A.G. Sykes, J. Chem. Soc., Dalton Trans., 14, (1980).

1.114 J. Simiplicio and R.G. Wilkins J. Amer. Chem. Soc., 91, 1325 (1969).

1.115 M. Mori and J.A. Weil, J. Amer. Chem. Soc., 89, 3732 (1967).

1.116 U. Thewalt, unpublished work (1969).

1.117 U. Thewalt and R.E. Marsh, J. Amer. Chem. Soc., 89, 6364 (1967).

1.118 M.R. Hyde and A.G. Sykes, J. Chem. Soc., Dalton Trans., 1550 (1974).

1.119 G. Mclendorf and A.E. Martell, Inorg. Chem., 15, 2662 (1976).

1.120 A. Hoffman and H. Taube, Inorg. Chem., 7, 1971 (1968).

1.121 T. Shibahara, S. Koda and M. Mori, Bull. Chem. Soc. Jpn., 46, 2070 (1973).

1.122 T. Shibahara and M. Mori, Bull. Chem. Soc. Jpn. 45, 1433 (1972)

1.123 S. Fallab, H.P. Hunold, M. Maeder and P.R. Mitchell, J. Chem. Soc., Chem. Commun. 469 (1981).

1.124 Y. Sasaki, K.Z. Suzuki, A. Matsumoto and K. Saito. Inorg. Chem., 21, 1825 (1982).

CHAPTER TWO

2.1 N. Bloembergen, E.M. Purcell and R.V. Pound, Phys. Rev., 73(7), 679 (1948).

2.2 P. Mansfield, P.G. Morris, R.J. Ordidge, I.L. Pykett, V. Bangert, and R.E. Coupland, Phil. Trans. Roy. Soc. Lond., B289, 503 (1980).

2.3 W.V. House, IEEE Trans. Nucl. Sci., 27(3), 1220 (1980).

2.4 P.C. Lauterbur and Ching-Ming Lai, IEEE Trans, Nucl. Sci., 27(3), 1227 (1980).

2.5 E.R. Andrews, IEEE Trans. Nucl. Sci., 27(3), 1232 (1980).

2.6 L.E. Crooks, IEEE Trans. Nucl. Sci., 27(3), 1239 (1980).

2.7 J.R. Singer, IEEE Trans. Nucl. Sci., 27(3), 1245 (1980).

2.8 J. Mallard, J.M.S. Hutchinson, W.A. Edelstein, C.R. Ling, M.A. Foster and G. Johnson, Phil. Trans. Roy. Soc. London, B289, 519 (1980).

2.9 P. Brunner and R.R. Ernst, J. Magn. Reson., 33, 83 (1979).

2.10 F. Bloch, W.W. Hansen, and M. Packard, Phys. Rev., 70, 474 (1946).

2.11 W. Lamb, Phys. Rev., 60, 817 (1941).

2.12 N.F. Ramsey, Phys. Rev., 77, 567 (1950).

2.13 Ibid., 78, 699 (1950).

2.14 Ibid., 86, 243 (1952)

2.15 J.W. Emsley, J. Feeney, and L.H. Sutcliffe, "High Resolution Nuclear Magnetic Resonance Spectroscopy" Pergamon Press, Oxford (1966).

2.16 (a) H.F. Hameka, J. Chem. Phys., 40, 3127 (1964).

(b) L.C. Snyder and R.G. Parr., J. Chem. Phys., 34, 827 (1961).

2.17 N.F. Chamberlain, "The Practice of NMR Spectroscopy with Spectra-Structure Correlations for Hydrogen-1" Plenium Press, New York and London (1974).

2.18 G.P. Betteridge and R.M. Golding, J. Chem. Phys., 51(6), 2497 (1969).

2.19 R. Freeman, G.R. Murray, and R.E. Richardson, Proc. Roy. Soc, (London), A242, 455 (1957).

2.20 S. Fujiwara, F. Yajima, and A. Yamasaki, J. Magn. Reson, 1, 203 (1969).

2.21 N. Juranić. J. Chem. Phys., 74(7), 3690 (1981).

2.22 R.L. Martin and A.M. White, Nature, 223, 394 (1969).

2.23 R. Weis and J.G. Verkade, Inorg. Chem., 18, 529 (1979).

2.24 N. Juranic, Inorg. Chem., 19, 1093 (1980).

2.25 N. Juranic, Spectrochim. Acta, 36A, 249 (1980).

2.26 W.C. Dickinson, Phys. Rev., 80, 563 (1950).

2.27 N. Juranić, M.B. Čelap, D. Vučelić, M.J. Milinar, and P.N. Radivojša, J. Magn. Reson., 35, 319 (1979).

2.28 D.M. Doddrell D.T. Pegg and M.R. Bendall, Aust. J. Chem., 32 1 (1979).

2.29 D.M. Doddrell and M.R. Bendall, J. Magn. Reson., 33, 659 (1979).

2.30 A. Yamasaki, T. Aoyama, S. Fukiqara, and K. Nakamura, Bull. Chem. Soc. Jpn., 51(2), 643 (1978).

2.31 A. Abragam, "The Principles of Nuclear Magnetism", the international series of monographs on physics (W.C. Marshall and D.H. Wilkinson, gem. eds.), Oxford University Press © 1961. Chapters 5-8.

2.32 E.R. Andrew, "Nuclear Magnetic Resonance", Cambridge Monographs on Physics (N. Feather and D. Shoenberg, gen. eds.), Cambrdige University Press, 1955, P. 114.

2.33 P. Debye, "Polar Molecules"; New York, Dover Publications, Inc., 1945 Chapter 5.

2.34 A. Carrington and A.D. McLachlan, "Introduction to Magnetic Resonance", Harper's Chemistry Series (S.A. Rice ed.), © 1967, Harper and Row, New York, Evanston, and London P. 189.

2.35 H.W. Spiess, "NMR Basic Principles and Progress" Volume 15, P. 55 (P. Diehl, E. Fluck and R. Kosfeld eds.), Springer-Verlag, Berlin, Heidelberg and New York.

2.36 PS. Hubbard, Phys. Rev., 131, 1155 (1963)

2.37 D.K. Green and J.G. Powles, Proc. Phys. Soc., Lond., 85, 87 (1965).

2.38 R.F. Schneider, J. Chem. Phys., 48(11), 4905 (1968).

2.39 L. Brillouin, "Tensors in Mechanics and Elasticity" Academic Press. New York, London, 1964, Chapters 1-3.

2.40 U. Haeberlen, Adv. in Magn. Reson., Suppl. 1, New York, Adacemic Press, 1976.

2.41 A.D. Buckingham and S.M. Malm, Mol. Phys, 22, 1127 (1971).

2.42 J.A.B. Lohman and C. MacLean Chem. Phys., 35, 269 (1978).

2.43 J.A.B. Lohman and C. MacLean J. Magn. Reson., 42, 5 (1981).

2.44 J.A.B. Lohman and C. MacLean Mol. Phys., 38(4), 1255 (1979).

2.45 J.A.B. Lohman and C. MacLean, Chem. Phys. Lett., 58(4), 483 (1978).

2.46 K.A. Valiev, Sov. Phys. JETP, 10, 77 (1960).

2.47 K.A. Valiev, Sov. Phys. JETP, 11, 883 (1960).

2.48 K.A. Valiev and B.M. Khabibullin, Russ. J. Phys. Chem., 35, 1118 (1961).

2.49 K.A. Valiev, J. Struct. Chem. U.S.S.R., 3, 630 (1962).

2.50 K.A. Valiev, J. Struct. Chem. U.S.S.R., 5, 477 (1964).

2.51 H.G. Hertz, Ber. Bunsenges. Phys. Chem., 77, 531 (1973).

2.52 H.G. Hertz, Ber. Bunsenges, Phys. Chem., 77, 688 (1973).

2.53 C. Deverell, Mol. Phys., 16, 491 (1969).

2.54 C. Deverell, Prog. Nucl. Magn. Reson. Spectrosc., 4, 235 (1969) (J.W. Emsley, J. Feeney, and L.H. Sutcliffe eds.). Pergamon Press.

2.55 J.D. Halliday, R.E. Richards, and R.R. Sharp, Proc. Roy. Soc. (London), A313, 45 (1969).

2.56 A.I. Mishustin and Yu. M. Kessler, J. Solution Chem., 4(9), 779 (1975).

2.57 Y.M. Kessler, A.I. Mishustin, and A.I. Podkovyrin, J. Solution Chem., 6, 111 (1977).

2.58 V. Gutmann and E. Wycheri, Inorg. Nucl. Chem. Lett., 2, 257 (1966).

2.59 J.S. Perelygin, Thesis, Ivanova, 1974.

2.60 A. Regis and J. Corset, Can. J. Chem., 51, 3577 (1973).

2.61 C.N.R. Rao, H. Molec. Struct., 19, 493 (1973).

2.62 R.E. Burton and J. Daly, Trans. Faraday Soc., 66, 1281 (1970).

2.63 B.M. Rode, Chem. Phys. Lett., 20, 366 (1973).

2.64 P.V. Kostetski, V.T. Ivanov, Yu. A. Ovchinnikov, and G. Shchembelov, FEBS Lett., 30, 205 (1973).

2.65 A.H. Narten, F. Vaslow, and H.A. Levy, J. Chem. Phys., 58, 5017 (1973).

2.66 V. Gutmann, "The Donor-Acceptor Approach to Molecular Interactions", Plenum, New York, 1978.

2.67 B. Lindman and S. Forsen, in "NMR Basic Principles and Progress" (P. Diehl, E. Fluck, and R. Kosfeld, Eds), Vol. 12, Springer-Verlag New York/Berlin, 1976.

2.68 R.G. Bryant, Ann. Rev. Phys. Chem., 29, 167 (1978).

2.69 G.N. Lewis, "Valence and Structures of Atoms and Molecules", The The Chemical Catalog Co., New York, 1923.

2.70 V. Gutmann, Coord. Chem. Revs., 15, 207 (1975).

2.71 V. Gutmann, Coord. Chem. Revs., 18, 225 (1976).

2.72 V. Gutmann, Electrochim. Acta, 21, 661 (1976).

2.73 W.M. Goldschmidt, "Geochemistry" (A. Muir Ed.), Clarendon Press, Oxford, 106 (1958).

2.74 V. Gutmann, Öst. Chem. Ztschr., 4, 1 (1976).

2.75 V. Gutmann, Öst. Chem. Ztschr., 6, 1 (1976).

2.76 V. Gutmann and H. Mayer, Structure and Bonding, 31, 49 (1976).

2.77 H. Keitaibl, H. Völlenkle, and A. Wittmann, Mh. Chem., 103, 1360 (1972).

2.78 V. Gutmann, Rev. Chim. Roun., 22, 679 (1977).

2.79 G. Leroy and G. Louterman-Leloup., J. Mol. Struct., 28, 33 (1975).

2.80 G. Leroy, G. Louterman-Leloup, J. Graultier, and M. Schroer, J. Mol. Struct., 25, 205 (1975).

2.81 B.M. Rode, Chem. Phys. Lett., 32, 38 (1975).

2.82 B.M. Rode, M. Breuss, and P. Schuster, Chem. Phys. Lett., 32, 34 (1975).

2.83 E. Grunwald and S. Winstein, J. Am. Chem. Soc., 70, 846 (1948).

2.84 E.M. Kosower, J. Am. Chem. Soc., 78, 5700 (1956).

2.85 E.M. Koswer, J. Amer. Chem. Soc., 80, 3253 (1958).

2.86 Ibid, 80, 3261, (1958), E.M. Koswer, J. Amer. Chem. Soc., 80, 3267 (1958).

2.87 E.M. Kosower, J. Amer. Chem. Soc., 80, 3267 (1958).

2.88 E.M. Kosower and E.P. Klinedinst. J. Amer. Chem. Soc., 78, 7483 (1956).

2.89 K. Dimroth, C. Reichhardt, T. Siepmann, and F. Bohlmann, Ann. Chem., 661, 1 (1963).

2.90 I. Lindqvist, "Inorganic Adduct Molecules of Oxo-Compounds". Springer-Verlag, Berlin/Grottingen/Heidelberg, 1963.

2.91 R.H. Erlich and A.I. Popov, J. Amer. Chem. Soc., 93, 5620 (1971).

2.92 G. Gonzalez, U. Mayer, and V. Gutmann, Inorg., Nucl Chem. Lett., 15, 155 (1979).

CHAPTER THREE

3.1 J.H. Bigelow, Inorg. Synth., 2, 225(1946).

3.2 J.B. Work, Inorg. Synth., 2, 221(1946).

3.3 R.D. Lindholm, Inorg. Synth., 18, 67(1978).

3.4 H.F. Bauer, W.C. Drinkard, Inorg. Synth., 8, 202(1966).

3.5 M. Shibita, Nippon Kagaku Zasshi, 87(8), 771(1966).

3.6 G.G. Schlessinger, Inorg. Synth., 9, 160(1967).

3.7 H. Diehl, H. Clark and H.H. Willard, Inorg. Synth., 6, 186(1939).

3.8 F. Basolo, R.K. Murmann, Inorg. Synth. 4, 171(1953).

3.9 M. Linhard and H. Flygare, Z. Anorg. Alleg. Chem., 262, 328(1950).

3.10 M. Linhard and H. Siebert, Z. Anorg. Alleg. Chem., 278, 287(1955).

3.11 T. Moeller and G.L. King, Inorg. Synth., 4, 168(1953).

3.12 H. Siebert, Z. Anorg. Alleg. Chem., 327, 63(1964).

3.13 M. Shibata, J. Jpn. Chem. (Kagaku No Ryoiki), 90, 9 (1970).

3.14 A. Haim and W.K. Wilmarth, Inorg. Chem., 1, 573(1962).

3.15 J.C. Bailer Jr., Inorg. Synth., 2, 222(1946).

3.16 J. Springbørg and C.E. Schäffer, Inorg, Synth., 14, 63-81(1973).

3.17 W.G. Jackson and C.M. Begbie, Inorg. Synth., 21, 119(1982).

3.18 W. Strecker and H. Oxenius, Z. Anorg. Alleg. Chem., 218, 151(1934).

3.19 E.P. Harbulak and M.J. Albinak, Inorg. Synth., 8, 196(1966).

3.20 H.F. Holtzclaw Jr., D.P. Sheetz and B.D. McCarty, Inorg. Synth., 4, 176(1953).

3.21 K. Konya, H. Nishikawa, and M. Shibita, Inorg. Chem., 7(6) 1165 (1968).

3.22 A. Werner, Lieb. Ann., 386, 103(1912).

3.23 G.B. Kauffman, S.F. Abott, S.E. Clark, J.M. Gibson and R.D. Meyers, Inorg., Synth., 18, 69(1978).

3.24 M. Mori, M. Shibata and E. Kyuno, Bull. Chem. Soc. Jpn., 29(8) (1956).

3.25 M. Shibata, Chem. and Chem. Ind., 20(9), 116(1967).

3.26 K. Ohkawa, J. Fujita and Y. Shimura, Bull. Chem. Soc., Jpn., 88(1), 66(1965).

3.27 M. Linhard, M. Weigel and H. Flygare, Z. Anorg. Alleg, Chem., 263, 233(1950).

3.28 D. Dodd and M.D. Johnson, J. Organomet. Chem., 52, 1(1973).

3.29 M. Linhard and M. Weigel, Z. Anorg. Alleg, Chem., 263, 245(1950).

3.30 P.H. Crayton, Inorg., Synth., 1, 207-213(1963).

3.31 G. Schlessinger, Inorg. Synth., 6, 175-191(1960).

3.32 D.A. House and D.A. Gainsford, Inorg. Chim. Acta., 3(3), 367(1969).

3.33 M. Mori, J.A. Weil and M. Ishiguro, J. Amer. Chem. Soc., 90, 615(1968).

3.34 J.A. Wiel, D.L. Duffy and D.A. House, J. Inorg. Nucl. Chem., 3, 2053(1969).

3.35 J. Calderazzo and C. Floriani, J. Chem., Soc. (A), 946(1969).

3.36 T.K. Leipert and D.W. Marquardt, J. Magn. Reson., 24, 181(1976).

3.37 T.C. Farrar and E.D. Becker, "Pulse and Fourier Transform NMR" Academic Press, New York, 1971.

3.38 D.T. Pegg, D.M. Doddrell, M.R. Bendall and A.K. Gregson, Aust. J. Chem., 29, 1885(1976).

3.39 K. Van Putte, J. Magn. Reson., 2, 174 (1970).

3.40 R.J. Buist, Private Communication.

3.41 N.R. Draper and H. Smith, "Applied Regression Analysis, 2nd Ed., Wiley, New York, 1981, Chapter 10.

3.42 R.E. Lenkenski, Private Communication

3.43 "CRC Handbook of Chemistry and Physics", 59th Edition, editor R.C. Weast, 1978-1979.

3.44 T. Birchall and J.P. Johnson, Can. J. Chem., 57, 160 (1979).

3.45 A.V. Hill, Proc, Roy, Soc., London Series A, 127, 9(1930).

CHAPTER FOUR

4.1 H. Hartmann and H. Sillescu, Theor. Chim. Acta, 2, 371(1964).

4.2 A. Yamasaki, F. Yajima and S. Fujiwara, Inorg. Chim. Acta, 2, 39 (1968).

4.3 F. Yajima, Y. Koike, H. Yamasaki and S. Fujiwara, Bull. Chem. Soc. Jpn., 47(6), 1442(1974).

4.4 N. Juranic, M. B. Celap, D. Vucelic, M.J. Malinar and P.N. Radivojsa, Spectrochim. Acta, A35, 997(1979).

4.5 R.G. Kidd and R.J. Goodfellow, in "NMR and The Periodic Table" (B.K. Harris and B.E. Mann, Eds.), Chapter 9, Academic Press, New York, 1978.

4.6 Commission on the Nomenclature of Inorganic Chemistry, Pure Appl. Chem., 28, 1(1971).

4.7 D.M. Doddrell and M.R. Bendall, Aust. J. Chem., 25, 2239(1972).

4.8 H.H. McConnell and C.H. Holm, J. Chem. Phys., 25, 1289(1956).

4.9 H.W. Spiess, H. Haas and H. Hartmann, J. Chem. Phys., 50, 3057 (1969).

4.10 H. Yamatvera, Bull. Chem. Soc. Jpn., 37, 95(1958).

4.11 R.A.D. Wentworth and T.S. Piper, Inorg. Chem., 4, 709(1965).

4.12 K. Matsumoto, H. Kuroya and T. Okamoto, Nippon Kagaku Zasshi, 9(7), 650 (1970).

4.13 A.B.P. Lever, "Inorganic Electronic Spectroscopy", Elsevier Publishing Company, 1968.

4.14 A. Gierer and K. Wirtz, Z. Naturforsch., A8, 532(1953).

4.15 B.L. Cohen, "Concepts of Nuclear Physics" McGraw-Hill Book Company 1971, Appendix II.

4.16 J.S. Griffith and L.E. Orgel, Trans. Faraday Soc., 53, 601(1957).

4.17 L. Ramakrishnan, S. Soundarajan, V.S.S. Sastry, and R. Ramakrishna, Coord. Chem. Rev., 22, 123 (1977).

4.18 P. Rigny and F. Virlet, J. Chem. Phys., 47(11), 4645(1967).

4.19. C. Deverell, Mol. Phys., 18(3), 319(1970).

4.20 R. Adler and A. Lowenstein, J. Magn. Reson., 5, 248(1971).

4.21 J. Wilinski and R.J. Kurland, Inorg. Chem., 12, 2202(1973).

4.22 W.T. Huntress, Adv. in Magn. Reson., 4, 1(1970), New York, Academic Press.

4.23 D.R. Eaton, C.V. Rogerson and A.C. Sandercock, J. Phys. Chem., 86, 1365(1982).

4.24 M.T. Emerson, E. Grunwald, M.L. Kaplan and R.A. Kromhout, J. Amer. Chem. Soc., 82, 6307(1960).

4.25 O. Ya. Samoilov, Zh. Fiz. Khimii, 20, 1411(1946).

4.26 D.P. Stevenson, J. Phys. Chem. 67, 2145(1965).

4.27 H.S. Frank and W.Y. Yen, Discuss Faraday, Soc., 24, 133(1957)

4.28 A.G. Marshall, J. Chem. Phys.,52, 2527(1970)

CHAPTER FIVE

5.1 Y. Nakashima, M. Muto, I.Takagi and K. Kawano.,Chem. Lett., 1075 (1975).

5.2 A. Yamasaki, Y. Miyakoshi, M. Fujita, Y. Yoshikawa and H. Yamatera J. Inorg. Nucl. Chem., 41, 473 (1979).

5.3 J.W. Lehman and B.M. Fung,Inorg. Chem., 11(1), 214 (1972).

5.4 J.H. Russell, V.P. Chacko and R.G. Bryant, Texas A&M University NMR Newsletter No.288, 29 (1982).

5.5 G.C. Levy and R.L. Lichter, Nitrogen 15 NMR Spectroscopy, Wiley, New York, (1979).

5.6 K.D. Rose and R.G. Bryant, Inorg. Chem., 16, 1332 (1979).

5.7 A. Yamasaki and K. Nakamura, Rep. Univ. Electro-Communs., 28, 507 (1978).

CHAPTER SIX

6.1 A. Yamasaki, F. Yajima and S. Fujiwara, Inorg. Chim. Acta, 2(1), 1968.

6.2 H. Yoneda and Y. Nakashima, Bull. Chem. Soc. Jpn., 47(3), 669 (1974).

6.3 C.J. Ballhausen,"Introduction to Ligand Field Theory, McGraw Hill, New York, p.107 (1962).

6.4 K.A. Valiyev and M.M. Zripov, Zh. Struckt. Khim., 7, 494 (1966).

6.5 V.P. Tarasov, V.I. Privalov and Yu. A. Buslaev, Mol. Phys., 35, 1047 (1978).

6.6 F.W. Wehrli and S. Wehrli, J. Magn. Reson, 44, 197 (1981).

6.7 G.M. Bancroft and R.H. Platt, Adv. In Inorg. and Radio Chem., 15, 59 (1972).

6.8 G.M. Bancroft, Coord. Chem. Rev., 11, 247 (1973).

6.9 C.K. Jorgensn, "Oxidation Numbers and Oxidation States" Springer, New York, pp. 84-85 (1969).

CHAPTER SEVEN

7.1 B.C. Wang and W.P. Schaeffer, Science, 165, 1404 (1969).

7.2 R. Marsh and W.P. Schaeffer, Acta, Crystallogr., 21, 246 (1968).

CHAPTER EIGHT

8.1 R.M. Fuoss, J. Amer. Chem. Soc., 80, 5059 (1958).

8.2 D.B. Rorbacher, Inorg. Chem., 5, 1891 (1966).

8.3 R.G. Pearson and P. Ellgen, Inorg. Chem., 6(7), 1379 (1967).

8.4 F. Marshall Beringer and E. Melvin Gindler, J. Amer. Chem. Soc., 77, 3200 (1955).

8.5 J.E. Prue, J. Chem. Soc., 7534 (1965).

8.6 A. Haim and W.K. Wilmarth, Inorg. Chem., 1, 573 (1962).

8.7 E.B. Fleischer, S. Jacobs and L. Mestichelli, J. Amer. Chem. Soc., 90, 2527 (1968).

8.8 J. Halpern, R.A. Palmer and L.M. Blakley, J. Amer. Chem. Soc., 88, 2877 (1966).

8.9 M.L. Tobe, "Inorganic Reaction Mechanisms", T. Nelson and Sons (London), 1972.

8.10 M. Zerner and M. Gouterman, Theoret. Chim. Acta, 4, 44 (1966).

CHAPTER NINE

9.1 R.N. Schwartz, J. Magn. Reson., 24, 205 (1976).

9.2 N. Juranic, Inorg. Chem., 22, 521 (1983).

Appendix II

A-II.1 P. Pascal. "Nouveau Traite de Chimie Minerale", Masson, Paris 27(1), 665 (1967).

A-II.2 A.A. Van der Giessen, "Chemical and Physical Properties of Iron(III)-Oxide Hydrate", Philips Res. Rep. Suppl., 12, 1 (1968).

A-II.3 M. Yamamoto and T. Iwata, Proc. Intern. Conf. Magn., Nottingham (1964), Inst. Phus. Soc., London (1965)

A-II.4 A.L. Mackay, "Reactivity of Solids", Ed. J.H. de Boer, Elsevier Publishing Co., New York, 4, 571 (1961).

A-II.5 Y. Yabuta, N. Kinomura, M. Shimada, F. Kanamura and M. Koizumi, J. Solid State Chem., 33, 25[illegible] (1980).

A-II.6 B.A. Goodman and D.G. Lewis, J. Soil Sc., 32, 351 (1981).

A-II.7 J.D. Bernal, D.R. Dasqupta and A.L. MacKay, Clays Minerals, Bull., 4, 15 (1959).

A-II.8 M.J. Ridge, B. Molony and G.R. Boell, J. Chem. Soc.(A), 594 (1967).

A-II.9 R.F. Conley, J. Amer. Ceram. Soc., 50, 124 (1967).

A-II.10 F. Gazzarini and G. Lanzavecchia, "Reactivity of Solids", Wiley-Interscience, New York, 6,57 (1968).

A-II.11 R. Schrader and G. Buttner, Z. Anorg. Chem., 320, 220 (1963).

A-II.12 Goldsztaub, Bull. Soc. Fr. Miner, 58, 6 (1935).

A-II.13 M.H. Francombe and H.P. Rooksby, Clays Minerals Bull., 4, 1 (1959).

A-II.14 A.A. Van der Giessen, J. Inorg. Nucl. Chem., 28, 2155 (1966).

A-II.15 G. Kruss and R. Lorentz, Z. Anorg. Allgem. Chemie, 200, 18 (1931).

A-II.16 K.M. Towe and W.F. Bradley, J. Coll. Interf. Sc., 24, 384 (1967).

A-II.17 S. Okamoto, H. Sekizawa and S.I. Okamoto, "Reactivity of Solids", Chapman and Hall, London, 7, 341 (1972).

A-II.18 G. Denes, Private Communications

A-II.19 E. Wolska, Z. Kristallogr., 154, 69 (1981).

A-II.20 J.M.D. Coey and P.W. Readman, Earth Planet Sc. Lett., 21, 45 (1973).

A-II.21 K. Ruebenbauer and T. Birchall, Hyperfine Interact., 7, 125 (1979); GMFPS, a modified version of GMFP by G. Denes (unpublished).

A-II.22 F. Van der Woude, Phys. Stat. Sol., 17, 417 (1966).